The Pennsylvania State University
The Graduate School

OPTIMIZED DESIGN OF CYCLIC PRESSURE PULSING IN NATURALLY FRACTURED RESERVOIRS USING NEURAL-NETWORK BASED PROXY MODELS

A Dissertation in
Petroleum and Natural Gas Engineering
by
F. Emre Artun

Submitted in Partial Fulfillment
of the Requirements
for the Degree of

Doctor of Philosophy

August 2008

The dissertation of F. Emre Artun was reviewed and approved* by the following:

Turgay Ertekin
Professor and Program Chair of Petroleum and Natural Gas Engineering
George E. Trimble Chair in Earth and Mineral Sciences
Dissertation Co-Advisor, Co-Chair of Committee

Robert W. Watson
Associate Professor of Petroleum and Natural Gas Engineering
Dissertation Co-Advisor, Co-Chair of Committee

Luis F. Ayala
Assistant Professor of Petroleum and Natural Gas Engineering

Mirna Urquidi-Macdonald
Professor of Engineering Science and Mechanics

Majid A. Al-Wadhahi
Assistant Professor of Petroleum and Natural Gas Engineering
Sultan Qaboos University, Oman
Special Member

*Signatures are on file in the Graduate School.

Abstract

Stimulation of oil wells with cyclic pressure pulsing using gases is an IOR method that is effectively applicable to fractured reservoirs. Fractures provide a large contact area for the injected gas to diffuse through and penetrate into the low-permeability matrix. Also, high permeability of the fracture system provides easy delivery of the injected gas and produced oil. The process attracts operators because of shorter payback periods and lower investment requirements as compared to field-scale flooding projects. Designing a cyclic pressure pulsing project requires optimization of the design parameters such as the amount of injected gas, injection rate, and lengths of injection, soaking, and production periods. Due to the computational cost of simulating a large number of scenarios, it is an arduous task to determine the aforementioned design parameters, and to optimize the process.

In this study, neural-network based proxy models are used to assess the feasibility of these processes in reservoirs with different characteristics, and to develop optimized design schemes to maximize the efficiency of the process. The method of approach includes understanding the mechanics of the process via reservoir simulation studies. Artificial neural network (ANN) based proxy models that accurately mimic the reservoir model efficiently in terms of the computational time are developed. First, the methodology is tested with the reservoir model of the Big Andy Field where cyclic CO_2 (since 1985) and cyclic N_2 (since 1996) injection have been utilized. Developed proxies were able to estimate the expected magnitudes of some of the critical performance indicators for a given set of process design parameters for CO_2 and N_2 injection. An inverse proxy is developed that goes beyond the capabilities of a reservoir model by providing optimized combination

of design parameters for a given set of desired performance characteristics. Then, the methodology is extended to reservoirs with different characteristics by including reservoir properties in the knowledge base. Universal proxies are developed which can accurately output the performance indicators when the reservoir characteristics and design parameters are input. The hybrid neuro-genetic approach is utilized for optimization studies. This approach uses the genetic algorithm (GA) as the optimization tool. GA uses the neural-network based proxy approximator for evaluation of the specified objective function for computational efficiency. By changing the design parameters, it searches for the best design scenario that would maximize/minimize the objective function that is specified based on the nature of the problem. The reservoir model used in this study is a single-well, compositional reservoir model with a dual-porosity system. A detailed parametric study is conducted using the reservoir model to develop a better understanding of how operational parameters and reservoir conditions affect the performance of the process. Peak oil rate, discounted incremental oil production, and net present value (NPV) are used for performance evaluation. It was observed that the injected gas volume in each cycle is the most critical parameter in affecting the performance. Injecting the same volume at a higher rate for a shorter period of time is found to be more effective than injecting for a longer time at a lower rate. While soaking has little effect as compared to other design parameters, optimization of soaking would yield higher recovery and NPV. It was observed that the initial pressure/temperature of the reservoir, and therefore, the initial fractions of gas/liquid phases affect the process efficiency significantly.

Table of Contents

List of Figures

List of Tables

Nomenclature

A	Drainage area, acres
b	Decline coefficient
C	Context neuron activations
D_i	Initial decline rate
e	Output error
F	Future value
h	Formation thickness, ft
i	Interest rate
k	Effective permeability, md
k_h	Effective matrix permeability in the horizontal direction (used when k_x=k_y), md
k_x	Effective matrix permeability in the x-direction, md
k_y	Effective matrix permeability in the y-direction, md
k_v	Effective matrix permeability in the vertical (z) direction, md
k_z	Effective matrix permeability in the z-direction, md
k_m	Matrix permeability, md
k_f	Fracture permeability, md
k_r	Relative permeability

k_{ro}	Relative permeability to oil
k_{rog}	Relative permeability to oil in the two-phase oil-gas system at irreducible water
k_{roi}	Initial relative permeability to oil
k_{row}	Relative permeability to oil in a two-phase water-oil system (no gas present)
k_{rw}	Relative permeability to water
k_{rwi}	Initial relative permeability to water
k_{rg}	Relative permeability to gas
k_{rgi}	Initial relative permeability to gas
N_I	Number of inputs
N_O	Number of outputs
N_{HN}	Number of hidden neurons
N_p	Population size (number of individuals)
N_{TP}	Number of training patterns
n	Number of periods in economic calculations
n_{max}	GA maximum number of generations
P	Present value
$P(t)$	GA population at generation, t
p	Pressure, psia
p_c	GA crossover probability
p_i	Initial pressure, psia
p_m	GA mutation probability
R	Correlation coefficient
q_o	Oil flow rate, STB/d

q_g	Gas flow rate, MCF/d
S	GA data structure
S_o	Oil saturation
S_w	Water saturation
S_g	Gas saturation
S_{oi}	Initial oil saturation
S_{wi}	Initial water saturation
S_{gi}	Initial gas saturation
T	Temperature, ^{o}F
t	Target (actual) output; EA/GA iteration index; time
t_{ip}	Injection period of a cycle
t_p	Time to reach the peak rate
t_{pp}	Production period of a cycle
t_{sp}	Soaking period of a cycle
U	Utilization factor
v	Weights in links between hidden and output layers
w	Weights in links between input and hidden layers
X_f	Fracture spacing, ft
x	Input neuron activations; GA individual
y	Output neuron activations
z	Hidden neuron activations

Greek

α	Learning rate
δ	Error information term
ϕ	Porosity
ϕ_m	Matrix porosity
ϕ_f	Fracture porosity

Abbreviations

ANN	Artificial neural networks
API	American Petroleum Institute
BTU	British Thermal Unit
CF	Contribution factor
CI	Cumulative injection
CO_2	Carbon dioxide
COP	Cumulative oil production
CP	Cumulative production
EA	Evolutionary algorithms
EP	Evolutionary programs
GA	Genetic algorithms
GOR	Gas-oil ratio
GUI	Graphical-user-interface
IOP	Incremental oil production
IOR	Improved oil recovery
IP	Injection period
MSCF/MCF	A thousand standard cubic-feet

MW	Molecular weight
N_2	Nitrogen
NCF	Net cash flow
NPV	Net present value
OIP	Oil-in-place
PP	Production period
RNN	Recurrent neural networks
SCF	Standard cubic feet
SG	Specific gravity
SP	Soaking period
SR	Stimulation ratio
STB	Standard barrels
TTP	Time-to-peak
WOR	Water-oil ratio

Acknowledgments

My doctoral studies at Penn State have been extremely rewarding for my personal and professional development. I would like to take this opportunity to express my gratitude to people who have contributed to my experiences during my studies.

First and foremost, I would like to thank my advisor, Prof. Turgay Ertekin, for his constant guidance, support, and friendship from the very first day until the completion of my studies. He has been very supportive and helpful during challenging times both in my research and in my personal life. I also learned a lot from him in his classes and during our discussions. I am grateful to him for making my research and learning experiences enjoyable.

I would like to express my sincere gratitude to my co-advisor, Dr. Robert Watson, for his constant guidance, support, and friendship during my studies. He has been very helpful by sharing his suggestions and experiences continuously during our meetings, which contributed significantly to the value of this research work.

I would like to extend my appreciation to my committee members, Prof. Mirna Urquidi-Macdonald, Dr. Luis Ayala and Dr. Majid Al-Wadhahi for their interest in serving in my committee. They all provided valuable recommendations, which made it possible for me to approach my research from different points of view.

I gratefully acknowledge the research grant from Miller Energy Technologies. I would like to thank Mr. Bernie Miller for his suggestions during our meetings and for providing the field data used in this study.

My friends have always been very helpful and supportive, and I feel very lucky to have them around. I would like to thank Dr. Claudia Parada for patiently

sharing his knowledge and experiences and discussing our research during our coffee breaks. I would like to thank my office-mate and friend Mario Farias for sharing the endless hours of working in 222 Hosler and for our discussions about cyclic pressure pulsing and reservoir simulation. I would like to thank Dr. Razi Gaskari of Merrick Systems for sharing his ideas regarding the neural network architectures for my research.

I am indebted to my friends; Başar Basbuğ, Burcu Ünal, and Doruk Alp for their endless emotional support and for taking care of me when I broke my ankle, and had the surgery. I want to thank Mehmet Tarman and Umut Gökcesu, with whom I went to high school, college, and graduate school together. I am grateful for their friendship, suggestions and support throughout the years. I would also like to thank Dr. Çağlan Kumbur, Murat Yaşar, Anı Şimşek-Gökcesu, Ahmet Turhan, Pamir Cırdı, Şafakcan Tunçdemir, Seyit Ural, Öykü Aşıkoğlu, Ceyda Çoruh and all others for being great friends and sharing many great moments during the past few years. Without them, it would have been very hard to achieve what I have achieved.

Many of my friends and my family were not here with me, but they have always been very supportive. I am thankful to them for their support and belief in me, which made it possible for me to successfully complete my studies.

F. Emre Artun
University Park, Pennsylvania
August 2008

To my father, Bilsel,
my mother, Nilgün,
and my sister, Selin.

"Our true mentor in life is science."
M. K. Atatürk

Chapter 1

Introduction

With the current world energy demand and supply profile, improved oil recovery (IOR) methods have become significantly important in recent years. There are many different types of IOR methods that are efficiently applicable in different classes of reservoirs. To develop a successful IOR application, selecting the appropriate IOR method and designing the process are of equally significant importance. Economic success of an IOR project mainly depends on the effectiveness of the method in that specific reservoir and the way it is designed.

Cyclic pressure pulsing using different types of gases is an IOR method that is effectively applicable specifically to fractured reservoirs. The process is also known as *huff 'n' puff*, which was first introduced to define the cyclic steam stimulation process to improve heavy oil recovery. In low-permeability reservoirs that are dissected by a network of interconnected fractures, solution channels, and vugs, waterflooding and gas flooding are not fully effective, since the injected fluid tends to channel through the high conductivity network and bypass the low-permeability, oil-bearing matrix (Felsenthal and Ferrell, 1967; Raza, 1971). In this type of reservoirs, cyclic pressure pulsing with gas has been found to be effective. Fractures provide a large contact area for the injected gas to diffuse through and penetrate into the low-permeability matrix. Also, high permeability of fracture system results in an easy delivery of both the injected gas and produced oil. Because it is a single-well process, well-to-well connectivity is not required. Another char-

acteristic of cyclic pulsing process that attracts operators' attention is that the payback period is very short as compared to that of field-scale flooding projects. This makes the single-well cyclic pressure pulsing process low-risk with a relatively lower initial investment requirement and a shorter payback period. The process is characterized by three distinct stages as shown in Figure 1.1 with its impact on the change in oil flow rate with time:

1. Injection period: During this period, the gas is injected into the reservoir. Length of this period depends on the treatment amount, the capability of the field unit to provide gas, and the number of wells that are to be treated.

2. Soaking period: After the injection period, the well is shut-in to wait for the injected gas to interact with reservoir fluids by diffusing from fractures into the matrix. From the field experience stated in the literature, this period is typically 2-4 weeks.

3. Production period: After soaking is completed, the well is put on production to produce oil, water, and gas. Typically, a large amount of gas is produced at the beginning of the period, while the oil rate starts to rise and reaches a peak rate. After this point, production may continue until the economic limits are reached.

The motivation for this study is the limited number of studies concerning this method in the literature that focus on specific reservoirs and the optimization of operational conditions that is not broadly investigated. The applicability and effectiveness of the process can vary significantly from one type of reservoir to another one. Like in any other IOR application, it is a challenging task to consider all variables involved in the process and develop rule-based guidelines for the practicing engineer. However, with the significant improvements in the computational power and development of new effective tools for modeling and optimization in recent years, it is now possible to develop a better understanding about the applicability and limitations of the process in different reservoirs and under different operating conditions. In this dissertation, a comprehensive study of the high-performance modeling and optimization of cyclic pressure pulsing process is presented. This study focuses on naturally fractured reservoirs because the recovery mechanism involved in this process is favorable in fractured systems.

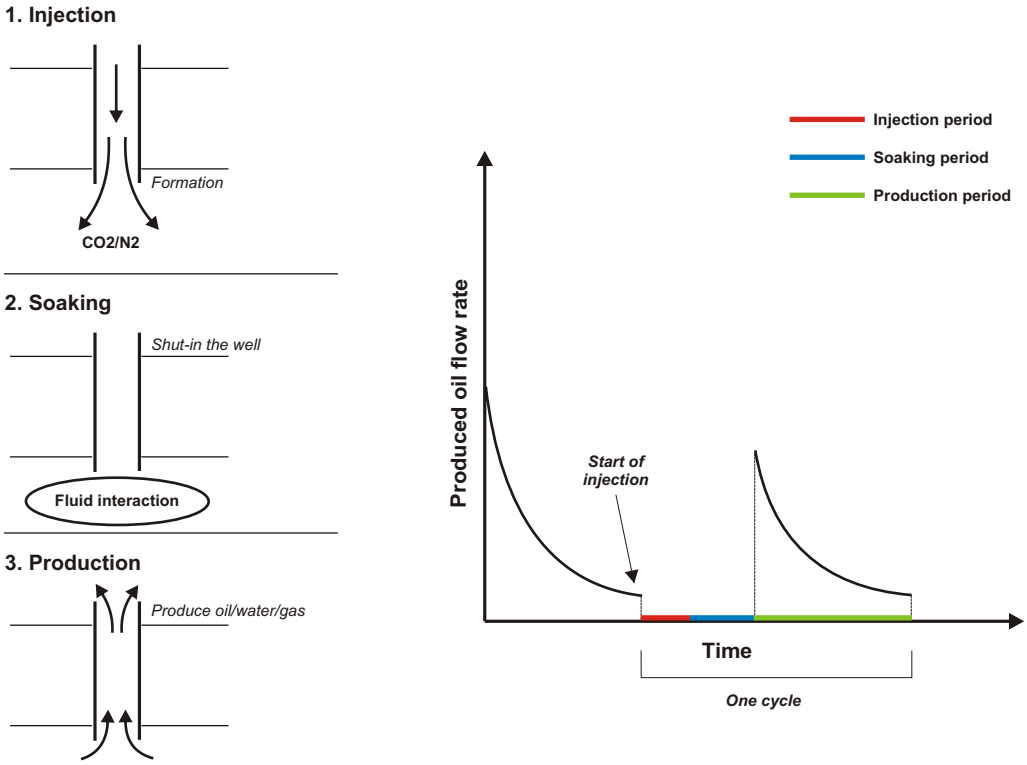

Figure 1.1. Overview of the cyclic stimulation process and its resulting impact on the produced oil flow rate.

This dissertation is organized as follows:

- In Chapter 2, a summary of the previous work done on cyclic pressure pulsing process is presented. Also, in a separate section a summary of various reservoir engineering optimization studies that utilized intelligent systems is given.
- Chapter 3 includes the problem statement and study objectives.
- Chapter 4 includes theoretical background about the methods that are used in this study. Explanations of artificial neural networks, genetic algorithms, and how they are incorporated to the study through the hybrid neuro-genetic approach are discussed. Algorithmic explanations of neural networks and genetic optimization techniques are presented.
- Chapter 5 includes design and development of reservoir-specific neural network proxy approximators. These models are developed specifically for the

Big Andy Field in Kentucky. An overview of the study area, description of the reservoir model, the structures of the networks that are developed, the problems that are faced, and how they are overcome, are explained. An application of the methodology to one of the leases in the Big Andy Field is presented as a guideline to the practicing engineer.

- Chapter 6 includes design and development of universal neural network proxy approximators. Characterization of the reservoir model to generalize the methodology presented to different reservoirs is presented. Architectures and structures of different neural networks for the injected gas, reservoir fluid, and the design scheme are explained.

- Chapter 7 includes a detailed parametric study that investigates how the operational parameters and reservoir characteristics affect the performance of the cyclic pressure pulsing process. Comparative analyses based on the economics and oil production are presented and discussed.

- Chapter 8 includes the optimization studies that were done with the neuro-genetic approach, which couples the neural-network based proxies with the genetic algorithm to perform a stochastic search through the response surface generated by the neural network. Results of optimization studies with different design schemes and objective functions are presented and discussed.

- Chapter 9 includes a summary of the study, conclusions and recommendations for future work to improve on the current study.

Chapter 2

Literature Review

Although the cyclic pressure pulsing process is not as popular as other IOR methods, there are a number of studies that have been presented in the petroleum engineering literature concerning it since late 1960's. In this chapter, first, a summary of these studies is given to present results of experimental and modeling studies and field applications. Later, some previous examples of the application of intelligent systems in various reservoir engineering optimization problems are introduced. The chapter concludes with a summary of all studies that were considered.

2.1 Cyclic Pressure Pulsing for Improved Oil Recovery

The idea of cyclic pressure pulsing has evolved after field-scale cyclic gas injection applications (Cook, 1957; Crosby and Cochran, 1960), where produced associated gas is injected into the reservoir from which it was produced. The purpose of this is pressure maintenance to improve oil recovery. During 1960's, cyclic pressure pulsing method was introduced as an improved method of conventional waterflooding, because of water channeling and oil bypassing problems in waterflooding of highly-fractured reservoirs. An experimental study (Owens and Archer, 1966) and results of an accidental cyclic waterflooding operation in the Grayburg reservoir of Permian Basin (Felsenthal and Ferrell, 1967) were presented in the literature. The

process was found to be feasible in the sense that injection was sped up from the slow imbibition rates to injection capacity rates, and a shorter pressuring phase compared to waterflooding was important for economic considerations. Water and nitrogen/ethane cycling experiments showed that injecting gas (nitrogen/ethane) ahead of water could increase the chances of success of the process. They also stated that pressure pulsing should be applied in high capacity, partially depleted, fractured reservoirs containing some free gas saturation. Menzie and Nielsen (1963) and Cook *et al.* (1967) set forth the initial motivation for cyclic injection of CO_2 by experimenting with its usefulness in vaporizing crude oil for improved oil recovery.

Raza (1971) conducted water and gas cycling experiments using Berea, Bandera sandstones and Austin chalk limestones. He found out that there is a critical oil saturation below which cyclic pulsing is ineffective, and this critical saturation is different for each porous medium. He also stated that gas cycling is better than water cycling, because it is not dependent on the critical oil saturation. He compared CO_2, N_2, and CH_4, and he observed that N_2 and CH_4 both have the similar effects in increasing the pressure, but higher amounts of CO_2 is required for the same pressure increase because of its higher compressibility.

The first field application utilizing gas huff 'n' puff was reported by Shelton and Morris (1973). They proposed injecting rich hydrocarbon gases to increase the reservoir energy and reduce the oil viscosity instead of steam, which is not found to be effective in stimulating deep and thin formations. They stated that while the increase in reservoir energy is a short-term benefit, viscosity reduction is a long-term benefit for the future of the well. One of the conclusions that they made was about the soaking period. They observed that soaking has a significant effect mainly on the initial production rate (peak rate), and longer soaking would decrease the peak rate because of dissipation of the pressure.

Stright *et al.* (1977) conducted a numerical simulation study that used the variable bubble-point formulation to model cyclic CO_2 injection in a bottom-water-drive reservoir to determine the feasibility of the process. They used some field data that employed the use of a small slug of CO_2 to evaluate the results using history matching with the numerical model. 1,890 MCF of CO_2 was injected over a 20-hour period, and the well was permitted to soak for 22 days. They concluded that the process efficiency was poor, and the viscosity reduction effect was offset

by increased water saturations in the coning region.

During 1980's, a number of studies were reported about using CO_2 huff 'n' puff, instead of steam, for heavy oil recovery. Field applications in southern Arkansas (Khatib *et al.*, 1981) and in Turkey (Bardon *et al.*, 1986; Göndiken, 1987), laboratory tests (Sankur and Emanuel, 1983; Sayegh and Maini, 1984), and numerical simulation studies (Patton *et al.*, 1982) indicated favorable improved oil recovery results due to oil swelling and viscosity reduction caused by CO_2. Claridge (1984) made a summary of these studies explaining the recovery mechanisms involved in the process. Haskin and Alston (1989) presented results of CO_2 huff 'n' puff applications in 28 wells in Texas. They provided a methodology to predict the incremental oil recovery, and they observed that soaking times longer than 2-3 weeks would not be feasible.

In late-1980's, heavy-oil huff 'n' puff applications started shifting towards light-oil applications. Hsu and Brugman (1986) conducted a single-well, compositional simulation study for the Paradis Field in Louisiana by history-matching two cycles, and predicting the performance of the third cycle. According to the parametric studies that they have conducted, they observed that the primary mechanisms favoring the process are: 1) vaporization of intermediate components, 2) oil viscosity reduction, and 3) oil phase swelling. They also observed that soaking has little effect (from 5 to 40 days), while injected gas amount has the most important effect on recovery. In their study, contamination of CO_2 with up to 20% N_2 or CH_4 had little effect. During the second cycle incremental oil significantly dropped, which showed that the third cycle would not be feasible. Monger and Coma (1988) tested 14 Berea cores from south Louisiana for CO_2 to improve the recovery of 32° API light crude oil. They also concluded that the injected gas amount is more important than soaking time (18-52 days), and efficacy of the process declines during the second cycle.

Miller (1990) presented field results of 200 CO_2 huff 'n' puff treatments (340 to 4,130 MSCF each) over a four-year period in the Big Sinking Field, Kentucky. Emanuel *et al.* (1991) analyzed a 120-ton, 2-day CO_2 injection process with analytical decline curve calculations and with a radial, compositional reservoir model. They observed that the amount of injected gas has the most significant effect and soaking period beyond 2 weeks does not have a significant effect. Monger *et al.*

(1991) conducted laboratory tests and compared them with field results achieving less than 1 MSCF/STB of efficiency. They concluded that the method is more feasible in depleted reservoirs rather than water-drive reservoirs.

Thomas and Monger-McClure (1991) performed field production data analysis from 14 fields in Louisiana and Kentucky, to understand how the incremental production and stimulated oil production rates increase with different design parameters. They observed that diffusion is important for soaking, and mechanisms related to diffusion, phase behavior, and relative permeability effects are more significant than reservoir re-pressurization. They emphasized the benefit of an extended soak, and concluded that holding back-pressure on producing wells is favorable, and that the recovery improves with oil swelling. They provided well selection and operational guidelines. They achieved an average CO_2 utilization factor of 1.3 MSCF/STB.

Towler and Wagle (1992) conducted black-oil modeling study to analyze the process in low-pressure, solution-gas-drive reservoirs. They observed that relatively dead oils are more likely to respond than gas-rich live oils, and relative permeability hysteresis and reservoir pressure increase are significant mechanisms in the success of the process. Biswas (1993) used a compositional model to evaluate the impact of different reservoir conditions and process design variables on the recovery after cyclic CO_2 injection in water-drive reservoirs. He observed that while the recovery increases with the slug size, it is a design variable that would be optimized considering the utilization efficiency. It is stated that the length of the soaking period does not affect the incremental recovery and it should be minimized such that the molecular diffusion can take place. It was observed that the process is not sensitive to the well spacing and is sensitive to the bottom-hole pressure. An important conclusion is reported that the effect of heterogeneities in the reservoir is very insignificant. This is due to the fact that the process is a single-well process and near-wellbore phenomena dominate the process rather than portions of the reservoir located external to the wellbore.

Bardon *et al.* (1994) and Miller *et al.* (1994) presented results of the cyclic CO_2 utilization in the Shoemaker Ridge Field in Kentucky since 1985. The first treatment included 2 hours of injection of 345-4,140 MSCF CO_2, followed by 1-2 weeks of soaking, and resulted in an average utilization of 0.63 MSCF/STB. Since

it is a low-pressure depleted reservoir, low dissolution of CO_2 resulted in a lower viscosity reduction than other field applications reported previously.

Wolcott *et al.* (1995) and Shayegi *et al.* (1996) presented experimental investigations of the process on light crude oil from the Timbalier Field, Louisiana. They tested mainly CO_2 injection, while investigating the benefits of using other types of gases. Based on the study of Wolcott *et al.* (1995), cyclic CO_2 stimulation can be successfully employed in steeply-inclined reservoirs, and chasing the CO_2 slug with nitrogen would improve the performance of the process. Shayegi *et al.* (1996) compared the results using CO_2 with the results using N_2 and CH_4. In their study, it was observed that pure N_2 would recover half of what could be recovered using CO_2 and CH_4. CO_2/N_2, CO_2/CH_4 mixtures yielded 2-3 times more recovery than these obtained using pure gases. They also stated that at high pressures CO_2/N_2 mixtures gave the best results.

Wehner and Prieditis (1996) used a radial, compositional model to analyze the process. They observed that main recovery mechanism is gas trapping by hysteresis, and majority of the gas trapping occurred during the first cycle (multiple cycles are not favorable). They have achieved an utilization factor of 10 MSCF/STB. They found out that the process is not dependent on reservoir heterogeneity and a longer soak of more than a few days would not help to improve the recovery. As in other similar studies, they observed that different injection pressures do not affect the process efficiency, while the most important parameter is the total amount of gas injected.

Miller and Hamilton-Smith (1998) presented the results of CO_2 cyclic injection in the Big Sinking Field, Kentucky, between 1985-1994 during which, 390 treatments in 240 wells resulted in a utilization efficiency of 1.2 MSCF/STB and 180,000 STB of incremental oil production. Because of the high cost of CO_2, they tried to use rich gas produced from the same reservoir, and exhaust gas (CO_2/N_2). They concluded that the exhaust gas is more efficient than the rich gas in terms of the utilization efficiency, but using rich gas from the reservoir is more economic than the exhaust gas. Longer soak times are needed when using rich or exhaust gas rather than using CO_2 alone.

In a recent study at Penn State, Abboud (2005) investigated the effect of vaporization on the recovery by cyclic injection of pure N_2 and N_2/O_2 mixtures with

laboratory PVT cell tests. A Mid-Continent light crude oil sample from the Big Andy Ridge Field, Kentucky was used. It is observed that lighter components of the crude oil were vaporized and oxygen contributed to the increase in the mobility of the oil. In another recent study, Mohammed-Singh *et al.* (2006) presented results of 16 CO_2 huff 'n' puff treatments in Trinidad and Tobago, together with a summary of published studies on CO_2 cyclic stimulation, and a screening criteria for these operations. The major conclusions they made were consistent with previous studies. They stated that viscosity reduction and swelling of oil by CO_2 are the major mechanisms for improved recovery, and the stimulation ratio of the oil rate mainly depends on the amount of gas that is injected per foot of the pay.

Dong *et al.* (2006) presented results of experimental and modeling studies of pressure cycling with methane to increase the heavy-oil recovery from thin reservoirs. The process includes injection of methane and water successively to repressure the reservoir and force the gas back into solution. Moussine *et al.* (2007) presented an improved cyclic steam injection method in which the injected gas mixture includes exhaust gases (CO_2 and nitrogen). This provides higher recovery compared to steam alone, as the energy released by the gas-steam generator is used more efficiently. Also, dissolution of exhaust gases provides additional reduction in the oil viscosity. They conducted simulation studies to determine optimum operating conditions of the process. They concluded that the optimum soaking time varies with the volume of gas injected and effectiveness of the process increases with higher oil-column thickness. In another recent study, Asghari and Torabi (2007) presented core experiments of CO_2 huff-n-puff. They observed that fractured light-oil reservoirs with high matrix permeability at immiscible and near-miscible conditions favor the process.

2.2 Intelligent Systems for Reservoir Engineering Optimization Problems

Since their introduction to the petroleum industry, intelligent systems have been applied to many different types of optimization problems. Most of these problems presented in the literature are based on development of artificial neural network

(ANN) based proxies that can accurately mimic reservoir, or other types of simulation models. Also known as *neuro-simulation*, applications of this methodology are found in field development, history matching, design optimization, and candidate well selection for hydraulic fracturing and treatments. The motivation behind this process arises from the development of a high-performance response surface that could provide desired outputs in an efficient manner in terms of the computational time.

Mohaghegh *et al.* (1996) presented a study for candidate well selection for hydraulic fracturing of gas storage wells. They developed a hybrid neuro-genetic approach, which couples ANN with a genetic algorithm (GA) to evaluate different wells for hydraulic fracturing and provide a list of candidate wells based on available data. The intelligent system also provides the optimum fracturing design for the proposed well.

Many developments have been made for the purpose of optimum field development studies. Centilmen *et al.* (1999), and Doraisamy *et al.* (2000) developed ANN proxies that output production profiles for different well placement configurations. By decreasing the computational time significantly, developed proxies are used to evaluate a large number of well placement scenarios in a very short time to select the configuration that maximizes the cumulative oil production. Gökcesu (2005) developed ANN proxies for the same purpose, and coupled them with GA to search for optimum well placement strategies to maximize the cumulative oil production. Güyagüler *et al.* (2000) and Johnson and Rogers (2001) also coupled proxies with GA to select the injector wells for a waterflooding operation to maximize the net present value (NPV).

Yeten *et al.* (2003) proposed an optimization procedure that utilizes GA with several acceleration routines that include an artificial neural network, a hill climber, and a near-well upscaling technique to optimize type, location, and trajectory of a non-conventional well. Yan and Minsker (2006) proposed an adaptive neural network genetic algorithm (ANGA) procedure for optimization of water resources problems. Zangl *et al.* (2006) used ANN and GA for a gas storage management application.

As a scheduling application, Patel *et al.* (2005) used GA to optimize scheduling of cyclic steam injection process in Bakersfield, California. While maximizing

the process efficiency, they introduced steam availability and transportation constraints for a large number of wells to come up with the optimum scheduling of cyclic steam injection operations.

Ayala and Ertekin (2005) presented a study to develop optimum production protocols for the implementation of the gas-cycling operations for pressure maintenance of gas/condensate reservoirs. They developed both a forward-looking network that mimics a compositional reservoir model, and an inverse-looking network that outputs design parameters once several performance criteria are provided.

Mohaghegh *et al.* (2006) presented a methodology to develop surrogate, full-field reservoir models. They utilized fuzzy pattern recognition to determine the key performance indicators of the reservoir model to decrease the dimensionality of the model. They validated the methodology by implementing it to a giant Middle East oil field. Cullick *et al.* (2006) and Silva *et al.* (2007) used neural networks to develop non-linear proxies that provide accurate predictions that are similar to a reservoir-simulation model. They presented history-matching applications with a reduced number of reservoir simulations. Yu *et al.* (2008) used genetic programming (GP) to develop proxies to classify reservoir models as good or bad, in terms of the history-match error to reduce the number of simulations required for history-matching.

In a recent study at Penn State, Parada (2008) developed a toolbox which includes a number of neural-network based proxies for different types of IOR processes. By using this toolbox, it is possible to screen and design miscible injection, waterflooding, and steam injection processes in different reservoirs.

2.3 Summary

Based on the studies that have been reviewed in the previous sections, we can conclude that there are significant number of studies that have been done on cyclic pressure pulsing for improved oil recovery. These studies can be grouped into three categories: 1) Experimental studies, 2) Modeling studies, 3) Field studies. Most of the studies have been done on pure CO_2 injection and there are studies that considered using rich hydrocarbon gases, and pure nitrogen, and mixtures of these gases with CO_2. Initial motivation of the cyclic injection process has

given to the use of CO_2 instead of steam to recover heavy oil with applications in Turkey, California, and Arkansas. Subsequently, its application was considered for medium and light oils, and successful field applications were reported in Kentucky, Texas, and Louisiana. The recovery mechanisms in-play can be grouped under two categories as 1) increased reservoir pressure, and 2) changes in phase behavior.

Mechanisms related to phase behavior include oil viscosity reduction, oil swelling, vaporization of lighter components, reduction of water permeability due to trapped gas and reduced water saturation, and reduction of interfacial tensions. Success of CO_2 injection applications are mainly due to viscosity reduction and oil swelling as the primary mechanisms.

In most of the studies, it was stated that the amount of injected gas has the most significant effect on the improved recovery. It was observed that soaking period is necessary for interaction of reservoir fluids with the injected gas, but soaking more than 2 weeks does not improve the recovery significantly. Soaking mainly affects the peak oil rate after the injection, and it is due to diffusion.

Reservoir characteristics and operational design parameters are two main components that influence the performance of a cyclic injection process. Although there are many studies that have been done, there is not a complete understanding of how to design these processes for the reservoir of interest to attain maximum efficiency. Considering studies that utilize intelligent systems for optimization of petroleum engineering problems, it can be suggested that presented methods can be applied to develop an understanding of how to design the process for a given reservoir with certain conditions.

Chapter 3

Problem Statement

In order to achieve success in any IOR application, significant effort must be expended to design and assess the feasibility of the IOR project. As indicated in Chapter 2, there have been both successful and unsuccessful applications of gas cyclic pressure pulsing presented in the literature. This fact points out the importance of the requirement of a careful consideration to assess the feasibility of the process in the reservoir of interest. First of all, it needs to be addressed whether the characteristics of the reservoir would favor this process. Once it is determined that the reservoir is an ideal candidate, some other decisions must be made to design the process. At that stage, the following questions should be answered:

- What should be the amount of injected gas?
- What should be the injection rate?
- How long should be the injection, soaking, and production periods?
- For a multi-cycle process, for how many cycles should the process continue?

It is the reservoir engineer's responsibility to assure that the process is designed in the most efficient way from the point of view of economics. Maximum efficiency for a given period of time can be obtained *vis-à-vis* two important goals:

1. Maximizing the income due to the produced oil
2. Minimizing the operational costs due to the injected gas

These two economic parameters can be derived from the process design parameters, and performance indicators, which are the outcomes of the process such as the cumulative oil production, peak oil rate, time to reach the peak oil rate, cycle oil production rates, gas-oil-ratio (GOR), *etc.*

Numerical reservoir simulation is an industry standard to evaluate such projects with the currently available computer power. After constructing a reservoir model, the reservoir engineer would use that model to evaluate different design scenarios, analyze the outcomes mentioned above, and make suggestions on designing the process with the highest efficiency. However, due to the heavy computational and laborious work required to make simulation runs for a number of different scenarios, it is not possible to evaluate all possible scenarios and pick the best one in confidence in a short period of time.

To overcome the heavy computational work problem, developing proxy (surrogate) models can present a potential solution. These models do not require heavy computational time and can process a huge number of scenarios within a fraction of a second. Artificial neural networks (ANN) are excellent candidates for this type of applications, because of their capabilities in mapping non-linear input/output relationships of highly sophisticated systems. Neural-network based proxies are widely used in many fields to mimic computationally-demanding simulation models. Once a reliable proxy model is developed, it can be coupled with an optimization tool to search for the best design scenario that would maximize the efficiency. Evolutionary algorithms (EA) are heuristic optimization techniques which are analogous to Darwin's evolution theory of survival of the fittest. Because of the stochastic behavior of the search process, these algorithms do not get stuck at the local minima/maxima. This makes them powerful in problems where the search space is discrete, instead of continuous, where there are many local minima/maxima that may mislead the optimization algorithm. In this study, we investigate the usefulness of these methods to develop optimized design scenarios for cyclic pressure pulsing processes, and to evaluate the effectiveness of the process for the reservoir of interest. Given this, the ultimate goals of this study are:

1. To understand the fluid flow dynamics of cyclic injection of CO_2 and N_2 into fractured reservoirs via reservoir simulation studies.

2. To develop optimized strategies in designing the process via utilization of intelligent systems.

Figure 3.1 shows a brief workflow of the process to be followed to achieve the aforementioned objectives. First, a representative reservoir model is to be constructed for the purpose of analyzing the process by conducting parametric studies. Next, a number of different design scenarios are to be generated. Then, utilizing the neuro-simulation methodology, which is explained in Section 4.1.4, two ANN proxies are to be developed: i) a forward proxy that can mimic the reservoir model for screening purposes, ii) an inverse proxy that can act as an inverse simulator and go beyond the reservoir model's capabilities for optimization purposes. The final step includes utilization of an optimization tool that uses the developed proxies to search for the best design scenario that would maximize/minimize a pre-defined objective function, which would be related to the efficiency of the process.

Figure 3.1. Workflow to be followed to achieve the objectives of this study.

Figure 3.2 shows a summary of the proxies that are developed and used for screening and optimization purposes. In the first part of the study, we are only looking at how design considerations affect the efficiency of cyclic pressure pulsing process in the reservoir of interest (upper portion of Figure 3.2). The study area is the Big Andy Field in Kentucky, where cyclic CO_2 (since 1985) and cyclic N_2 (since 1996) have been successfully utilized to improve the oil recovery. The reservoir model is constructed by using the available data from that field. In the second part of the study, the methodology is generalized to reservoirs with varying characteristics. The neural-network based proxies include reservoir characteristics, as well (lower portion of Figure 3.2).

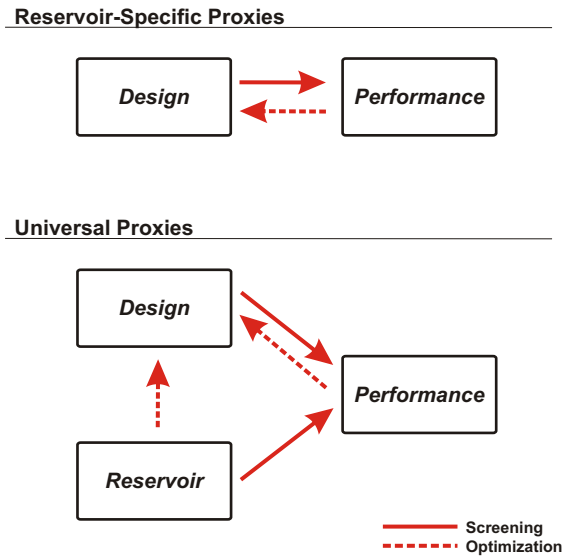

Figure 3.2. Development of ANN proxies for screening and optimization studies.

Chapter 4

Theory and Methods

In this chapter, the methods that are used in this study and the theory behind these methods are explained. First, artificial neural networks (ANN) are introduced, which are used to construct the proxy models. Backpropagation algorithm, recurrent neural networks, early stopping, and neuro-simulation methodology are presented. Next, genetic algorithms (GA) are defined and explained. The final section covers the hybrid neuro-genetic approach, which couples ANN proxies with GA for optimization.

4.1 Artificial Neural Networks

Artificial neural networks (ANN) draw much of their inspiration from the biological nervous system. It is therefore useful to have some knowledge of how these systems are organized.

Most living creatures, which have the ability to adapt to a changing environment, need a controlling unit that is able to learn. Higher developed animals and humans use very complex networks of highly specialized neurons to perform this task. The control unit (*i.e.*, the brain) can be divided in different anatomic and functional sub-units, each having certain tasks like vision, hearing, motor and sensor control. The brain is connected by nerves to the sensors and actors in the rest of the body. The human brain consists of a very large number of *neurons*, about 10^{11} on average. These can be seen as the basic building bricks for the central nervous system (CNS). The neurons are interconnected at points called *synapses*

(Haykin, 1998). The complexity of the brain is due to the massive number of highly interconnected simple units working in parallel, with an individual neuron receiving input from up to 10,000 others. The neuron contains all structures of an animal cell. The complexity of the structure and of the processes in a simple cell is enormous. Even the most sophisticated neuron models in artificial neural networks seem comparatively toy-like (Haykin, 1998).

Structurally the neuron can be divided in three major parts: the cell body (soma), the dendrites, and the axon, see Figure 4.1 for an illustration. The dendrites receive the signals from other neurons. The signals are electrical impulses, and transmitted with a chemical process. Chemical transmitters modify the incoming signal, which is similar to what weights do in artificial neural networks. The received signals are then summed up in the soma. If sufficient input is received, the cell fires (*i.e.*, transmits the signal over its axon, to other cells.). This process occurs as a result of concentrations of different types of ions such as potassium, sodium, and chloride.

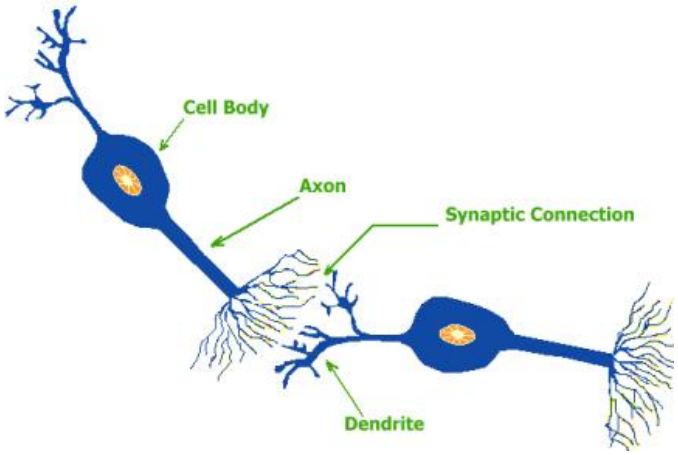

Figure 4.1. Schematic view of a bi-polar neuron, adapted from Mohaghegh (2000).

Artificial neural networks (ANN) can be broadly defined as information-processing systems, which mimic the human mind as a mathematical model representation of biological neural networks. ANN's have gained an increasing popularity in different fields of engineering during the past few decades, because of their capability to extract complex and non-linear relationships. In many ways, the mechanism of artificial neural networks have received their motivation from biological neural

networks. One of the key features is the ability of being fault tolerant, which can be explained as being able to recognize many different input signals that have not been seen before, or being tolerant to damages in the neural system (Fausett, 1994).

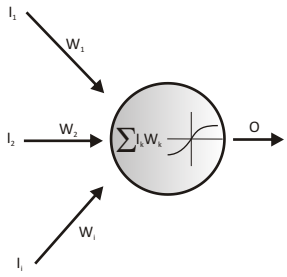

Figure 4.2. A neuron, reproduced from Mohaghegh (2000).

The simplest unit of a neural network is the neuron (processing element). Figure 4.2 shows a typical neuron. The basic information processing occurs like the following; outputs (I_n) coming from another neuron are multiplied by their corresponding weights (W_n), and summed. An activation function is then applied to the summation, and the output of that neuron is now calculated and ready to be transferred to another neuron (Mohaghegh, 2000). The internal state of a neuron after the activation function is applied, is called its *activation*. Thus, for the neuron shown in the figure, its activation, y, would be equal to $f(\sum I_k W_k)$; where $f(x)$ can be any activation function.

A neural network can be characterized by its:

1. Pattern of connections between the neurons (*i.e., its architecture*),
2. Method of determining the weights on the connection links (*i.e., its training algorithm*),
3. Activation functions.

Figure 4.3 shows a simple network with 2 inputs, 1 hidden layer of 3 neurons, and 1 output. Some common activation functions that are used include:

- Logistic (binary sigmoid) function: $f(x) = \frac{1}{1+e^{-x}}$
- Tan-sigmoid (bipolar sigmoid) function: $f(x) = \frac{2}{1+e^{-2x}} - 1$

- Hyperbolic tangent function: $f(x) = \frac{e^x - e^{-x}}{e^x + e^{-x}}$
- Linear function: $f(x) = x$

In addition to petroleum engineering and many other engineering disciplines, artificial neural networks have been used in many different kinds of applications such as signal processing, control, pattern recognition, medicine, speech recognition, speech production, and business (Fausett, 1994).

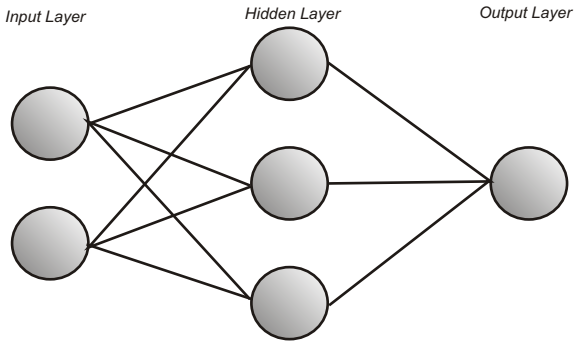

Figure 4.3. A simple network.

4.1.1 Backpropagation Algorithm

Also known as the *generalized delta rule*, backpropagation algorithm is a gradient descent method that minimizes the total squared error of the output computed by the network. It played a major role in the reemergence of neural networks in late 1980's. It was introduced as a training method of multilayer networks to overcome the limitations of single-layer networks (Fausett, 1994).

Backpropagation algorithm is a supervised training technique (*i.e.*, mapping a given set of inputs to a specified set of target outputs), and includes three stages: 1) Feed-forward of the input training pattern, 2) Calculation and back-propagation of the error, 3) Adjustment of weights. The overall goal is to train the network such that it can:

- Respond correctly to the input patterns that are used for training (memorization)
- Give reasonable responses to similar, but not identical, input patterns (generalization)

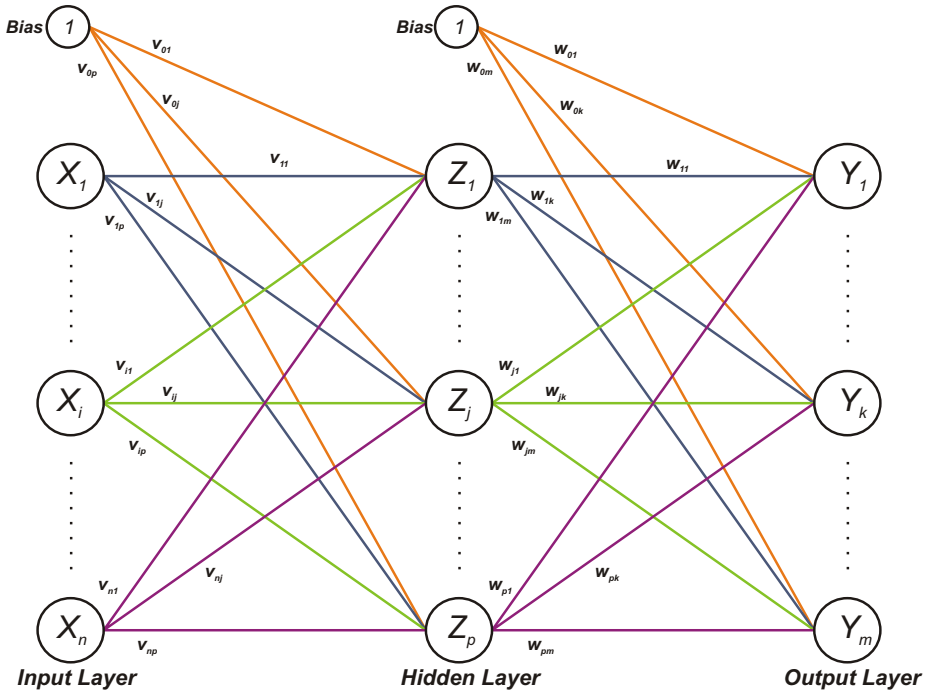

Figure 4.4. Architecture of a multilayer network, reproduced from Fausett (1994).

Figure 4.4 shows a multi-layer, fully-connected network with one hidden layer. There are n input neurons in the input layer, p hidden neurons in the hidden layer, and m output neurons in the output layer. There are biases also shown in this figure whose activation value are constant during the training (1, in this case). While the number of inputs and outputs are based on the nature of the problem studied, the number of hidden neurons is a part of the network design process and must be optimized by the designer. In Neuroshell (1998), a rule-of-thumb formula is presented to calculate the number of the hidden neurons, which is mostly based on experience:

$$N_{HN} = \frac{N_I + N_O}{2} + \sqrt{N_{TP}} \tag{4.1}$$

where N_I is the number of inputs, N_O is the number of outputs, and N_{TP} is the number of training patterns. It should be noted that this is not a theoretical formula, and this number would not necessarily be the best estimate of the number of hidden neurons. However, it can be used as a good start for the optimization process. Algorithm 1 shows a step-by-step explanation of the backpropagation

algorithm.

Algorithm 1 Backpropagation Training Algorithm

initialize weights (small random values)
while stopping condition is **false do**
  for each training pair **do**
    Feedforward stage:
    - each input unit receives signal, and broadcasts it to all units in the layer above (hidden units)
    - each hidden unit sums its weighted input signals, applies its activation function to calculate its output, and sends this signal to all units in the layer above (output layer)
    - each output unit sums its weighted input signals, and applies its activation function to calculate its output
    Error backpropagation stage:
    for both hidden units and output units **do**
      compute: *error*, and *error information* term
      compute: *weight correction* term
    end for
    Weight adjustment stage:
    update weights and biases
  end for
  test for stopping condition
end while

Let us look at each step in this algorithm. We start with initializing weights on each link randomly. It is a common practice to initialize the weights randomly between -0.5 and 0.5. Then, the network is presented with input signals for each input unit. Input units transmit these signals to the layer above, which is the hidden layer (or the 1^{st} hidden layer in a multi-hidden-layer network). Each hidden unit sums its weighted input signals:

$$z_{in,j} = v_{0j} + \sum_{i=1}^{n} x_i v_{ij} \tag{4.2}$$

Then the activation function is applied to each hidden unit:

$$z_j = f(z_{in,j}) \tag{4.3}$$

Similarly, output units receive signals from hidden units and sums its weighted

input signals:

$$y_{in,k} = w_{0k} + \sum_{j=1}^{p} z_j w_{jk} \tag{4.4}$$

Then the activation function is applied to each hidden unit:

$$y_k = f(y_{in,k}) \tag{4.5}$$

After the activations of output units are calculated, the backpropagation process starts. The error in each output is calculated by subtracting the output, y_k from the target (actual) output, t_k:

$$e_k = t_k - y_k \tag{4.6}$$

Then the *error information*, *weight correction*, and *bias correction* terms are calculated:

$$\delta_k = e_k f'(y_{in,k}) \tag{4.7}$$

$$\Delta w_{jk} = \alpha \delta_k z_j \tag{4.8}$$

$$\Delta w_{0k} = \alpha \delta_k \tag{4.9}$$

where; α is the *learning rate*. For the weight updates between hidden and output layers, each hidden unit sums the *delta inputs* from the units in the layer above:

$$\delta_{in,j} = \sum_{k=1}^{m} \delta_k w_{jk} \tag{4.10}$$

Then, the *error information*, *weight correction*, and *bias correction* terms are calculated:

$$\delta_j = \delta_{in,j} f'(z_{in,j}) \tag{4.11}$$

$$\Delta v_{ij} = \alpha \delta_j x_i \tag{4.12}$$

$$\Delta v_{0j} = \alpha \delta_j \tag{4.13}$$

Finally, the weights on links between input and hidden layers, and hidden and output layers are calculated:

$$v_{ij}(new) = v_{ij}(old) + \Delta v_{ij} \tag{4.14}$$

$$w_{jk}(new) = w_{jk}(old) + \Delta w_{jk} \tag{4.15}$$

This process is repeated for all training patterns, until a pre-specified stopping condition is achieved. Processing of each training data is known as a *training event*, or, *iteration*. When all training data are processed once, one *epoch* (training cycle) is completed. Each training data can be processed either by random selection, or by rotation. After each training event, average mean-squared error is calculated. Achieving minimum mean-squared errors of outputs and maximum number of epochs are among most common stopping conditions. The algorithm above is explained for one hidden layer networks, but it can easily be extended to multi-hidden-layer networks.

In this study, all forward-looking proxies are trained using the backpropagation algorithm. The algorithm is successfully applied to both reservoir-specific and universal proxy models that are presented in Chapters 5 and 6.

4.1.2 Recurrent Neural Networks

First introduced by Jordan (1986), recurrent neural networks were developed to learn sequential and time-varying patterns. Elman (1990) introduced a *partially recurrent* network that has all the connection being feedforward, except having a specific group units (context layer) that receives feedback signals from the previous time step. Architecture of these simple recurrent networks are illustrated in Figure 4.5. The algorithm is the same with the backpropagation algorithm explained in Algorithm 1, except using the context units. At time t, the activations of the context units are the activations (output signals) of the hidden units at the previous time step (*i.e.*, previous training pattern). The weights from the context

units to the hidden units are trained in exactly the same manner as the weights from the input units to the hidden units. At each time step, after the activations of hidden units are calculated, they are copied to the context units for use in the next training event (Fausett, 1994). A simplified version of backpropogation training with recurrent connections is explained in Algorithm 2.

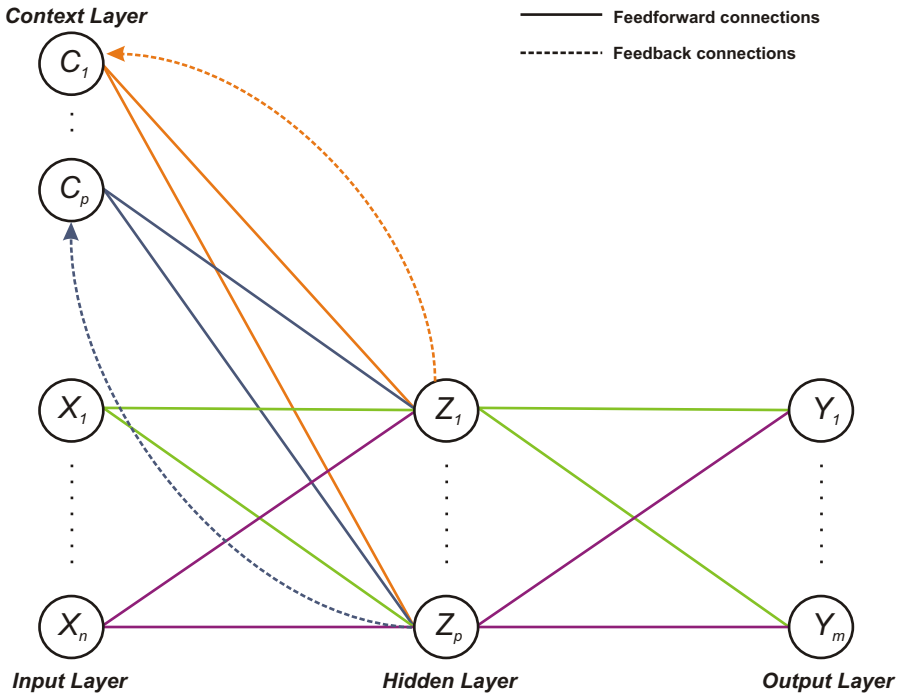

Figure 4.5. Architecture of a multilayer network with recurrent connections, reproduced from Fausett (1994).

Another popular recurrent network was introduced by Rumelhart *et al.* (1986). In this network, outputs from the network at one time step become the inputs at the next time step. These networks can be trained for several time steps by making copies of the net (with the same weights), training each copy, and then averaging the weight updates. This process is known as backpropagation in time (Fausett, 1994). Recurrent neural networks are very popular in solving time-dependent systems. In this study, they are used in the development of inverse proxies. The usefulness of this algorithm in cyclic injection process and how it is applied is explained in Section 5.5.

Algorithm 2 Backpropagation for Networks with Recurrent Connections

initialize weights (small random values)
while stopping condition is **false do**
  for each training pair **do**
    Feedforward stage:
    - each input unit receives signal, and broadcasts it to all units in the layer above (hidden units)
    - each hidden unit sums its weighted input signals, applies its activation function to calculate its output, and sends this signal to all units in the layer above (output layer)
    - each output unit sums its weighted input signals, and applies its activation function to calculate its output
    Feedback stage:
    each hidden unit copies its activation to its context unit
    Error backpropagation stage:
    for both hidden units and output units **do**
      compute: *error*, and *error information* term
      compute: *weight correction* term
    end for
    Weight adjustment stage:
    update weights and biases
  end for
  test for stopping condition
end while

4.1.3 Improving Generalization: Early Stopping

There are several methods, which are used to improve the generalization abilities of neural networks and to prevent *overtraining*. *Early stopping* is the most common one because of its easy implementation.

In this method, the available data set is divided into three. First dataset is used for *training* the network by computing the gradients and updating weights and biases. Second dataset is the *validation* dataset. During training, the network is applied to this data set, and the error is recorded. Typically, during training, the training error would continuously decrease. Validation error would also decrease as the training error. However, at some point, the validation error would start to stabilize and then, would start to increase (Figure 4.6). At this point, the network would start to overfit the data. Typically, the training should be stopped after a number of iterations from the point the validation error does not decrease

(improve). This number is to be inputted by the user.

Third data set is the *testing* data set and it is not used during training. This data set is used after the training is completed, to analyze the generalization capabilities of the network in predicting cases that it has not seen before. It is usually a good practice to plot training, validation, and testing errors continuously during training. If testing error starts to increase before the validation error increases, this would show that the data sets are not divided properly (Demuth *et al.*, 2006). In this study, all neural networks are trained with early stopping.

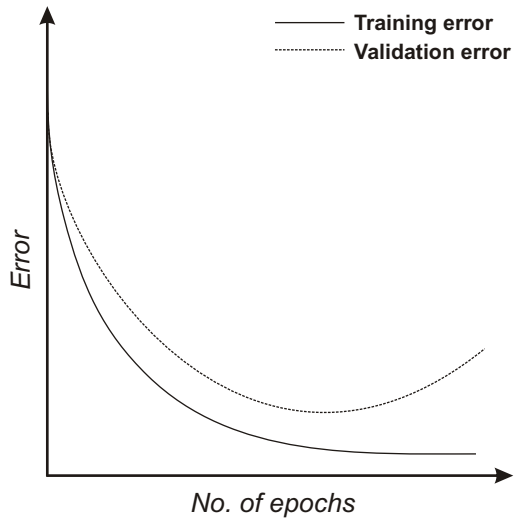

Figure 4.6. Typical behavior of training and validation errors during training.

4.1.4 Neuro-Simulation Methodology

Neuro-simulation can be defined as the process of coupling simulation models based on hard computing with artificial neural networks (ANN) to develop approximator proxies that can mimic simulation models accurately. When an approximator for a model is constructed, it is aimed to retain the size and scope of the problem, while capitalizing on the existence of simpler empirical relationships between decision variables and selected model outcomes (Johnson and Rogers, 2000). In their paper, Johnson and Rogers (2000) showed that ANN are superior to linear and non-linear regression equations, since they impose fewer constraints on the functional form of

the relationships between variables.

In the petroleum engineering literature, there are a number of studies that uses ANN's as substitutes for reservoir models. Although they can be never used to model the actual physical phenomena of reservoir fluid flow dynamics, they can be developed to map specific input/output relationships of the reservoir system. Section 2.2 includes example works that utilized this methodology for different kinds of optimization problems.

Once a reservoir model of the field/well of interest is constructed, this model can be used to run a number of different design scenarios that are created for a given problem. Outcomes of the simulation runs, *key performance indicators*, can be collected in a *knowledge base*. This knowledge base, which includes different design scenarios and corresponding performance indicators can be fed into a neural network for training. When the network is trained with an appropriate training method, it can be tested by comparing with simulator outputs to see if it can provide accurate predictions. If the network is validated and it can make predictions with a reasonable accuracy, it can be used as a proxy (surrogate) model to evaluate a number of other design scenarios. A typical flowchart of the neuro-simulation methodology for proxy construction is shown in Figure 4.7.

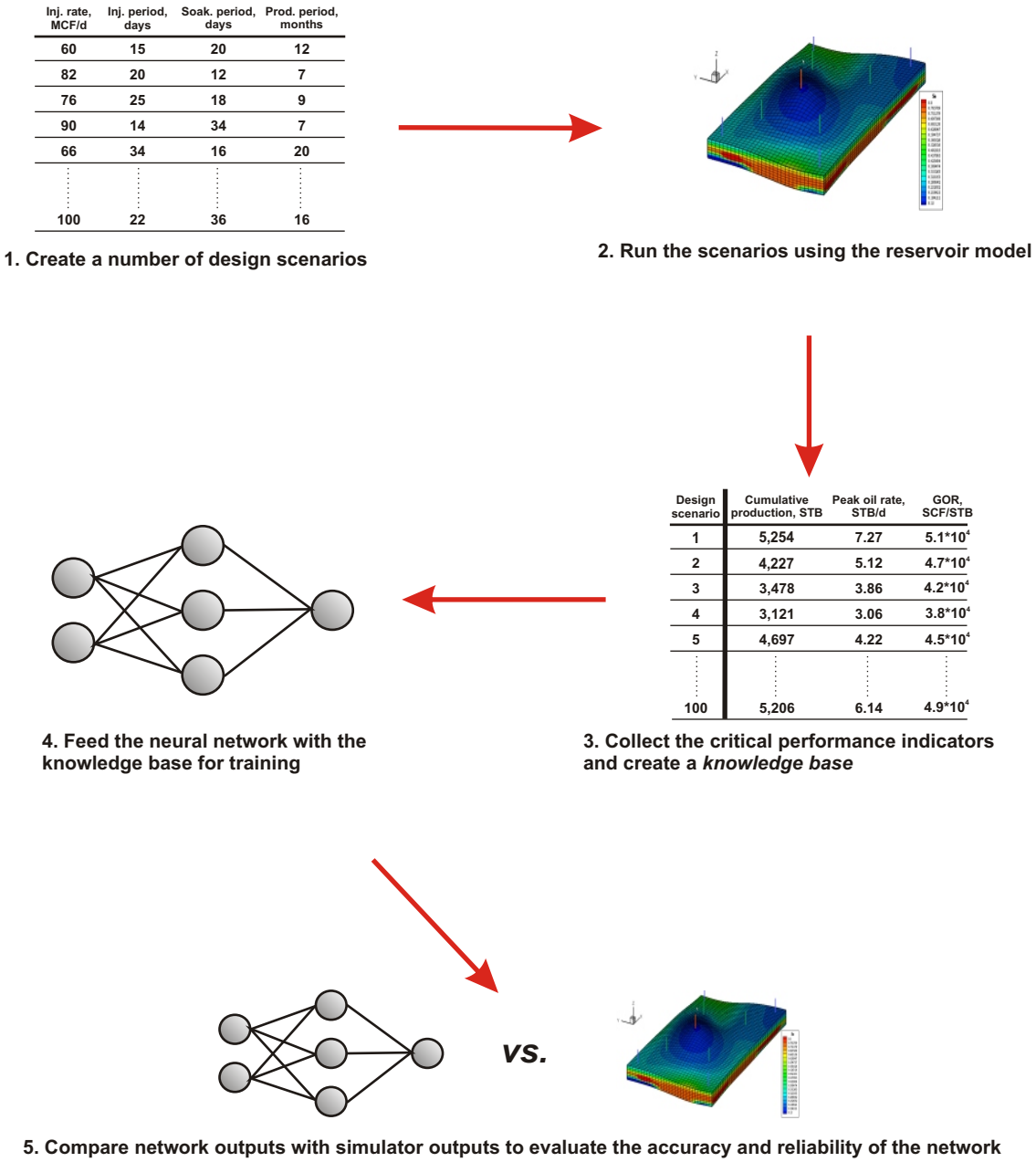

Figure 4.7. Flowchart of the neuro-simulation methodology for proxy construction.

4.2 Genetic Algorithms

There has been a growing interest in problem solving systems, which are based on evolution and hereditary. Such systems maintain a population of potential solutions, which have selection processes that are based on fitness of individuals, and *genetic* operators that are analogous to Darwin's evolution theory. These evolution-based systems are known as evolution programs (EP), and have a structure like the one shown in Algorithm 3 (Michalewicz, 1994).

Algorithm 3 Evolution Programs

```
t ← 0
initialize P(t)
evaluate P(t)
while stopping condition is false do
  t ← t + 1
  select P(t) from P(t − 1)
  alter P(t)
end while
```

Evolution programs are probabilistic algorithms, which maintain a population of individuals, $P(t) = \{x_1^t, ..., x_n^t\}$, at iteration t. Each individual is a potential solution to the problem in hand. These individuals are represented in a data structure form, S. Each solution, x_i^t, is evaluated to give a measure of its *fitness*. Then, a new population, for iteration $t + 1$, is formed by selecting more fit individuals (selection). Some members of the new population may undergo transformations (alteration) via genetic operators to form new individuals (solutions). There are *mutation* type transformations, which create new individuals by a small change in a single individual ($m_i : S \rightarrow S$). There are also higher-order crossover type transformations, which create new individuals by combining parts from two or more individuals ($c_j : S \times S... \times S \rightarrow S$). After a number of generations, the algorithm converges to a near-optimum solution (Michalewicz, 1994).

The genetic algorithm (GA) is the most commonly used evolution program for both constrained and non-constrained optimization problems. While classical derivative-based optimization algorithms generate a single-point at each iteration, GAs generate a population of points at each iteration. This makes them a powerful tool in solving complex optimization problems with discontinuous search spaces

and having many local extrema. Derivative-based, gradient-following algorithms become insufficient in finding the global optimum of such kind of problems, where the objective function is discontinuous, non-differentiable, stochastic, or highly non-linear (Matlab, 2006).

Potential solutions in GA's are represented in the form of strings. The lengths of the strings depend on the range of the parameters (minimum and maximum) and also the precision with which the solutions are sought within this range. Binary strings with an alphabet size of two (0 and 1) are common, however any alphabet size may be employed. Some of the GA vocabulary is shown in Table 4.1, which would be make it easier to understand the terminology used in the explanation of GA's.

Table 4.1. The GA vocabulary (Güyagüler, 2002).

GA vocabulary	Engineering vocabulary
environment	objective function evaluator
population	set of solution vectors
chromosome, string	string encoded solution vector
gene	an element of the encoded string
fitness	function value
individual	data structure
generation	iteration
reproduce	carry on to the next iteration

Implementation of the algorithm starts with creating an initial random population. Population size is a parameter that must be defined. At any iteration step, the population is modified simultaneously, to generate a better population. This enables the algorithm to search different areas of the parameter space simultaneously. The individuals from this population are selected according to their fitness. Fitness is basically the objective function that is to be maximized/minimized. Individuals with higher fitness have higher chances to reproduce. The selection process can be done in different ways. However, most common techniques are stochastic tournament and roulette (Goldberg and Deb, 1991):

Stochastic tournament - This implementation is suited to distributed applications. Every time an individual is to be selected for reproduction, two of

them are chosen randomly, and the best one wins with some fixed probability, typically 0.8. This scheme can be enhanced by using more individuals on the competition.

Roulette - The individuals of each generation are selected for survival into the next generation according to a probability value that is proportional to the ratio of the individual fitness over total population fitness. This means that, on average the next generation will receive copies of an individual in proportion to the importance of its fitness value.

Elitism is a commonly-used extension to the selection process, which makes the best individual of the older generation be copied to the next generation without alteration. In this way, good solutions are not lost during the selection process.

The selected individuals are modified with two genetic operators: *crossover* and *mutation*. Crossover is a recombination operator. There are different ways of combining two individuals, but the most common one is the single-point cross over. Two individuals are selected and their strings are crossed over from a randomly selected crossing point. For example, if **01100101** and 10111001 were to be crossed over from 5^{th} gene, the offsprings would look like 10111**101** and **01100**001. Crossover is carried out with the probability, p_c, which is usually closer to 1. Mutation is the other operator, which reverses a gene within a string. When using binary strings, mutated gene would become 0 if it was 1, or vice versa. Mutation is done by the mutation probability, p_m, which is usually set at a very low value (closer to 0). Selection and crossover are processes by which individuals with good performance are selected and their building blocks are recombined. By this way, more and more copies of good schemata are created. Mutation is used to bring back some important bit values (genes) that may be lost during the selection process. Algorithm 4 shows a simplified explanation of the genetic algorithm as a modification of the evolution programs algorithm.

Algorithm 4 Genetic Algorithm

```
t ← 0
initialize P(t)
evaluate P(t)
while stopping condition is false do
  t ← t + 1
  evaluate P(t − 1)
  if elitism is on then
    copy x_best^{t−1} to P(t)
  end if
  select P(t) from P(t − 1)
  crossover selected individuals
  mutate selected individuals
  generate the next generation P(t + 1)
end while
return the best individual
```

4.3 The Hybrid Neuro-Genetic Approach

In this study, a *hybrid neuro-genetic approach* is used for optimizing the design of cyclic gas injection processes in a computationally-efficient manner. The hybrid neuro-genetic approach includes constructing proxy approximators with ANN, and using these approximators to calculate the objective function in GA. Coupling ANN with GA has been successfully applied in different kinds of petroleum engineering applications (Mohaghegh *et al.*, 1996; Güyagüler *et al.*, 2000; Johnson and Rogers, 2001; Yeten *et al.*, 2003; Zangl *et al.*, 2006). Johnson and Rogers (2000) showed that the ANN can be used as an accurate approximator when they are used for objective function evaluation. As a fast evaluator, this also makes it easier and faster to optimize the GA parameters. They also showed that the optimal solution is insensitive to different compositions of training samples that are used for network training. Figure 4.8 shows the optimization process. A number of potential solutions, represented by strings are fed into the neural-network proxy. Each solution is evaluated based on the proxy output. Next generation of solutions are created via genetic operators. This method is successfully applied to optimize the design of the cyclic pressure pulsing process using the developed proxies. Optimization studies using the neuro-genetic approach are presented in Chapter 8.

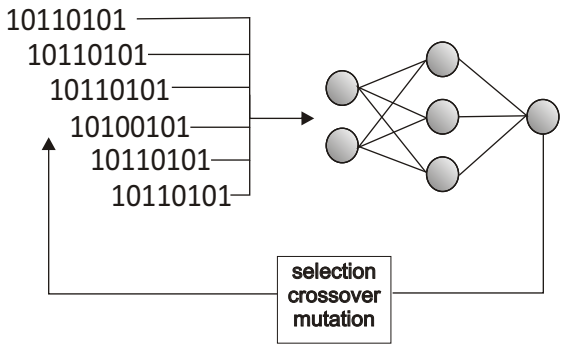

Figure 4.8. The hybrid neuro-genetic approach for high-performance optimization.

Chapter 5

Development of Reservoir-Specific Proxies

In this chapter, the design and development of reservoir-specific proxy models for the cyclic pressure pulsing process are explained. First, an overview of the study area (Big Andy Field) is given, and the constructed single-well reservoir model is described. Then, the development of neural network structures, problems that were faced with, and how they were overcome during the development stage are presented. Definitions of the parameters are followed by the development of neural network architectures for forward and inverse problems. The prediction results are presented for pure N_2 and CO_2 injections with the relevant discussions. At the end of the chapter, a case study is presented, and main conclusions are summarized.

5.1 Study Area: The Big Andy Field, Kentucky

5.1.1 Background Information

The Big Sinking Field is located in Eastern Kentucky lying on the Western flank of the Appalachian Basin. Production started during the early 1900's, and the underlying reservoir is pressure depleted with a remaining pressure of about 50 psig. Having an average water saturation of 50%, the field has an average permeability of 19 md, and average porosity of 13%. Produced oil is Mid-Continent crude oil of 36° API gravity (Abboud, 2005). The composition of the sampled reservoir oil

from laboratary analysis is shown in Table 5.1.

Table 5.1. Composition of the oil sample taken from Well-19P (Abboud, 2005).

Component	Mole, %	Component	Mole, %
C_1	0.17	C_6	5.85
C_2	1.11	C_7	21.80
C_3	5.48	C_8	11.20
iC_4	1.22	C_9	8.87
nC_4	8.37	C_{10+}	20.96
iC_5	3.69	N_2	0.06
nC_5	11.22	CO_2	0.00

Most of the wells had been drilled in the early 1980's with a total of around 800 wells (Miller and Hamilton-Smith, 1998). The Big Sinking Field produces from three zones of the Silurian age, encountered at depths ranging from 800 ft to 1,200 ft. These three zones are known as the Corniferous 1^{st} pay, 2^{nd} pay, and 3^{rd} pay, which corresponds respectively to Upper and Lower Lockport and Keefer.

The Big Andy Field is an extension of the Big Sinking Field and is the current area of interest for production. It is a shallow (1,300 ft), naturally-fractured reservoir with a formation thickness of 40 ft. The stripper oil well production at the Big Andy Field is currently from the 3^{rd} pay zone: Keefer sandstone. The formation characteristics are listed in Table 5.2.

Table 5.2. Characteristics of the Big Sinking Field (Miller and Hamilton-Smith, 1998).

Depth, ft	1,300
Thickness, ft	40
Drainage area, acres	8
Porosity	0.13
Permeability, md	19
Water saturation	0.50
Pressure, psi	50
Produced gas-oil ratio (GOR), SCF/STB	1,500
Produced water-oil ratio (WOR), STB/STB	8
Temperature, °F	68
Oil gravity, °API	36

There is considered to be significant reservoir heterogeneity as a result of fracturing along near-vertical small-displacement faults. Figure 5.1 shows the structural map of depth to the top of Corniferous formation with the wells in the field.

5.1.2 Utilization of Cyclic Pressure Pulsing and Production History

Because of depletion, the field was waterflooded during the early 1980s. Waterflooding was ineffective due to presence of a fractured matrix. During 1985, cyclic gas injection testing was initiated using CO_2. With the start of continuous cyclic injection during 1989, 390 treatments were utilized on 240 wells until 1994 (Miller *et al.*, 1994). A total of 12,200 tons of liquid CO_2 was injected, resulting in 180,000 STB of incremental recovery, and 1.2 MSCF/STB of efficiency (Miller and Hamilton-Smith, 1998). It was observed that efficiency of treatments decreased with time, and less initial response was observed with larger volumes of CO_2. Figure 5.2 shows the production history of the Big Sinking Field during cyclic CO_2 utilization.

As a result of declining cyclic efficiency, and both increasing costs and shortage of CO_2 in the area, the CO_2 program was terminated during 1994. An investigation was made to improve the process with alternative gases. 1900 BTU casing head rich gas and 80% N_2 and 20% CO_2 were tested. Both alternatives showed improved responses after CO_2 utilization (Miller and Hamilton-Smith, 1998). In 1996 N_2 was introduced as the primary injection gas for the process. A nitrogen membrane unit was installed in the field to generate nitrogen on site at a cost much less than that for other gases. Nitrogen is selected because it has several advantages besides its cost. It is a user-friendly gas since it is inert, non-corrosive, and environmentally friendly (Miller and Gaudin, 2000). Since the reservoir pressure was as low as 50 psi because of depletion at that time, it was possible to inject N_2 at very low pressures (around 150 psig). Since it does not dissolve in the oil at low pressures as CO_2 would do, it can move further back into the reservoir, and can penetrate easier into the rock matrix (Miller and Gaudin, 2000).

Initial tests were undertaken by injecting 5% O_2 and 95% N_2 at 350 MSCF/d.

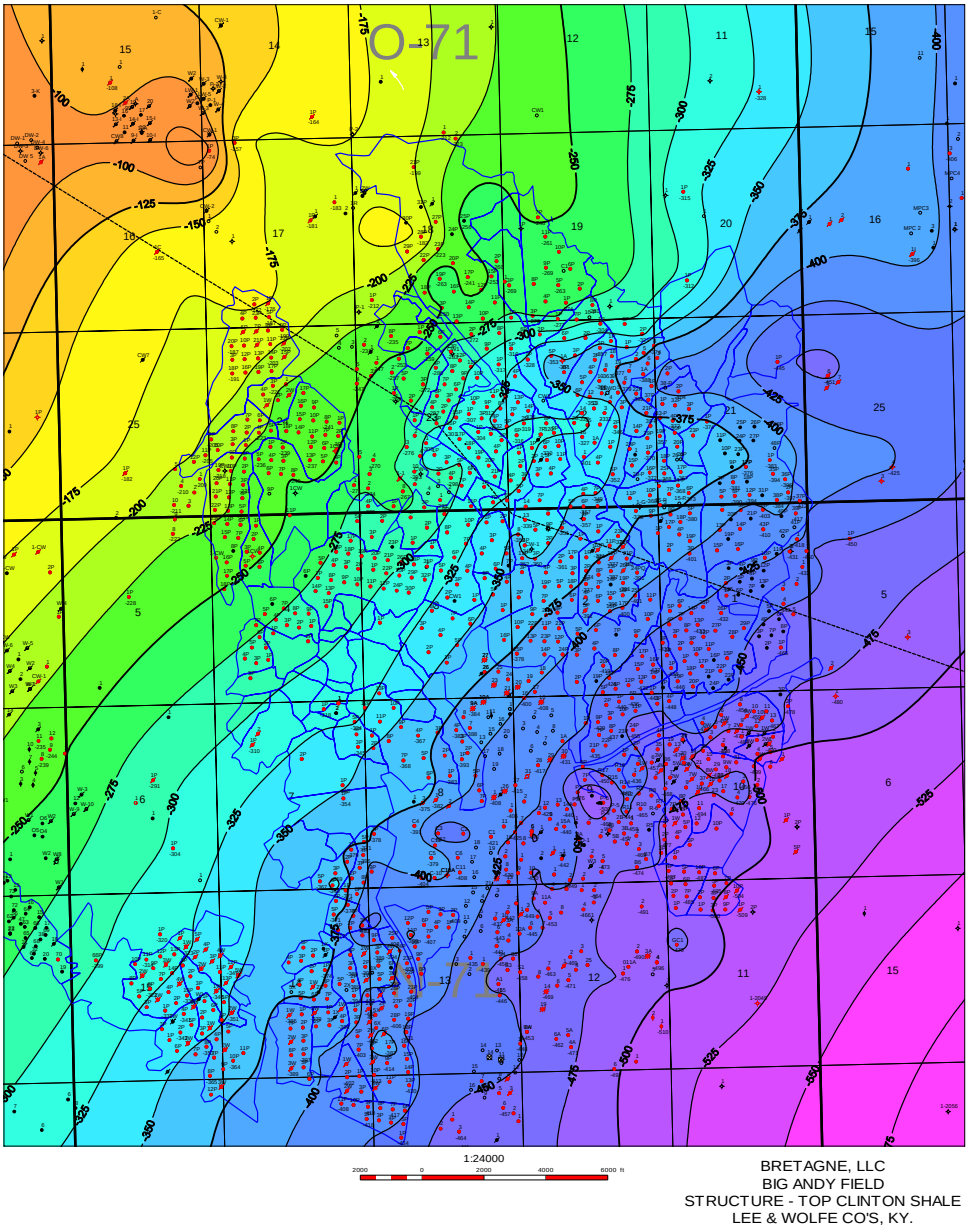

Figure 5.1. Structural depth-to-top map of the Corniferous formation, Big Andy Field (courtesy of Bretagne, LLC).

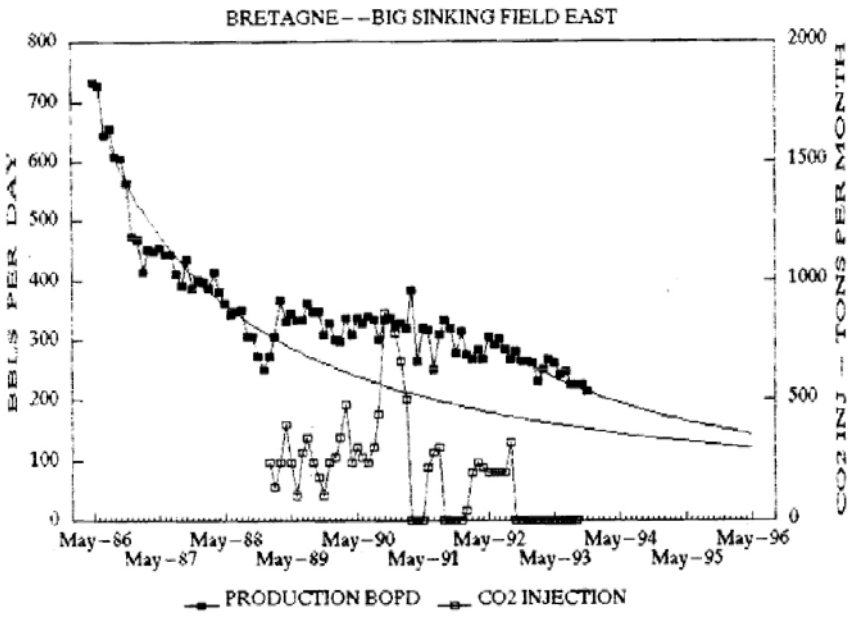

Figure 5.2. Production response during the cyclic CO_2 utilization in the Big Sinking Field, adapted from Miller *et al.* (1994).

After gaining experience, the injection volume was increased to 750 MSCF/d to expand the treatment. Nitrogen is injected down the annulus of producing wells with an injection rate of 20 to 100 MSCF/d per well depending on the stage of injection (Miller and Gaudin, 2000).

The process has been continuing since 1996. Currently, an average of 12,000 MSCF per lease area is provided by the membrane unit, and the current operating pressure is around 300 psig. Each well can take around 100 MSCF of gas, and the treatments continue until all wells are equalized with supply, or until a 30-day injection period is completed. After the injection, the wells are shut-in for soaking for a period of around 30 days (Abboud, 2005). Optimum treatment schemes are to be determined with this study. Figure 5.3 shows the cumulative production/injection history of N_2 utilization in the Big Andy Field. The plot of efficiency ratio (injection/increase in production) changing with time is shown on Figure 5.4.

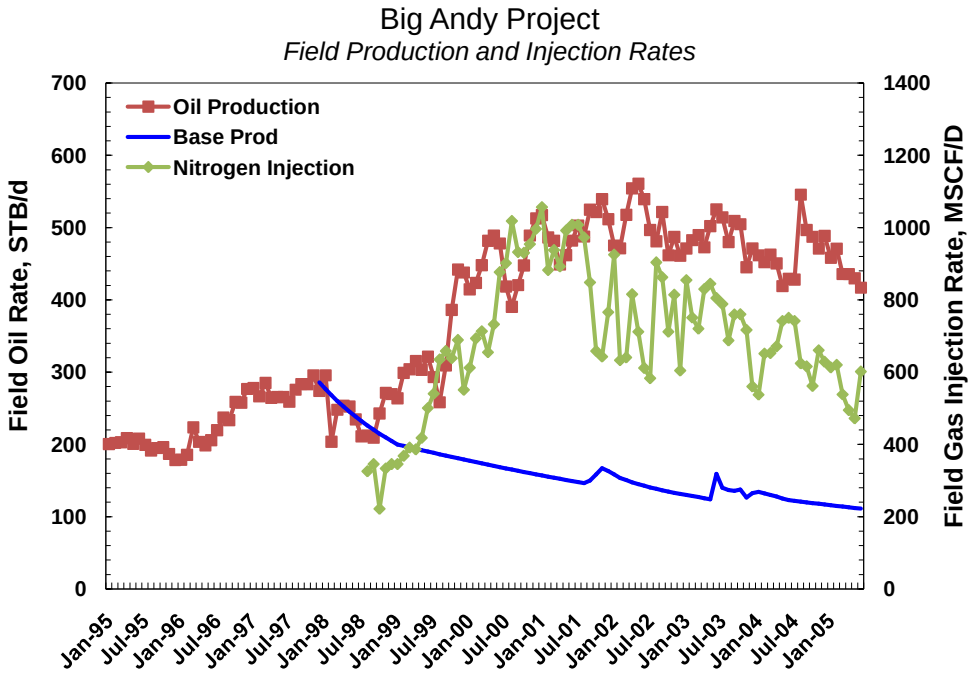

Figure 5.3. Production/injection history of cyclic N_2 utilization in the Big Andy Field, Kentucky (courtesy of Bretagne, LLC).

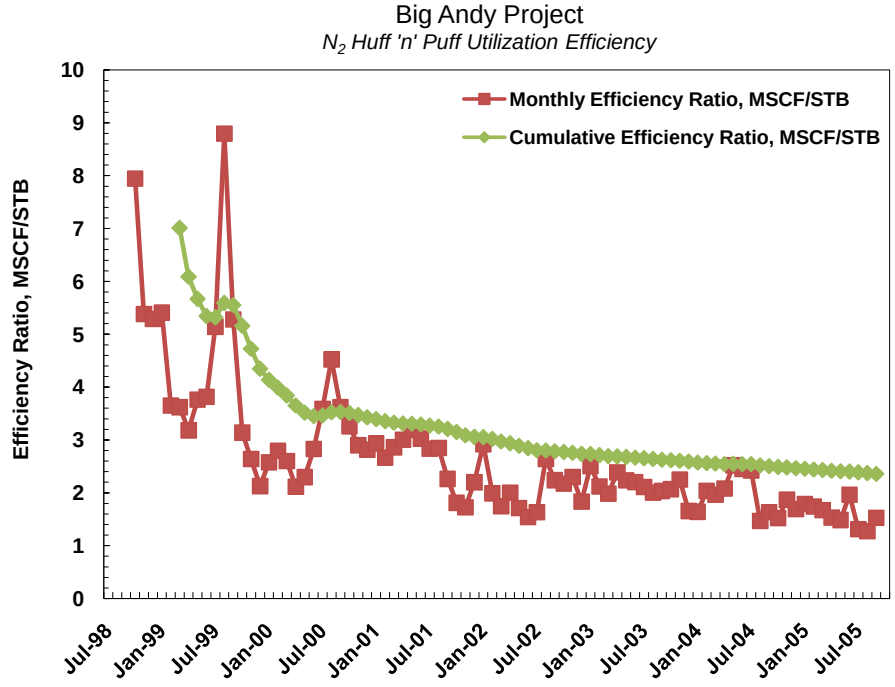

Figure 5.4. Efficiency ratio history of cyclic N_2 utilization in the Big Andy Field, Kentucky (courtesy of Bretagne, LLC).

5.1.3 Available Field Data

A set of available field data from the Big Andy Field have been compiled to construct a reservoir model for the field. The data include production histories, logs, core and fluid sample analyses for wells, leases, and the field. Table 5.3 shows a summary of the data.

Table 5.3. Available field data from the Big Andy Field.

Type of Data	Explanation
Field Data	
Production	Cumulative production and injection history for the field
Lease Data	
Reserves	Cumulative oil production and current reserves for 65 leases
Production	Production and injection history for 32 leases
Well Data	
Cores	Core analyses (porosity, permeability) from two wells
Fluid samples	Fluid hydrocarbon analyses including PVT and viscosity from 3 wells
Logs	Log evaluations (bulk density, thickness, water saturation, oil-in-place) for approximately 300 wells, GR, NP, DP, resistivity logs for one well. A seperate net pay and gross pay thickness information from 377 wells.

5.2 Reservoir Model

A single-well, compositional, dual-porosity reservoir model is constructed using a commercial simulator: CMG's Advanced Compositional Reservoir Simulator (GEM^{TM}). Reservoir characteristics are from the Big Andy Field. The grid system is 9×9 cartesian system, with each block representing 65 ft×65 ft square. This corresponds to 8 acres of drainage area, which is also a characteristic of the well spacing in the Big Andy Field. The reservoir characteristics are shown in Table 5.4.

Table 5.4. Characteristics of the single-well reservoir model.

Depth, ft	1,300
Thickness, ft	40
Drainage area, acres	8
Porosity (matrix)	0.13
Porosity (fracture)	0.01
Permeability, md (matrix)	19, 19, 1 (x, y, z)
Permeability, md (fracture)	100, 100, 1 (x, y, z)
Fracture spacing, ft	10, 10, 10 (x, y, z)
Water saturation	0.50
Pressure, psi	20
Temperature, °F	68

Some initial tests have been done on the model to understand the process. A test case was run at 100 MSCF/d by injecting nitrogen for 53 days, and soaking the system for 30 days. Figure 5.5 shows the nitrogen mole fraction in the fractures, during injection and soaking periods.

In this model, gas-phase diffusion is taken into account, which is the most important factor during the soaking. The effect of soaking is analyzed by varying soaking time while keeping other parameters constant. Figure 5.6 shows this analysis, where the peak oil rate and incremental oil production are plotted with varying soaking times for a cumulative treatment amount of 10,561 MCF. Results for both CO_2 and N_2 are shown. These figures show that peak rate and cumulative production of oil increases with soaking time up to a point after which they start to decline. This is due to the dissipation of pressure with time as also stated by Shelton and Morris (1973). These plots also show that it is possible to have a higher peak rate with N_2 compared to CO_2. On the other hand, higher incremental oil production is achieved with CO_2.

In another analysis, phase behavior effects during the soaking were studied. Phase envelopes in Figure 5.7 also indicate high solubility of CO_2 compared to N_2. After CO_2 injection, the pressure at the well block increased to 151.9 psia, while with N_2, a significantly higher pressure, 430.6 psia, was achieved. Changes in the oil saturation and liquid volume % with soaking time were analyzed with different amounts of gas injected (150 MSCF/d, 225 MSCF/d, and 300 MSCF/d). It was

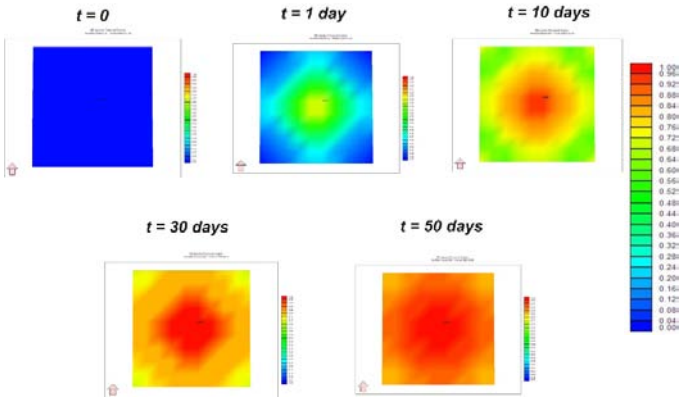

(a) Injection

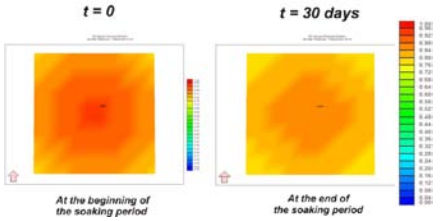

(b) Soaking

Figure 5.5. Nitrogen mole fraction in the fracture system during injection (100 MSCF/d) and soaking.

observed that in the case of CO_2 injection, the liquid volume % and oil saturation around the wellbore increases as the gas amount increases during soaking due to high dissolution of CO_2 in oil (Figure 5.8). This explains the higher amount of incremental oil recovery with CO_2 as compared to that of N_2. These observations show that mechanisms related to phase behavior are very important for the increase in oil production in the case of CO_2 injection. On the other hand, in the case of N_2 injection, the increase in the reservoir pressure is the major mechanism for improved oil recovery.

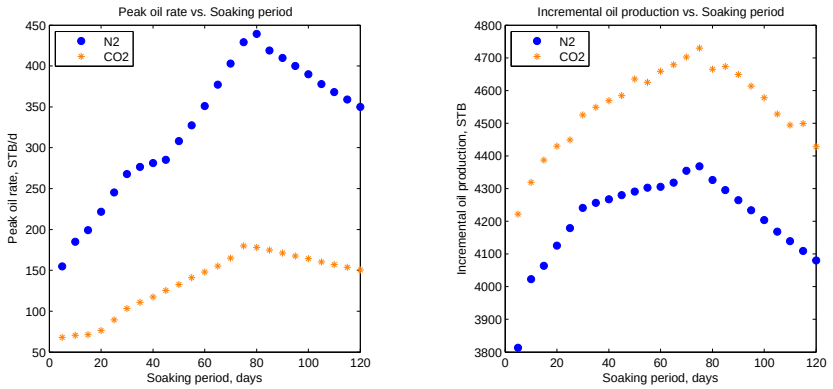

(a) Peak oil rate (b) Incremental oil production

Figure 5.6. Effect of soaking period on the peak oil rate and incremental oil production after a treatment amount of 10,561 MSCF.

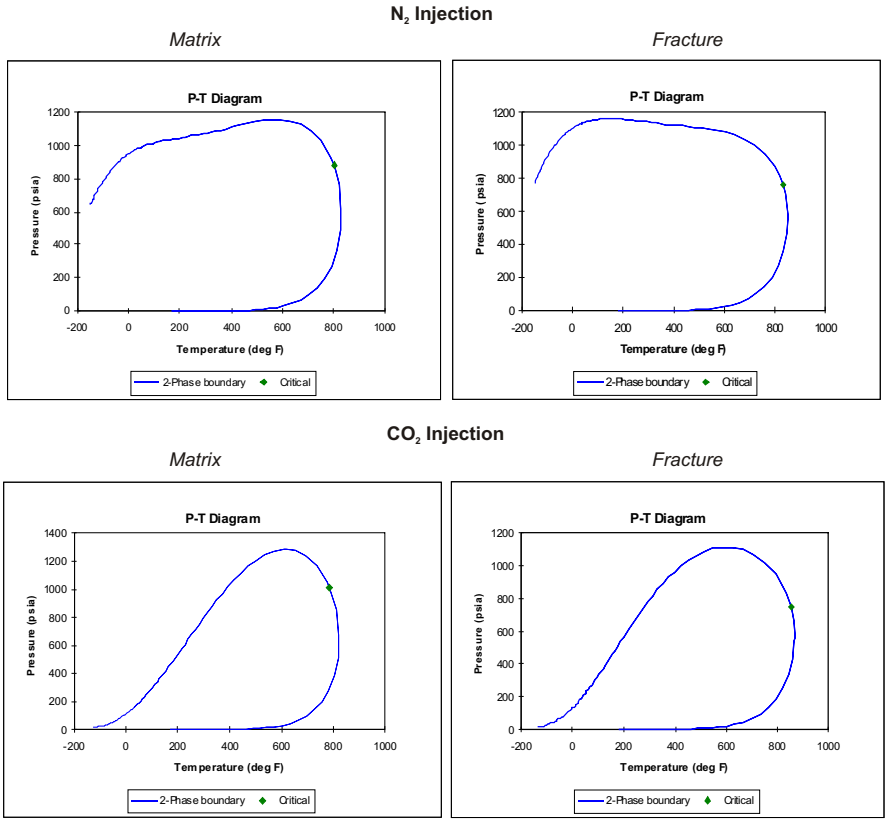

Figure 5.7. Phase envelopes of the mixtures around the wellbore in the matrix and fractures after the injection of N_2 and CO_2.

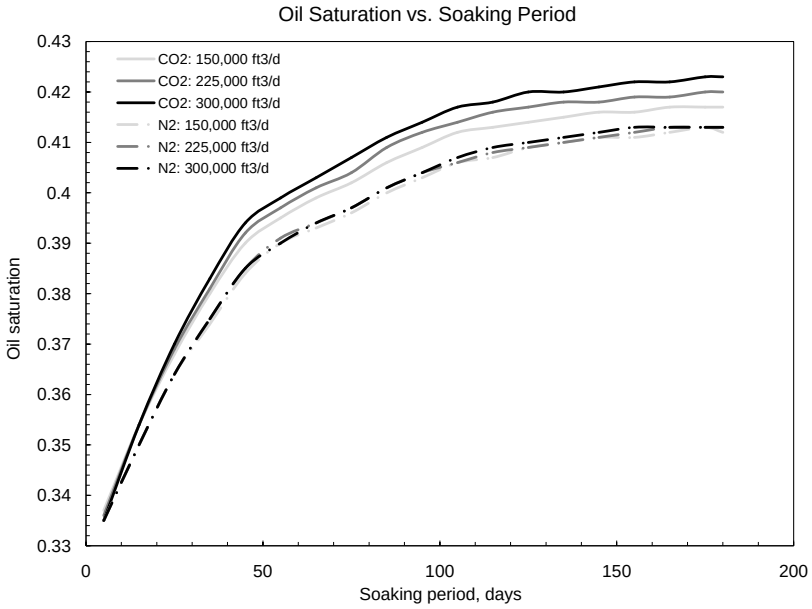

(a) Oil saturation

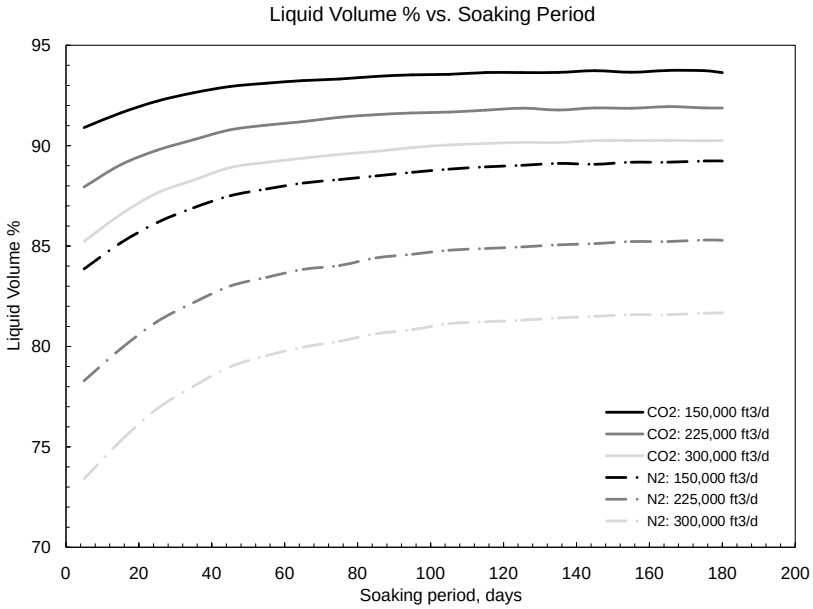

(b) Liquid volume %

Figure 5.8. Effect of soaking period on the oil saturation and liquid mole % around the well bore.

5.3 Data Preparation and Design Schemes for Cyclic Pressure Pulsing

The first step that needs to be taken in constructing proxy approximators is to define the variables that the proxy is going to use and the ranges of these variables. In this case, we would like the proxy to be an accurate approximator of the relationships between the *design parameters* and the *performance indicators* of the cyclic pressure pulsing process. In Chapter 3, some of these parameters are mentioned. In this section, we go through these variables in detail.

In modeling the multi-cycle cyclic pressure pulsing process, two design schemes are considered:

Design Scheme-1: Fixed-number-of-cycles scheme with variable injection volumes

Design Scheme-2: Variable-number-of-cycles scheme with constant injection volumes

The approach to the process design is different in these schemes from the modeling perspective. If the number of cycles to be modeled is known, each individual cycle can be controlled separately. On the other hand, if the number of cycles is controlled by other system characteristics, then it would not be possible to specify cycle design parameters separately. Since both design approaches are applicable in the field, both are studied to cover a wider range of applications. Figure 5.9 shows an illustration of these schemes with the expected input/output structures.

5.3.1 Design Scheme-1

In this design scheme, we are using a fixed number of cycles (5), so the number of cycles is not used as a design parameter. Also, we are using pure N_2 and pure CO_2 injections, so the composition of the injected gas is not included as a design parameter. Considering these, the list of the process variables are shown in Table 5.5.

Although the design parameters are clear, some of the performance indicators must be defined at this point. Figure 5.10 show a typical oil flow rate change

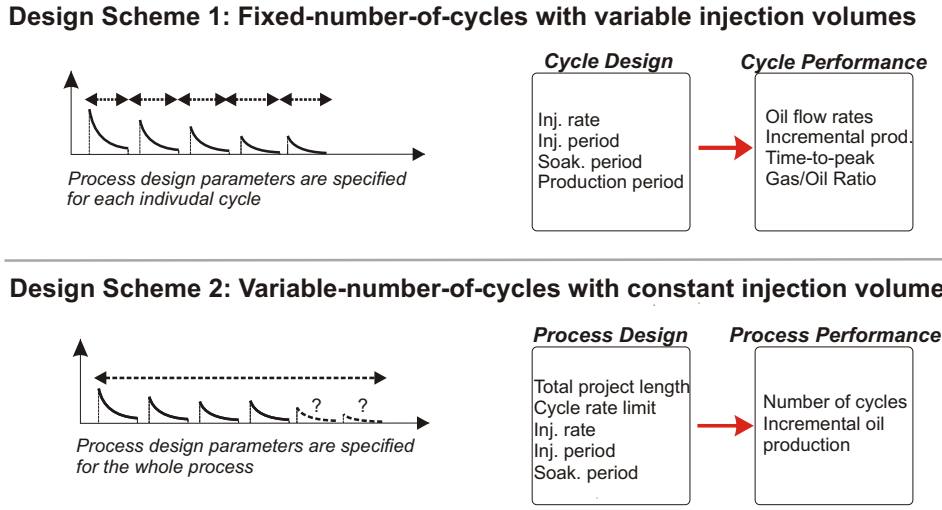

Figure 5.9. Design schemes of the cyclic pressure pulsing process.

Table 5.5. Process variables of the Design Scheme-1.

Design Parameters	Performance Indicators
Injection rate	Cumulative and incremental oil productions
Length of the injection period	Oil rates
Length of the soaking period	Peak oil rate (and stimulation ratio)
Length of the production period	Time to reach the peak rate
	Gas-oil-ratio (GOR)
	Gas rates

with time during a cycle of injection process. The oil rate immediately before the injection starts is defined as, q_{o0}. Then the injection starts, and the well is soaked for a period of time. Typically, the oil rate starts to rise after the well is put on production. It reaches a peak rate after a period called, time-to-peak, t_p, which may be as short as 1 day or longer depending on the reservoir characteristics. With the reservoir model of the Big Andy Field, it was observed that it may take from a week to 2 months for the oil rate to reach the peak. Thus, it was decided to consider this parameter as a performance indicator as well. The peak oil rate is defined as q_{o1}. After the peak, the oil production starts to decline like a typical oil well. The oil rate at the end of the cycle is q_{o2}. Since the well starts producing gas at the beginning of the cycle, the gas rate peaks as soon as the well is put

on production. Then, it also declines during the production. Gas rates at the beginning of the cycle, and at the end of the cycle are defined as q_{g1}, and q_{g2}, respectively. We are interested in predicting oil flow rates in a cycle to know the expected decline behavior of the well's oil production. As it is seen on the right hand side of Figure 5.10, we set our goal of predicting nine flow rates during the cycle, which are divided equally in terms of time.

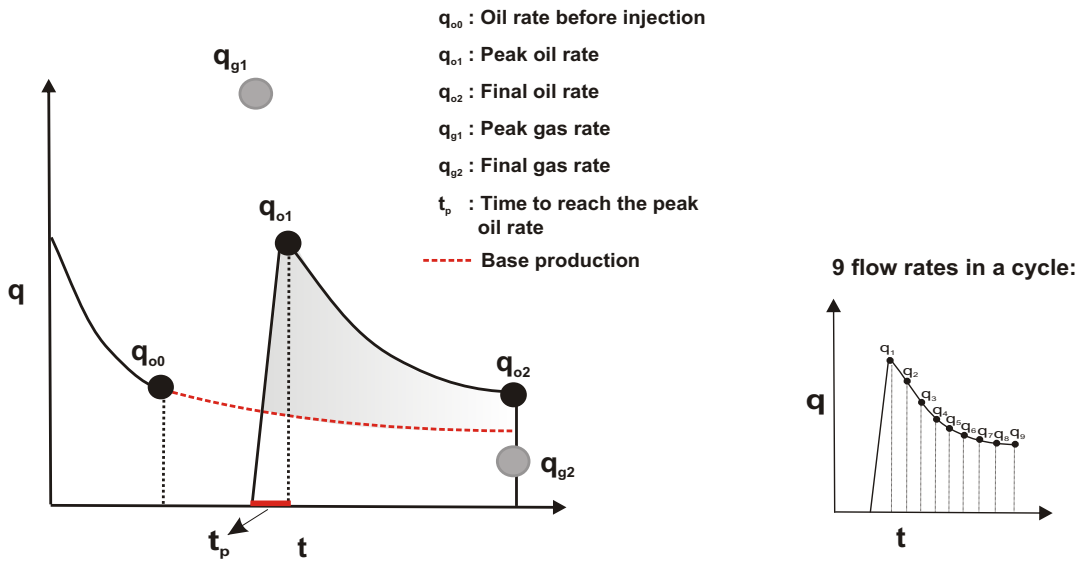

Figure 5.10. Illustrative definitions of performance indicators.

The *incremental oil production* (Pratz, 1982) is defined as the additional oil produced above the base cumulative production that would have been achieved without the IOR process. Thus, in Figure 5.10 the shaded area represents the incremental oil production. It is a more representative value for the well performance since it also considers the time period for injection and soaking where the production time is lost.

Stimulation ratio is defined as the ratio of the peak oil rate to the oil rate before injection and represents how much the well is stimulated from its last condition:

$$SR = \frac{q_{o1}}{q_{o0}} \tag{5.1}$$

After defining these variables, the next step is to define the ranges in which we want the proxies to be accurate approximators. Based on the operations at the

Big Andy Field, we determined the ranges of the design parameters for which we can create our knowledge base. Table 5.6 shows these ranges:

Table 5.6. Ranges of design parameters used in the Design Scheme-1.

Design Parameter	Minimum	Maximum
Injection rate, MSCF/d	50	100
Injection period, days	7	40
Soaking period, days	7	40
Production period, months	6	25
Amount of gas injected, MSCF	350	4,000

A dataset is created with uniformly-distributed, randomly-selected values of these variables. A total of 500 cases is generated for five cycles of injection of pure CO_2 and pure N_2. These cases were run using the model developed with a commercial reservoir simulator: CMG's Advanced Compositional Reservoir Simulator (GEM^{TM}). The outputs of these runs were collected based on the aforementioned performance characteristics. With the collection of these data, a knowledge base is created that is to be fed into the neural network for training and to construct the proxies.

Some analyses were made to identify some characteristics of the cyclic injection process and develop an understanding of the process. First a 2-layer (input/output) network is developed with no hidden layer. This network is trained using the hyperbolic-tangent transfer function. Weight matrix of this network is plotted as a Hinton Diagram (Figure 5.11). In this diagram, each value is represented by a rectangle whose size is associated with the magnitude, and whose color indicates the sign (green(+), red(-)). This diagram would show us the influence of each design parameter on performance indicators. As it can be seen in this plot, injected gas amount, injection period, and production period have the most influence. Production period has the most influence on late flow rates, as expected. Longer production periods provide lower flow rates at the end of the cycle. It is also observed that soaking period is not as significant as the other parameters.

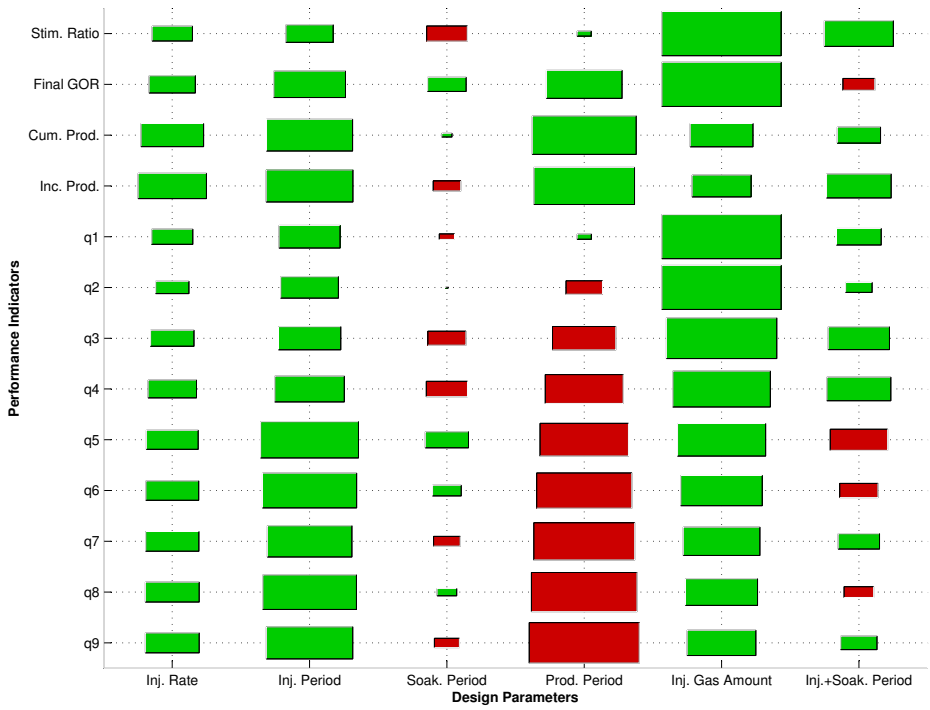

Figure 5.11. Hinton Diagram for the weight matrix between design parameters and performance indicators.

5.3.2 Design Scheme-2

In this design scheme, instead of using a fixed number of cycles, the project length and the economic oil production rate limit are specified. In this way, we let the system utilize as many cycles as possible within the specified time period. Therefore, the number of cycles becomes an outcome of the process as a function of the specified process design parameters. Since the number of cycles is going to be different in each design scenario, the cumulative oil production of the whole process is the only performance indicator. The overall list of the process variables are shown in Table 5.7. Based on the operations at the Big Andy Field, the ranges of the design parameters for this design scheme are determined as shown in Table 5.8. The rate limit is specified between 0.1-1.0 STB/d due to the stripper-production behavior of the field with abandonment rates in the range of 0.3-0.5 STB/d.

Table 5.7. Process variables of the Design Scheme-2.

Design Parameters	Performance Indicators
Injection rate	Incremental oil production
Length of the injection period	Number of cycles
Length of the soaking period	
Economic limit for the oil production rate	

Table 5.8. Ranges of design parameters used in the Design Scheme-2.

Design Parameter	Minimum	Maximum
Injection rate, MSCF/d	50	100
Injection period, days	7	40
Soaking period, days	7	40
Economic limit for the oil rate, STB/d	0.1	1.0
Total project length, years	1	10

5.4 Forward Problem

The *forward problem* includes developing a neural-network based proxy, which can accurately mimic the reservoir model. As shown in Figure 3.2, the developed proxy should provide accurate predictions of performance indicators using given design parameters. In this way, instead of running the numerical model and waiting for the results, the developed proxy can provide accurate predictions of the specific performance criteria in a computationally-efficient manner.

5.4.1 Design Scheme-1

The structure of the proxy of this scheme is shown in Figure 5.12. As can be seen, we have 4 design parameters and 16 performance indicators. In a neural network, where we include five injection cycles, we would have 20 design parameters and 80 performance indicators. The network that was developed for this part of the study had that structure with a single hidden layer of 50 neurons. Tan-sigmoid function was used for activation in the hidden layer, and a linear function is used in the output layer. Among 500 cases, 350 were used for training, 100 used for validation, and 50 were used for testing. The network architecture is shown in Figure 5.13.

Predictions of performance indicators for pure N_2 and pure CO_2 injection using this network are presented next.

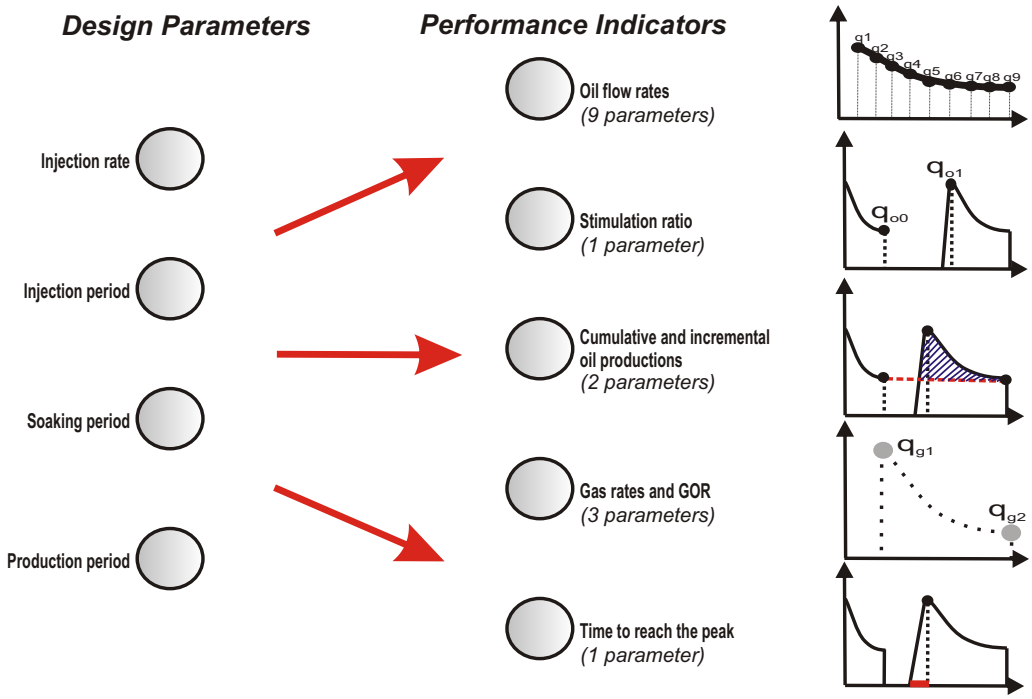

Figure 5.12. Structure of the forward proxy with fixed-number-of-cycles: Mapping from design parameters to performance indicators.

5.4.1.1 Pure N_2 Injection Predictions

Figure 5.14 and Figure 5.15 are the cross-plots for the performance predictions for parameters: time-to-peak, GOR, gas rates, stimulation ratio, cumulative and incremental oil productions. Figure 5.16 shows the oil rates during the cycle (q_1,...,q_9). Figure 5.17 and Figure 5.18 are other representations of the flow rate predictions: comparison with the actual production decline behavior of five cycles in each case. These plots clearly show that the network was able to accurately predict the production performance of the well during five cycles of injection. The correlation coefficients are also included on top of each plot, each represents a high level of accuracy with values between 0.96 and 1.00.

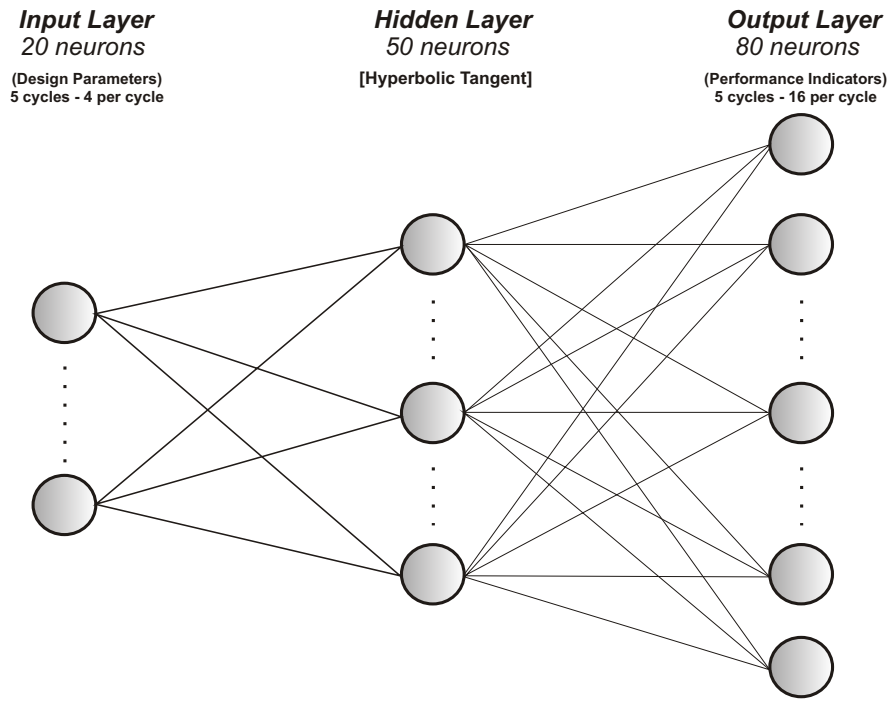

Figure 5.13. Network architecture for the forward problem with fixed-number-of-cycles.

5.4.1.2 Pure CO_2 Injection Predictions

Similar plots with the N_2 injection case are presented in this section. Figure 5.19 and Figure 5.20 are the cross-plots for the performance predictions for parameters: time-to-peak, GOR, gas rates, stimulation ratio, cumulative and incremental oil productions. Figure 5.21 shows the oil rates during the cycle (q_1,...,q_9). Figure 5.22 and Figure 5.23 are comparisons with the actual production behavior of five cycles in each case. Predictions are in the same range of accuracy with the N_2 injection case. The network was able to accurately predict the production performance of the well during five cycles of CO_2 injection. The correlation coefficients are also included on top of each plot, each represents high accuracy with values between 0.98 and 1.00.

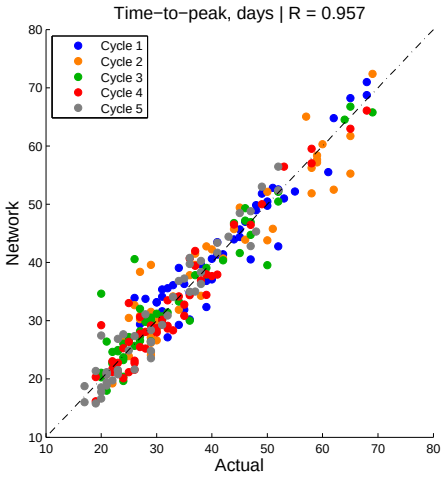

(a) Time-to-peak

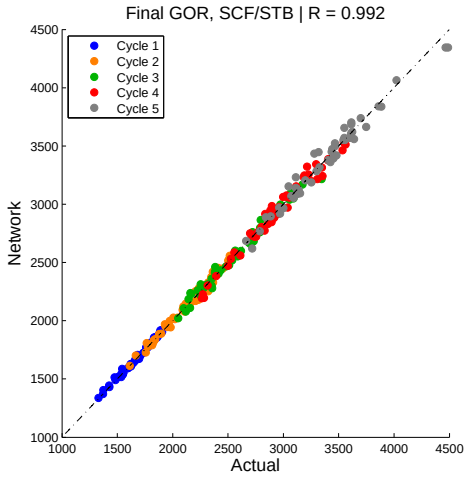

(b) Final gas-oil-ratio (GOR)

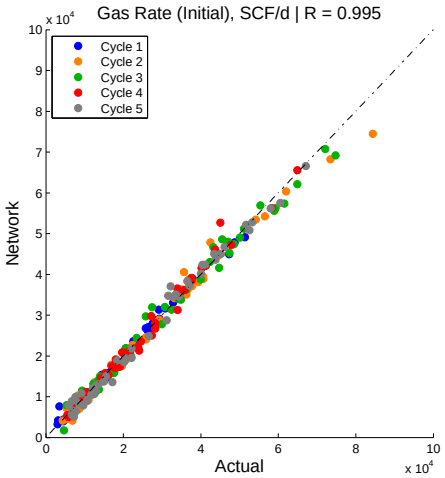

(c) Initial gas rate

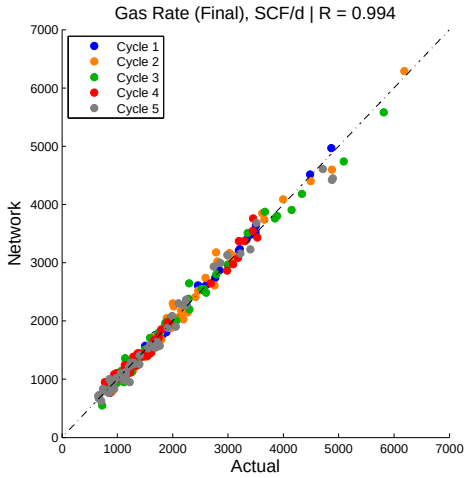

(d) Final gas rate

Figure 5.14. Pure N_2 injection: performance predictions.

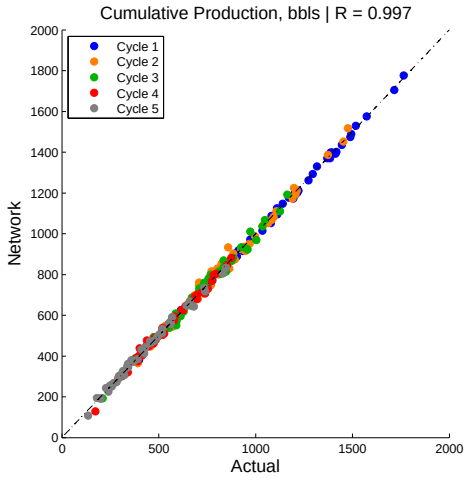

(a) Cumulative oil production

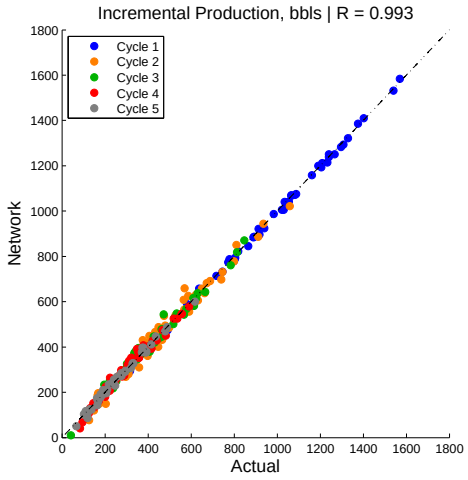

(b) Incremental oil production

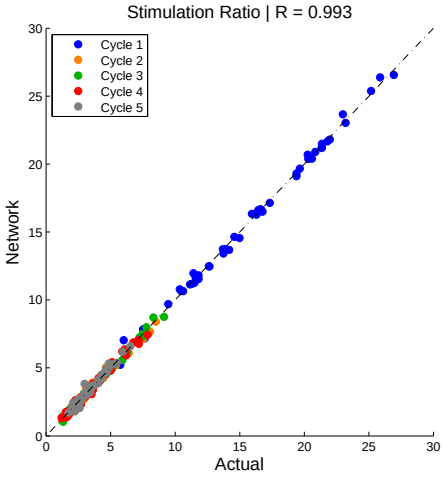

(c) Stimulation ratio

Figure 5.15. Pure N_2 injection: performance predictions (cont'd).

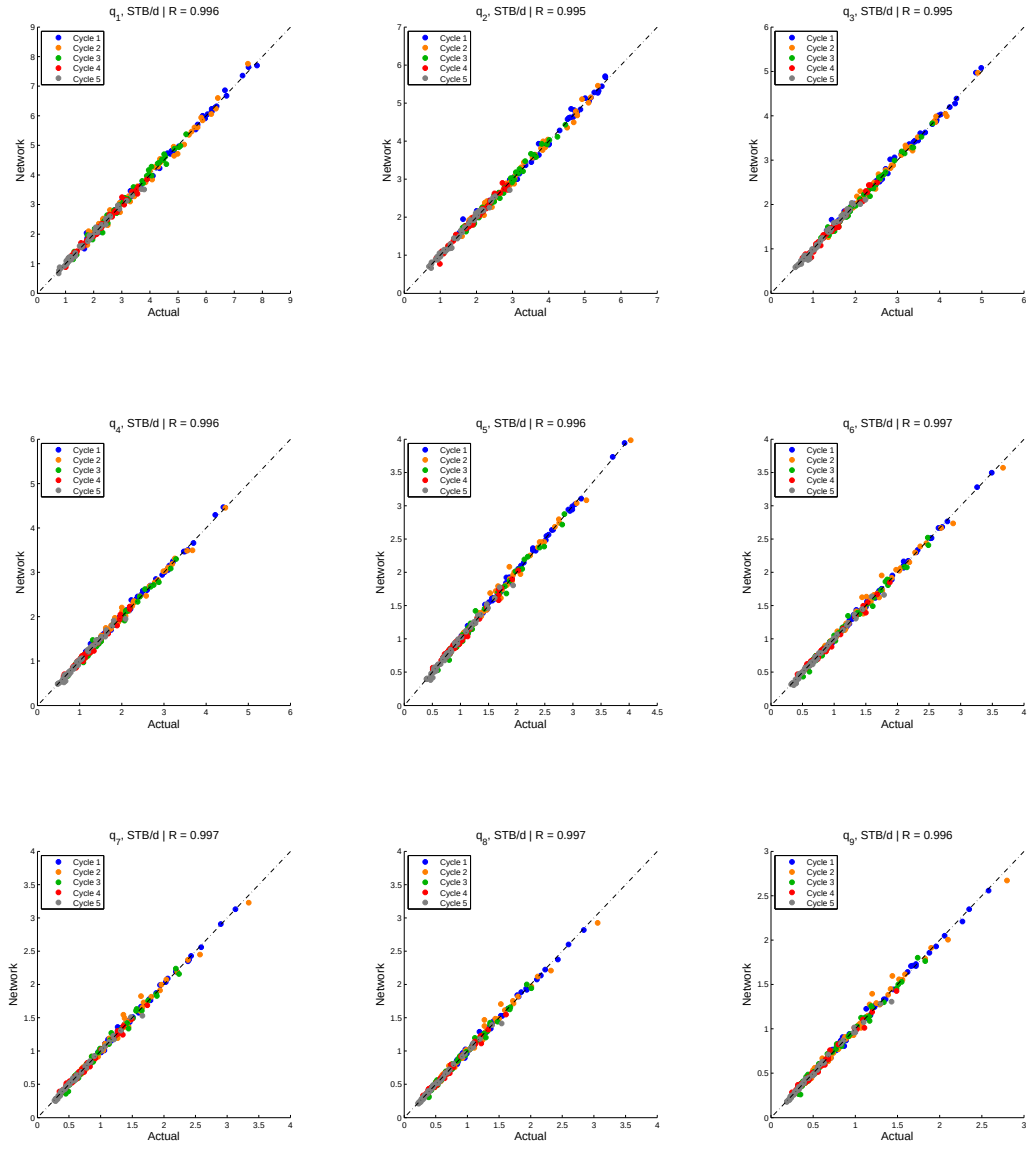

Figure 5.16. Pure N_2 injection: flow rate (q_1,...,q_9) predictions.

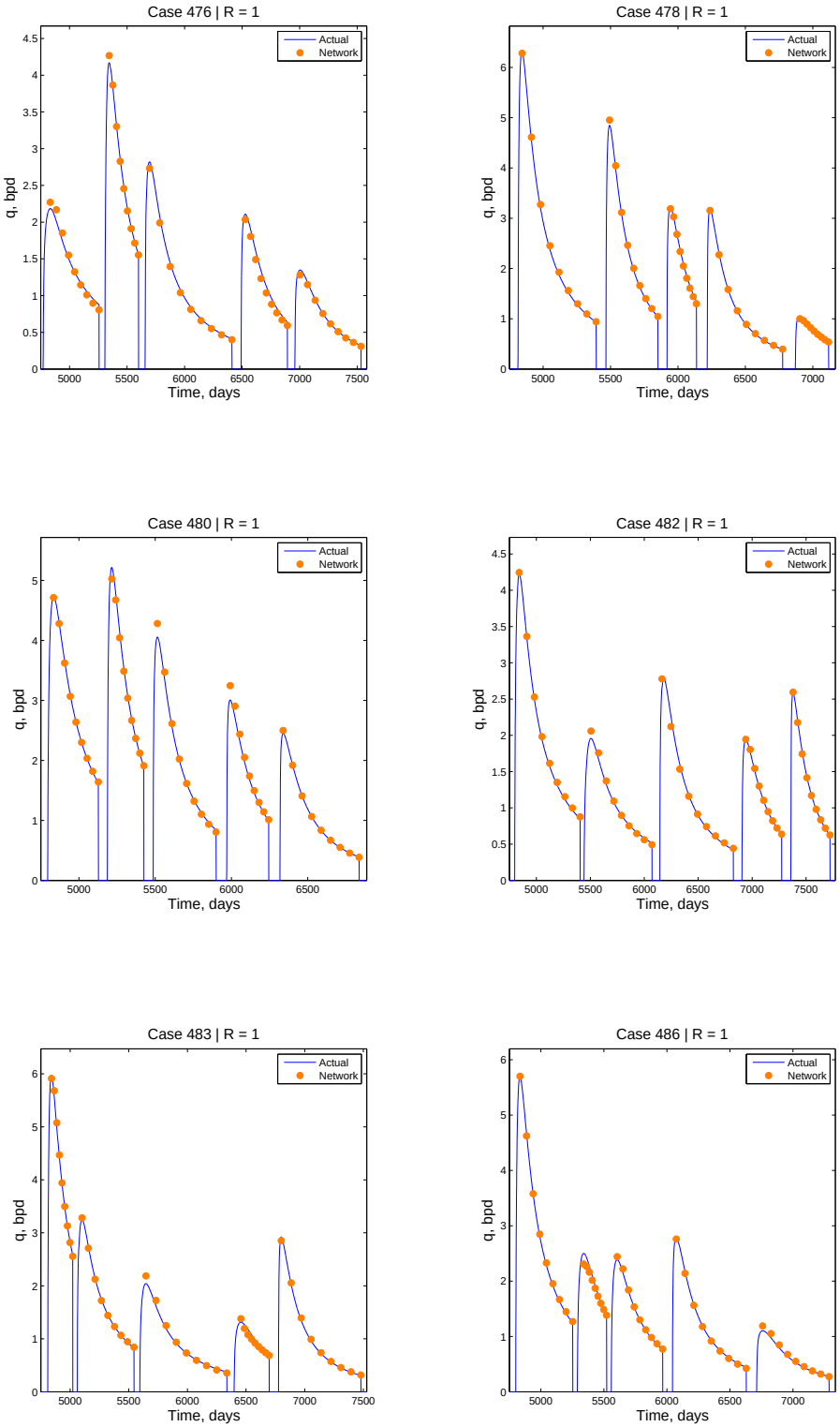

Figure 5.17. Pure N_2 injection: flow rate predictions - comparison with the actual production curves.

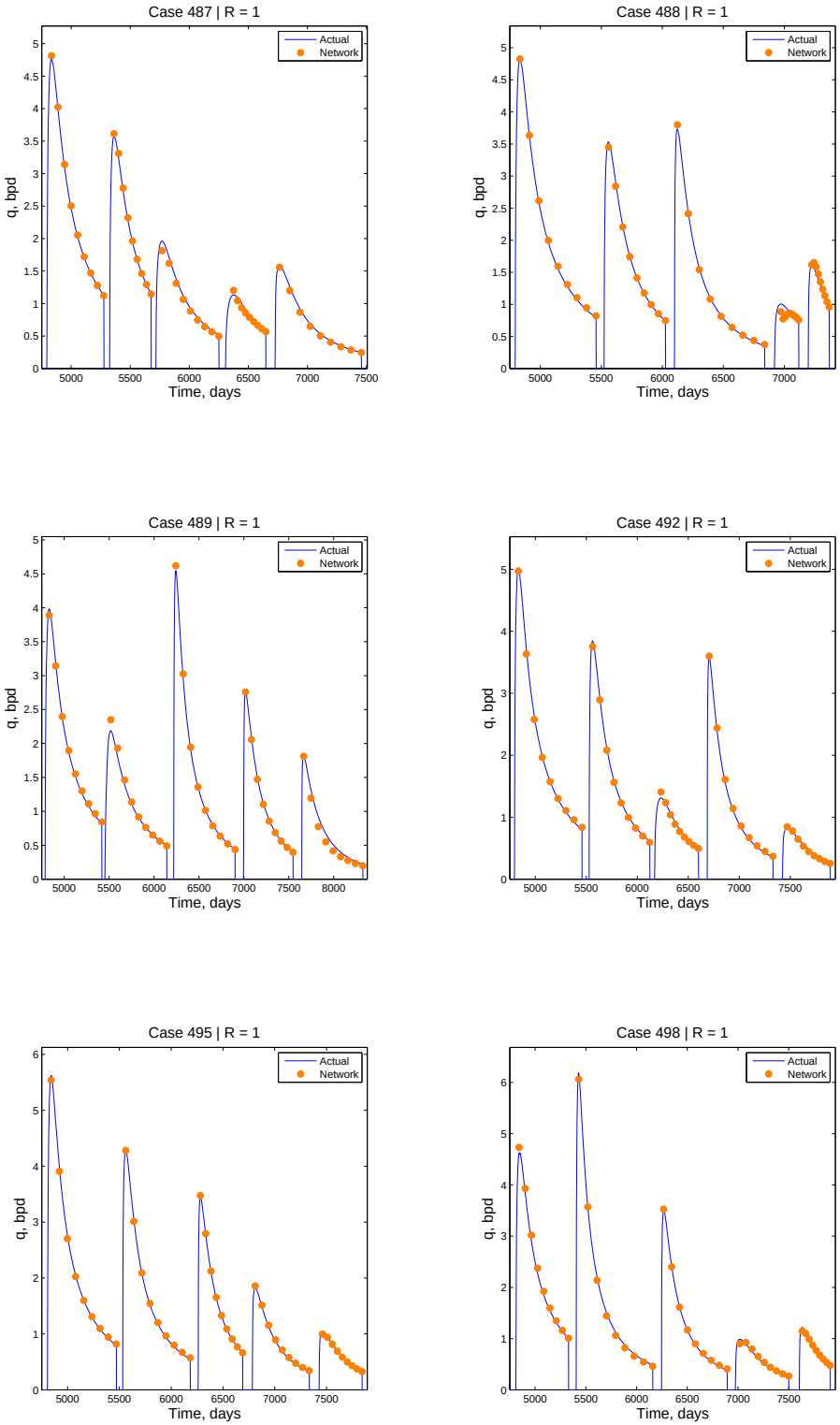

Figure 5.18. Pure N_2 injection: flow rate predictions - comparison with the actual production curves (cont'd).

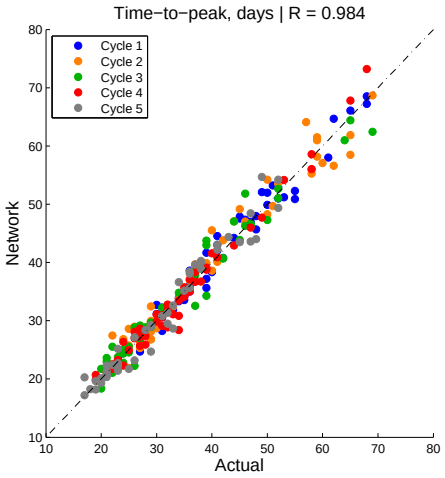

(a) Time-to-peak

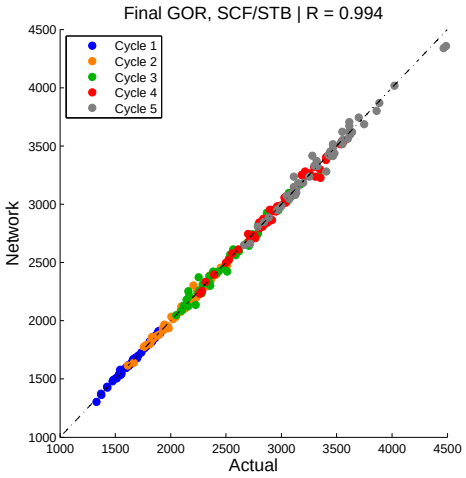

(b) Final gas-oil-ratio (GOR)

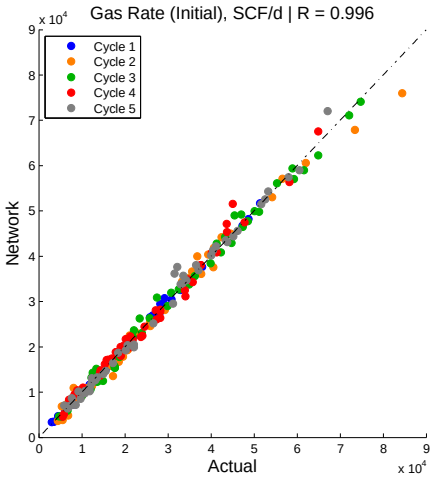

(c) Initial gas rate

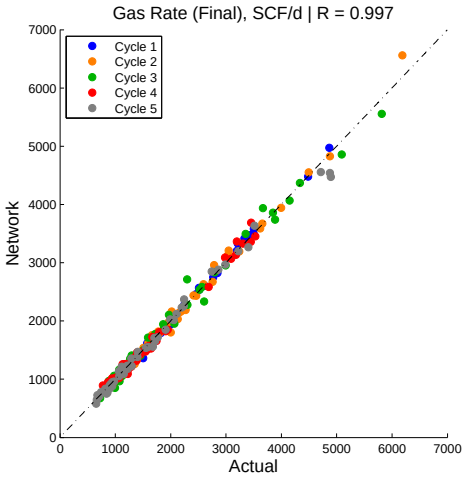

(d) Final gas rate

Figure 5.19. Pure CO_2 injection: performance predictions.

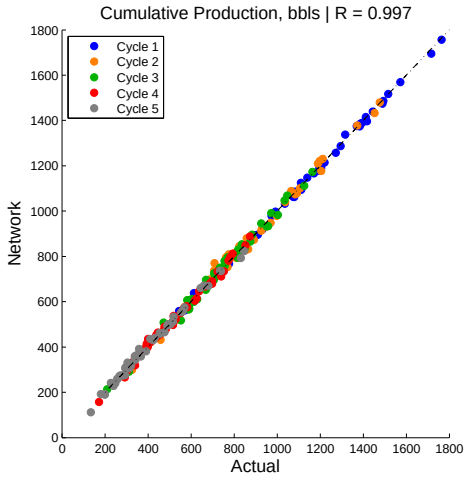

(a) Cumulative oil production

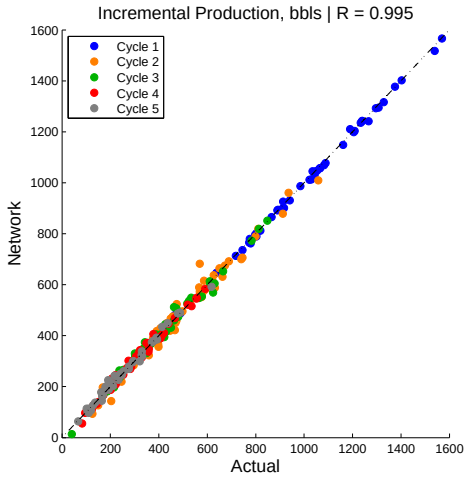

(b) Incremental oil production

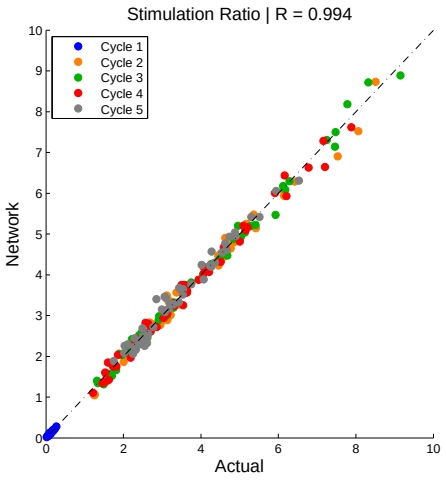

(c) Stimulation ratio

Figure 5.20. Pure CO_2 injection: performance predictions (cont'd).

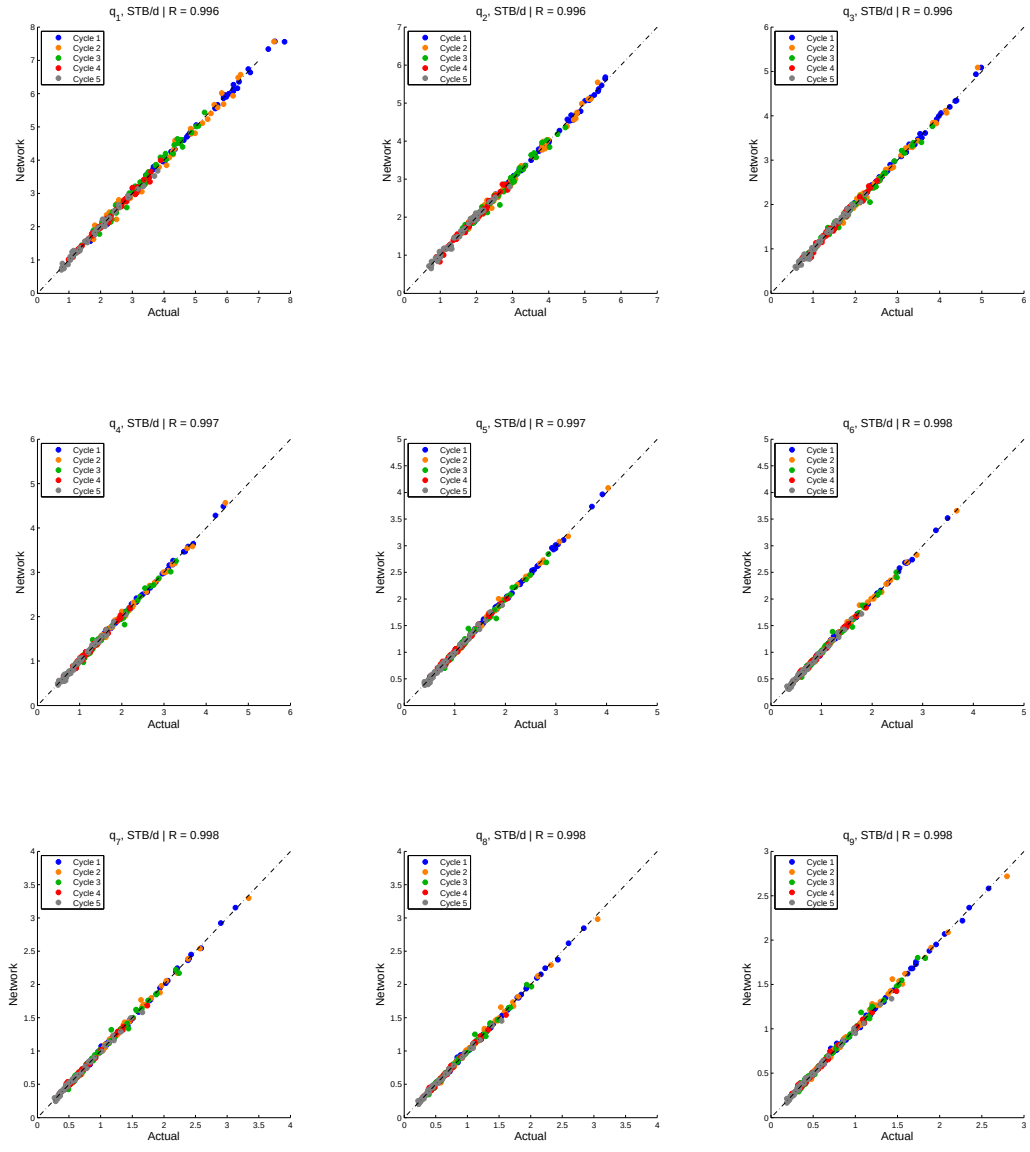

Figure 5.21. Pure CO_2 injection: flow rate (q_1,...,q_9) predictions.

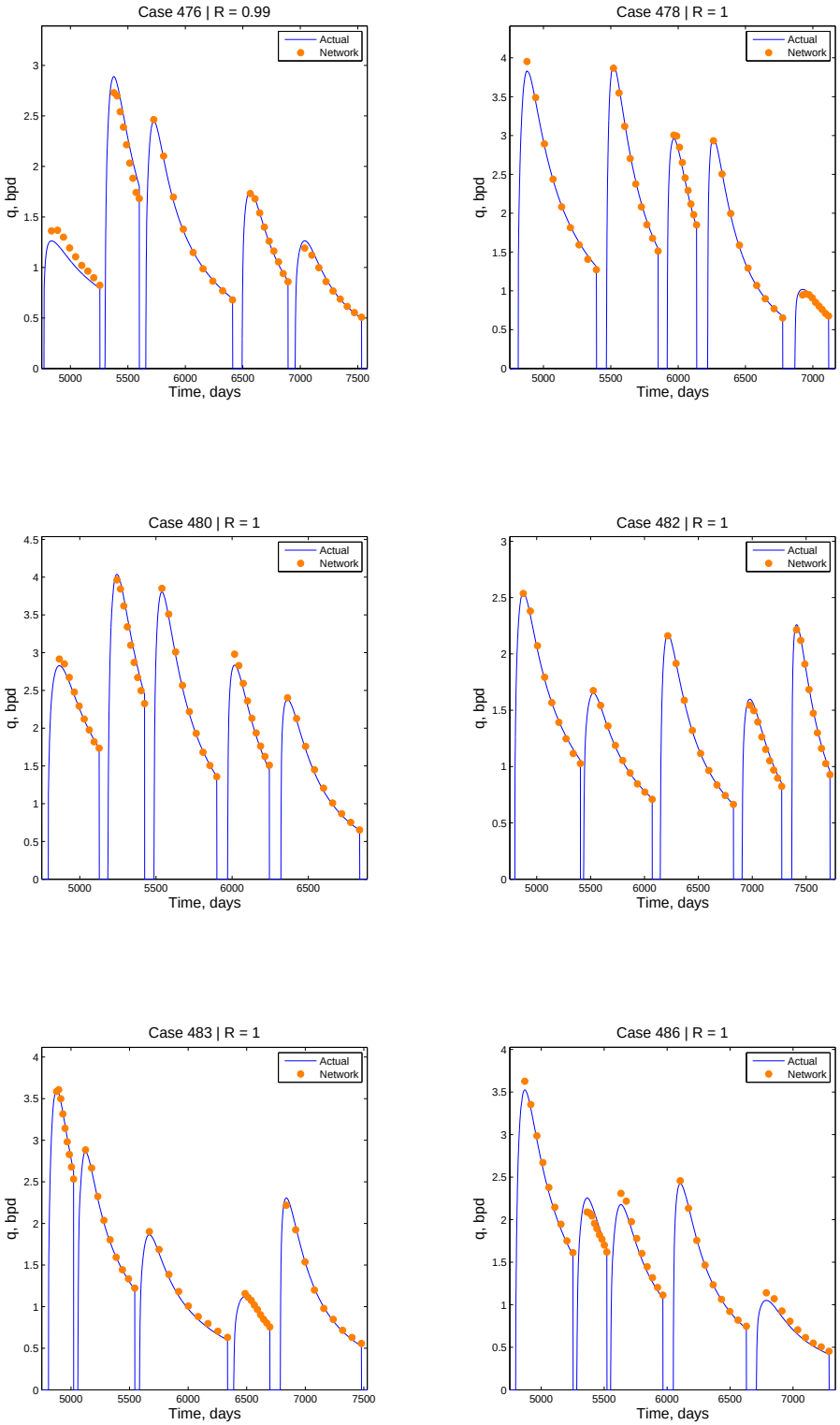

Figure 5.22. Pure CO_2 injection: flow rate predictions - comparison with the actual production curves.

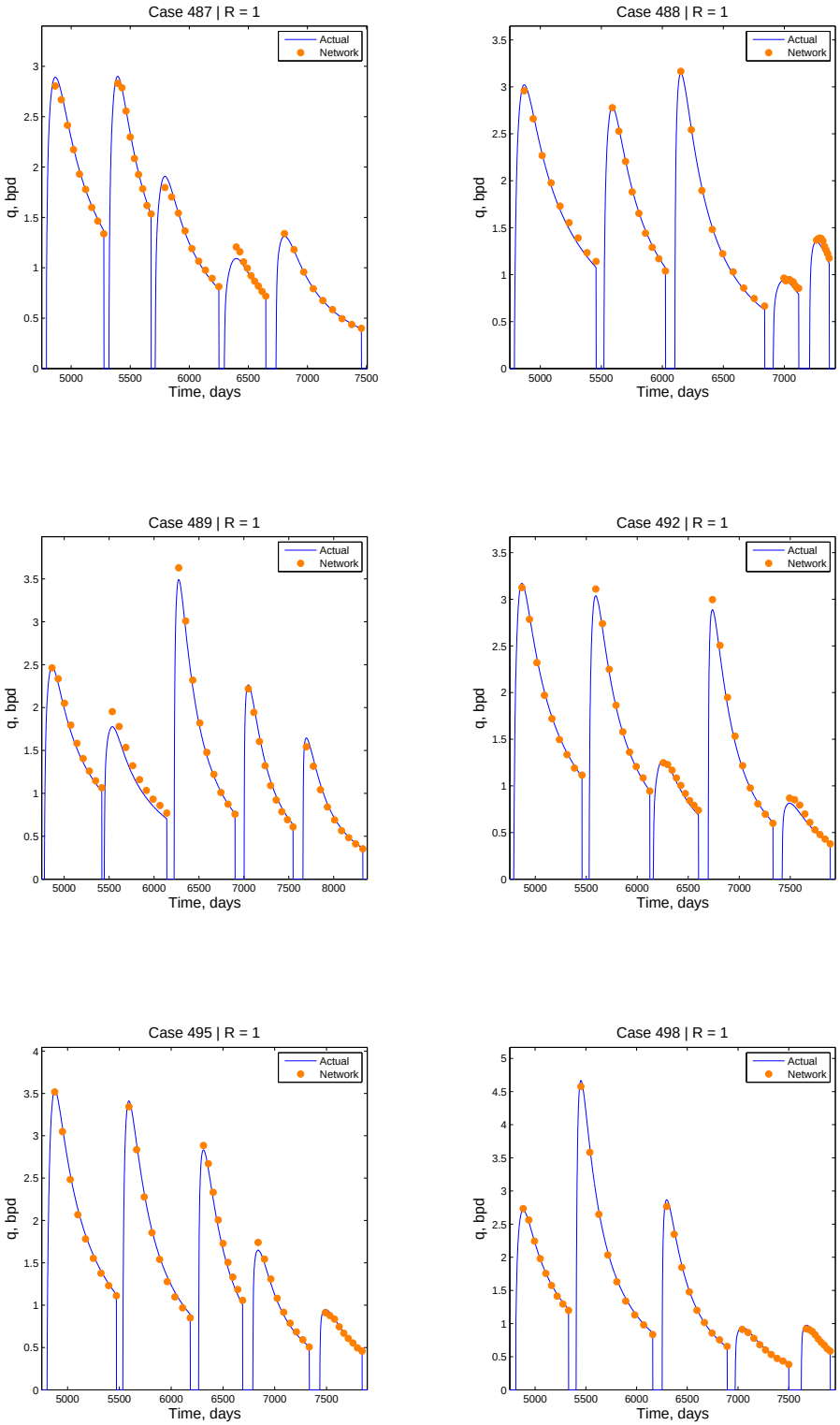

Figure 5.23. Pure CO_2 injection: flow rate predictions - comparison with the actual production curves (cont'd).

5.4.2 Design Scheme-2

The structure of the proxy of this scheme is shown in Figure 5.24. In this case, we have five design parameters and two performance indicators. The network that was developed for this part of the study had a simpler structure with a single hidden layer of 20 neurons. This is due to the fewer number of inputs and outputs. As in the previous case, tan-sigmoid function was used for activation in the hidden layer, and a linear function is used in the output layer. Among 500 cases, 350 were used for training, 100 used for validation, and 50 were used for testing. The network architecture is shown in Figure 5.25.

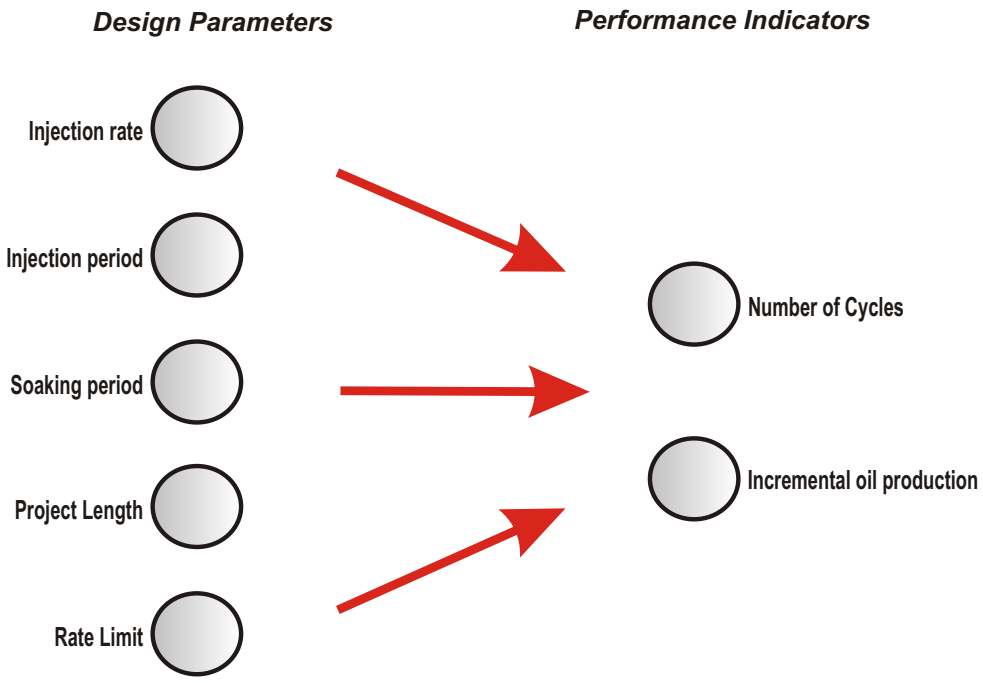

Figure 5.24. Structure of the forward proxy with variable-number-of-cycles: Mapping from design parameters to performance indicators.

Predictions of performance indicators using this network are presented below. Figure 5.26 is the predictions of incremental oil production and number of cycles for pure N_2 and CO_2 injections. Actual vs. network plots for incremental oil production shows a high correlation coefficient of 0.93 and 0.98 for N_2 and CO_2

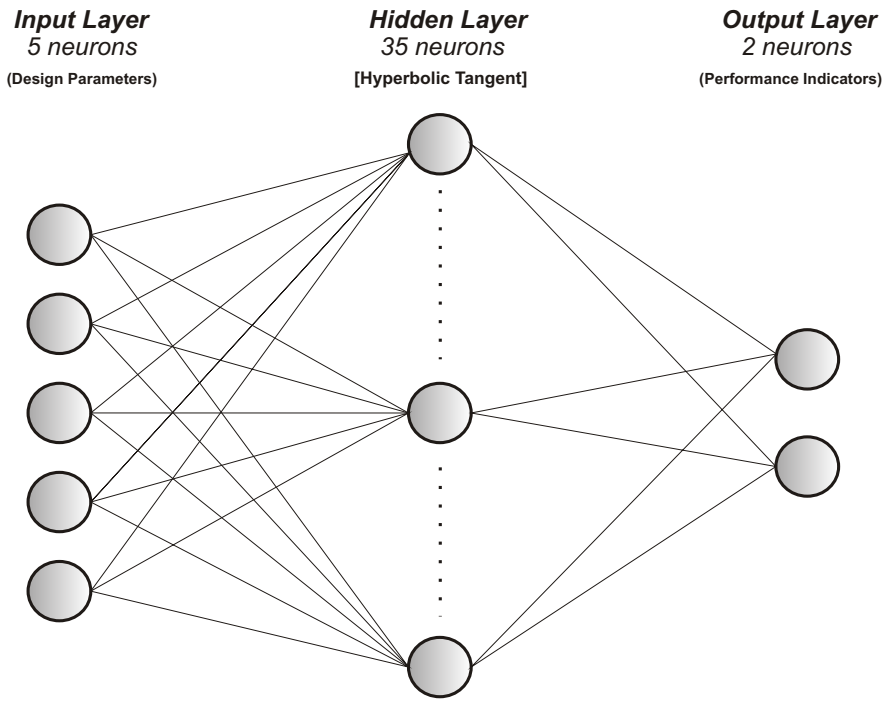

Figure 5.25. Network architecture for the forward problem with variable-number-of-cycles.

injection cases, respectively. The histogram charts for the number of cycles show the number of cases with ±0, 1, and 2 accurate predictions. In the case with N_2, 100% of the 100 testing cases were predicted with ±1 accuracy. Predictions with similar accuracy were obtained with the CO_2-injection case with 95% of the cases having ±1 accuracy for the number-of-cycles predictions.

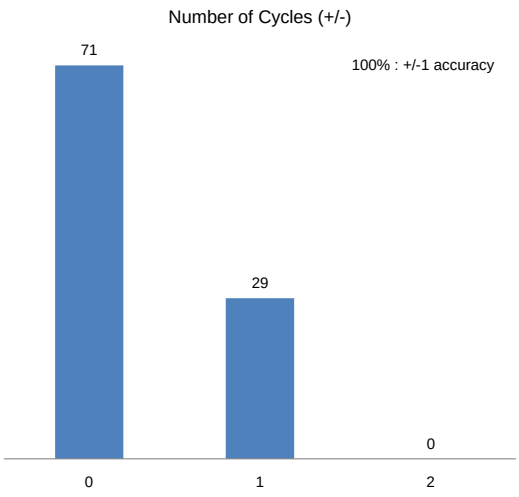

(a) N_2 - Number of cycles ($\pm$ accuracy)

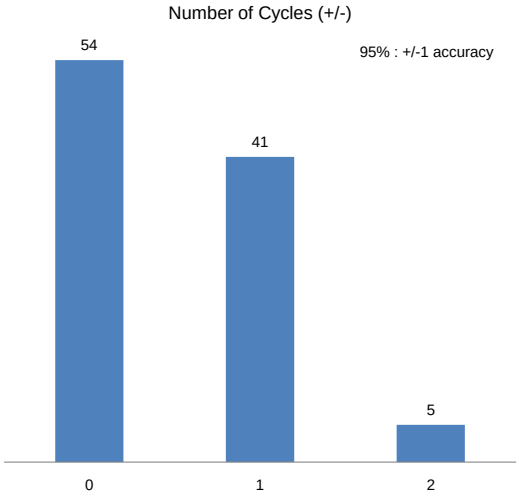

(b) CO_2 - Number of cycles ($\pm$ accuracy)

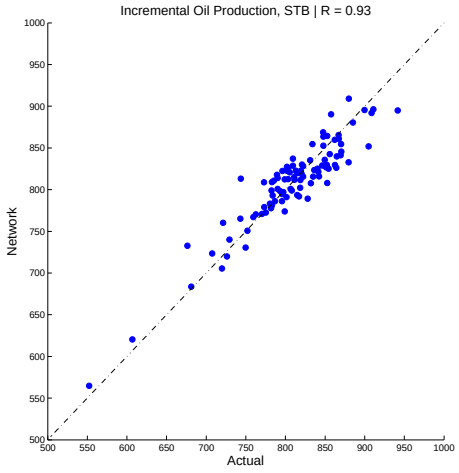

(c) N_2 - Incremental oil production

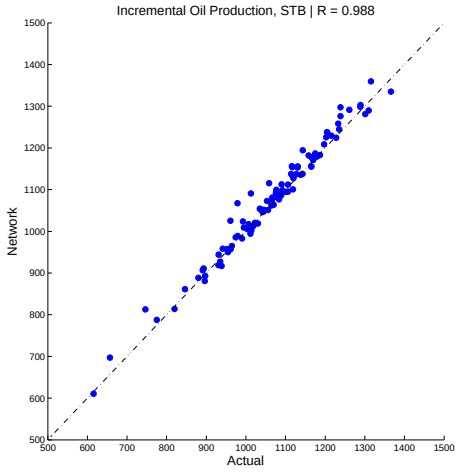

(d) CO_2 - Incremental oil production

Figure 5.26. Incremental oil production and number of cycles predictions of proxies developed for Design Scheme-2.

5.5 Inverse Problem

Inverse problems are often ill-posed problems (with no unique solution), where some model parameter(s) must be obtained from observed data. Thus, they are rather hard to solve using conventional methods.

In this study, the *inverse problem* includes developing an ANN proxy, which can act as an inverse simulator, going beyond the reservoir model's capabilities. As shown in Figure 3.2, the developed proxy should provide accurate predictions of design parameters once the performance indicators are given. In this way, if one can specify the desired performance from a system, the proxy can provide the corresponding design parameters (assuming the provided performance characteristics are within the ranges of proxy's prediction capabilities). The structure of this proxy would be the reverse of the forward one (Figure 5.27).

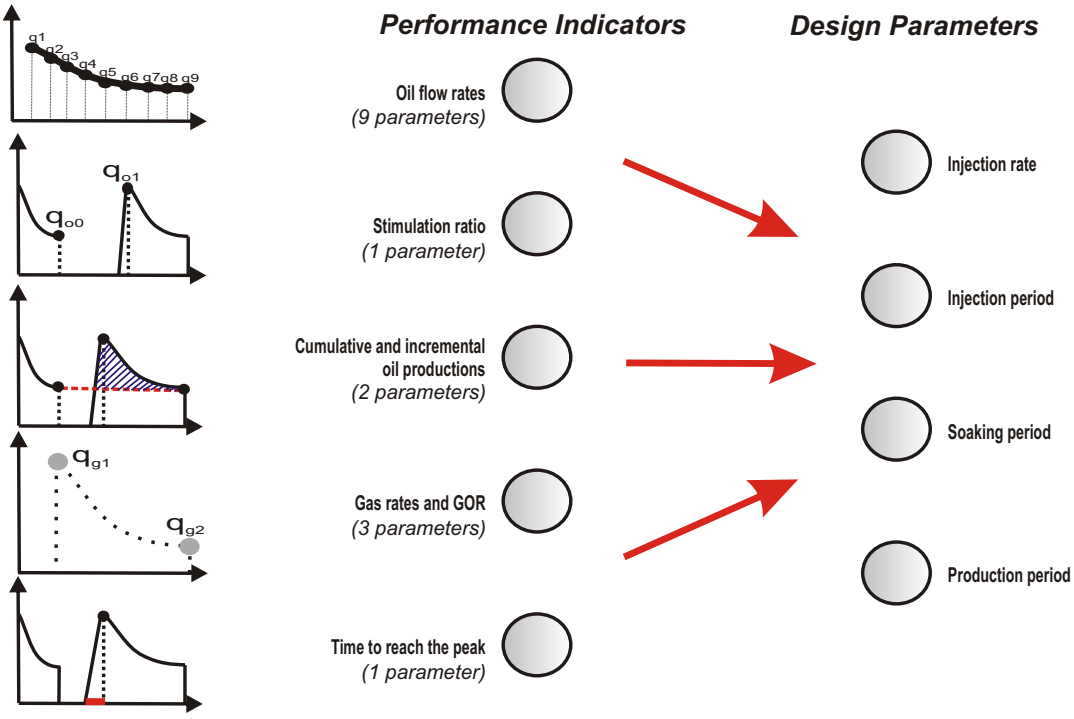

Figure 5.27. Structure of the inverse proxy: Mapping from performance indicators to design parameters.

As presented in the previous section, backpropagation algorithm worked well with the forward problem. However, in the inverse case backpropagation was not

as successful as the forward problem. As explained in Section 5.3.1, the amount of injected gas is the most important parameter that influences the performance of the well. In addition to that, soaking and injection periods can be counted together as the actual soaking period, since the soaking process actually starts immediately following the start of the injection. Because of these complexities, the backpropagation algorithm had difficulties in separately understanding the influences of soaking and injection periods, and the effect of the injection rate. These issues were handled by using output parameters, which are functions of other parameters (functional links) instead of using the primary design parameters.

For example, by using the summation of soaking and injection periods instead of one of them (such as soaking), we can still obtain the injection period, which would be the difference between total time and the soaking period (assuming the network would be able to accurately predict these two). Similarly, the injected gas amount could be used instead of injection rate. If we are able to obtain accurate estimates of the injection period, we would be able to obtain the injection rate from the amount of injected gas (Injection rate = Amount of gas / Injection period). These are simple modifications on the network output parameters to help the network learn the process better, without changing the dimensionality of the problem.

Another problem arose because of not distinguishing between different cycles. It was observed that the network was able to make accurate predictions when only the first cycle is presented. However, as the number of cycles that are included increased, the accuracy of the predictions became worse. This is to a certain degree expected, because we should consider that with each cycle, we inject some amount of gas, and perturb the reservoir system. The nature of the system changes with each cycle, so the effect of the same treatment (*i.e.*, same injection amount, same injection period, same soaking period) would change in each case based on the treatments in previous cycles. This problem has not arisen in the *forward* case, because the problem was simpler, and the influence of each design parameter was captured easily by the network even for different cycles of injection.

In order to overcome this problem, we looked for other types of networks that might be more useful in capturing the physical process. *Recurrent neural networks* (RNN) (explained in Section 4.1.2) have been found to be a candidate solution for a problem of this type, since they are powerful in capturing time-dependent

relationships. When using RNN, there are options of using a feedback from the hidden layer or the output layer. Among these two, the latter is more suited to our problem, which is also known as *backpropagation in time*. After trying two different architectures, slightly better predictions were obtained with backpropagation in time. The structure of this network is shown in Figure 5.28.

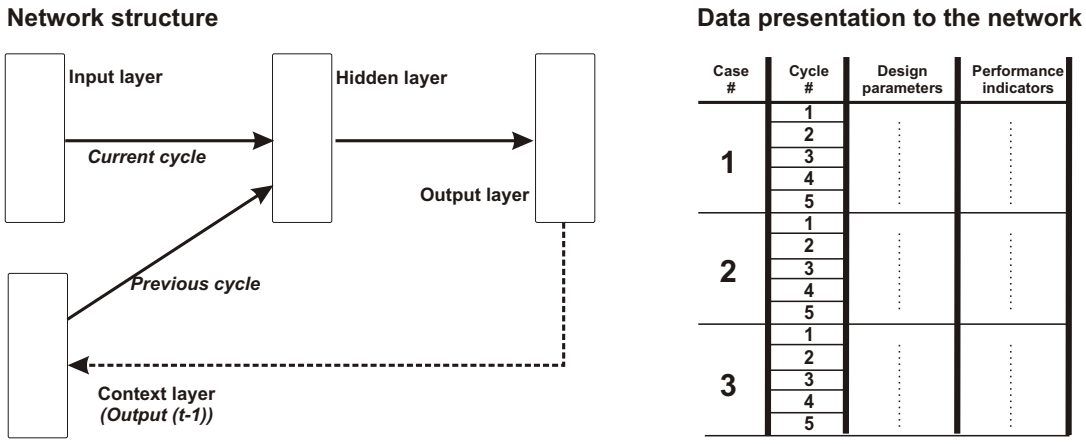

Figure 5.28. Structure of the recurrent network (with feedback from output) and the presentation of cyclic injection data to this network.

The first thing to be considered carefully is the presentation of data, shown on the right. In the *forward* case, we provided the network with data from all five cycles at each training event. In this case, each cycle is a training event itself. For example, in a given case, data of first cycle are given to the network. Outputs are the *design parameters* for that cycle. After updating the weights, the design parameters for the first cycle are copied to the *context layer*. Then, while the training event for the second cycle is executed, the context layer provides the hidden layer with the design parameters of the previous (first) cycle. In this way, the network knows that it is actually the second cycle that is being trained, and there was a cycle before that one (first cycle), which may have influenced the current cycle. This type of training has two important benefits:

Capturing the physical process - It helps the network to capture that the data provided it is actually a sequence of events. In this way, the network takes into consideration that outcomes of each cycle may also be under the influence of previous cycle(s).

Simplified network structure - Since we present one cycle at a time, we only need to have 16 inputs and 4 outputs (Presenting five cycles would have required 80 inputs and 16 outputs). However, the computational time would increase because of increased training data (5 times more data are used).

The architecture of the network with recurrent connections is shown in Figure 5.29.

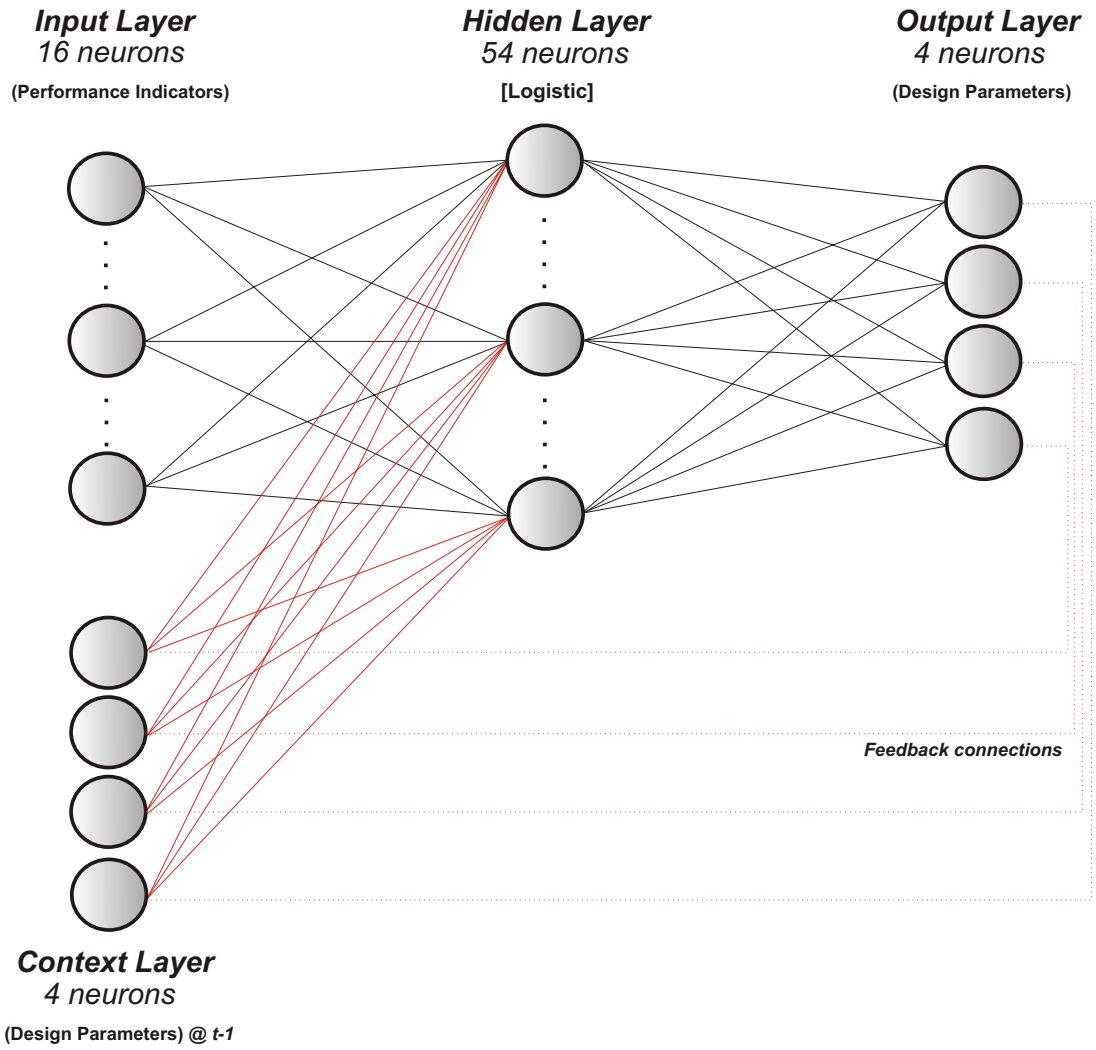

Figure 5.29. Network architecture for the inverse problem with recurrent connections.

Figure 5.30 and Figure 5.31 show the predictions of design parameters for N_2 and CO_2 injection, respectively. As can be seen, while the predictions for the injected gas amount and the production period are good, predictions for the injection period and the soaking period are less accurate. However, it should be

noted that correlation coefficient values of higher than 0.92 indicate reasonable accuracy for all parameters.

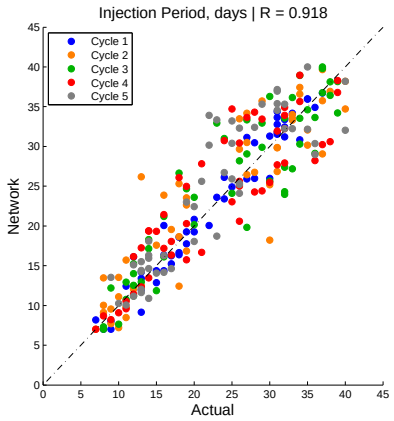

(a) Injection period

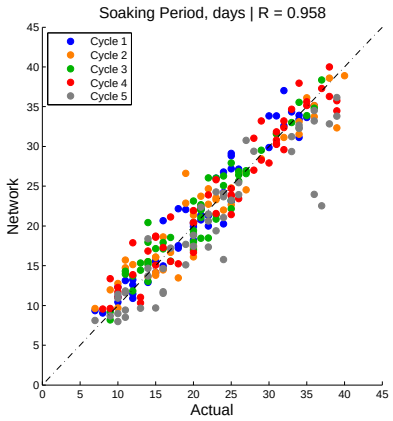

(b) Soaking period

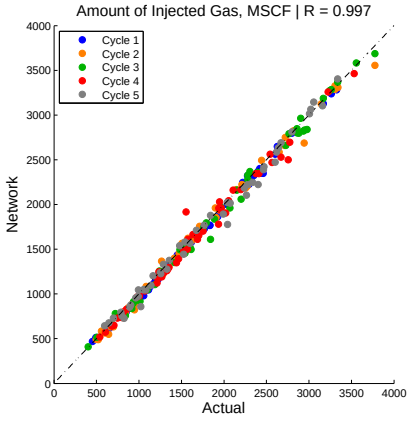

(c) Amount of injected gas

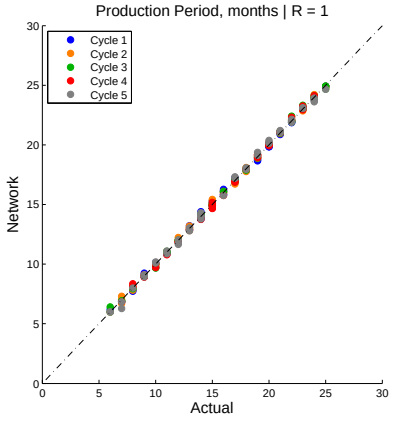

(d) Production period

Figure 5.30. Pure N_2 injection: performance predictions.

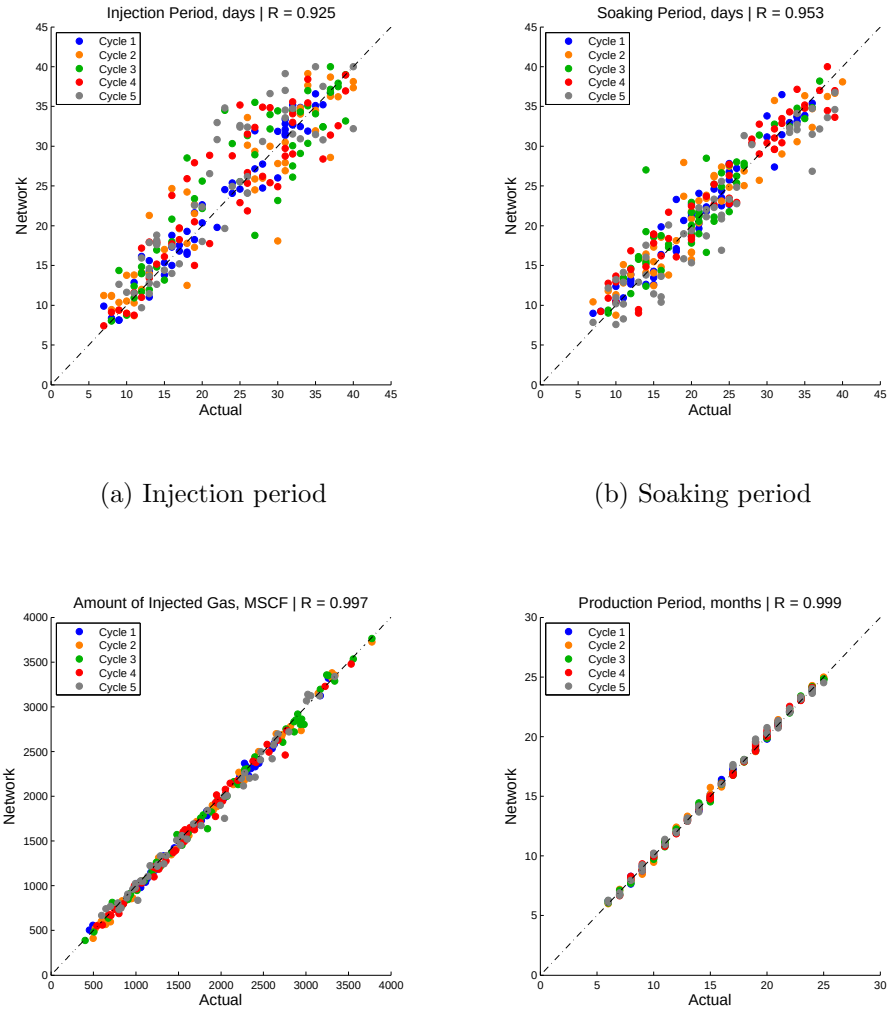

(a) Injection period

(b) Soaking period

(c) Amount of injected gas

(d) Production period

Figure 5.31. Pure CO_2 injection: performance predictions.

5.6 Case Study: The Sandy Ridge Unit

The Sandy Ridge Unit is one of the leases operated by Bretagne, LLC. in the Big Andy Field. Cyclic nitrogen utilization started during 1999 and is currently in the fourth cycle. Lease production is approximately 500 STB/month. It is aimed to apply the presented methodology to this specific lease area and analyze the outcomes. This provides an opportunity to go over the guidelines of this methodology for the practicing engineer.

First, oil production and gas injection histories of the lease are analyzed. The production history is approximated using decline curves for each cycle of production. The scope of the analysis is reduced to one representative well by considering the number of wells on production with time. Then, a representative reservoir model is constructed using the available reservoir information and the production history. A number of design scenarios are generated using Design Scheme-2 (explained in Section 5.3.2). Injection rate, injection and soaking periods, total project time, and cycle abandonment rate are varied. After running these scenarios using the reservoir model, outcomes are collected, and NPV for each case is forecasted. This knowledge base is used to develop a neural-network based proxy, that can be used to accurately predict the NPV and incremental oil production, once the design scenario is provided.

5.6.1 Production Data Analyses

Production data analyses were performed on the Sandy Ridge Unit for the purpose of developing decline behavior that would be representative of the change in oil-production rates with the number of nitrogen treatments. This lease is currently in the fourth cycle of cyclic utilization (Figure 5.32). The production history was approximated with decline curves using the empirical Arps Equation (Arps, 1945):

$$q(t) = \frac{q_i}{(1 + q_i b D_i)^{1/b}} \tag{5.2}$$

where q_i is the initial flow rate, D_i is the initial decline rate and b is the decline coefficient. An hyperbolic decline model is obtained for $0 < b < 1$. When $b = 0$ and $b = 1$, two special cases can be defined as:

$$q(t) = \begin{cases} \frac{q_i}{(1+q_i b D_i)} & \text{if } b = 1 \text{ (Harmonic decline),} \\ q_i e^{D_i t} & \text{if } b = 0 \text{ (Exponential decline).} \end{cases}$$

In this case, since q_i, the initial flow rate, is known, D_i, and b were estimated manually to get an approximate match between the actual production and estimated production rates. These parameters are shown in Table 5.9. It is seen that the decline behavior of each cycle is similar as peak rates vary with the number of cycles. Table 5.10 includes the information regarding the performance of each cycle such as the peak oil rate, incremental oil production, cycle abandonment rate, and cycle length.

Table 5.9. Decline curve parameters for the Sandy Ridge Unit production.

Parameter	Base	Cycle 1	Cycle 2	Cycle 3	Cycle 4
q_i	900	1,300	1,800	1,400	1,000
D_i	0.02	0.06	0.07	0.05	0.05
b	0.3	1	1	1	1

Table 5.10. Cyclic performance data for the Sandy Ridge Unit.

Parameter	Cycle 1	Cycle 2	Cycle 3	Cycle 4
Stimulation ratio	7.88	3.40	1.74	1.39
Peak oil rate, STB/month	1,261	1,810	1,265	1,000
Cycle-end oil rate, STB/month	532	728	720	-
Cycle length, months	28	23	24	-
Incremental oil prod., bbls	16,456	13,558	8,059	2,292

To reduce the scope of the analysis to one representative well, the number of wells on production at different times were considered (Figure 5.33). Based on Figure 5.33, 25 wells were determined to approximate the average production for each well. The monthly production in the lease area were divided by 25 wells and 30 days to estimate the daily average production for a representative well. Figure 5.34-a shows the average production history for one well in the Sandy Ridge Unit. Table 5.11 shows the performance of the individual cycles based on a single representative well's production.

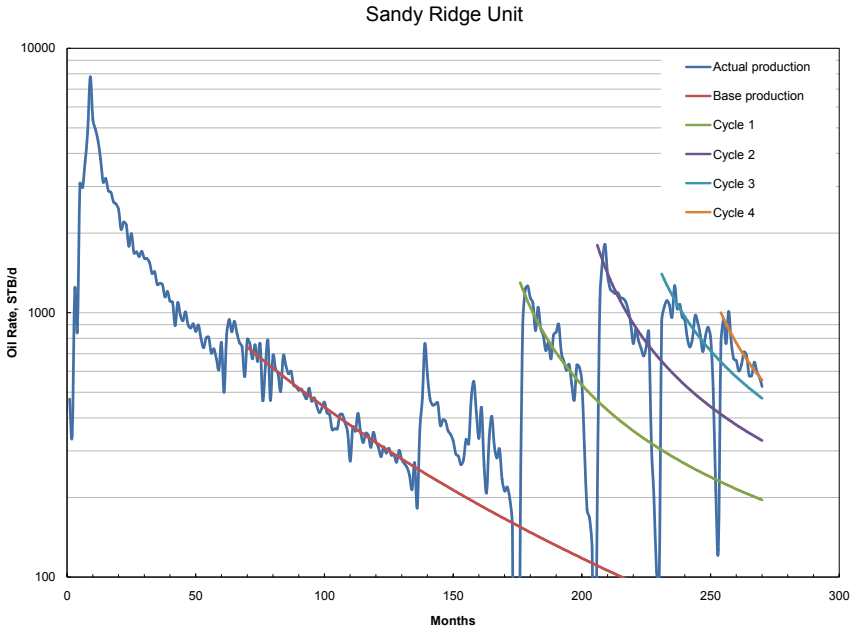

Figure 5.32. Production history of the Sandy Ridge Unit (courtesy of Bretagne, LLC).

Table 5.11. Cyclic performance data for representative well.

Parameter	Cycle 1	Cycle 2	Cycle 3	Cycle 4
Stimulation ratio	7.88	3.40	1.74	1.39
Peak oil rate, STB/month	1.68	2.41	1.69	1.33
Cycle-end oil rate, STB/month	0.71	0.97	0.96	-
Cycle length, months	28	23	24	-
Incremental oil prod., bbls	658.3	542.3	322.3	91.7

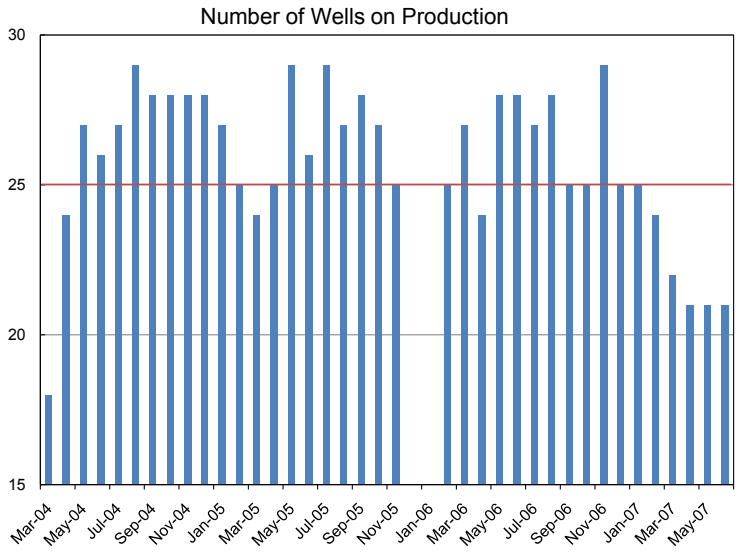

Figure 5.33. Number of wells on production in the Sandy Ridge Unit (courtesy of Bretagne, LLC).

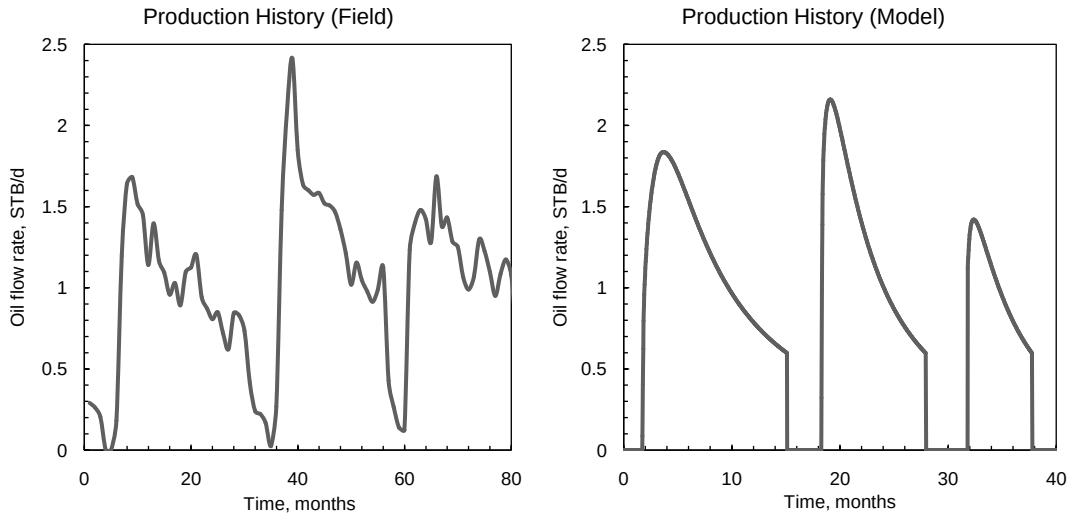

(a) Field (b) Reservoir model

Figure 5.34. Sandy Ridge Unit actual average production history for a representative well and reservoir model output.

A single-well reservoir model was constructed to perform optimization studies by evaluating different design scenarios. Oil composition in Table 5.1 was used to characterize the reservoir fluid. The nitrogen treatment volumes in the Sandy Ridge Unit were collected from the database. Average nitrogen volume per well was determined as 600 MCF for the first cycle and approximately 1,000-1,100 MCF during the second and third cycles, assuming an average of 25 active wells. Applying these treatments in the model and using a soaking time of 20 days for each cycle resulted in similar production behaviors of these cycles. Figure 5.34-b shows the oil production rate history of the well with peak rates around 1.8 STB/d, 2.4 STB/d, and 1.4 STB/d for three cycles.

5.6.2 Economic Calculations

Economic analyses were performed to understand how design considerations would affect the project financially and to develop design scenarios that would maximize the net present value (NPV) of a given cyclic injection project. Parameters used in the economic analyses are given in Table 5.12. Each project is evaluated by collecting monthly oil production and nitrogen injection volumes through the life of the project and calculating the net cash flow, NCF, at a given time:

$$NCF_t = NCF_{oil,t} - NCF_{N_2,t} - NCF_{op,t} \tag{5.3}$$

where $NCF_{oil,t}$ is the income component after paying taxes and royalty interest from the oil production. $NCF_{N_2,t}$ is the nitrogen generation and delivery component and $NCF_{op,t}$ is the well operating component. This net cash flow amount at a future time, t, can be brought to present using:

$$P = F\left(\frac{1}{(1+i)^n}\right) \tag{5.4}$$

where P is the present value, F is the future value, i is the interest rate, and n is the number of periods. In this manner, different projects can be evaluated with equal conditions at $t = 0$ by considering the time value of money.

Table 5.12. Parameters used in the economic analysis.

Oil price	.....	$	60.00	per STB of production
Nitrogen cost	.....	$	1.00	per MCF of injection
Operating cost	.....	$	400.00	per well per month
Royalty interest	.....	%	12.5	of the gross revenue
Taxes	.....	%	6.0	of the net revenue

5.6.3 Proxy Construction

Using the current reservoir model, a number of design scenarios were created and run. In these design scenarios, the project life in years, the cycle abandonment rate, injection rate, period, and soaking period were varied within the ranges shown in Table 5.13.

Table 5.13. Ranges of scenario design parameters.

Parameter	Minimum	Maximum
Project life, years	5	10
Cycle abandonment rate, STB/d	0.2	0.5
Injection rate, MCF/d	50	100
Injection period, days	10	40
Injection amount, MCF	500	4,000
Soaking period, days	10	40

Using the outcomes of these scenarios, it was aimed to develop a neural network model that can accurately predict the NPV, and the incremental oil that can be produced with a given project design scenario was developed. The design scenarios created within the specified ranges resulted in a NPV varying between \$17,000-\$31,000 and incremental production varying between 650-900 STB. The input/output structure of this network is shown in Figure 5.35.

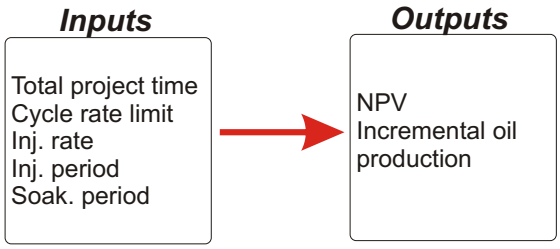

Figure 5.35. Input/output structure of the neural network model.

The developed network model was able to accurately predict NPV and incremental production with correlation coefficients higher than 0.95 (Figures 5.36 and 5.37).

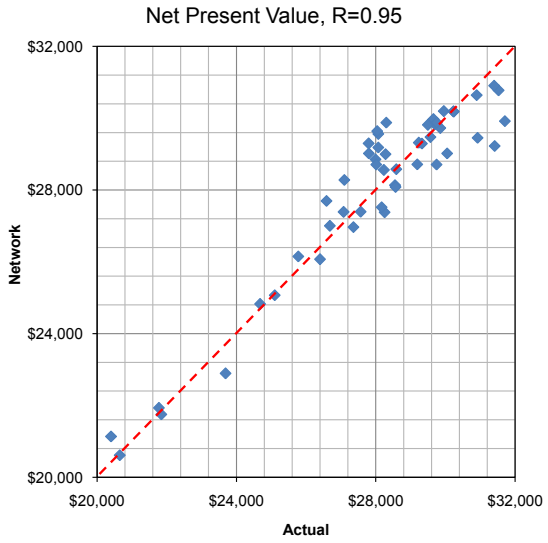

Figure 5.36. Actual vs. network-predicted NPV values using the developed network model.

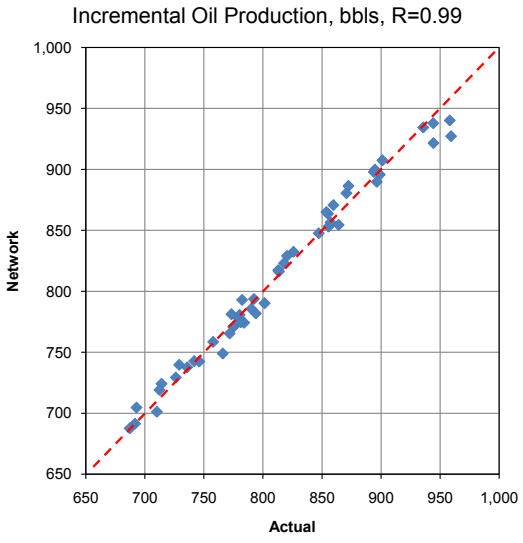

Figure 5.37. Actual vs. network-predicted incremental oil values using the developed network model.

5.7 Summary and Conclusions

A single-well, compositional, dual-porosity reservoir model was constructed, which incorporated reservoir characteristics of the Big Andy Field, Kentucky. Cyclic injection of N_2 and CO_2 were utilized in this model. It was observed that while N_2 causes a higher peak rate with the same amount of injection, CO_2 dissolves into the oil, increasing the oil saturation, and yielding more cumulative oil recovery. Soaking period mainly affects the peak oil rate. Longer soaking increases the peak oil rate up to a point, after which the rate starts to decline due to the dissipation of the pressure. It can also be stated that soaking process starts as soon as the injection starts. Thus, it is possible to have a more clear understanding of the effect of soaking period if these two periods are taken into consideration together. The amount of injected gas is the most important parameter affecting the incremental recovery, and the injection rate has a little effect.

Proxy approximators were developed using the neuro-simulation methodology. The forward proxy provides the critical performance indicators, once the design parameters are provided. Accurate predictions were obtained for both cases with nitrogen and CO_2. This showed that these proxies can mimic the reservoir model to output the desired performance indicators as the model would do. Similarly, inverse proxies were developed that can output the corresponding design parameters for a given set of performance indicators. These proxies went beyond the capabilities of the reservoir model, working backwards. The amount of injected gas and the production period were predicted with a very high accuracy. Injection and soaking periods were predicted with a less, but reasonable accuracy. This is most probably due to the physical soaking process, which actually starts with the injection as mentioned above.

In developing the proxy approximators two design schemes are considered depending on the way the cyclic pressure pulsing process is designed and applied in the field/model. In Design Scheme-1, a fixed number of cycles (in this case, it is 5) is implemented, and each cycle is designed separately with different injection characteristics. Injection rate, lengths of injection period, soaking period, and production period are specified separately for each cycle. This design scheme is powerful because it allows varying injection design characteristics for each cycle.

On the other hand, Design Scheme-2 allows different number of cycles in each case. Process economic production rate limit and process length is specified in designing the process. Production in each cycle is stopped when the oil production rate reaches the production rate limit. Another cycle of injection/production is then initiated, and this continues until the total time reaches the project length, which was also another specified design parameter. This design scheme is powerful because the number of cycles is not limited. Both design schemes are applicable in the field. Therefore, to cover a wider range of possibilities both schemes are implemented, and proxies are successfully developed for each design scheme.

At the end of the chapter, an example case study is presented. The methodology presented in the chapter is applied to one of the lease areas in the Big Andy Field. After considering the number of wells on production each month, the actual lease production history was converted to the production history of one representative well. 400 different design scenarios with Design Scheme-2 were applied to the reservoir model and the performance indicators were collected. Together with the incremental oil production, net present value (NPV) is also calculated for each design scenario. A neural-network proxy was trained with the knowledge base. The proxy was able to accurately predict the cumulative oil production and the NPV. With this case study, a guideline to the practicing engineer is presented to apply the presented methodology to a given well or lease area.

Chapter 6

Development of Universal Proxies

In this chapter, development and application of universal proxy models for the cyclic pressure pulsing process are presented. In this part of the study, it is aimed to generalize the methodology presented in Chapter 5 to reservoirs of different characteristics. This includes development of more complicated proxies which, when trained, could capture the influence of reservoir characteristics together with the operational design scenarios. In this way, the developed proxies can be used as general screening tools applicable to different reservoirs. In addition to variations in reservoir rock properties, well drainage area (*i.e.*, well spacing), and initial conditions of the reservoir; the study is repeated for three different types of oils to further generalize the approach. These fluids are characterized with compositions found in the literature and defined as black, volatile, and heavy oils with a conventional naming procedure as used in the petroleum engineering literature.

The chapter starts with description of the reservoir model. The description is divided into three subsections to describe the initial conditions and well spacing (Section 6.1.1), rock properties (Section 6.1.2), and fluid properties (Section 6.1.3). Then, the development of proxies are presented for Design Scheme-1 and Design Scheme-2, which were described earlier in Section 5.3. A hierarchical diagram that shows the proxies developed for different design schemes, injected fluids, and reservoir fluids is shown in Figure 6.1. This represents a total of 12 proxy models serving for different purposes. The results and discussions are presented throughout the chapter in this structure. For each design scheme, the prediction results and discussions are presented for cases with pure N_2 and CO_2 injection as ap-

plied to oils with different compositions (volatile, heavy, and black-oil, defined in Section 6.1.3). Finally, the chapter concludes with the summary and conclusions.

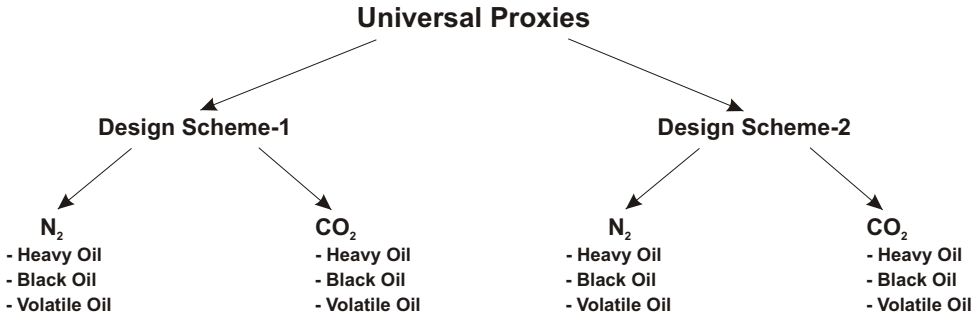

Figure 6.1. Hierarchical diagram of the proxies developed for different purposes in terms of design, injected fluid, and reservoir fluid.

6.1 Characterization of the Reservoir Model

The reservoir model is constructed using CMG's Advanced Compositional Reservoir Simulator (GEM^{TM}). It is a single-well, single-layer, compositional, dual-porosity reservoir model with a 17×17 cartesian grid system.

The production/injection well is located at the center of the model. For the injection well, the injection rate is specified as the well constraint since it is used as a process design parameter in this study. For the production well, the minimum bottom-hole pressure is specified as 14.7 psia as the only well production constraint.

Warren-Root's formulation (Warren and Root, 1963) is used to define the dual-porosity system. Fully-implicit scheme is used for the numerical solution. The gas-phase diffusion option is activated to represent the component mass flow from fractures into the matrix due to the compositional gradients. To construct a knowledge base that would cover a wide range of different reservoir characteristics and conditions, ranges of various reservoir characteristics and conditions are defined. While defining these ranges, it is aimed to cover a wide range of cases while considering the physical occurability of each case. These ranges of various parameters are shown in Table 6.1. In the following sections, the characterization of the reservoir will be explained in more details to discuss the ranges of some of the parameters

and to describe some of the other reservoir characteristics.

Table 6.1. Ranges of reservoir characteristics that are varied to construct universal proxies.

Parameter	Minimum	Maximum
Thickness, ft	10	100
Drainage area, acres	5	20
Porosity - matrix	0.12	0.20
Porosity - fracture	0.01	0.03
Permeability - matrix, md - i, j	0.1	100
Permeability - matrix, % - k	1	25
Permeability - fracture - i, j, k	10	10,000
Fracture spacing, ft - i, j, k	10	100
Reservoir temperature, °F	80	240
Initial reservoir pressure, psia	20	1,500
Initial water saturation	0.3	0.7

6.1.1 Initial Conditions and Well Spacing

The initial conditions are defined with the average reservoir pressure, temperature and water saturation. In this study, cyclic pressure pulsing process is investigated in depleted or partially-depleted reservoirs. Therefore, the average reservoir pressure is varied between 20 psia and 1,500 psia. The constant average reservoir temperature is varied between 80 F and 240 F. The initial water saturation is varied between 0.30 and 0.70. While incorporating the variations in the well-spacing, we wanted to narrow-down our analysis to developed fields. Thus, we determined the limits for the drainage area as 5 and 20 acres.

6.1.2 Rock Properties

Variations in the rock properties are included to have a universal range of formations with different volumetric, storage and transmissibility capacities. These include variations in the porosity and permeability in both matrix and fracture systems, thickness of the formation and the fracture spacing (intensity). Ranges of these parameters are shown in Table 6.1. While generating uniform distributions of

these parameters, a constraint is defined to assure that the fracture permeability is larger than the matrix permeability. While including anisotropy in the horizontal and vertical directions of the matrix permeability, fracture permeability is defined as an isotropic tensor (k_{f_x}=k_{f_y}=k_{f_z}).

Data analyses were performed during the data preparation stage. Initially, it was aimed to generate uniformly-distributed data sets to represent a wide range of different types of reservoir characteristics. It was expected that fracture permeability would have a significant effect on the recovery process. Its influence on the process performance was analyzed. Figure 6.2 shows how the peak oil rate changes with different fracture permeabilities. It is observed that at low-permeability regions (less than 2,000 md) the change in the peak oil rate is more significant than in the high-permeability regions (2,000 md - 10,000 md). Therefore, in low-permeability regions, dramatic changes in the process performance would be observed with even small changes in the fracture permeability. Because of this fact, we included more data from the low-permeability distribution instead of a uniform distribution. In this case, the neural network could capture the significant influence of the fracture permeability, by iterating on more data from the low-permeability region.

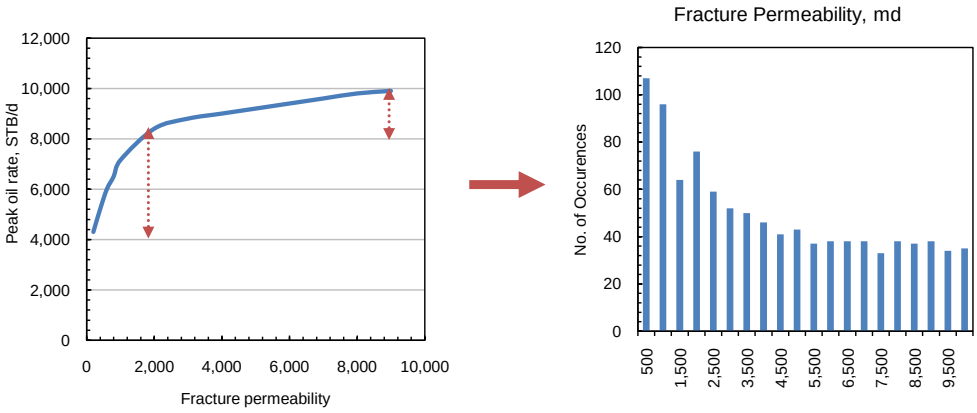

Figure 6.2. Effect of fracture permeability on the peak oil rate and re-designed histogram of generated data sets to capture its effect in both high-permeability and low-permeability regions.

In characterizing the reservoir rock, variations in the relative permeability curves are not included. Three-phase relative permeabilities for a sandstone reser-

voir are used that are generated using the Stone's Second Model (Stone, 1973) with an irreducible water saturation of 0.2, and residual oil saturation of 0.1. The relative permeability curves used in this study and the oil isoperms are shown in Figures 6.3 and 6.4, respectively.

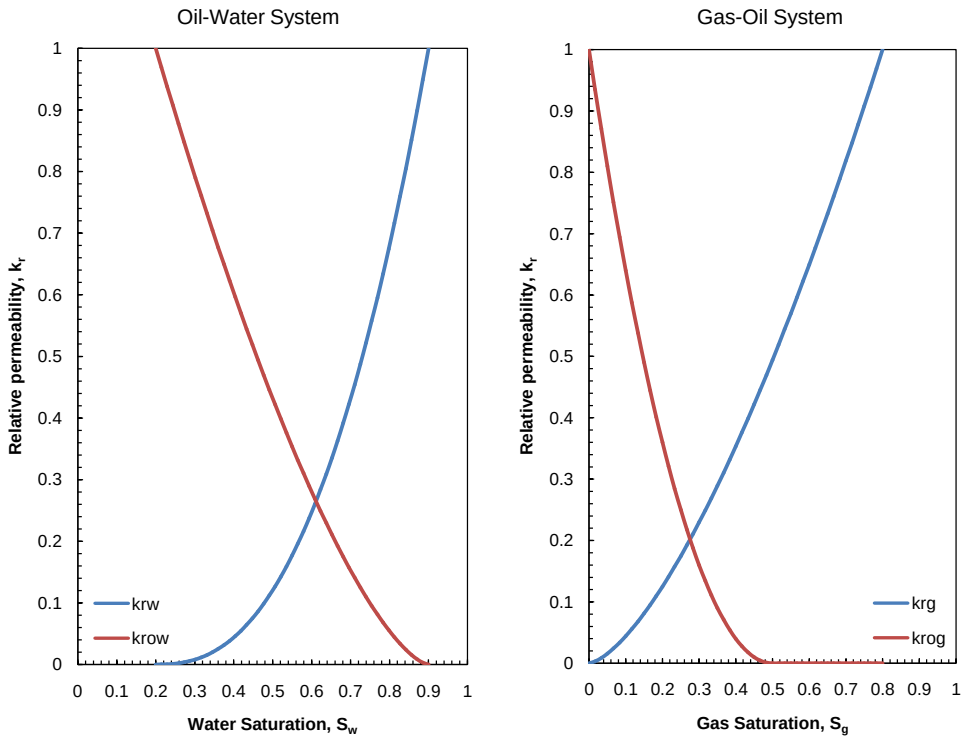

Figure 6.3. Three-phase relative permeability curves used in this study.

6.1.3 Fluid Properties

According to their phase behavior characteristics, a number of classifications of reservoir fluids have been made in the petroleum industry. Typically, at early stages of production from a reservoir, the produced reservoir fluid is characterized and many decisions that are made during the life of the reservoir are based on that definition (McCain, 1990). In the literature, cyclic pressure pulsing has been applied to both heavy and light oil reservoirs with both successful and unsuccessful results. Therefore, in order to generalize our approach, we wanted to extend the applicability of the universal proxies to different types of oils as a similar approach followed by Parada (2008). In this study, three different hydrocarbon compositions

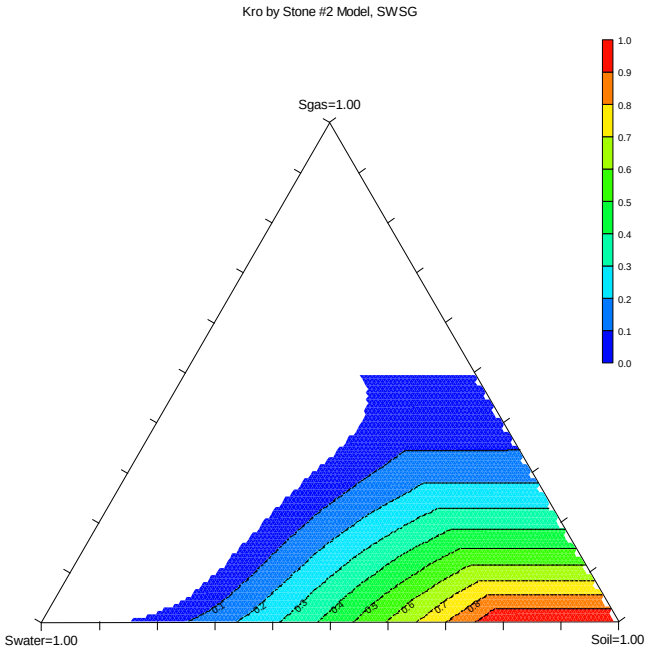

Figure 6.4. Oil isoperms generated using Stone's Second Model (Stone, 1973).

(heavy, black and volatile) are considered to cover a wide range of oil properties. Black oil (Rathmell *et al.*, 1971) and volatile oil (Papp *et al.*, 1998) compositions are from the literature. Heavy oil composition that is used is a real sample taken from a heavy oil reservoir in the Middle East, which is currently producing under steam injection (Parada, 2008). These compositions are shown in Table 6.2. Phase envelopes of these fluids are shown in Figure 6.5. The quality lines are also shown for different volume fractions of liquid and gas phases inside the 2-phase region. The black oil's critical temperature is higher than typical reservoir temperatures (100-250 F). For the volatile oil, the critical temperature is closer to typical reservoir temperatures. 2-phase region's temperature range is smaller than the one of black oil. The quality lines of the black oil are distributed uniformly within the 2-phase region. For the volatile oil, the quality lines are displaced upwards toward the bubble point curve. The phase envelope of the heavy oil is constructed by using laboratory data obtained from a differential liberation experiment. It is important to note that the fluid is in liquid phase for pressures above 430 psia. As a typical characteristic of heavy oil compositions, the bubble-point pressures are very low as compared to other types of oil compositions (Parada, 2008). In Section 7.2.3, a

discussion is presented on how the initial pressure/temperature conditions of the reservoir affects the performance of the cyclic pressure pulsing process.

Table 6.2. Compositions of three fluids used to characterize the reservoir fluid.

Component	Black Oil	Volatile Oil	Heavy Oil
CO_2	3.20	0.51	0.11
N_2	0.03	1.80	0.69
C_1	27.81	46.80	10.78
C_2	8.21	8.09	0.12
C_3	5.99	10.91	0.42
iC_4	0.31	4.26	0.30
nC_4	4.10	6.86	0.30
iC_5	1.30	3.71	0.29
nC_5	2.30	3.81	0.26
C_6	4.62	4.73	0.64
C_{7+}	42.13	8.52	86.09
SG	0.875	0.782	0.925
MW (g)	223.0	156.0	531.8

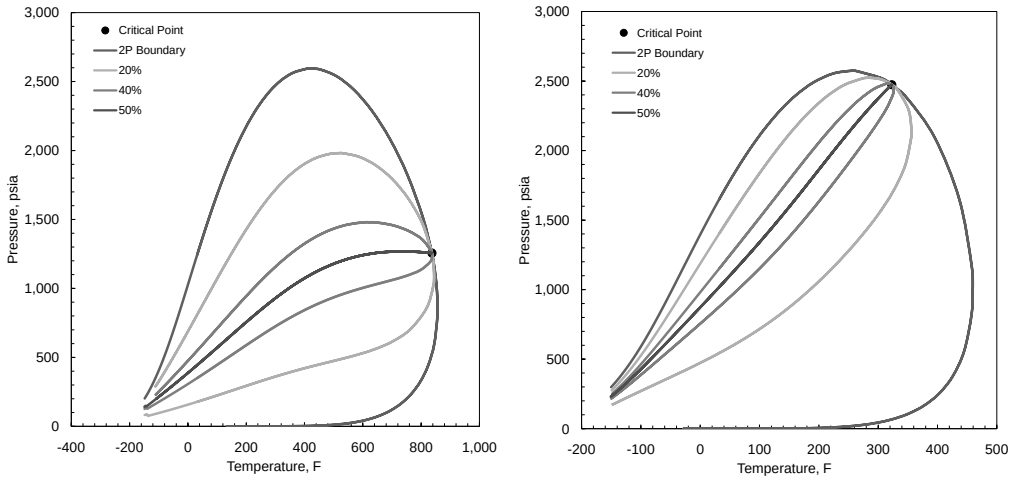

(a) Black oil

(b) Volatile oil

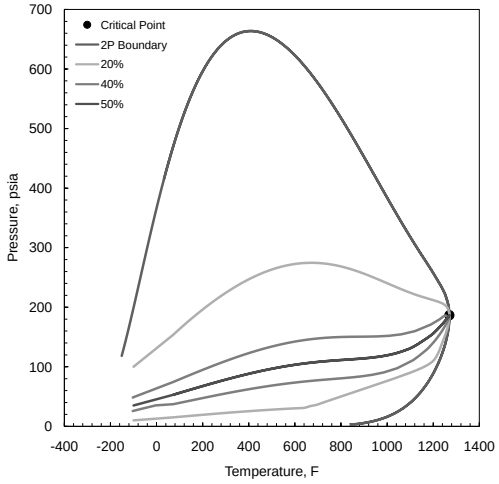

(c) Heavy oil

Figure 6.5. Phase envelopes of three different reservoir fluids used in this study.

6.2 Design Scheme-1

As explained in Section 5.3.1, the process is designed with a fixed number of cycles (5). Therefore, the number of cycles is not used as a process design parameter. In Section 5.3.1, the list of variables used is presented in Table 5.5. In this part of the study, the proxies that are developed include variation in reservoir characteristics. Therefore, the set of input parameters for the neural network includes reservoir characteristics as well as the process design parameters. Table 6.3 shows the reservoir characteristics that are included as inputs. The list also includes some parameters that are derived from other reservoir characteristics. These additional parameters improved the performance of the training of the neural networks.

Table 6.3. Reservoir characteristics that are included in the set of inputs.

Thickness, ft	h
Drainage area, acres	A
Porosity - matrix	ϕ_m
Porosity - fracture	ϕ_f
Permeability - matrix, md - i, j	$k_{m_{x,y}}$
Permeability - matrix, md - k	k_{m_z}
Permeability - fracture - i, j, k	k_f
Fracture spacing, ft - i, j, k	X_f
Reservoir temparature, °F	T
Initial reservoir pressure	p_i
Initial water saturation	S_{wi}
Initial oil saturation	S_{oi}
Initial relative perm. to water	k_{rwi}
Initial relative perm. to oil	k_{roi}
Fracture/Matrix permability ratio	$k_f/k_{m_{x,y}}$
Size of the reservoir, acre-ft	Ah
Oil-in-place, acre-ft	$AhS_o\phi_m$

Considering the variation in the reservoir characteristics the variety of possible different reservoir conditions, the ranges of the design parameters are selected as shown in Table 6.4. The input/output structure of the proposed proxies is shown in Figure 6.6.

Table 6.4. Ranges of design parameters used in the Design Scheme-1.

Design Parameter	Minimum	Maximum
Injection rate, MSCF/d	20	100
Injection period, days	5	50
Soaking period, days	5	50
Production period, months	3	12
Amount of gas injected, MSCF	100	5,000

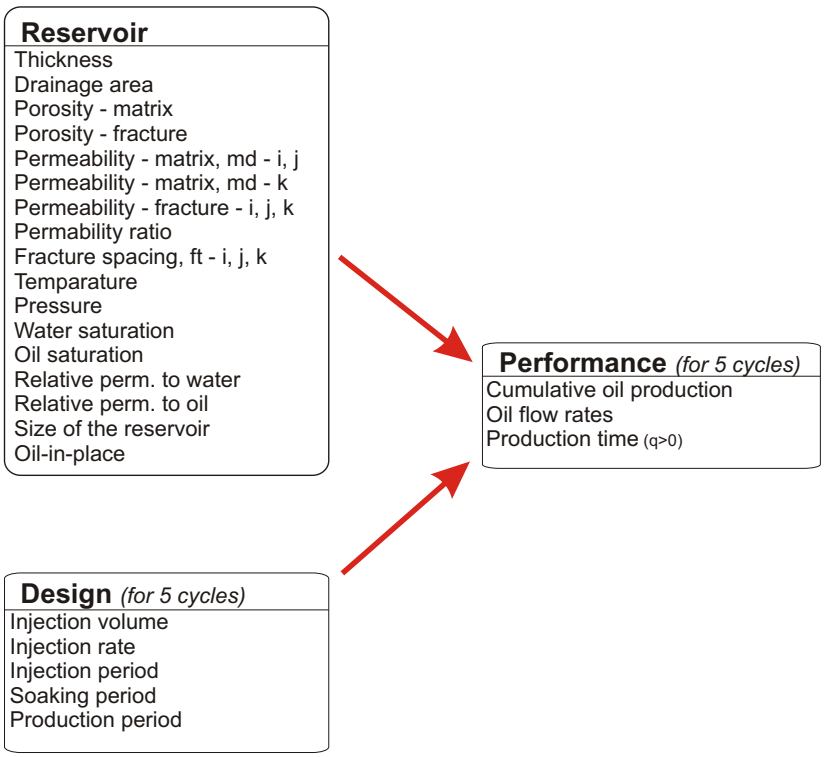

Figure 6.6. Structure of the universal proxy with Design Scheme-1: Mapping from reservoir and design characteristics to performance indicators.

Together with the cumulative oil production for each cycle, nine flow rates during the production period are selected as target outputs. This provides an understanding of the production decline behavior after each cycle of injection. Although the length of the production period is specified as a design parameter, it is observed that in a number of cases the production does not last until the end of the specified production period. This results in the collection of flow rates that asymptotically approach zero, rather than the flow rates of the actual producing time. To overcome this problem, we defined another performance indicator, which represents the actual producing time in a given cycle. This time is the actual producing time before the oil flow rate becomes zero. Accordingly, nine flow rates are collected at equally-divided time intervals between the time the peak rate is achieved and the time when the oil flow rate drops to 0 STB/d in each cycle.

Typically, the architecture of an artificial neural network is determined after careful consideration of the number of inputs, outputs, training patterns, and the complexity of the problem to be solved. We can recall from Chapter 5 that successful mapping from the process design parameters to the process performance indicators in the same reservoir is achieved using a single-layer network. However, in this part of the study, we are trying to develop universal proxies that could work in different reservoirs. We expect that the proxies would capture the influence of different reservoir characteristics and provide accurate approximations of the performance of the cyclic pressure pulsing process once the injection design scenarios are given. Therefore, it is likely that the most optimum network architecture would be more complex not only because of the higher number of inputs involved but also, and more importantly, due to the inclusion of a new type of input set, reservoir characteristics. However, it is also known from practice that additional hidden layers increase the complexity of the neural network. Higher than the optimum number of hidden layers typically worsen the training performance of a neural network. Therefore, it is necessary to find out the most optimum architecture with the best training performance and generalization capabilities.

In this case, it is observed that a 2-layer neural network architecture resulted in better training and testing performance as compared to a single-layer network. This is expected due to the increased complexity of the problem. While 3-layer and 4-layer networks were also tested, they did not perform as well as a 2-layer

network. Therefore, it is concluded that the architecture with two hidden layers is the more feasible one for this problem. After optimizing the number of neurons in each layer, the final architecture included 45-74-68-55 neurons in input, hidden and output layers, respectively. The architecture is illustrated in Figure 6.7.

After considering the memory requirements for storage, scaled conjugate-gradient backpropagation training algorithm (Demuth *et al.*, 2006) is utilized. It was observed that taking the *logarithm* of input and output data to reduce the range of the data improved the performance of networks. Data in the logarithmic scale then are normalized between -1 and 1. Among a total of 1,700 cases with different design and reservoir characteristics, 1,200 are used for training, 300 are used for validation, and 200 are used for testing.

In the next two sections, the prediction results of the developed neural networks are presented for pure N_2 injection and pure CO_2 injection, respectively. Crossplots of the cumulative oil production and peak oil rate, and flow rate predictions in different reservoirs are presented. Due to the initial high pressure of the reservoir the cumulative oil production and the peak oil rate of Cycle 1 is in a higher range than other cycles. Because of this, crossplots of Cycle-1 are shown separately from other cycles.

6.2.1 Pure N_2 Injection Predictions

After a neural network is trained, weights in the connection links may be analyzed to understand the contribution of the each individual input to the network. This essentially gives information about the importance of each input parameter in predicting the output parameters. Before presenting the prediction results of the developed neural networks, let us analyze the contribution of each input parameter on the performance of the cyclic pressure pulsing process using nitrogen. As we recall, the input set consists of reservoir characteristics and the process design parameters for five cycles of injection. Table 6.5 shows the contribution factors of each input parameter on the sum of outputs. The table includes the neural network models that were trained for heavy, black and volatile oil compositions. With this analysis, it is possible to make comments on the importance of each reservoir property in this process.

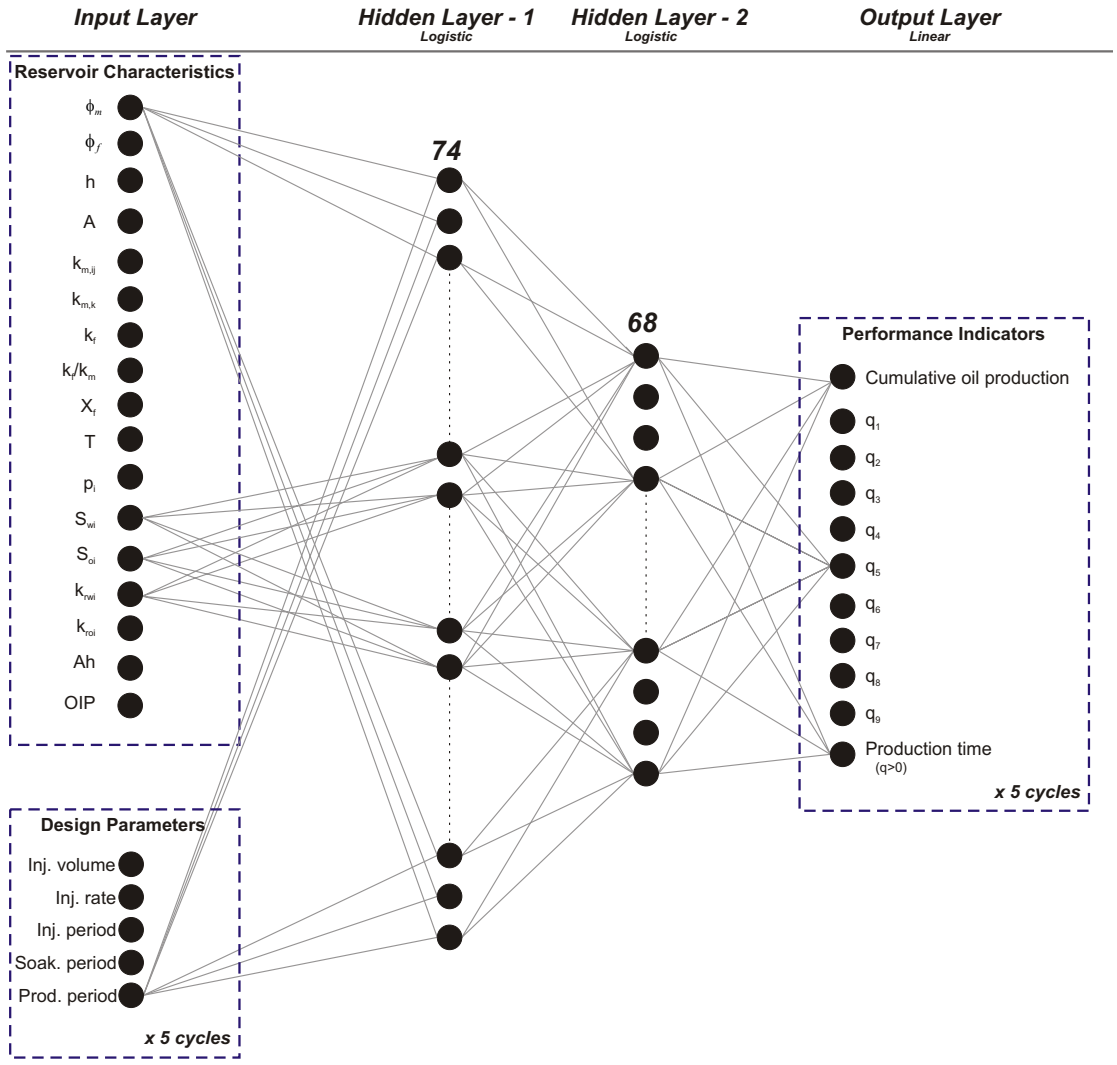

Figure 6.7. Network architecture for the universal proxy with Design Scheme-1.

In all three types of oils, fracture permeability, ratio of fracture permeability to matrix permeability, oil-in-place, area, Ah product, and oil saturation are the parameters that contributed most. It is interesting to note that while the contribution of matrix permeability itself is not very significant, the ratio of fracture permeability to matrix permeability is at a very high rank. This ratio defines the contrast between the two permeabilities. Fracture permeability provides the delivery of the injected gas to further portions of the reservoir, while the matrix

permeability defines the rate of diffusion from the fractures to the matrix. Due to the phase behavior characteristics, contribution of initial pressure and temperature of the reservoir are more pronounced in the volatile oil than black and heavy oils. Parameters with a '*' superscript are the design parameters. We see that most of the contribution comes from the reservoir characteristics. Among the design parameters, as a confirmation of earlier studies, volume of the injected gas is the most critical parameter, affecting the performance. Injection period, injection rate, and production rate are at a comparable rank in all three cases. Soaking period contributes the least.

Table 6.5. Contribution factors of each input parameter on the sum of outputs for each neural network model developed for N_2 injection.

	Heavy Oil		Black Oil		Volatile Oil	
Rank	Input	C.F.	Input	C.F.	Input	C.F.
1	k_f	5.08	k_{roi}	4.78	k_f	4.96
2	k_f/k_m	3.53	k_f	4.53	T	4.63
3	k_{rwi}	3.28	k_f/k_m	3.78	k_f/k_m	3.93
4	OIP	3.02	OIP	3.25	k_{roi}	3.93
5	S_{oi}	2.32	S_{oi}	3.07	OIP	3.51
6	S_{wi}	2.16	Ah	1.97	S_{oi}	2.07
7	A	2.09	A	1.96	A	2.01
8	k_{roi}	1.89	T	1.88	p_i	1.94
9	Ah	1.80	S_{wi}	1.72	Ah	1.76
10	h	1.59	p_i	1.50	h	1.76
11	k_{m_z}	1.54	Inj. Vol.*	1.41	Inj. Vol.*	1.52
12	Inj. Vol.*	1.52	k_{rwi}	1.37	S_{wi}	1.38
13	X_f	1.36	k_{m_z}	1.19	k_{rwi}	1.34
14	T	1.34	h	1.19	Inj. Period*	1.09
15	$k_{m_{x,y}}$	1.31	ϕ_m	1.18	k_{m_z}	1.13
16	ϕ_m	1.29	Inj. Period*	1.17	ϕ_m	1.11
17	Inj. Rate*	1.23	Inj. Rate*	1.16	Inj. Rate*	1.01
18	Inj. Period*	1.20	X_f	1.16	Prod. Period*	0.91
19	p_i	1.17	Prod. Period*	1.14	$k_{m_{x,y}}$	0.91
20	Prod. Period*	1.13	$k_{m_{x,y}}$	0.92	X_f	0.83
21	ϕ_f	0.83	Soak. Period*	0.92	Soak. Period*	0.83
22	Soak. Period*	0.80	ϕ_f	0.62	ϕ_f	0.75

6.2.1.1 Volatile Oil

The reservoir hydrocarbons may exist both in the gas and liquid phases depending on the pressure and temperature of the reservoir. Because of the phase behavior characteristics of the volatile oil (Figure 6.5), the gas saturation may be higher than the oil saturation within the pressure (less than 1,500 psia) and temperature (80-240 F) ranges studied in this study. This results in low oil saturation, very low relative permeability to oil, and low oil production rates. Within the pressure and temperature ranges that the knowledge base is generated, the oil saturation at initial conditions are the lowest among the three compositions used in this study. The average oil saturation of all cases is 0.07 with the highest 0.33 and lowest 0.00. As a result of this distribution, there were extreme cases with low production rates outputted by the reservoir model. In reality, it is not practical to produce from these type of reservoirs, but in this case it is a good practice to train and test the neural-network proxy with these extreme cases to determine its capabilities.

Table 6.6 shows the correlation coefficients of the predictions of the neural network when applied to training, validation and testing data sets. Figure 6.8 shows the actual and network-predicted total production time. Figure 6.9 shows the cross-plots of actual and network-predicted cumulative oil productions and peak oil rates. Because of the large difference in the range of production amounts of the first cycle and other cycles, Cycle 1 and Cycle 2-5 are shown in two different plots. Figure 6.9-a is the cumulative oil production of Cycle-1 and Figure 6.9-b shows the cumulative oil production of Cycles 2 through 5. Figure 6.9-c is the peak oil rate of Cycle-1 and Figure 6.9-d shows the peak oil rates of Cycles 2 through 5. Both correlation statistics and visual plots show that the network is able to predict the critical performance indicators within high levels of accuracy. In Figures 6.10 through 6.12, comparison of the actual production histories and predicted flow rates are presented for three different cases. We see that while the order of flow rates change significantly in each case, the network is still able to capture the decline behavior of each production cycle. In all of the cases, highest error is seen in the peak oil rate. Also, in cases with very small rates (*e.g.*, Figure 6.12, Cycle-5), high error in the predictions is observed. However, at a rate less than 1 STB/d, the overall effect on the cumulative production is insignificant.

Table 6.6. Correlation coefficients of N_2 injection/Volatile Oil/Design Scheme-1 neural network model.

	Cycle 1	**Cycle 2**	**Cycle 3**	**Cycle 4**	**Cycle 5**
Training					
Cumulative Oil Production	1.00	0.99	0.99	0.99	0.99
$t_{q>0}$	0.98	0.99	0.99	0.98	0.98
Flow Rates	0.99	0.99	0.99	0.99	0.99
Validation					
Cumulative Oil Production	0.99	0.94	0.98	0.97	0.97
$t_{q>0}$	0.89	0.89	0.89	0.78	0.80
Flow Rates	0.95	0.97	0.98	0.98	0.97
Testing					
Cumulative Oil Production	0.98	0.98	0.98	0.96	0.97
$t_{q>0}$	0.92	0.83	0.83	0.87	0.88
Flow Rates	0.97	0.98	0.99	0.98	0.98

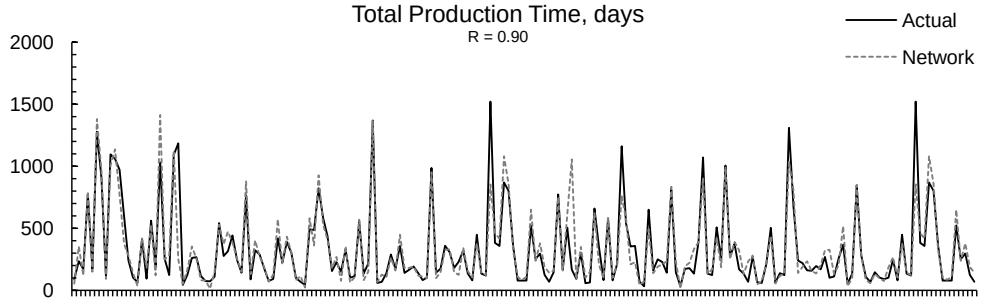

Figure 6.8. Pure N_2 injection/Volatile Oil/Design Scheme-1: Total production time predictions.

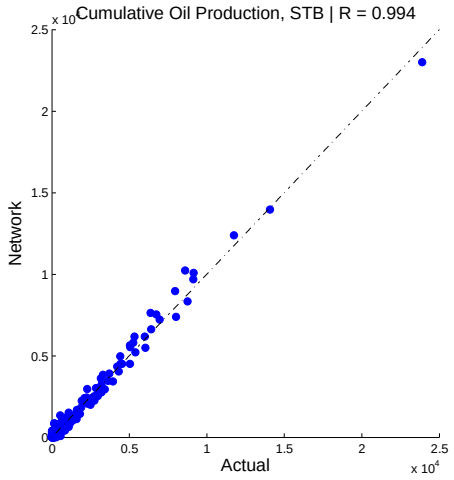

(a) Cumulative oil production - Cycle 1.

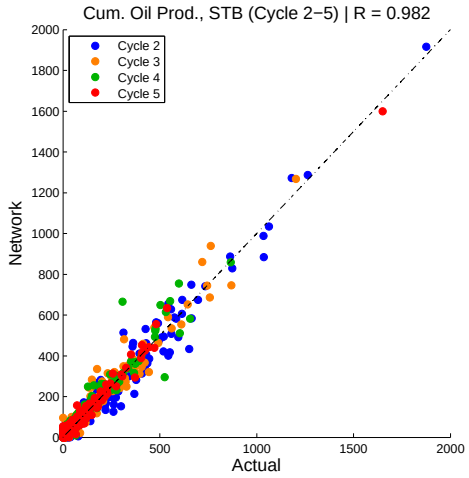

(b) Cumulative oil production - Cycles 2-5.

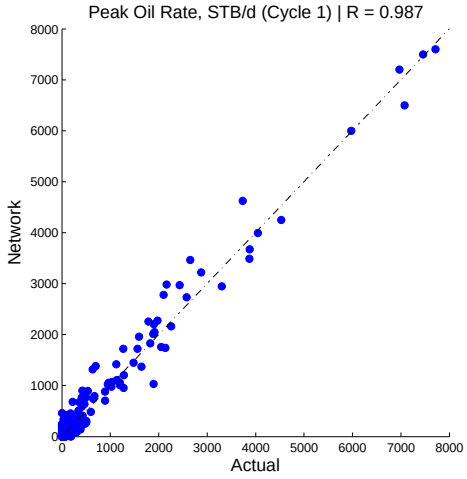

(c) Peak oil rate - Cycle 1.

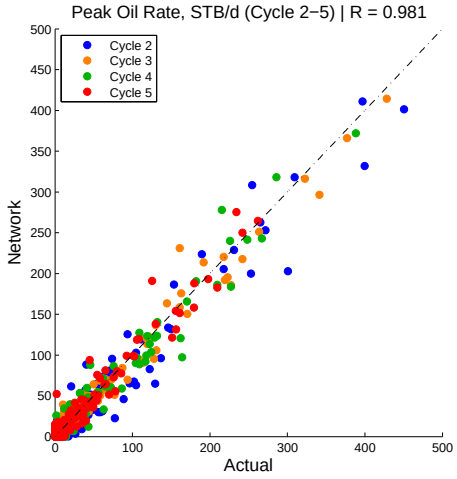

(d) Peak oil rate - Cycle 2-5.

Figure 6.9. Pure N_2 injection/Volatile Oil/Design Scheme-1: Cumulative oil production and peak oil rate predictions.

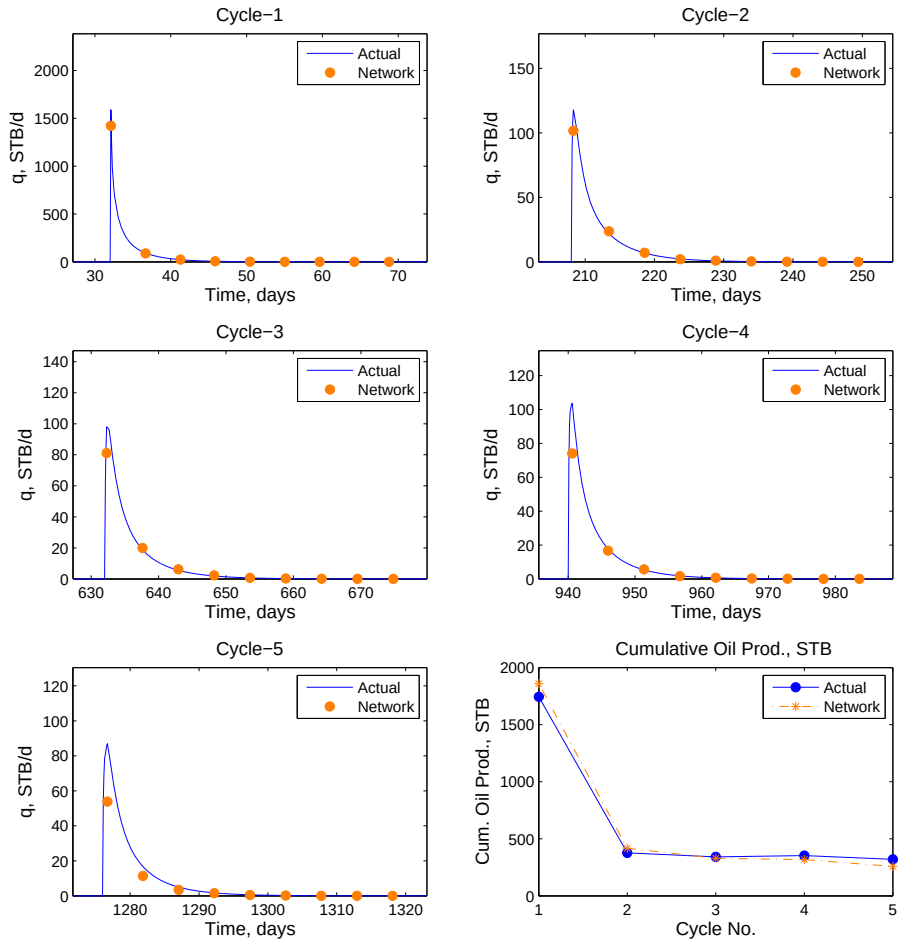

h	75 ft	$k_{m_{x,y}}$	45 md	T	215 F
A	15 acres	k_{m_z}	5.4 md	p_i	341 psia
ϕ_m	0.16	k_f	5260 md	S_{wi}	0.510
ϕ_f	0.02	X_f	35 ft	S_{oi}	0.015

Figure 6.10. Example Case 1 - Pure N_2 injection/Volatile Oil/Design Scheme-1: flow rate predictions - comparison with the actual production curves.

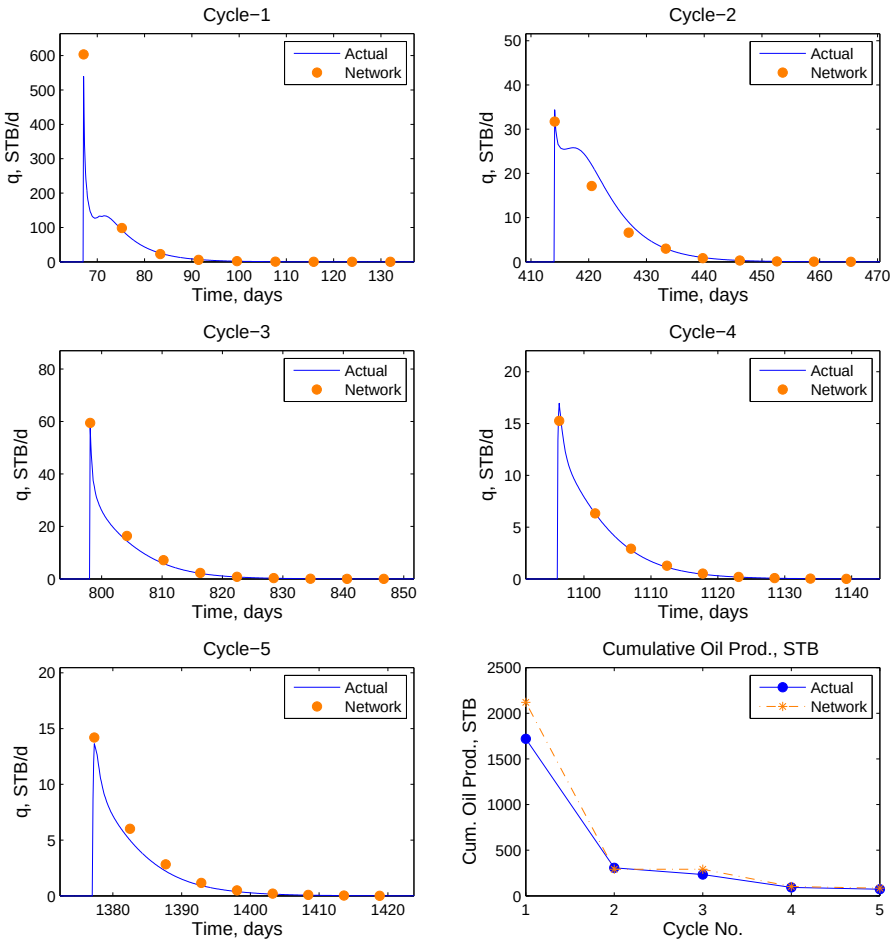

h	86 ft	$k_{m_{x,y}}$	38 md	T	178 F
A	20 acres	k_{m_z}	2.66 md	p_i	659 psia
ϕ_m	0.11	k_f	4042 md	S_{wi}	0.640
ϕ_f	0.01	X_f	940 ft	S_{oi}	0.039

Figure 6.11. Example Case 2 - Pure N_2 injection/Volatile Oil/Design Scheme-1: flow rate predictions - comparison with the actual production curves.

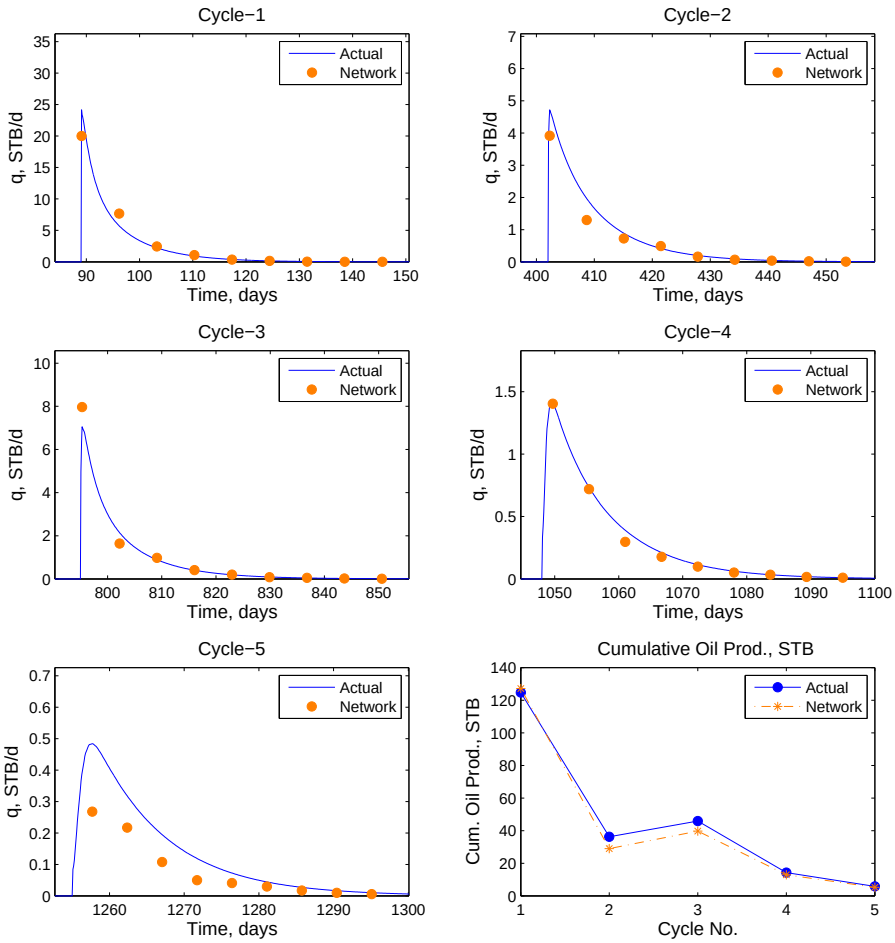

h	90 ft	$k_{m_{x,y}}$	50 md	T	152 F
A	9 acres	k_{m_z}	10.5 md	p_i	161 psia
ϕ_m	0.10	k_f	940 md	S_{wi}	0.410
ϕ_f	0.02	X_f	89 ft	S_{oi}	0.009

Figure 6.12. Example Case 3 - Pure N_2 injection/Volatile Oil/Design Scheme-1: flow rate predictions - comparison with the actual production curves.

6.2.1.2 Heavy Oil

As contrasted to volatile and black oils, the liquid portion of heavy-oil hydrocarbons dominates over the gas phase. Much higher initial oil saturations are obtained in the knowledge base ranging between 0.10 and 0.70. The average oil saturation is 0.48. Therefore, among the three compositions, higher liquid production is observed with heavy oil.

Table 6.7 shows the correlation coefficients of the predictions of the neural network when applied to training, validation and testing data sets. Figure 6.13 shows the actual and network-predicted total production time. It should be noted that the total producing time is much longer than the cases with black oil and volatile oil, which is a direct consequence of the phase behavior characteristics. As a result of higher liquid saturation, liquid production lasts for a much longer time.

Figure 6.14 shows the cross-plots of actual and network-predicted cumulative oil productions and peak oil rates. Because of the large difference in the range of production amounts of the first cycle and other cycles, Cycle 1 and Cycle 2-5 are shown in two different plots. Figure 6.14-a is the cumulative oil production of Cycle-1 and Figure 6.14-b shows the cumulative oil production of Cycles 2 through 5. Figure 6.14-c is the peak oil rate of Cycle-1 and Figure 6.14-d shows the peak oil rates of Cycles 2 through 5. Both correlation statistics and visual plots show that the network is able to predict the critical performance indicators with a high degree of accuracy. In Figures 6.15 through 6.17, comparison of the actual production histories and predicted flow rates are presented for three different cases. It is observed while the magnitude of the flow rates change significantly from one cycle to another, the network is able to make accurate predictions. Again, the peak oil rate is the one with highest error due to its instantaneous nature. However, the predictions are always found to be within a reasonable degree of accuracy.

Table 6.7. Correlation coefficients of N_2 injection/Heavy Oil/Design Scheme-1 neural network model.

	Cycle 1	**Cycle 2**	**Cycle 3**	**Cycle 4**	**Cycle 5**
Training					
Cumulative Oil Production	0.98	0.97	0.97	0.97	0.96
$t_{q>0}$	0.95	0.97	0.97	0.96	0.97
Flow Rates	0.98	0.97	0.95	0.94	0.95
Validation					
Cumulative Oil Production	0.98	0.96	0.96	0.93	0.78
$t_{q>0}$	0.91	0.83	0.83	0.82	0.90
Flow Rates	0.97	0.96	0.94	0.92	0.85
Testing					
Cumulative Oil Production	0.98	0.95	0.97	0.96	0.81
$t_{q>0}$	0.91	0.82	0.82	0.77	0.95
Flow Rates	0.97	0.96	0.95	0.92	0.86

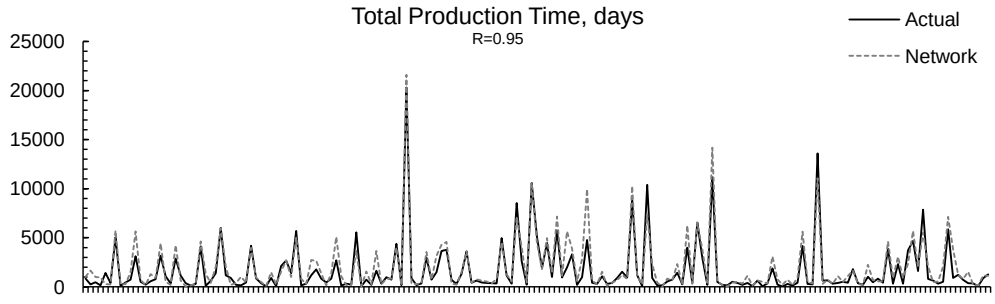

Figure 6.13. Pure N_2 injection/Heavy Oil/Design Scheme-1: Total production time predictions.

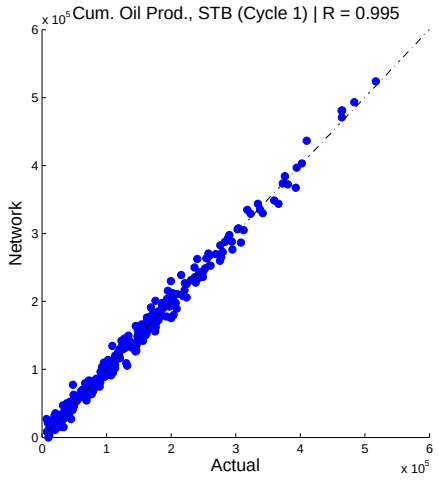

(a) Cumulative oil production - Cycle 1.

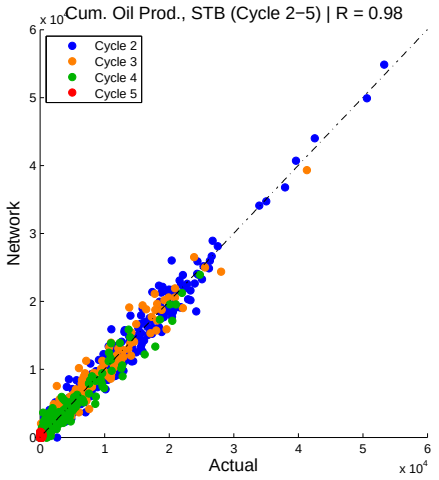

(b) Cumulative oil production - Cycles 2-5.

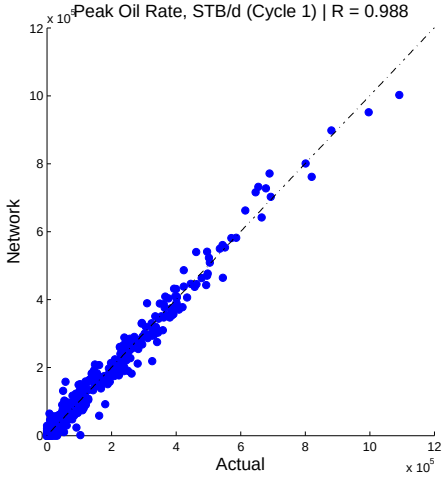

(c) Peak oil rate - Cycle 1.

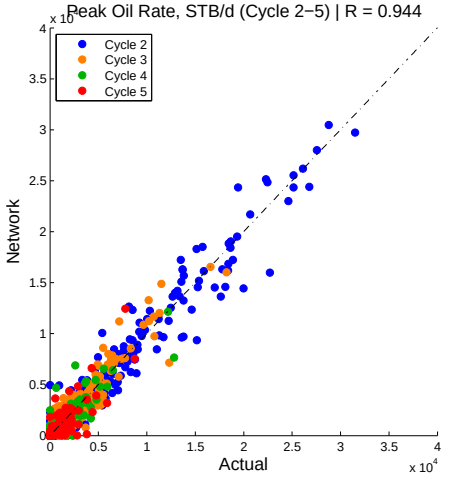

(d) Peak oil rate - Cycle 2-5.

Figure 6.14. Pure N_2 injection/Heavy Oil/Design Scheme-1: Cumulative oil production and peak oil rate predictions.

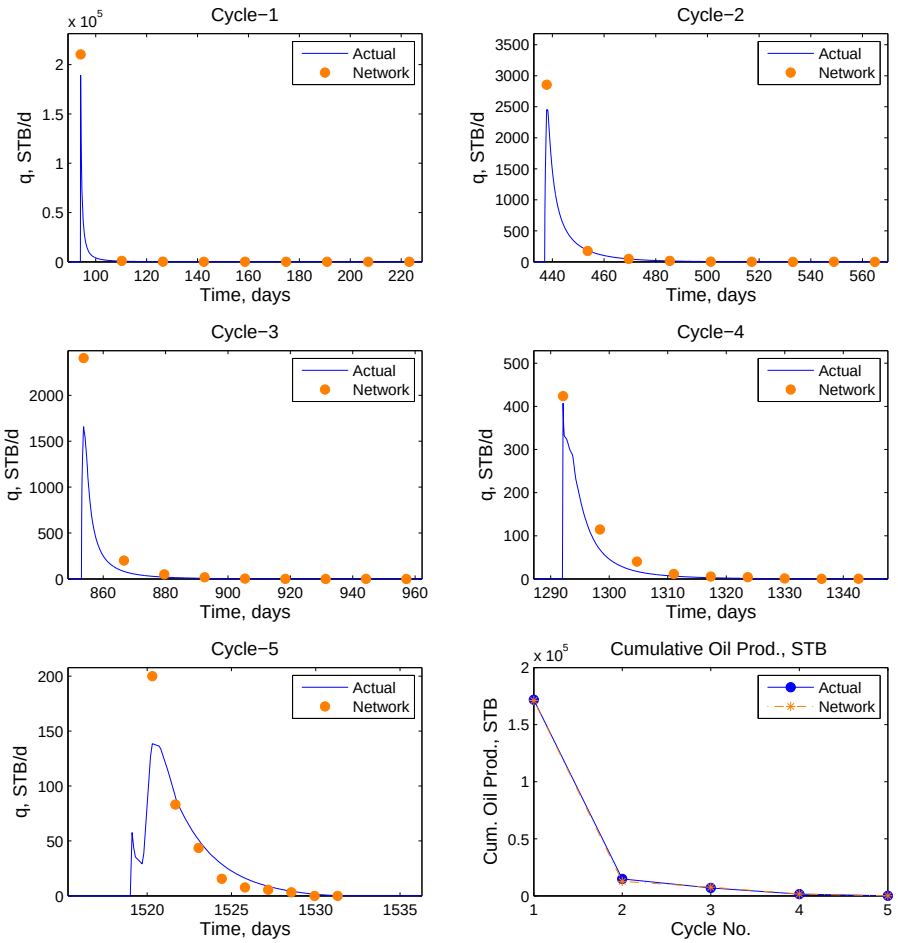

h	91 ft	$k_{m_{x,y}}$	59 md	T	235 F
A	7 acres	k_{m_z}	12.39 md	p_i	802 psia
ϕ_m	0.14	k_f	1,011 md	S_{wi}	0.42
ϕ_f	0.02	X_f	71 ft	S_{oi}	0.58

Figure 6.15. Example Case 1 - Pure N_2 injection/Heavy Oil/Design Scheme-1: flow rate predictions - comparison with the actual production curves.

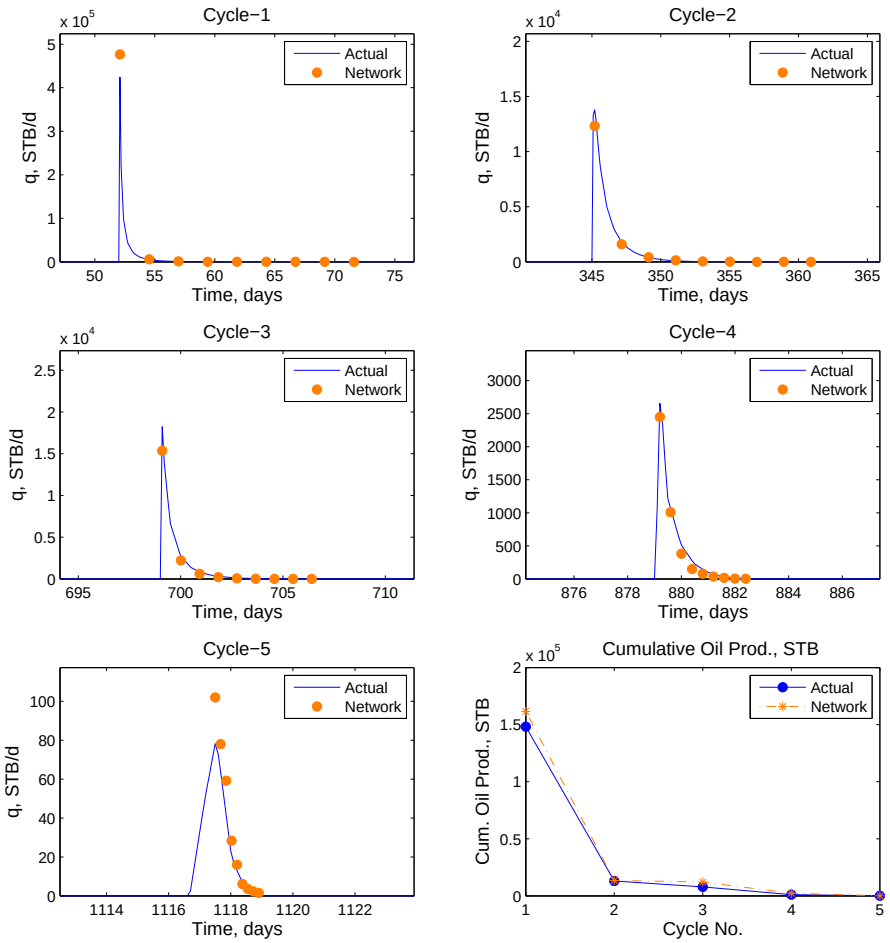

h	76 ft	$k_{m_{x,y}}$	96 md	T	190 F
A	10 acres	k_{m_z}	2.88 md	p_i	705 psia
ϕ_m	0.10	k_f	3,012 md	S_{wi}	0.61
ϕ_f	0.02	X_f	87 ft	S_{oi}	0.39

Figure 6.16. Example Case 2 - Pure N_2 injection/Heavy Oil/Design Scheme-1: flow rate predictions - comparison with the actual production curves.

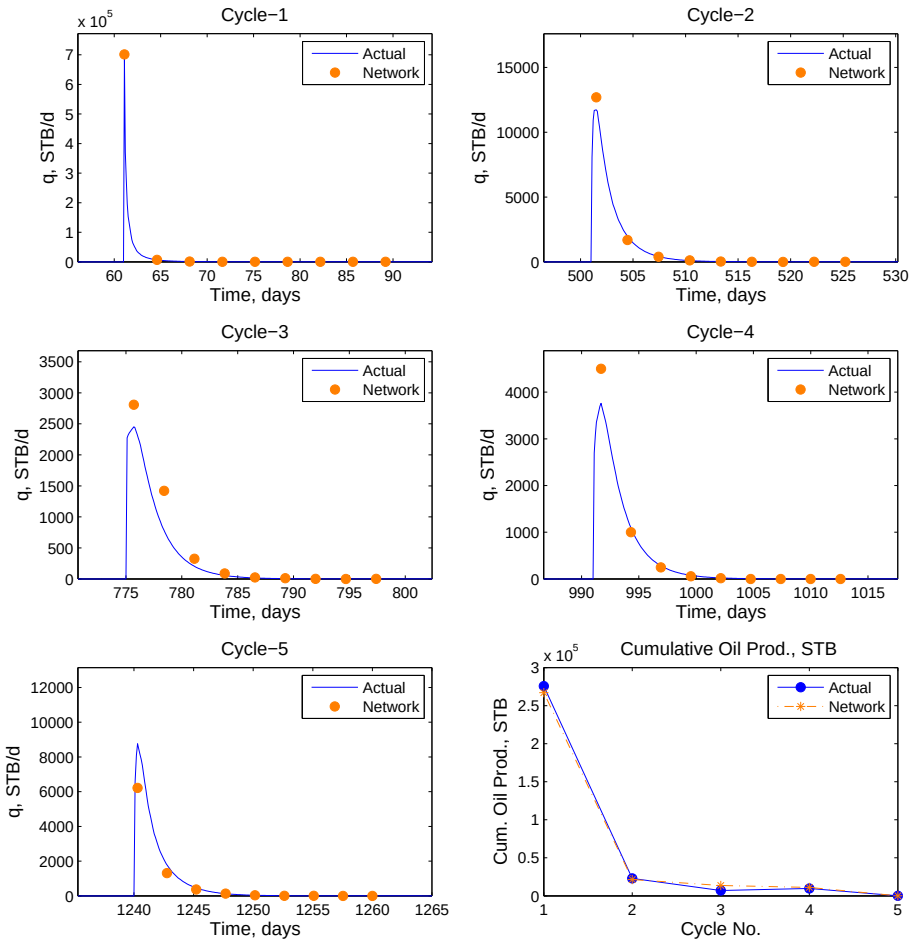

h	38 ft	$k_{m_{x,y}}$	66 md	T	161 F
A	10 acres	k_{m_z}	5.28 md	p_i	689 psia
ϕ_m	0.11	k_f	4,339 md	S_{wi}	0.37
ϕ_f	0.01	X_f	53 ft	S_{oi}	0.58

Figure 6.17. Example Case 3 - Pure N_2 injection/Heavy Oil/Design Scheme-1: flow rate predictions - comparison with the actual production curves.

6.2.1.3 Black Oil

With the black oil cases, initial oil saturations are obtained in the knowledge base ranging between 0.01 and 0.62. The average oil saturation is 0.24, which is at an intermediate level as compared to heavy and volatile oils. Table 6.8 shows the correlation coefficients of the predictions of the neural network when applied to training, validation and testing data sets. Figure 6.18 shows the actual and network-predicted total production time. Figure 6.19 shows the cross-plots of actual and network-predicted cumulative oil productions and peak oil rates. In Figures 6.20 through 6.22, comparison of the actual production histories and predicted flow rates are presented for three different cases. It is important to note that in Example Case-3 where the flow rate after the first cycle is very close to zero, the neural network output very low flow rates. This shows that the network is able to provide accurate predictions in rather extreme conditions.

Table 6.8. Correlation coefficients of N_2 injection/Black Oil/Design Scheme-1 neural network model.

	Cycle 1	**Cycle 2**	**Cycle 3**	**Cycle 4**	**Cycle 5**
Training					
Cumulative Oil Production	0.99	0.99	0.98	0.98	0.98
$t_{q>0}$	0.98	0.99	0.99	0.98	0.98
Flow Rates	0.99	0.97	0.98	0.98	0.98
Validation					
Cumulative Oil Production	0.98	0.96	0.89	0.88	0.90
$t_{q>0}$	0.93	0.91	0.91	0.89	0.93
Flow Rates	0.95	0.91	0.92	0.80	0.80
Testing					
Cumulative Oil Production	0.98	0.81	0.88	0.87	0.82
$t_{q>0}$	0.90	0.92	0.92	0.93	0.91
Flow Rates	0.96	0.95	0.94	0.82	0.80

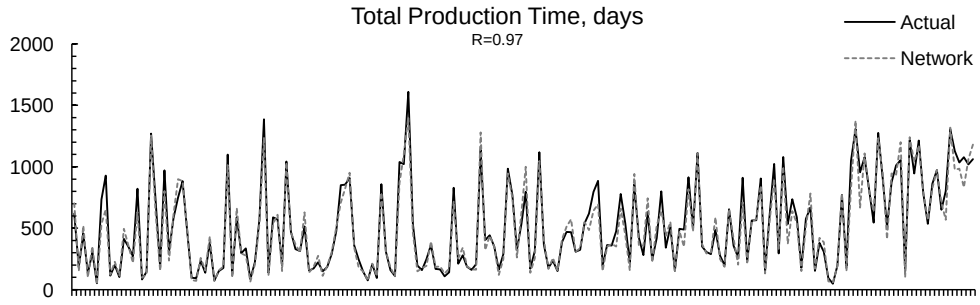

Figure 6.18. Pure N_2 injection/Black Oil/Design Scheme-1: Total production time predictions.

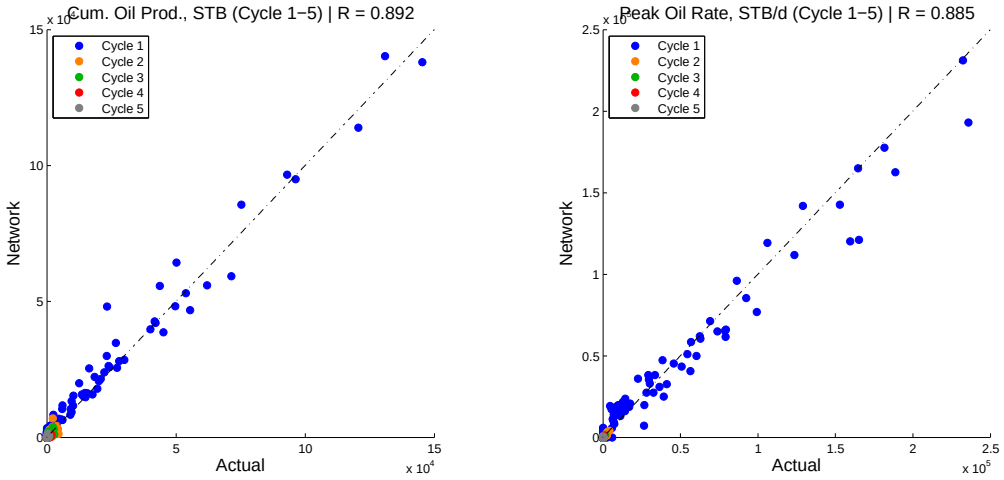

(a) Cumulative oil production - Cycle 1-5.

(b) Peak oil rate - Cycle 1-5.

Figure 6.19. Pure N_2 injection/Black Oil/Design Scheme-1: Cumulative oil production and peak oil rate predictions.

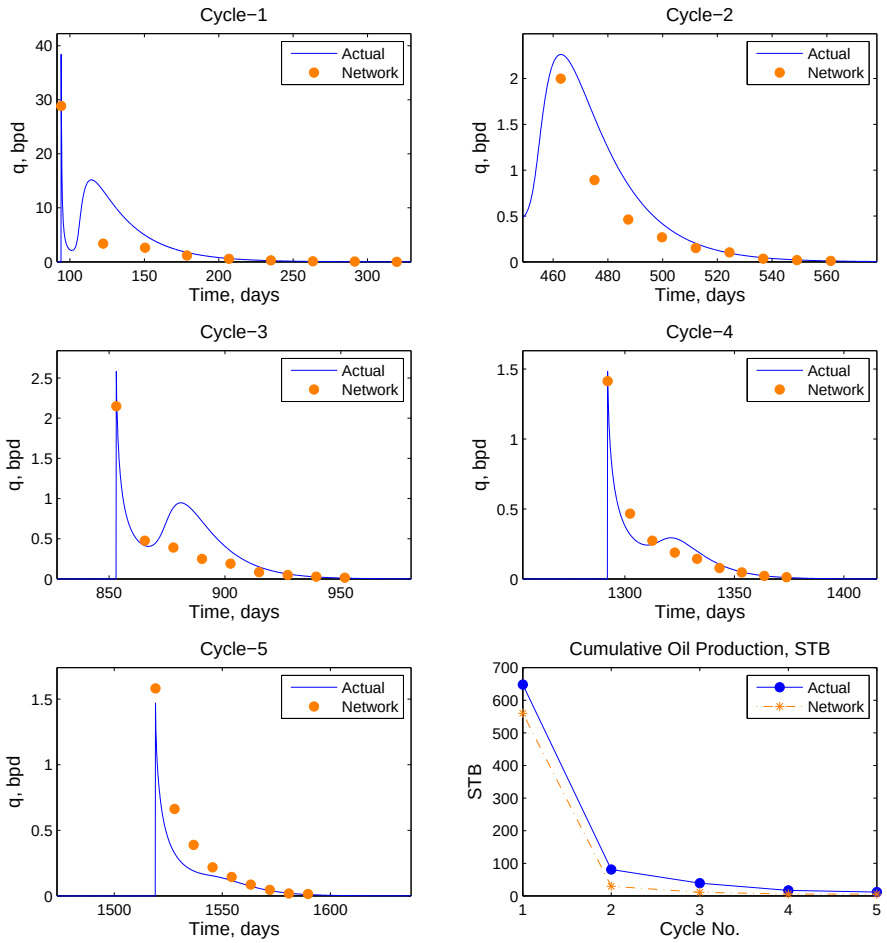

h	91 ft	$k_{m_{x,y}}$	59 md	T	235 F
A	7 acres	k_{m_z}	12.39 md	p_i	802 psia
ϕ_m	0.14	k_f	1,011 md	S_{wi}	0.42
ϕ_f	0.02	X_f	71 ft	S_{oi}	0.58

Figure 6.20. Example Case 1 - Pure N_2 injection/Black Oil/Design Scheme-1: flow rate predictions - comparison with the actual production curves.

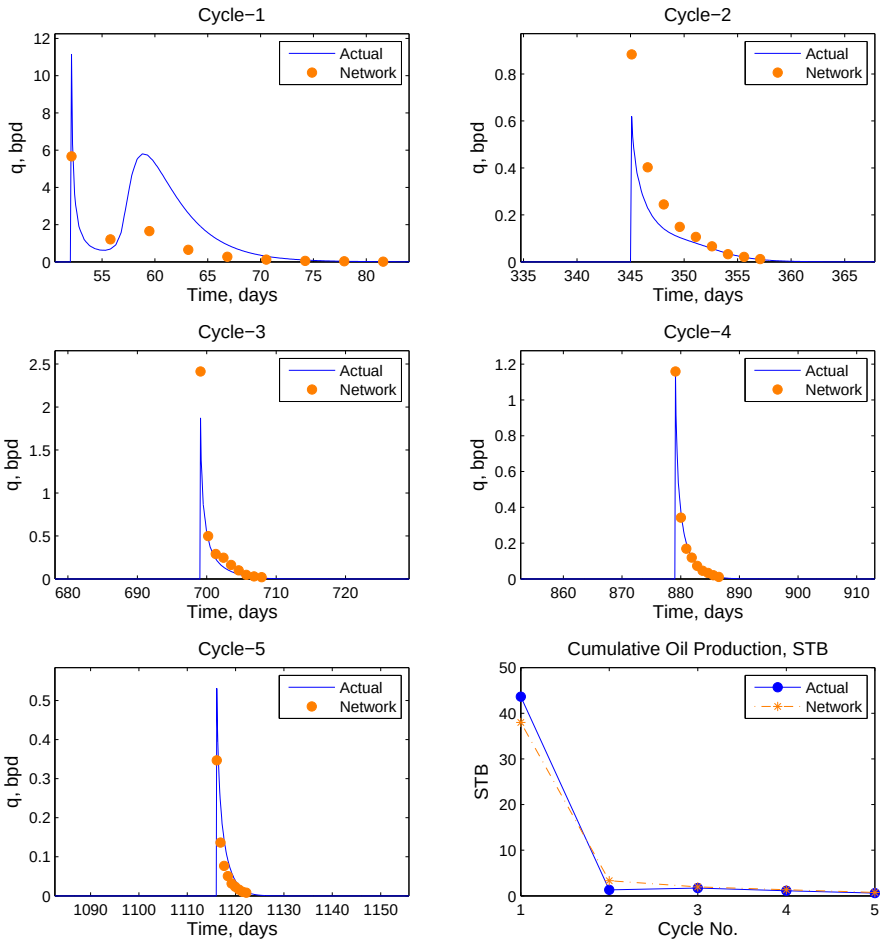

h	94 ft	$k_{m_{x,y}}$	58 md	T	174 F
A	7 acres	k_{m_z}	12.76 md	p_i	689 psia
ϕ_m	0.13	k_f	8,429 md	S_{wi}	0.46
ϕ_f	0.02	X_f	43 ft	S_{oi}	0.54

Figure 6.21. Example Case 2 - Pure N_2 injection/Black Oil/Design Scheme-1: flow rate predictions - comparison with the actual production curves.

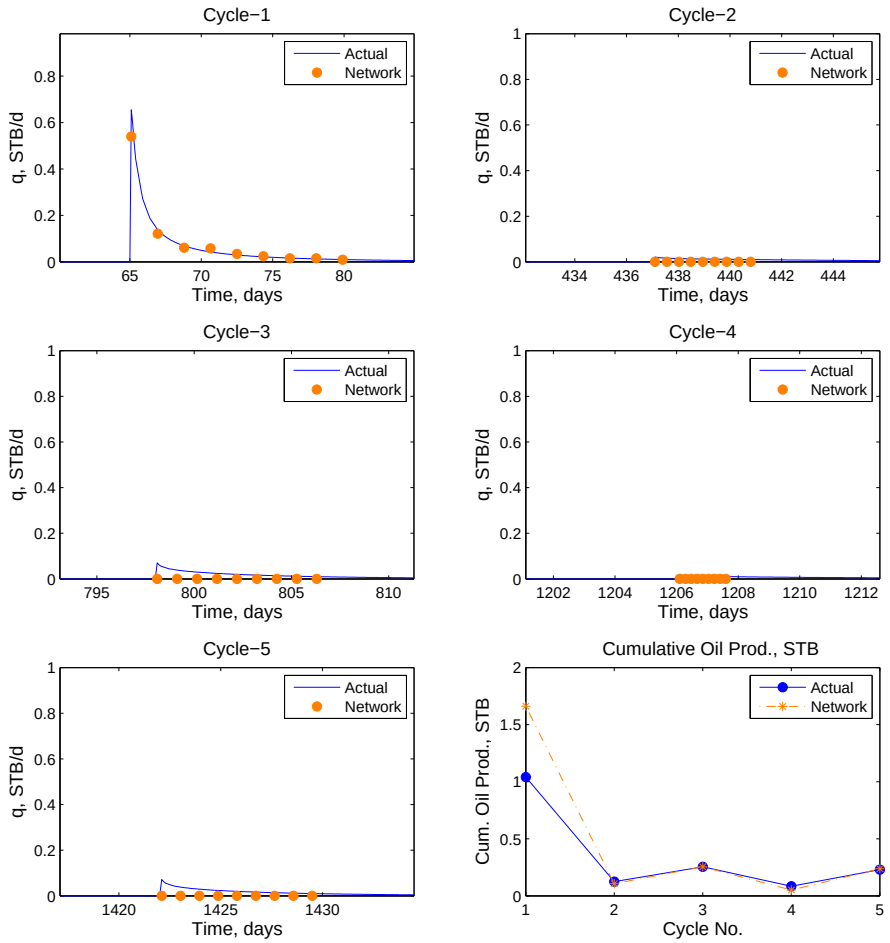

h	73 ft	$k_{m_{x,y}}$	70 md	T	129 F
A	18 acres	k_{m_z}	10.5 md	p_i	327 psia
ϕ_m	0.18	k_f	5328 md	S_{wi}	0.63
ϕ_f	0.02	X_f	55 ft	S_{oi}	0.10

Figure 6.22. Example Case 3 - Pure N_2 injection/Black Oil/Design Scheme-1: flow rate predictions - comparison with the actual production curves.

6.2.2 Pure CO_2 Injection Predictions

Table 6.9 shows the contribution factors of each input parameter on the sum of outputs for the cases with pure CO_2 injection. Neural network models for heavy, black and volatile oil compositions are shown in separate columns. The magnitude of each input's contribution factor is an indication of the importance of each reservoir property and process design parameter in the performance of the cyclic pressure pulsing process. Comparing with the case with nitrogen (Table 6.5), observations are, in general, similar. Similarly, in all three types of oils, fracture permeability, ratio of fracture permeability to matrix permeability, oil-in-place, area, Ah product, and oil saturation are the parameters that significantly contributed to the network more. The contribution of matrix permeability itself is limited. Contribution of initial pressure and temperature of the reservoir are more significant in the volatile oil than in black and heavy oils. Fracture porosity and fracture spacing are the other reservoir characteristics that have little contributions. In terms of the design parameters, volume of the injected gas is the most critical parameter. Injection period, injection rate, and production rate are at a comparable rank in all three types of oils. Soaking period is the least contributor.

6.2.2.1 Volatile Oil

Table 6.10 shows the correlation coefficients of the predictions of the neural network when applied to training, validation and testing data sets. Figure 6.23 shows the actual and network-predicted total production time. Figure 6.24-a is the cumulative oil production of Cycle-1 and Figure 6.24-b shows the cumulative oil production of Cycles 2 through 5. Figure 6.24-c is the peak oil rate of Cycle-1 and Figure 6.24-d shows the peak oil rates of Cycles 2 through 5. Both correlation statistics and visual plots show that the network is able to predict the critical performance indicators with a high accuracy. In Figures 6.25 through 6.27, comparison of the actual production histories and predicted flow rates are presented for three different cases. These results show that a similar level of accuracy is obtained with the CO_2 injection case as with the N_2 injection.

Table 6.9. Contribution factors of each input parameter on the sum of outputs for each neural network model developed for CO_2 injection.

	Heavy Oil		Black Oil		Volatile Oil	
Rank	Input	C.F.	Input	C.F.	Input	C.F.
1	k_f	4.27	k_{roi}	4.78	k_f	4.73
2	k_f/k_m	3.00	k_f	4.64	T	3.88
3	k_{rwi}	2.97	k_f/k_m	4.02	k_f/k_m	3.75
4	S_{oi}	2.44	OIP	3.09	k_{roi}	3.19
5	OIP	2.26	S_{oi}	2.74	OIP	2.96
6	k_{roi}	2.22	S_{wi}	1.82	A	2.18
7	A	2.22	A	1.80	S_{oi}	2.01
8	S_{wi}	2.19	T	1.79	p_i	1.97
9	Ah	1.99	Ah	1.66	Ah	1.73
10	h	1.87	k_{rwi}	1.62	k_{rwi}	1.67
11	Inj. Volume*	1.53	p_i	1.52	h	1.65
12	k_{m_z}	1.44	Inj. Volume*	1.41	Inj. Volume*	1.44
13	T	1.35	h	1.40	S_{wi}	1.41
14	p_i	1.30	ϕ_m	1.39	ϕ_m	1.27
15	Inj. Rate*	1.25	k_{m_z}	1.36	X_f	1.17
16	X_f	1.24	Inj. Period*	1.15	k_{m_z}	1.11
17	Inj. Period*	1.23	Inj. Rate*	1.15	Inj. Rate*	1.11
18	$k_{m_{x,y}}$	1.21	Prod. Period*	1.13	Inj. Period*	1.09
19	Prod. Period*	1.20	X_f	1.01	Prod. Period*	1.08
20	ϕ_m	1.19	Soak. Period*	0.93	$k_{m_{x,y}}$	0.98
21	Soak. Period*	0.99	$k_{m_{x,y}}$	0.86	Soak. Period*	0.97
22	ϕ_f	0.83	ϕ_f	0.67	ϕ_f	0.89

Table 6.10. Correlation coefficients of CO_2 injection/Volatile Oil/Design Scheme-1 neural network model.

	Cycle 1	**Cycle 2**	**Cycle 3**	**Cycle 4**	**Cycle 5**
Training					
Cumulative Oil Production	0.99	0.98	0.98	0.98	0.98
$t_{q>0}$	0.97	0.98	0.98	0.97	0.97
Flow Rates	0.98	0.98	0.99	0.98	0.98
Validation					
Cumulative Oil Production	0.98	0.92	0.96	0.97	0.97
$t_{q>0}$	0.93	0.93	0.93	0.91	0.93
Flow Rates	0.95	0.97	0.97	0.97	0.97
Testing					
Cumulative Oil Production	0.98	0.96	0.96	0.97	0.96
$t_{q>0}$	0.95	0.90	0.90	0.93	0.93
Flow Rates	0.98	0.97	0.97	0.98	0.97

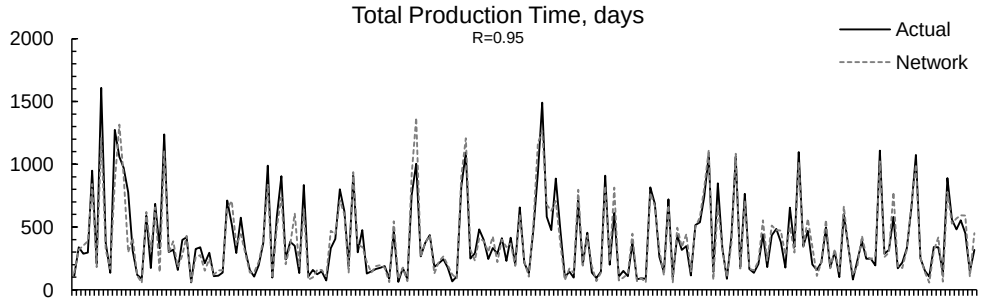

Figure 6.23. Pure CO_2 injection/Volatile Oil/Design Scheme-1: Total production time predictions.

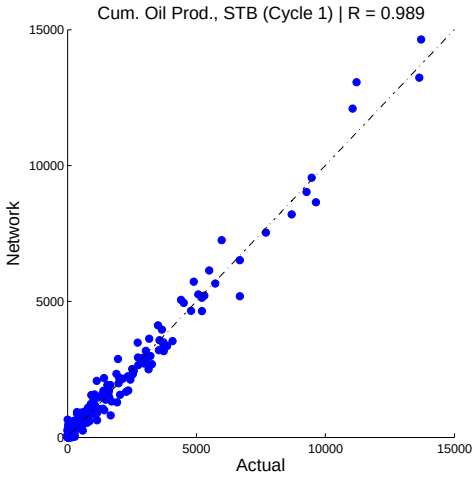

(a) Cumulative oil production - Cycle 1.

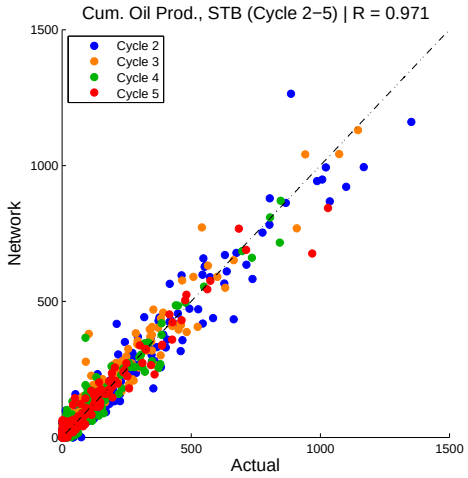

(b) Cumulative oil production - Cycles 2-5.

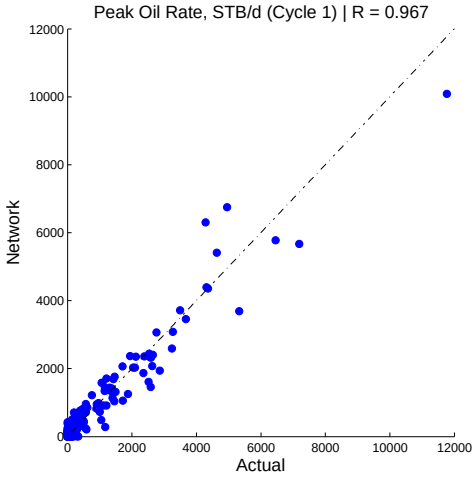

(c) Peak oil rate - Cycle 1.

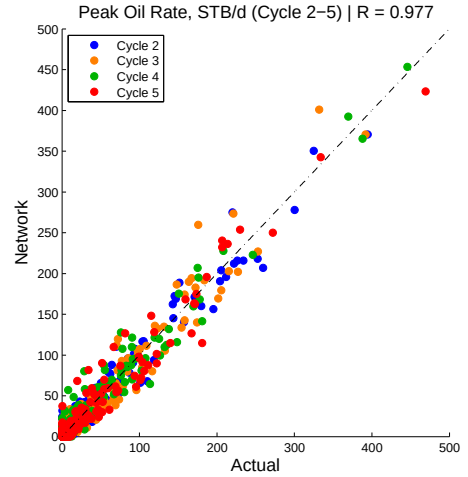

(d) Peak oil rate - Cycle 2-5.

Figure 6.24. Pure CO_2 injection/Volatile Oil/Design Scheme-1: Cumulative oil production and peak oil rate predictions.

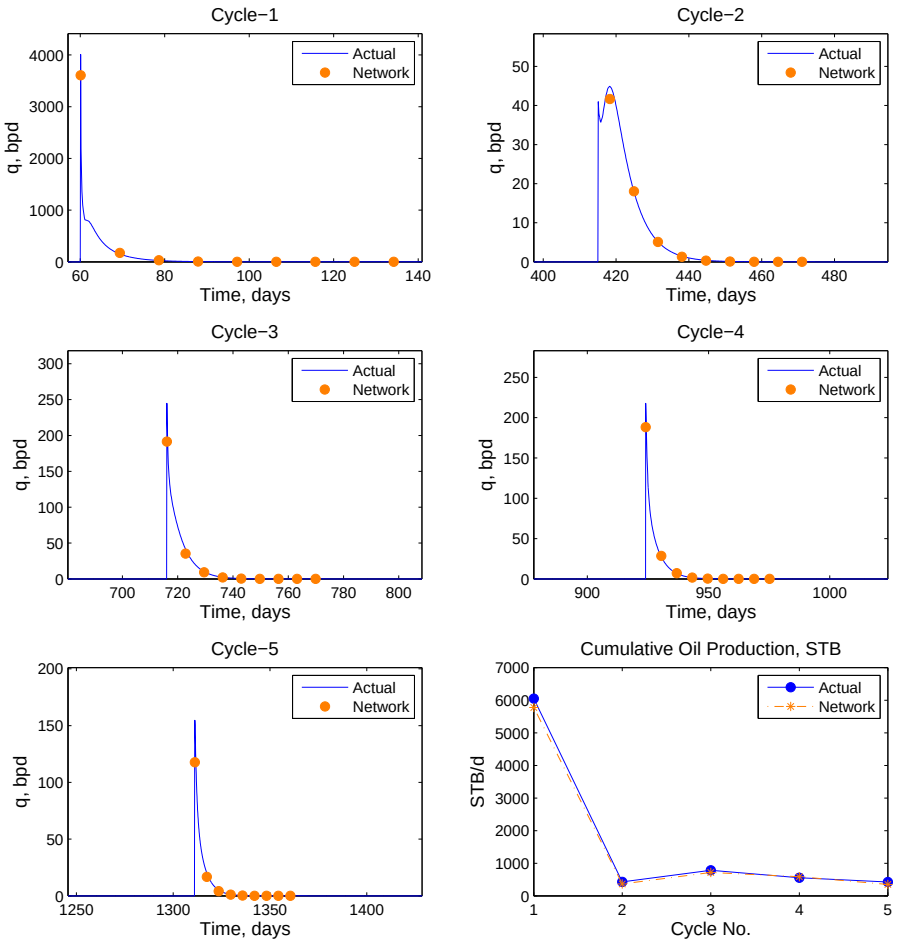

h	38 ft	$k_{m_{x,y}}$	26 md	T	225 F
A	17 acres	k_{m_z}	4.42 md	p_i	1,352 psia
ϕ_m	0.19	k_f	8,249 md	S_{wi}	0.57
ϕ_f	0.02	X_f	44 ft	S_{oi}	0.11

Figure 6.25. Example Case 1 - Pure CO_2 injection/Volatile Oil/Design Scheme-1: flow rate predictions - comparison with the actual production curves.

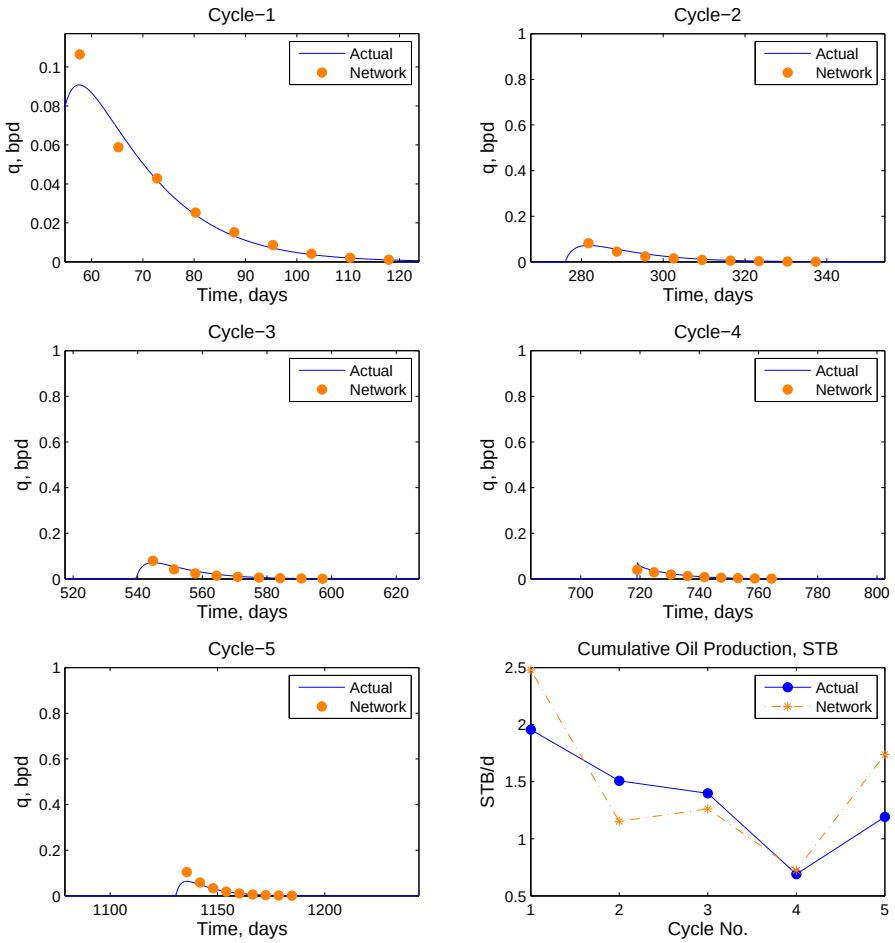

h	74 ft	$k_{m_{x,y}}$	19 md	T	80 F
A	9 acres	k_{m_z}	1.33 md	p_i	232 psia
ϕ_m	0.19	k_f	1,288 md	S_{wi}	0.62
ϕ_f	0.02	X_f	51 ft	S_{oi}	0.02

Figure 6.26. Example Case 2 - Pure CO_2 injection/Volatile Oil/Design Scheme-1: flow rate predictions - comparison with the actual production curves.

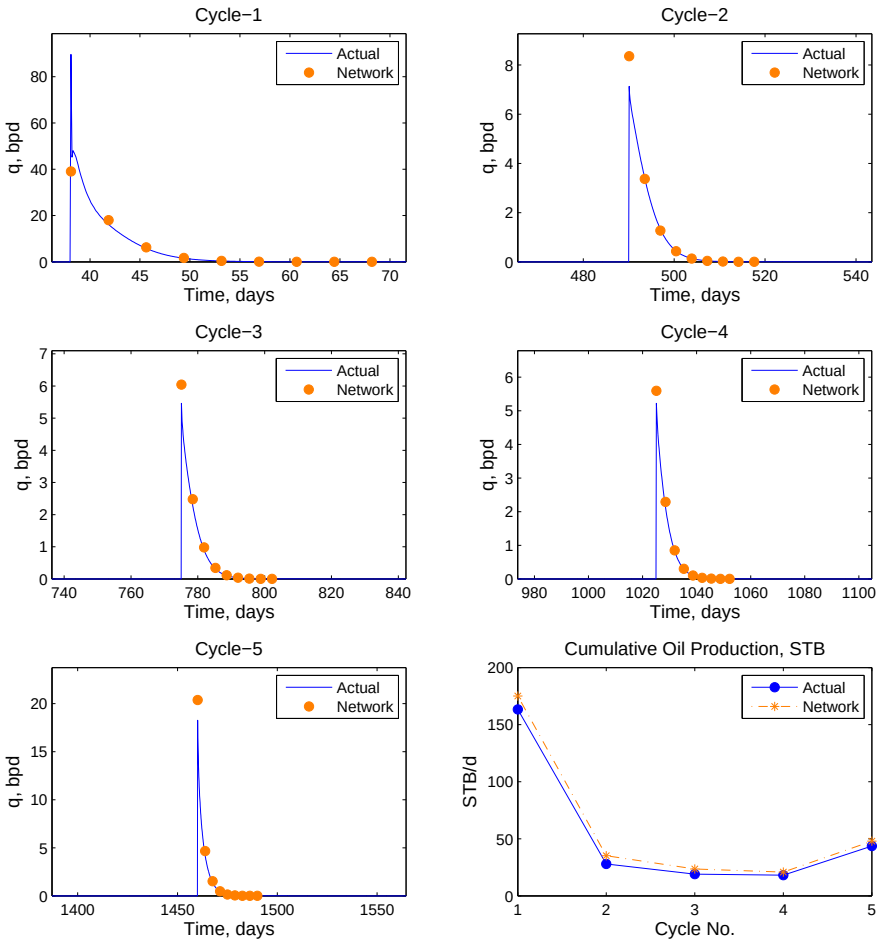

h	84 ft	$k_{m_{x,y}}$	99 md	T	129 F
A	15 acres	k_{m_z}	12.87 md	p_i	222 psia
ϕ_m	0.16	k_f	7,526 md	S_{wi}	0.50
ϕ_f	0.02	X_f	27 ft	S_{oi}	0.02

Figure 6.27. Example Case 3 - Pure CO_2 injection/Volatile Oil/Design Scheme-1: flow rate predictions - comparison with the actual production curves.

6.2.2.2 Heavy Oil

As in the case with nitrogen, higher oil production is observed with heavy oil because of the phase behavior characteristics that yield higher liquid hydrocarbon saturation than volatile and black oils. Correlation coefficients of the predictions of the trained neural network model are shown in Table 6.11. Correlation coefficients are shown separately for training, validation and testing data sets. Figure 6.28 shows the actual and network-predicted total production time. Again, a longer total producing time is observed than with black oil and volatile oil. Figure 6.29 shows the cross-plots of actual and network-predicted cumulative oil productions and peak oil rates. The cumulative oil production of Cycle-1 is shown in Figure 6.29-a and Cycles 2 through 5 are shown in Figure 6.29-b. Figure 6.29-c is the peak oil rate of Cycle-1 and Figure 6.29-d shows the peak oil rates of Cycles 2 through 5. Both correlation statistics and plots show that the network is able to predict the critical performance indicators with a high degree of accuracy for the pure CO_2 injection case in a heavy oil reservoir. In Figures 6.30 through 6.32, comparison of the actual production histories and predicted flow rates are presented for three different cases. These plots also show that the predicted flow rates are in good agreement with the actual production histories as output by the simulator.

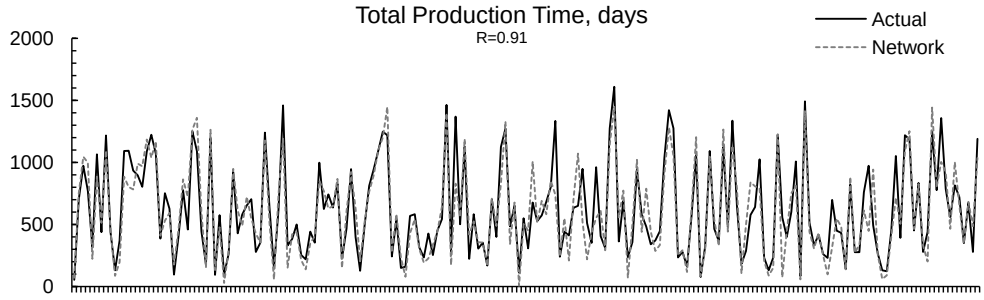

Figure 6.28. Pure CO_2 injection/Heavy Oil/Design Scheme-1: Total production time predictions.

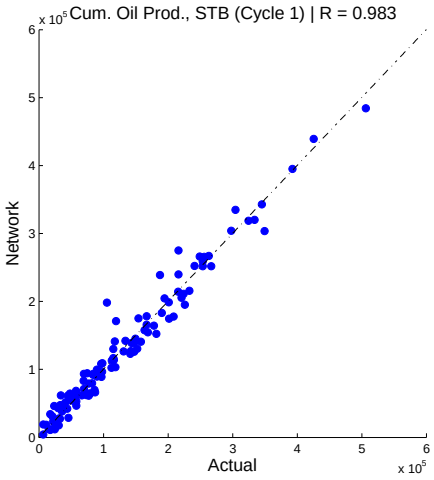

(a) Cumulative oil production - Cycle 1.

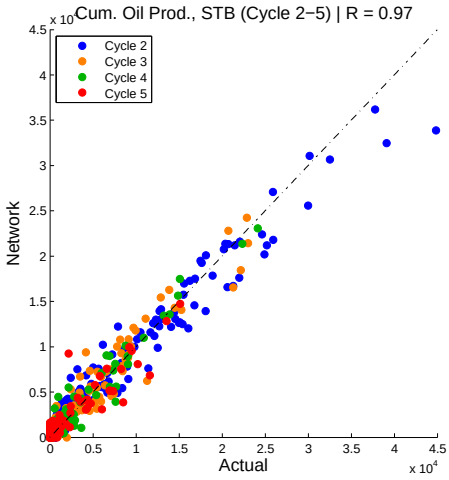

(b) Cumulative oil production - Cycles 2-5.

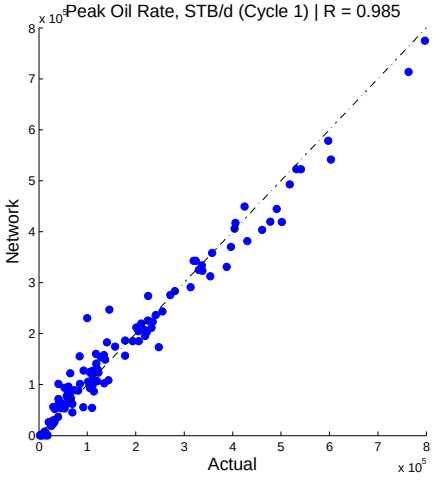

(c) Peak oil rate - Cycle 1.

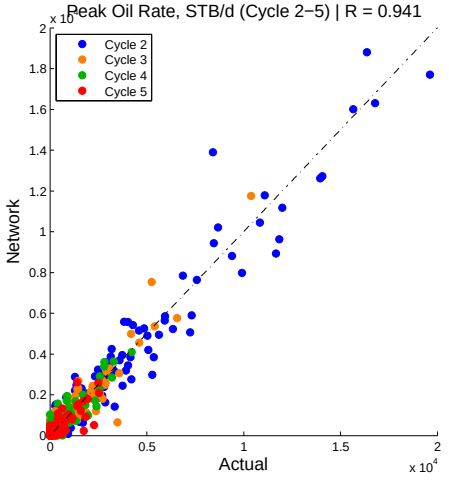

(d) Peak oil rate - Cycle 2-5.

Figure 6.29. Pure CO_2 injection/Heavy Oil/Design Scheme-1: Cumulative oil production and peak oil rate predictions.

Table 6.11. Correlation coefficients of CO_2 injection/Heavy Oil/Design Scheme-1 neural network model.

	Cycle 1	**Cycle 2**	**Cycle 3**	**Cycle 4**	**Cycle 5**
Training					
Cumulative Oil Production	0.98	0.97	0.97	0.96	0.86
$t_{q>0.001}$	0.95	0.96	0.96	0.94	0.94
Flow Rates	0.98	0.97	0.95	0.94	0.95
Validation					
Cumulative Oil Production	0.98	0.95	0.95	0.93	0.86
$t_{q>0.001}$	0.88	0.84	0.84	0.80	0.80
Flow Rates	0.97	0.94	0.93	0.93	0.90
Testing					
Cumulative Oil Production	0.98	0.94	0.95	0.91	0.88
$t_{q>0.001}$	0.85	0.82	0.82	0.81	0.81
Flow Rates	0.97	0.94	0.94	0.88	0.87

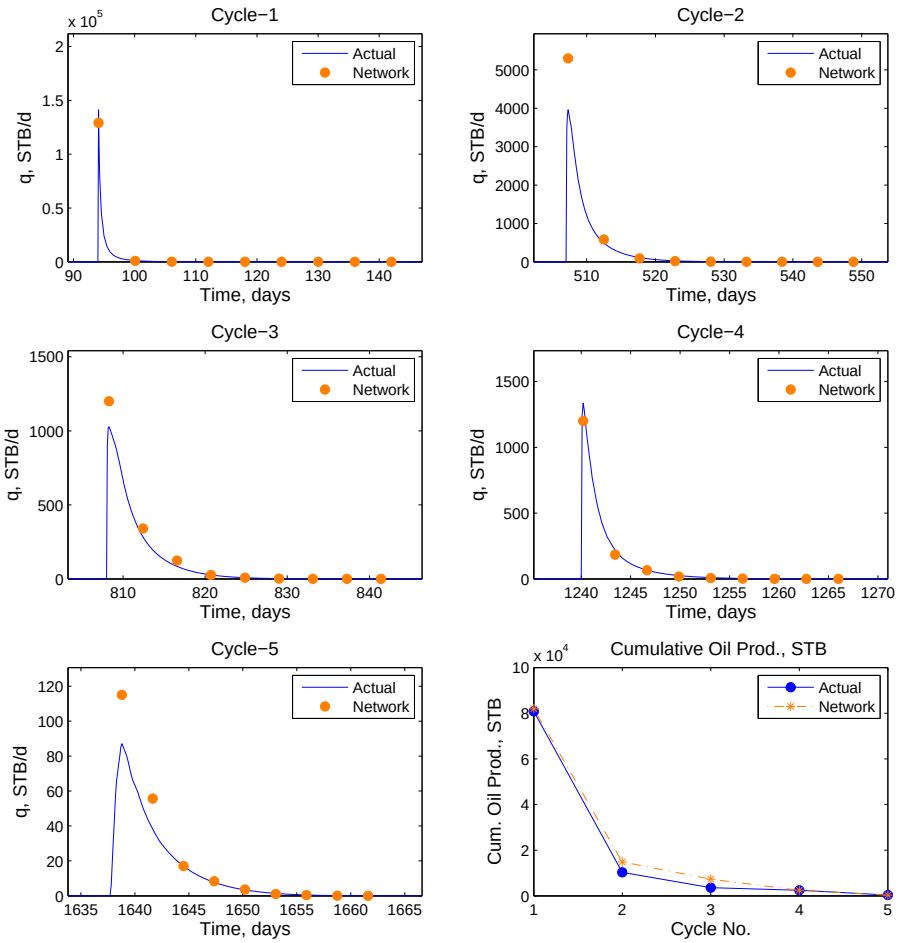

h	21 ft	$k_{m_{x,y}}$	26 md	T	109 F
A	16 acres	k_{m_z}	4.42 md	p_i	299 psia
ϕ_m	0.15	k_f	8,780 md	S_{wi}	0.41
ϕ_f	0.02	X_f	84 ft	S_{oi}	0.55

Figure 6.30. Example Case 1 - Pure CO_2 injection/Heavy Oil/Design Scheme-1: flow rate predictions - comparison with the actual production curves.

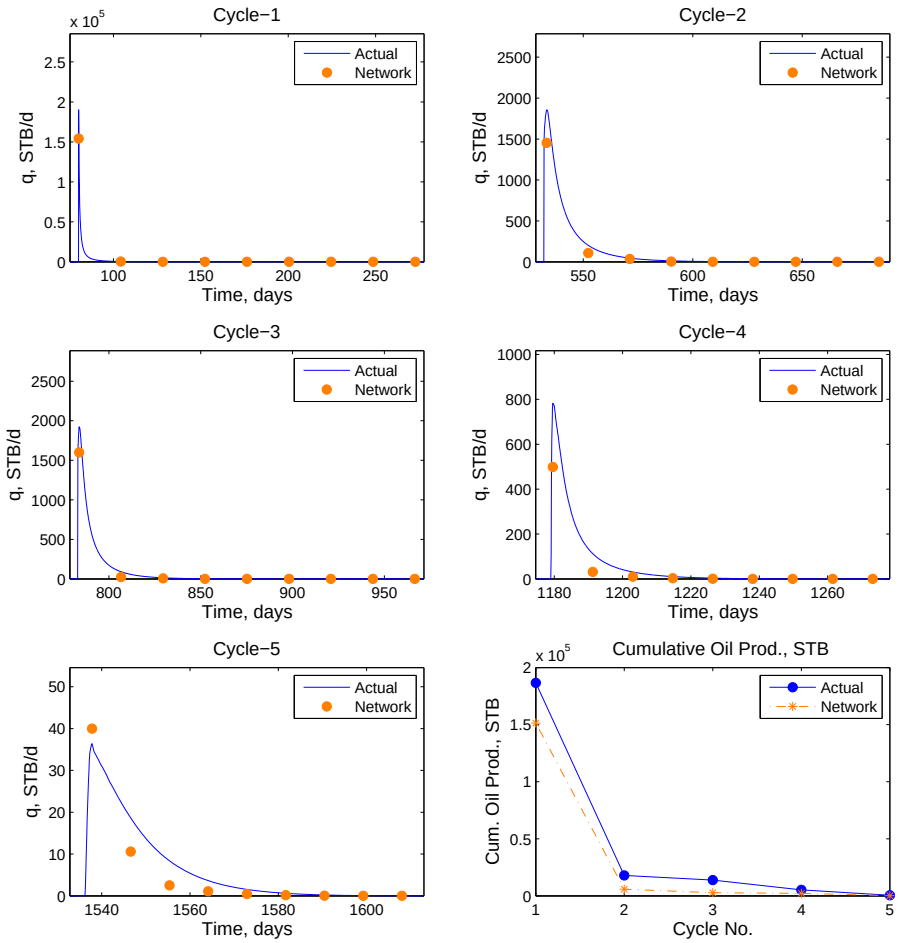

h	39 ft	$k_{m_{x,y}}$	68 md	T	90 F
A	15 acres	k_{m_z}	2.04 md	p_i	1,328 psia
ϕ_m	0.19	k_f	2,740 md	S_{wi}	0.45
ϕ_f	0.02	X_f	96 ft	S_{oi}	0.55

Figure 6.31. Example Case 2 - Pure CO_2 injection/Heavy Oil/Design Scheme-1: flow rate predictions - comparison with the actual production curves.

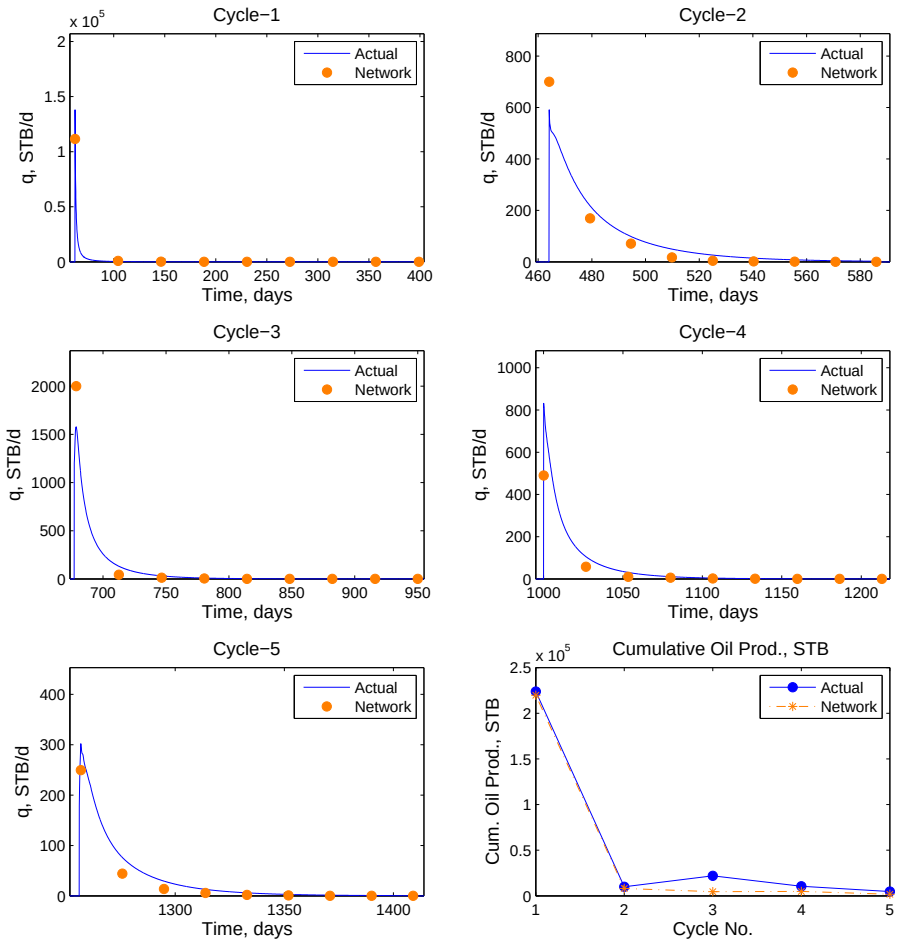

h	73 ft	$k_{m_{x,y}}$	9 md	T	120 F
A	9 acres	k_{m_z}	1.26 md	p_i	903 psia
ϕ_m	0.18	k_f	759 md	S_{wi}	0.38
ϕ_f	0.01	X_f	42 ft	S_{oi}	0.62

Figure 6.32. Example Case 3 - Pure CO_2 injection/Heavy Oil/Design Scheme-1: flow rate predictions - comparison with the actual production curves.

6.2.2.3 Black Oil

Table 6.12 shows the correlation coefficients of the predictions of the neural network when applied to training, validation and testing data sets. Figure 6.33 shows the actual and network-predicted total production time. Figure 6.34 shows the cross-plots of actual and network-predicted cumulative oil productions and peak oil rates. In Figures 6.35 through 6.37, comparison of the actual production histories and predicted flow rates are presented for three different cases. Again, similar levels of accuracy with the nitrogen injection are obtained in this case.

Table 6.12. Correlation coefficients of CO_2 injection/Black Oil/Design Scheme-1 neural network model.

	Cycle 1	**Cycle 2**	**Cycle 3**	**Cycle 4**	**Cycle 5**
Training					
Cumulative Oil Production	0.99	0.99	0.99	0.98	0.98
$t_{q>0.001}$	0.98	0.99	0.99	0.98	0.98
Flow Rates	0.99	0.97	0.98	0.98	0.97
Validation					
Cumulative Oil Production	0.97	0.86	0.95	0.91	0.92
$t_{q>0.001}$	0.91	0.94	0.94	0.92	0.90
Flow Rates	0.98	0.80	0.87	0.94	0.93
Testing					
Cumulative Oil Production	0.97	0.85	0.89	0.88	0.91
$t_{q>0.001}$	0.94	0.94	0.94	0.92	0.92
Flow Rates	0.94	0.94	0.84	0.90	0.81

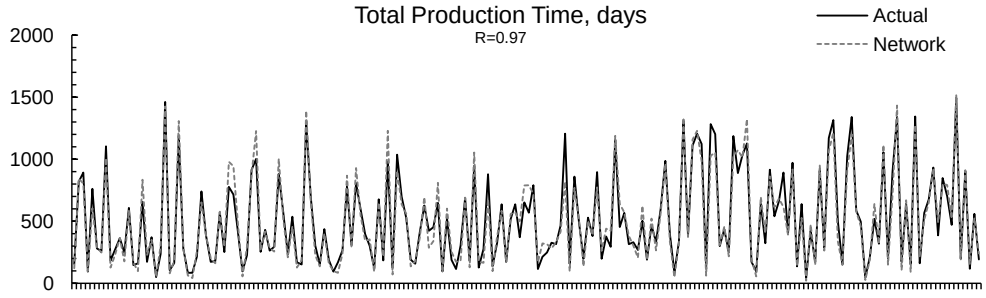

Figure 6.33. Pure CO_2 injection/Black Oil/Design Scheme-1: Total production time predictions.

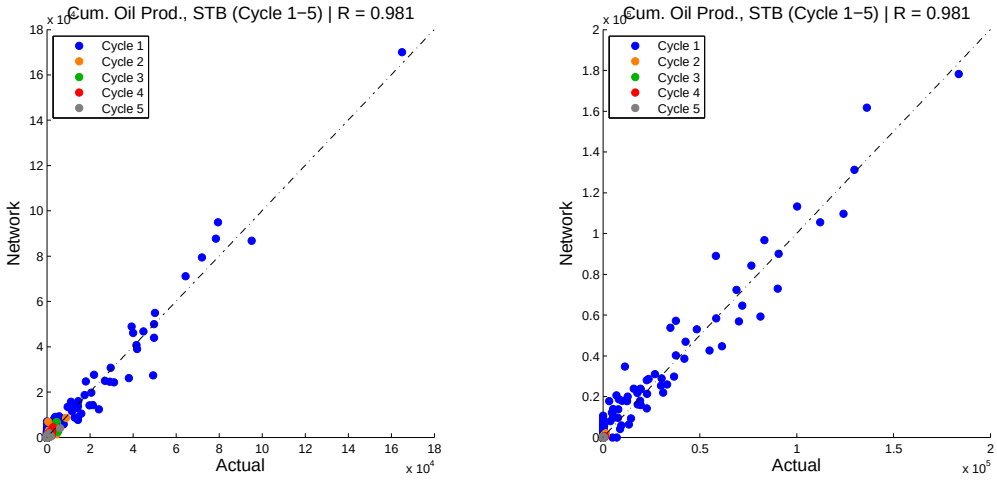

(a) Cumulative oil production - Cycle 1-5.

(b) Peak oil rate - Cycle 1-5.

Figure 6.34. Pure CO_2 injection/Black Oil/Design Scheme-1: Cumulative oil production and peak oil rate predictions.

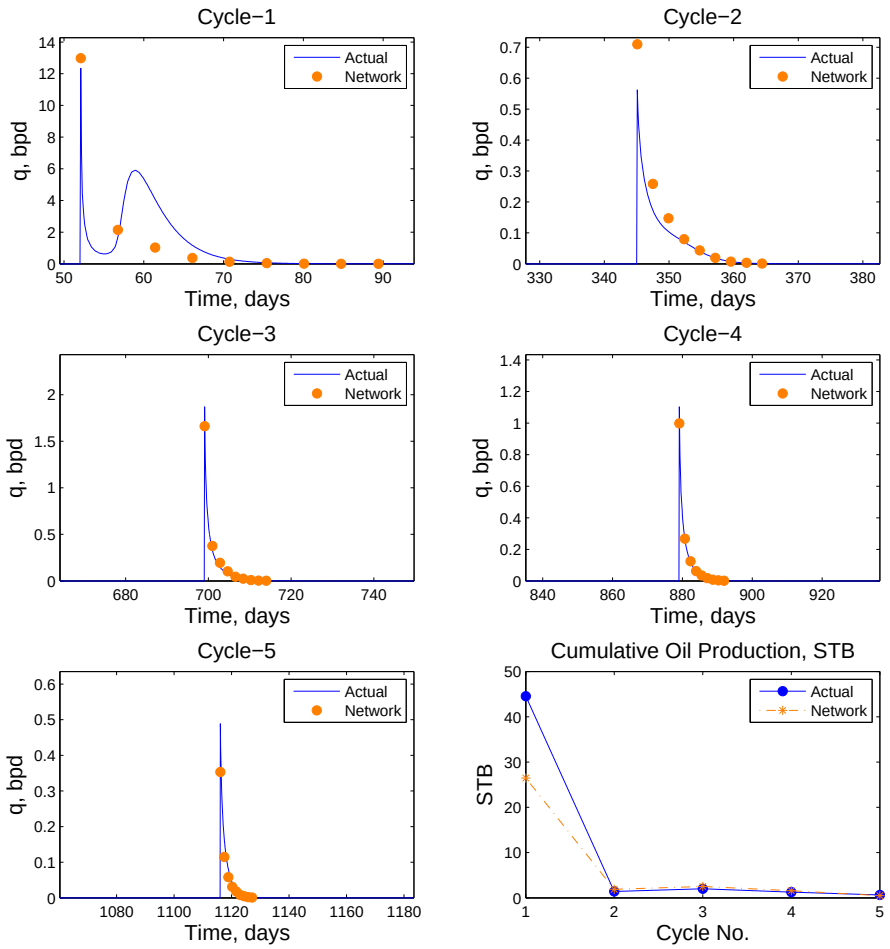

h	94 ft	$k_{m_{x,y}}$	58 md	T	174 F
A	7 acres	k_{m_z}	12.76 md	p_i	689 psia
ϕ_m	0.13	k_f	8,429 md	S_{wi}	0.46
ϕ_f	0.02	X_f	43 ft	S_{oi}	0.54

Figure 6.35. Example Case 1 - Pure CO_2 injection/Black Oil/Design Scheme-1: flow rate predictions - comparison with the actual production curves.

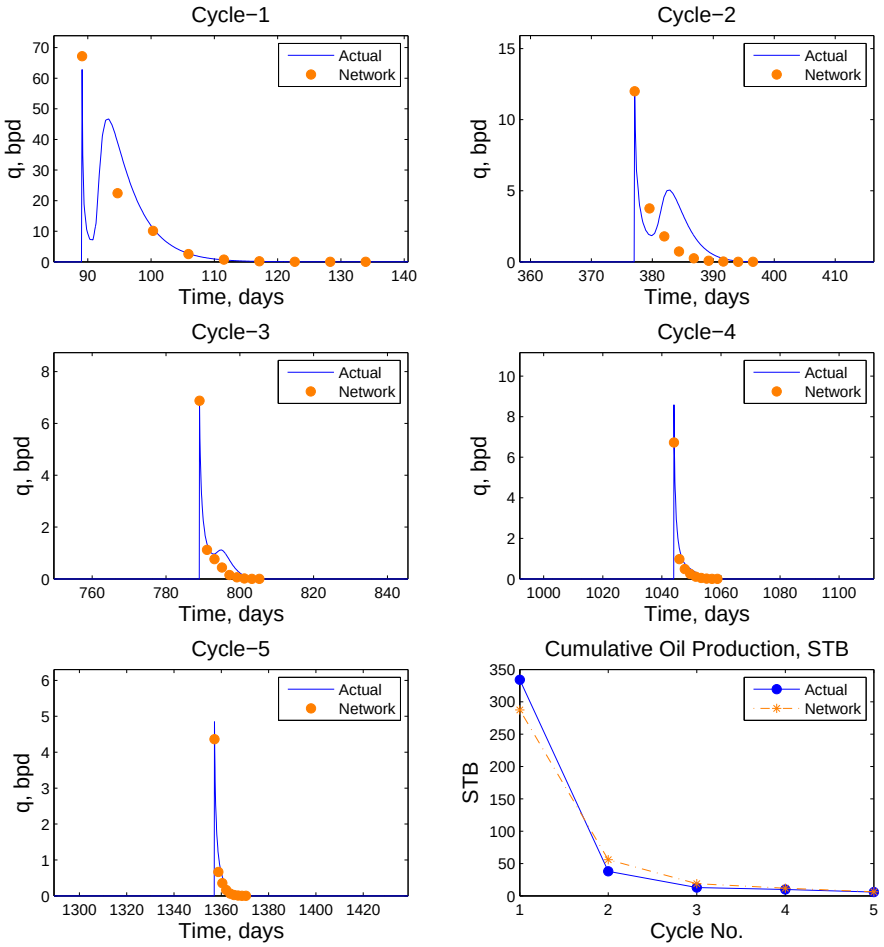

h	69 ft	$k_{m_{x,y}}$	36 md	T	232 F
A	5 acres	k_{m_z}	7.92 md	p_i	1,004 psia
ϕ_m	0.15	k_f	6,510 md	S_{wi}	0.53
ϕ_f	0.03	X_f	64 ft	S_{oi}	0.28

Figure 6.36. Example Case 2 - Pure CO_2 injection/Black Oil/Design Scheme-1: flow rate predictions - comparison with the actual production curves.

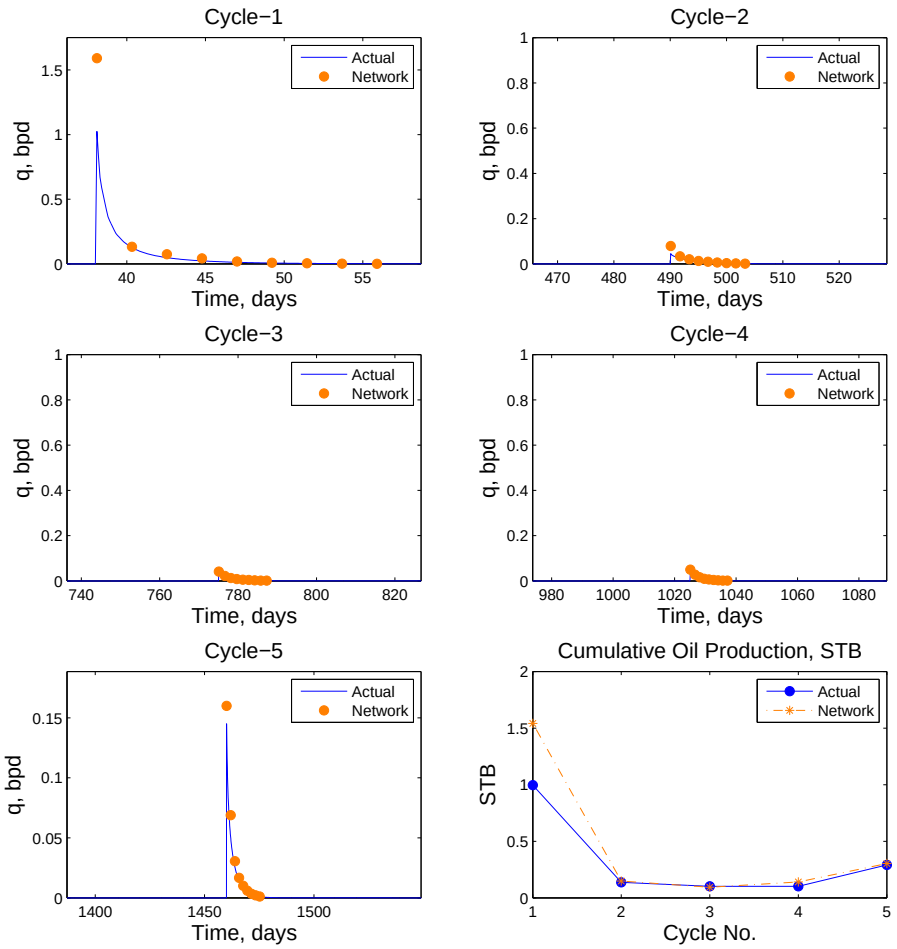

h	84 ft	$k_{m_{x,y}}$	99 md	T	129 F
A	15 acres	k_{m_z}	12.87 md	p_i	222 psia
ϕ_m	0.16	k_f	7.526 md	S_{wi}	0.50
ϕ_f	0.02	X_f	27 ft	S_{oi}	0.09

Figure 6.37. Example Case 3 - Pure CO_2 injection/Black Oil/Design Scheme-1: flow rate predictions - comparison with the actual production curves.

6.3 Design Scheme-2

In this design scheme, the project length and the economic oil production rate limit are specified to design the process together with the injection rate, injection period, and soaking period. Length of each cycle's production period is not specified and the production stops when the specified production rate limit is achieved in each cycle. The number of cycles is not specified and the system utilizes as many cycles as possible within the specified time period. The number of cycles is an outcome of the other process design parameters and the reservoir characteristics. Since the number of cycles is going to be different in each design scenario, the cumulative oil production of the whole process is the only performance indicator. The overall list of the process variables is shown in Table 5.7. The ranges of the design parameters are shown in Table 6.13. The input/output structure of the proposed proxies is shown in Figure 6.38.

Table 6.13. Ranges of design parameters used in the Design Scheme-2.

Design Parameter	Minimum	Maximum
Injection rate, MSCF/d	20	100
Injection period, days	5	50
Soaking period, days	5	50
Economic limit for the oil rate, STB/d	1	10
Total project length, years	1	5

Although this design scheme has a simpler structure in terms of the number of inputs and outputs involved, it was observed that inclusion of reservoir characteristics still required a more complex neural-network architecture as opposed to the ones presented in Chapter 5. After considering the number of inputs, outputs and training patterns involved in this design scheme, the most optimum neural-network architecture is determined to have 2 hidden layers with 30 and 20 neurons, respectively. In hidden layers, *hyperbolic tangent* transfer function is utilized. The architecture is shown in Figure 6.39. The input layer consists of reservoir characteristics and the design parameters of the process. The output layer consists of the cumulative oil production and the number of cycles. For training, Levenberg-Marquardt backpropagation algorithm (Demuth *et al.*, 2006) is used, which is

usually preferred for its faster computing characteristics. 1,200 cases are used for training, 300 for validation, and 200 for testing.

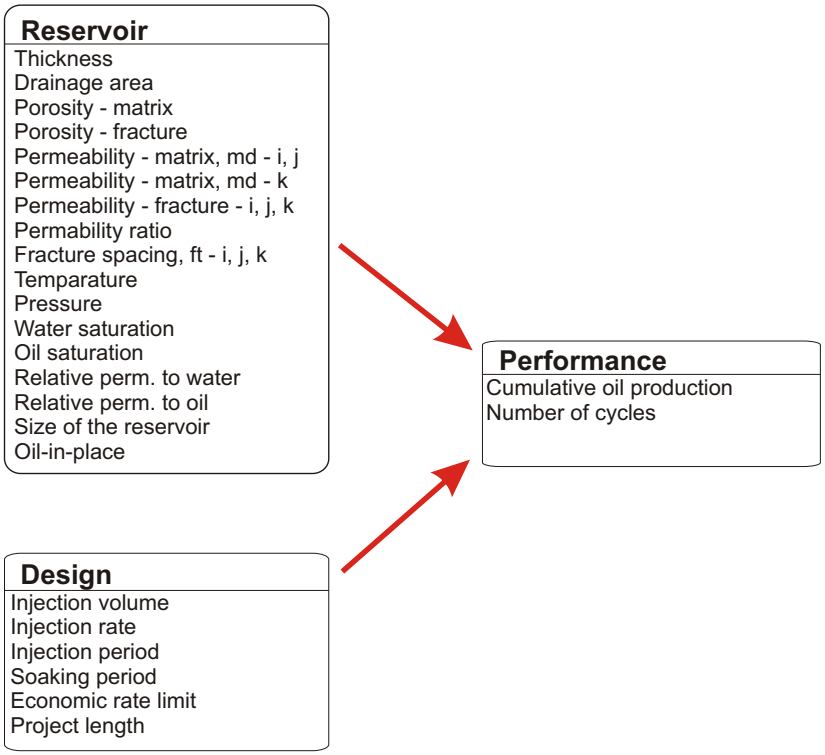

Figure 6.38. Structure of the proxy with variable-number-of-cycles: Mapping from reservoir and design characteristics to performance indicators.

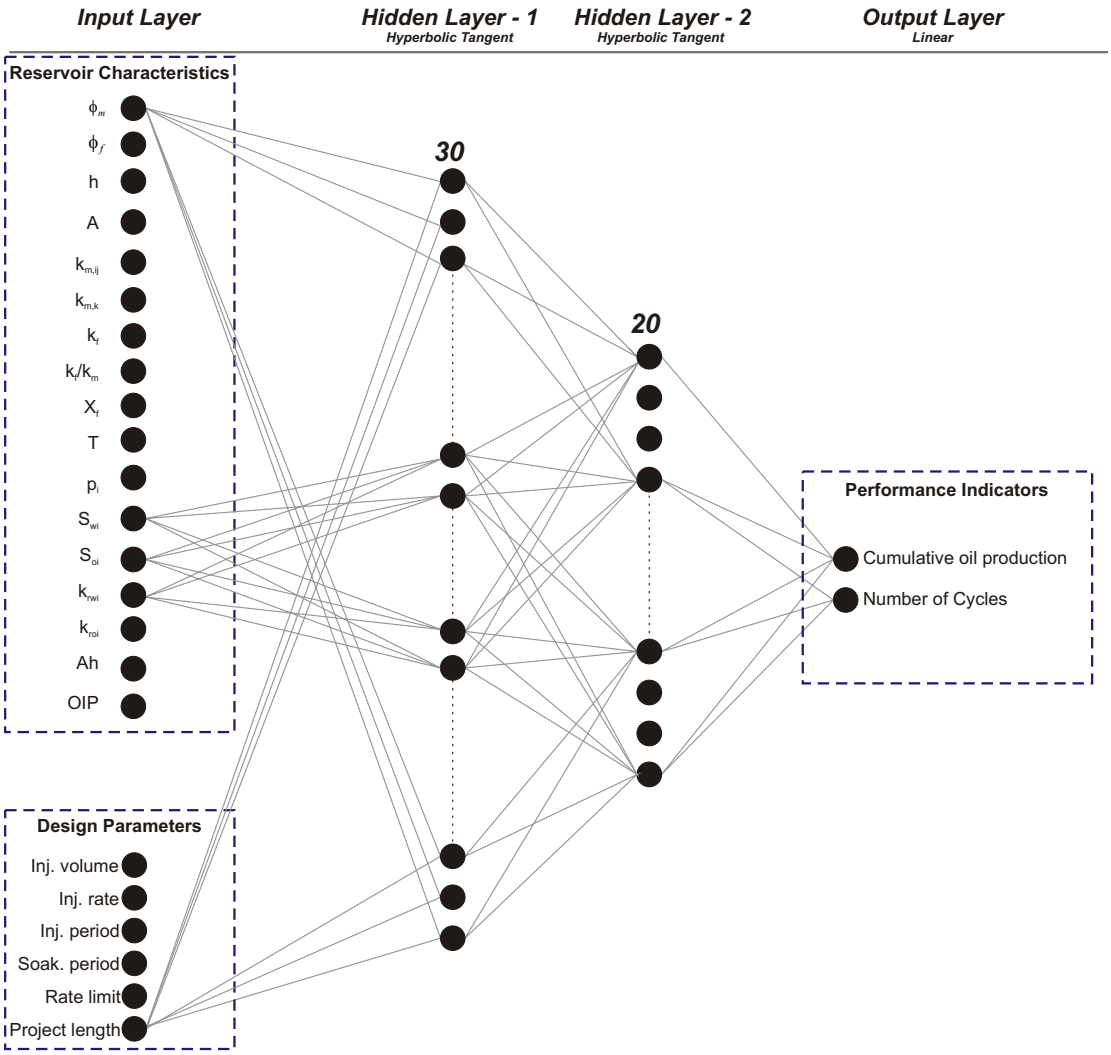

Figure 6.39. Network architecture for the universal proxy with Design Scheme-2.

6.3.1 Pure N_2 Injection Predictions

Figure 6.40 shows the histogram of the number-of-cycles predictions in terms of the accuracy of the prediction (0: correct prediction). Each color represents a different type of oil composition, and we see that in at least 90% of the cases, the neural network was able to predict the number of cycles within the ±2 cycles of accuracy range. Number of cycles is a difficult design parameter to predict, because it is not related directly to the physics of the process. Also, because of the way it is implemented in the numerical model (controlled by the oil flow rate constraint), there is a high chance that obtained number-of-cycles values are in the range of ± 1 cycle than the actual number of cycles. Considering these, the obtained accuracy in the predictions is acceptable. Figure 6.41 shows the testing results for cumulative oil production for heavy, black and volatile oils. These cross-plots show that correlation coefficients higher than 0.99 are obtained for each type of oil.

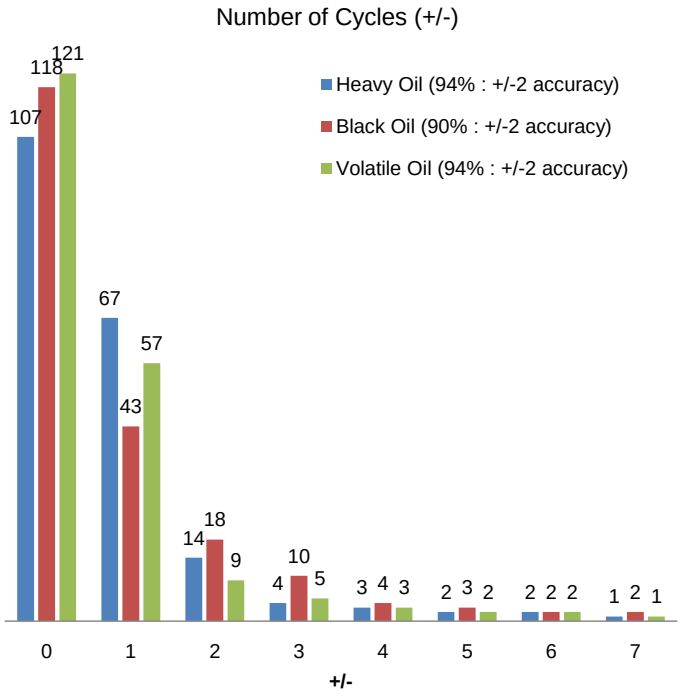

Figure 6.40. Pure N_2 injection/Design Scheme-2: Number of cycles predictions for heavy, black, and volatile oils.

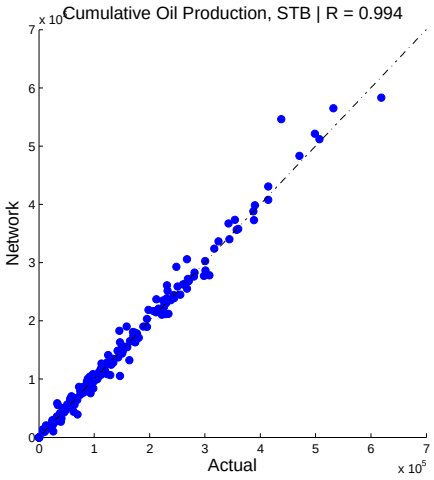

(a) Heavy oil

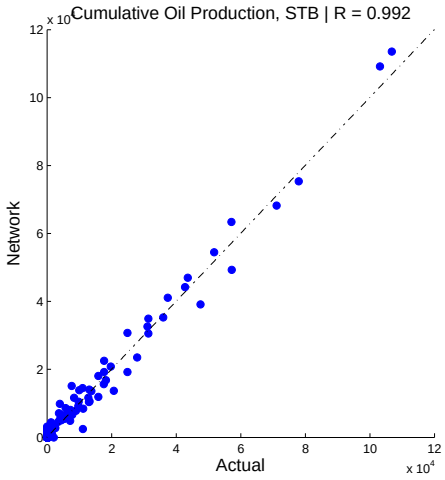

(b) Volatile oil

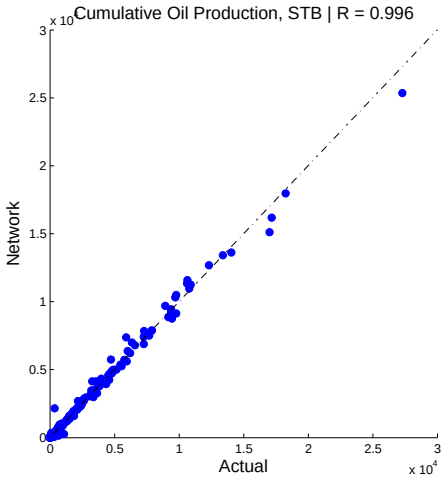

(c) Black oil

Figure 6.41. Pure N_2 injection/Design Scheme-2: Cumulative oil production predictions for heavy, black, and volatile oils.

6.3.2 Pure CO_2 Injection Predictions

Figure 6.42 shows the histogram of the number-of-cycles predictions in terms of the accuracy of the prediction for pure CO_2 injection cases. For volatile oil and black oil, in 94% of the cases and for heavy oil in 87% of the cases, the neural network was able to predict the number of cycles within the ± 2 cycles of accuracy range. Figure 6.43 shows the testing results for cumulative oil production for heavy, black and volatile oils. These cross-plots show that correlation coefficients higher than 0.95 are obtained for each type of oil. We see a relatively higher amount of dispersion in the case with heavy oil. In this design scheme, convergence problems were observed in some of the cases with CO_2 injection and heavy oil. Therefore, it is observed that these problems were carried into the training of the network. This resulted with a relatively higher amount of error in the predictions as compared to black and volatile oil compositions.

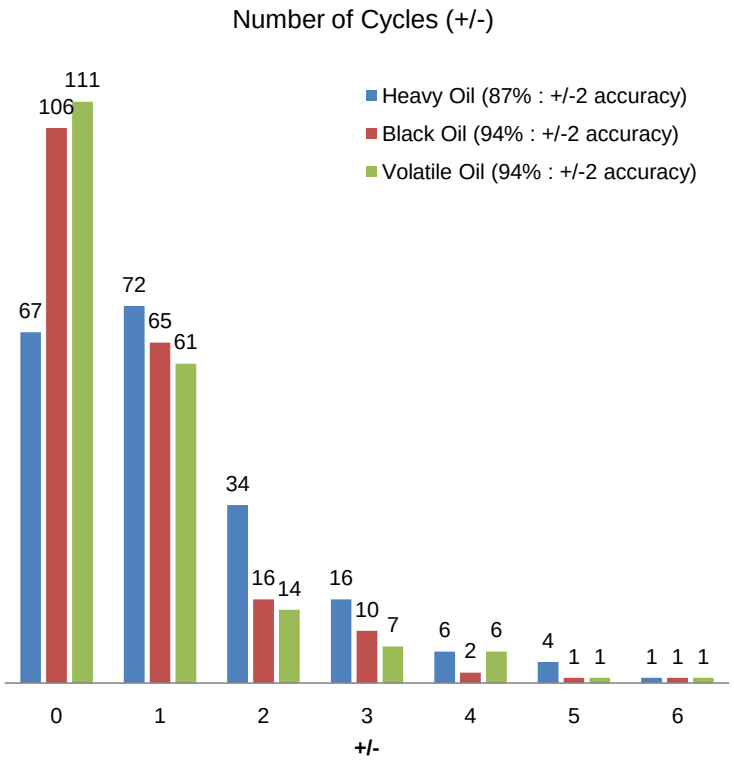

Figure 6.42. Pure CO_2 injection/Design Scheme-2: Number of cycles predictions for heavy, black, and volatile oils.

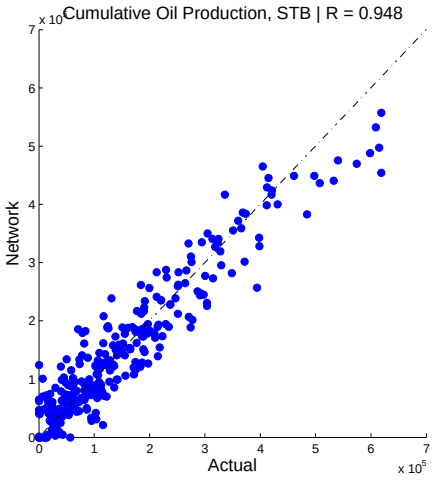

(a) Heavy oil

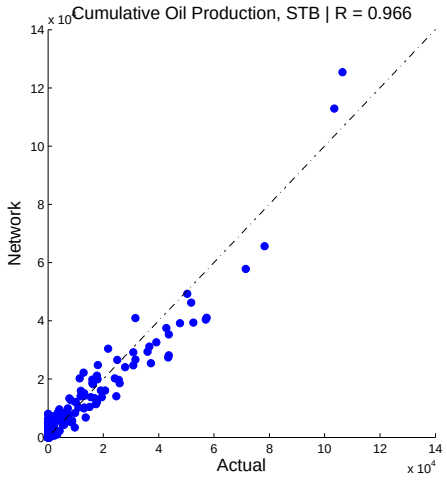

(b) Volatile oil

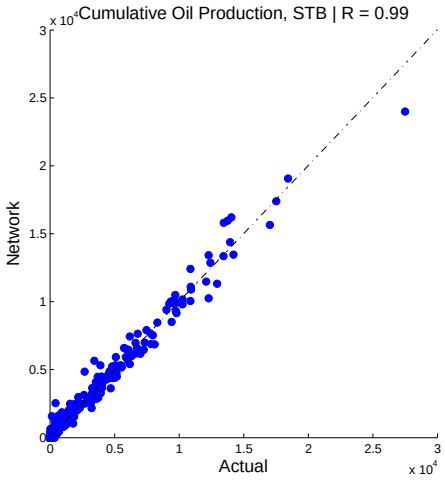

(c) Black oil

Figure 6.43. Pure CO_2 injection/Design Scheme-2: Cumulative oil production predictions for heavy, black, and volatile oils.

6.4 Summary and Conclusions

In this chapter, the methodology presented in Chapter 5 is generalized for reservoirs of varying characteristics. Universal neural-network proxies are developed that can predict the performance indicators for a given set of reservoir characteristics and design parameters. 12 neural networks were trained for each injected fluid, reservoir fluid and design scheme. The prediction results indicate that developed networks can predict the performance of the cyclic injection process accurately. The constructed proxy models are incorporated in a graphical-user-interface (GUI) application, which is presented in the Appendix. Other main conclusions of this chapter are summarized as follows:

1. When the level of complexity in the neural network architecture is increased in parallel with the complexity of the problem, the generalization capabilities of a neural network may improve. After including the reservoir characteristics as an additional layer of complexity in the problem, a 2-layer neural network provided better results than a 1-layer neural network. This was confirmed during the development of neural networks for Design Scheme-2 (Section 6.3).

2. Taking the logarithm of input and output data improved the training performance by scaling down the ranges of the data. This helped the network to predict a wide range of flow rates (significantly high peak oil rates and lower cycle flow rates).

3. During the data preparation stage, it is important to understand the significance of each input parameter on the provided outputs. This was possible in this study, since a reservoir model is used to generate data, which we had the full control of. After observing that the reservoir system under consideration is highly sensitive to changes in the fracture permeability when it is less than 2,000 md, re-distribution of the input data improved the neural network (Section 6.1.2, Figure 6.2).

4. After training the neural network, analyses of weights in connection links provide valuable information about the influence of each input parameter on the outputs. If there is a prior knowledge about the problem under consider-

ation, this can also be used as a way of confirming whether the network was trained in the right direction or not.

5. Analysis of the connection weights displayed in Tables 6.5 and 6.9 indicate similarities between CO_2 and N_2 injection. The common observation is that the fracture permeability, ratio of fracture permeability to matrix permeability, oil-in-place, area, Ah product, and oil saturation are the most critical parameters that affect the performance. Due to the phase behavior characteristics, contribution of initial pressure and temperature of the reservoir are more pronounced in the volatile oil than black and heavy oils. Among the design parameters, volume of the injected gas is the most critical parameter that affects the performance. Injection period, injection rate, and production rate are at a comparable rank in all three cases. Soaking period is the least contributor. These results confirmed the previous observations about the design parameters.

Chapter 7

Parametric Studies for Performance Evaluation

In this chapter, results of parametric studies are presented. First, parametric studies are performed to develop a better understanding of how operational parameters affect the process performance in the Big Andy Field. These include analyses of various design parameters such as the injection rate, lengths of injection and soaking periods, and cycle rate limits. Incremental oil production, peak oil rate and net present value (NPV) are considered as the performance criteria. Combined analyses of the design parameters are presented with contour plots. These results are presented in the first part of the chapter. The second part of the chapter focuses on the reservoir characteristics. It is aimed to develop a better understanding of the reservoir conditions that favor the cyclic pressure pulsing process. Comparative discussions are presented between cases with CO_2 and N_2 on different reservoir fluids (heavy, black and volatile oils). Area, thickness, fracture/matrix permeabilities, pressure and temperature are the reservoir characteristics that are studied.

7.1 Analyses of Design Parameters

Using the reservoir model developed for the Big Andy Field, performance of a cycle of nitrogen injection is analyzed. The objective is to understand how the net present value (NPV), peak oil rate and incremental oil production would be

affected using different treatment volumes, injection rates, and soaking periods. NPV calculations are made based on the formulation given in Section 5.6.2. Economic parameters are given in Table 5.12.

7.1.1 Injection Volume

Figures 7.1, 7.2, and 7.3 show how the peak oil rate, incremental oil production, and net present value change with different injection volumes. These three figures are for soaking periods of 10, 30, and 50 days, respectively. It is seen that with higher injection volumes, peak oil rate linearly increases. However, incremental oil production and net present value increase at a slower rate, and starts to stabilize as the injection rate approaches 100 MCF/d. When we look towards the vertical axes for each injection rate (increasing injection periods), we see that the production and NPV stabilizes towards 50 days of injection. Therefore, we conclude that for this reservoir up to 50 days of injection at a rate of 100 MCF/d incremental recovery may be maximized, together with the NPV assuming the economic parameters in Table 5.12 are valid.

For longer soaking periods of up to 50 days, the result is an increase in the oil production and net present value. The similarity between the net present value and incremental production should also be noted. This confirms the fact that while the initial peak oil rate is important, the cumulative oil production is the most important criterion from the economics perspective. We also see that as the soaking time increases from 10 days to 30 and 50 days, we see an increase in the peak oil rate and the incremental oil production. However, when we look at the NPV, there is little or no change as we increase the soaking period. This is most probably due to the fact that the income from increased oil production balances the lost time of production. With higher oil prices, there is a possibility that the NPV increase due to the increase in oil production would be more pronounced.

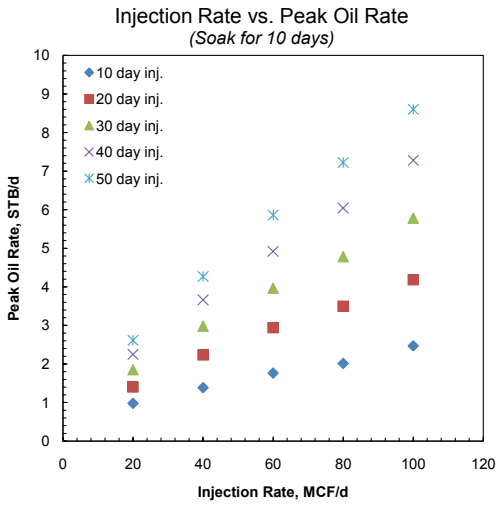

(a) Peak oil rate

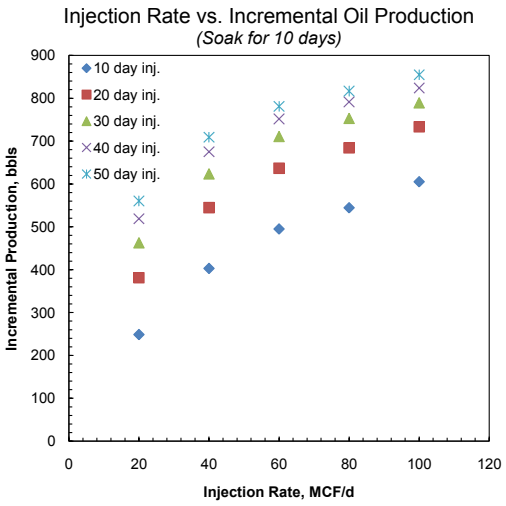

(b) Incremental oil production

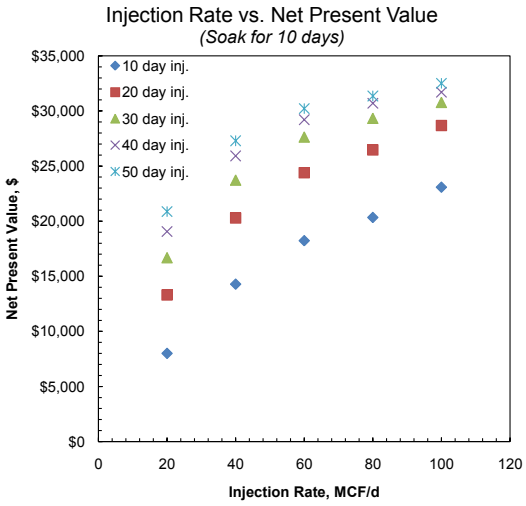

(c) NPV

Figure 7.1. Injection rate vs. peak oil rate, incremental production, and NPV (soaking for 10 days).

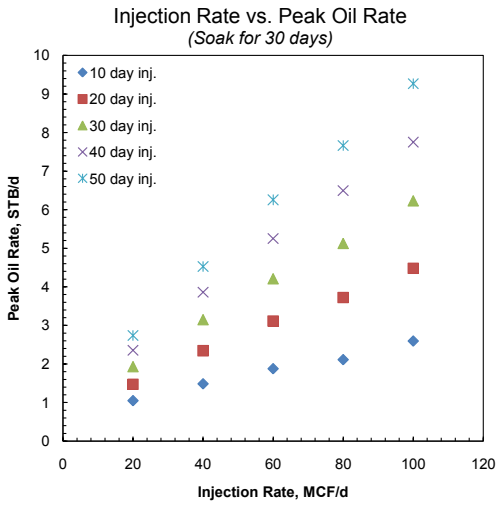

(a) Peak oil rate

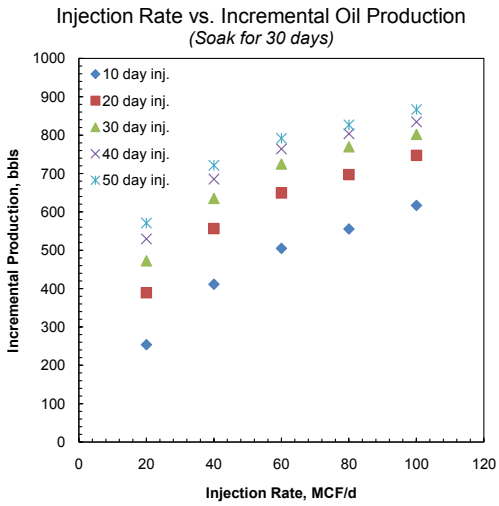

(b) Incremental oil production

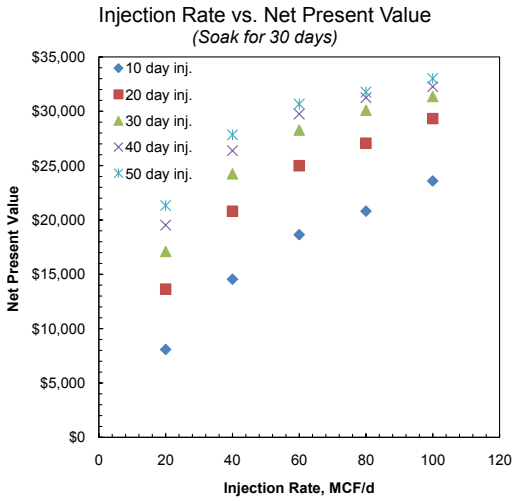

(c) NPV

Figure 7.2. Injection rate vs. peak oil rate, incremental production, and NPV (soaking for 30 days).

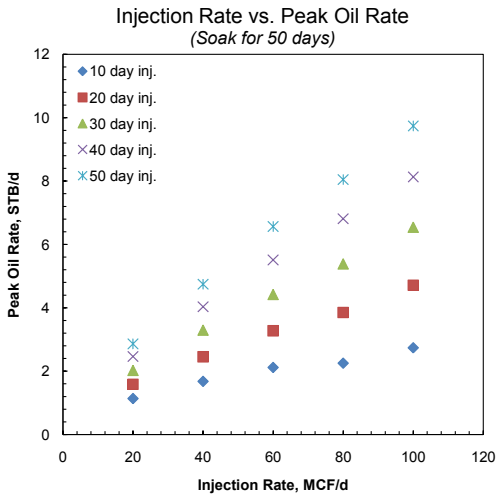

(a) Peak oil rate

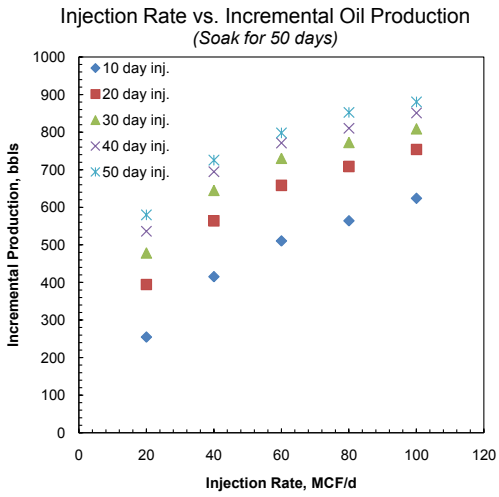

(b) Incremental oil production

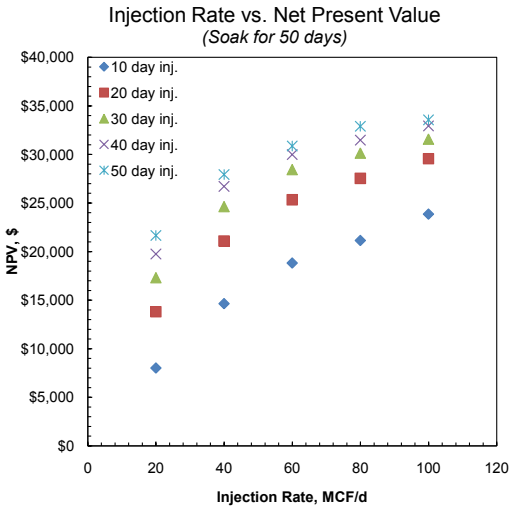

(c) NPV

Figure 7.3. Injection rate vs. peak oil rate, incremental production, and NPV (soaking for 50 days).

7.1.2 Injection Rate

To understand the importance of injection rate, the same treatment amount, 800 MCF, is applied with different injection rates (or, injection periods). Figures 7.4, 7.5, and 7.6 show peak rate, incremental production, and net present value when the treatment is done in 10, 20, and 40 days. Soaking period is also varied between 20 days and 50 days. In these plots, it is seen that injecting at a lower rate and for a longer time results in higher peak rates. However, the injection rate is low, and resulting pressure gradients do not allow for the gas to penetrate into further portions of the reservoir. When the well is put on production, initially a high amount of injected gas is produced. This results in reduced incremental oil production and thus, reduced net present value. Also, as in the earlier graphs, it can be observed that soaking of up to 50 days can help to improve the amount of incremental recovery.

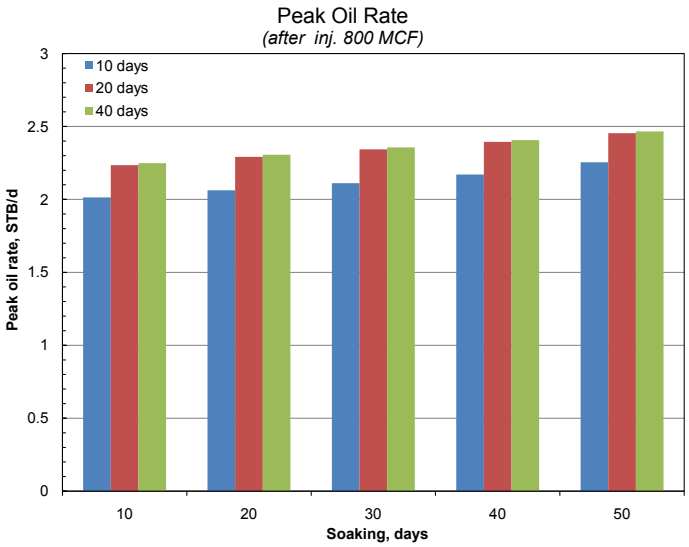

Figure 7.4. Peak oil rate after injection of 800-MCF with varying injection rates.

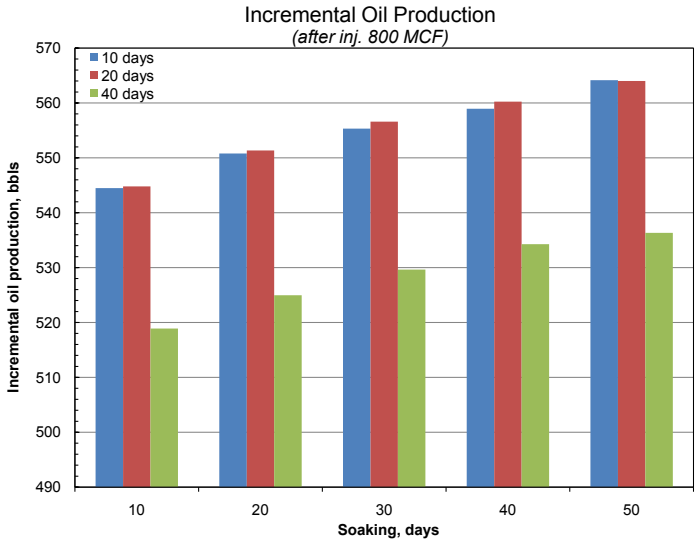

Figure 7.5. Incremental oil production after injection of 800-MCF with varying injection rates.

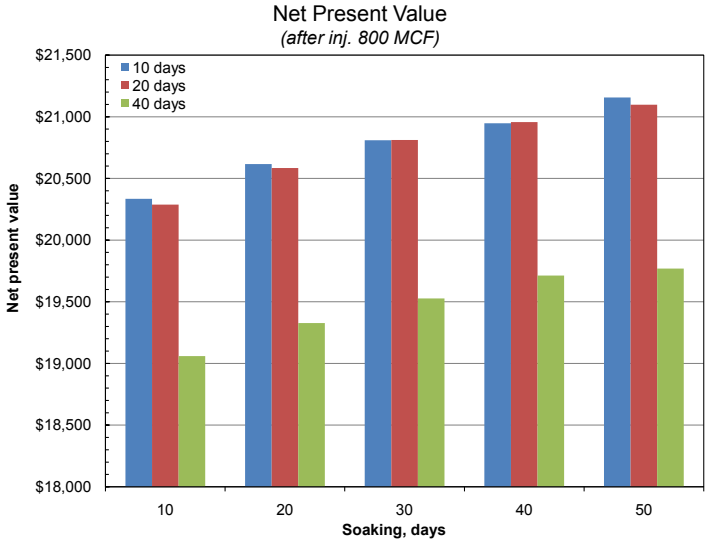

Figure 7.6. NPV after injection of 800-MCF with varying injection rates.

7.1.3 Soaking

Figure 7.7 shows that it is possible to have higher incremental production (2.5% more) with longer soaking periods of up to 60 days, and as the treatment volume increases this increase in production can be more significant as observed in the previous analyses. Figure 7.8 shows the change in NPV with soaking period for different treatment volumes. It is seen that for higher volumes of injection, longer soaking is necessary to maximize the NPV. For 250 MCF of injection, after 20 days of soaking the NPV starts to decrease. This value is around 25-30 days for 300 MCF, and around 50 days for 350 MCF. For 400 MCF, NPV continues to increase with soaking for 60 days. From these observations, it can be concluded that a shorter injection period with a high rate is more feasible than lower rate and longer injection period for the same volume of gas. This was also observed in the previous analyses (*e.g.*, Figure 7.6). We also conclude that soaking as much as 60 days can increase the net present value of the project when the injected volume is 400 MCF. This is again due to the fact that the additional production is higher than the lost production during soaking.

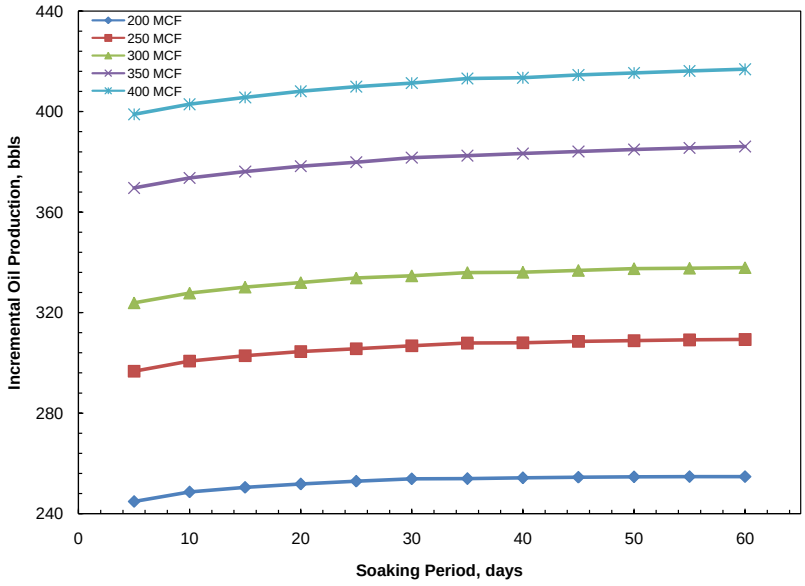

Figure 7.7. Soaking vs. incremental production for different treatment volumes.

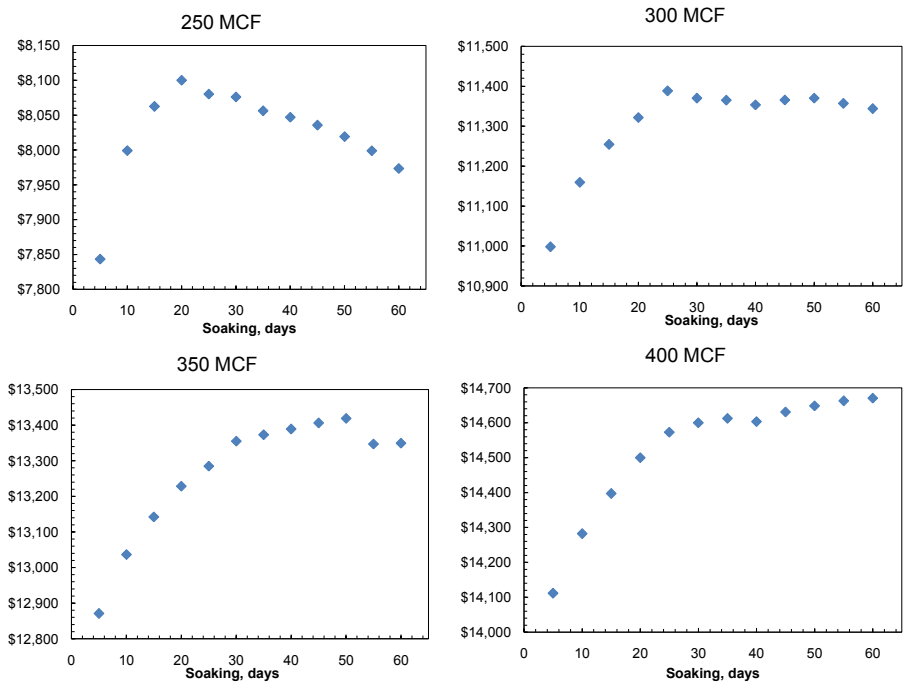

Figure 7.8. Soaking vs. NPV for different treatment volumes.

7.1.4 Combined Analyses for CO_2 and N_2 Injections

In this section, combined analyses of the following design parameters are analyzed:

- Cycle injection volume
- Soaking period
- Cycle rate limit
- Cumulative injection volume

Analyses are made for both pure N_2 and CO_2 injection. The performance indicators are the incremental oil production, net present value and current incremental oil production. current incremental production is calculated by converting the incremental production to today's value at interest rate, i, using the present value equation:

$$IOP_{current} = \frac{IOP}{(1+i)^n} \tag{7.1}$$

Net present value calculations are made using the economic parameters in Table 7.1. The cost difference between N_2 and CO_2 should be noted ($1.00 vs. $4.50). In these analyses, the knowledge base that was obtained during the application of Design Scheme-2 on the reservoir model of the Big Andy Field is used.

Table 7.1. Parameters used to calculate the NPV.

Oil price	.....	$	100.00	per STB of production
Nitrogen cost	.....	$	1.00	per MCF of injection
CO_2 cost	.....	$	4.50	per MCF of injection
Operating cost	.....	$	500.00	per well per month
Royalty interest	.....	%	12.5	of the gross revenue
Taxes	.....	%	6.0	of the net revenue

7.1.4.1 Cycle Injection Volume vs. Soaking Period

Areal distribution plots of incremental production, current incremental production and NPV with changing soaking period and cycle injection volumes of N_2 and CO_2 are shown in Figure 7.9. It is an expected result to see higher incremental oil production with higher soaking and higher injection volumes in each cycle. We see the incremental production is maximized at the region of soaking period of 30-40 days and cycle injection volume higher than 3,000-4,000 MCF/cycle. Also, the higher incremental production with CO_2 is an expected result because of the dissolution of CO_2 in the oil.

Distributions in the middle of the page are current incremental oil production values. In this case, the oil production is converted into today's value using the interest formula presented above. In both CO_2 and N_2, it is observed that the maximized area shifted toward the intermediate zone for soaking, which is 20-30 days. This is expected because of the loss of production time during the soaking period. While higher soaking period increases the cumulative oil recovery, the time value of the oil production comes into the picture and optimum soaking period of 20-30 days is observed. In the case with CO_2, we also see higher production when there is longer soaking than 30 days. This is due to the fact that longer soaking allows more CO_2 to be dissolved. In this case, higher oil production is overcoming the lost production during the shut-in period. The hot area is still in the high-injection-volume region since the injected volume is not related to the time value of the production.

The plots in the last row are the NPV distributions. As expected, they are consistent with oil productions converted to today's productions. However, NPV is a more realistic indicator because of the inclusion of the cost of the injected gas in the formulation. Since the hot area is still in the high-injection-volume region, it is clear that the cost of the gas price is not affecting the process NPV significantly with the given oil price of \$100/bbl. Because of the cost difference between CO_2 and N_2, the ranges of the NPV values are different. With nitrogen (\$1/MCF), NPV changes between \$72,000 and \$80,000. In the case with CO_2, the range is between \$65,000 and \$73,000. This indicates that nitrogen is a better choice with these reservoir conditions and with these oil and gas prices.

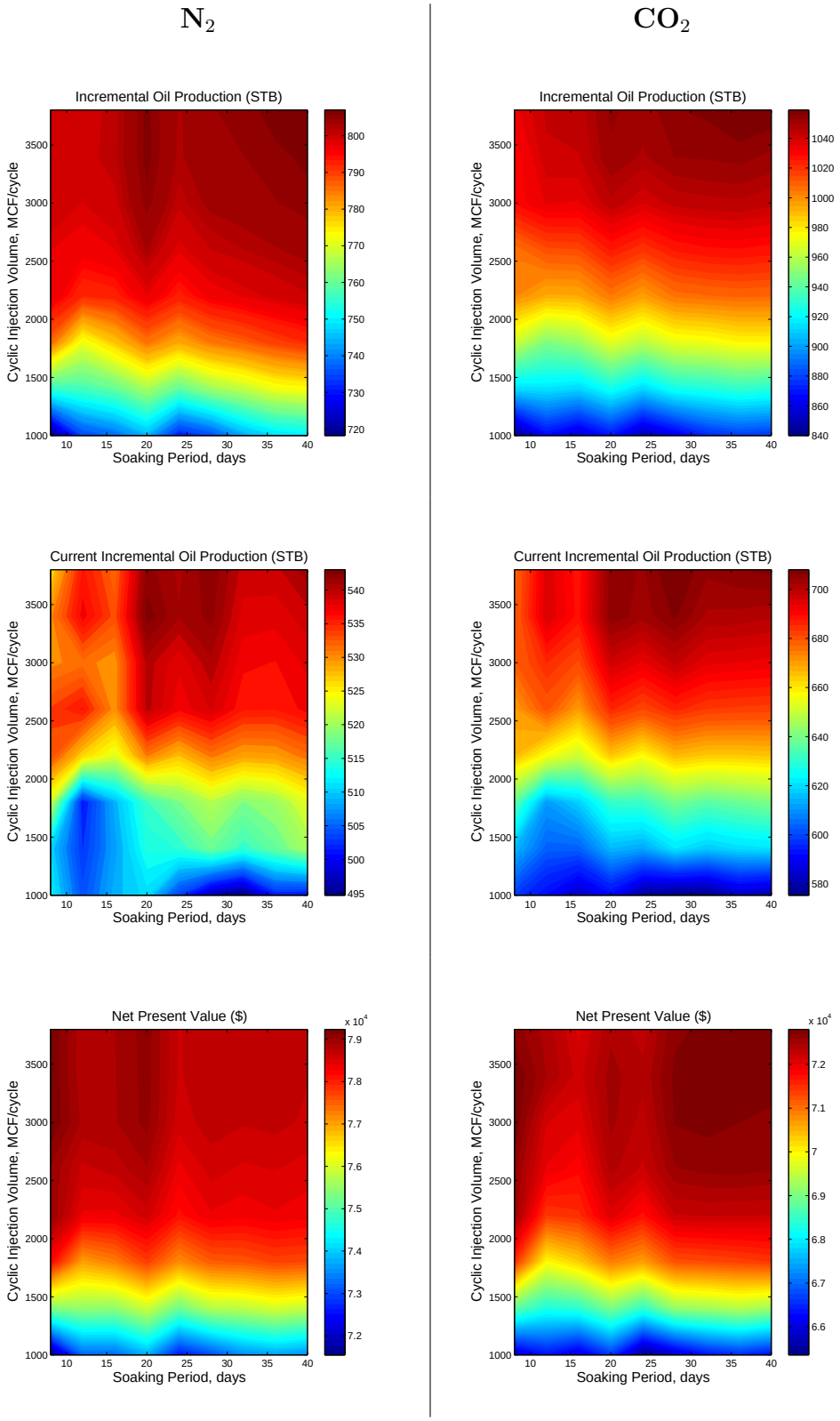

Figure 7.9. Areal distribution plots of incremental production, current (discounted) incremental production and NPV with changing soaking period and cycle injection volumes of N_2 and CO_2.

7.1.4.2 Cycle Injection Volume vs. Cycle Rate Limit

In this section, the analyses are based on the cycle injection volume and the cycle rate limit. Figure 7.10 shows the areal contour plots of how the performance indicators are changing with the cycle rate limit and cycle injection volume. Because the reservoir of interest is a stripper-production reservoir, the cycle rate limit is varied between 0.1 STB/d and 1.0 STB/d. In these plots, it is seen that stopping the cycle oil production at 1.0 STB/d before starting the next injection maximizes the oil production. When the injected gas is CO_2, the NPV is maximized toward the middle region where the rate limit is between 0.6 and 0.8 STB/d. However, it is still close to the higher rate limits rather than lower limits. This brings the conclusion that the existing energy in the reservoir helps the process to be more efficient.

7.1.4.3 Cumulative Injection Volume vs. Number of Cycles

In this section, the parameters under consideration are the number of cycles and the cumulative injection volume rather than cycle injection volume. Number of cycles is a critical parameter and typically higher number of cycles is not desired due to increased costs with higher volumes of injected gas. However, it is still an important parameter to determine how many times the injection process would be efficient. When the same cumulative volume of gas is considered, the number of cycles needs to be determined. Figure 7.11 shows the areal contour plots of how the performance indicators are changing with the number of cycles and cumulative injected volume. Higher oil production is an expected result of higher number of cycles and cumulative injection. On the other hand, when we look at current incremental production, we see that the most optimum number of cycles is 2. It is important to note that here the cost of the injected gas is not included in the calculations. When we include the cost of the injected gas and use NPV as our criterion, we see different results with CO_2 and N_2. Nitrogen, as a lower cost gas, provides high NPV's in a large region where the number of cycles is changing between 3 and 7, and the cumulative injection is changing between 8,000 and 16,000 MCF. On the other hand, when the injected gas is CO_2 a 3-cycle process is the most optimum. It is still desirable to inject high volumes of gas (between

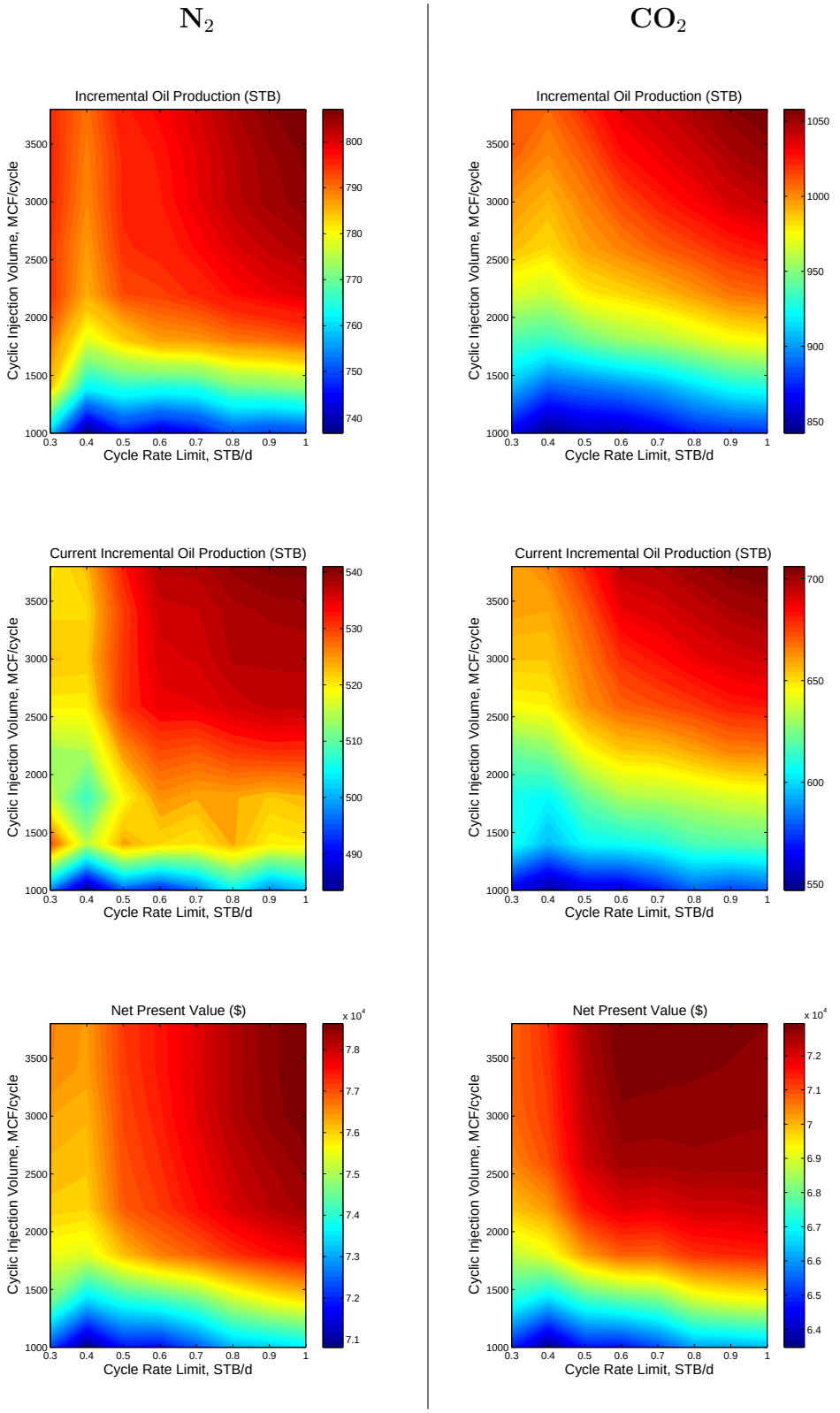

Figure 7.10. Areal distribution plots of incremental production, current (discounted) incremental production and NPV with changing cycle rate limit and cycle injection volumes of N_2 and CO_2.

8,000 and 16,000 MCF). However, since each cycle brings in injection and soaking periods during when the well is shut-in, each cycle also results in loss of production time. Therefore, due to the high cost of CO_2, this significantly affects the NPV in a negative way. As a result, we see less number of cycles (3) as the most optimum number of cycles.

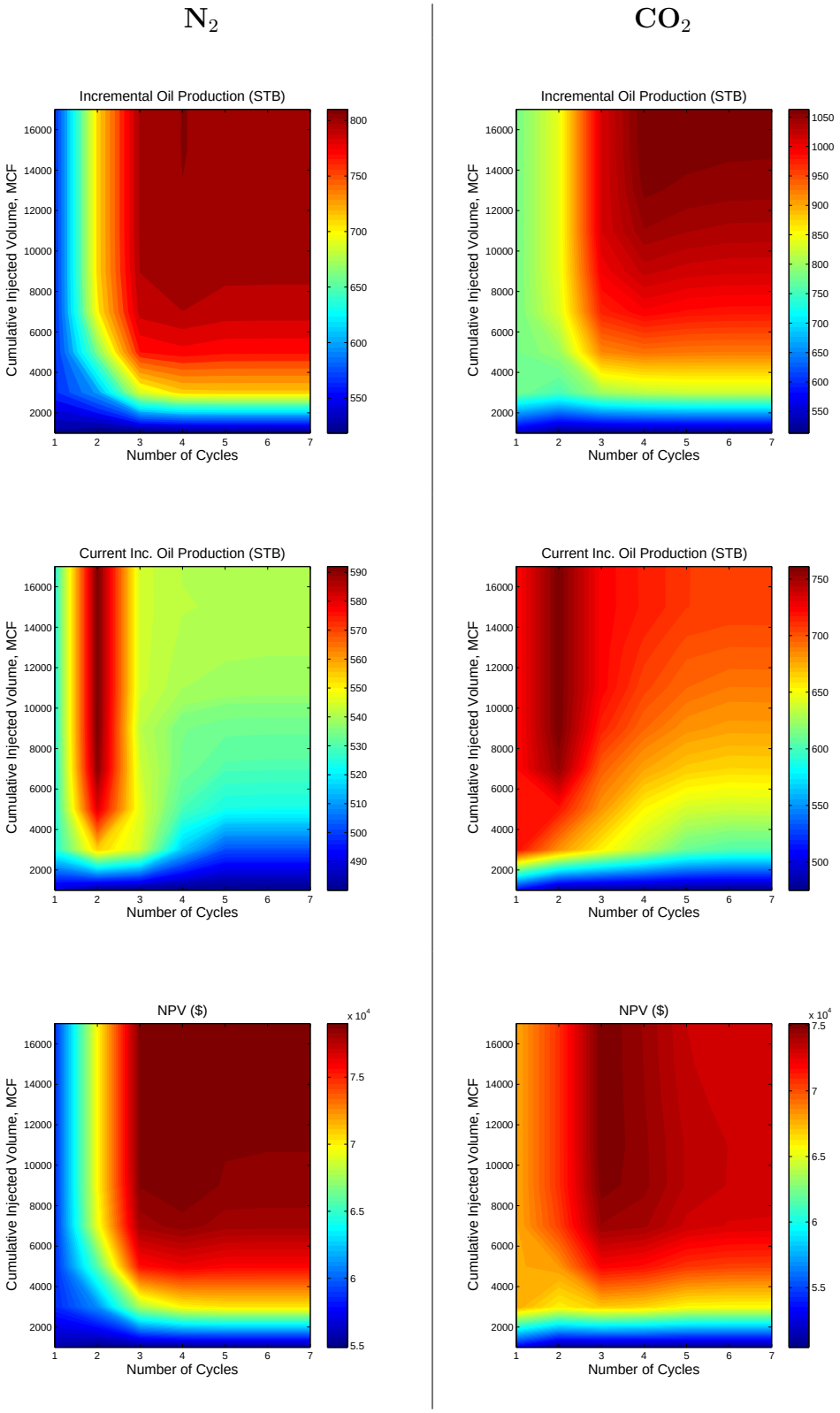

Figure 7.11. Areal distribution plots of incremental production, current (discounted) incremental production and NPV with changing number of cycles and cumulative injection volumes of N_2 and CO_2.

7.2 Analyses of Reservoir Characteristics

In this section analyses of critical reservoir characteristics on the process efficiency are presented. The reservoir characteristics that are investigated are area/thickness, fracture/matrix permeabilities and initial pressure/temperature of the reservoir. The performance indicator that is used to compare each case is defined as the utilization factor, the ratio of the incremental production to the volume of injected gas. The utilization factor is then divided by the $Area \times Thickness$ product, to normalize the result to the size of the reservoir to obtain a representative indicator per unit volume. Therefore, the utilization factor that is used in this section is defined as:

$$U = \frac{IOP}{CI \times A \times h} \tag{7.2}$$

where IOP is the incremental oil production, and CI is the cumulative volume of the injected gas. The analyses are presented for heavy, black and volatile oils and for N_2 and CO_2 injection cases.

7.2.1 Area/Thickness

Contour plots in Figure 7.12 shows the areal distribution of the utilization factor changing with different areas and thicknesses. Since the utilization factor was calculated per $acre - ft$, these distributions are not biased by the size of the reservoir. In the case of heavy oil, which is shown at the top, we see a concentration in the region where the drainage area is at the lowest range (5-8 acres). This is due to the high viscosity of heavy oil that prevents the oil from being effectively transported to the well from further portions of the reservoir. Therefore, the cyclic injection of CO_2 and N_2 are effective in producing heavy oil from the near vicinity of the well. We also see that the efficiency of the process is maximum when the thickness is between 30-50 ft. The similarity between CO_2 and N_2 is an indication of the similar effectiveness of these two gases in an heavy oil reservoir.

In the case of black oil, which is shown at the middle, we see a more homogeneous distribution especially with the case with CO_2. A high-efficiency region is observed for a thickness range of 30-50 ft for CO_2 and 20-40 ft for nitrogen. In terms of the area, we see a homogeneous distribution as compared to heavy oil.

High-efficiency regions are observed in a wide range of area values for both N_2 and CO_2. The behavior of volatile oil is similar to that of black oil. With both CO_2 and N_2, high-efficiency regions are distributed in an homogeneous manner in terms of the area. Also, low-thickness region (20-50 ft) shows better utilization factor. These results indicate similarities to that of black oil.

As a conclusion, it is observed that, the process is more effective in thin reservoirs. In all cases regardless of the type of reservoir fluid and injected gas, thicknesses ranging between 20-50 ft produced more favorable results in terms of the process efficiency. In terms of the area, we see higher efficiency with smaller area (5-8 ft) with heavy oil. For the cases with volatile and black oil, it is seen that the process efficiency is not significantly affected by the area significantly.

7.2.2 Matrix/Fracture Permeability

Contour plots in Figure 7.13 show the areal distribution of the utilization factor changing with different matrix and fracture permeabilities. As in the previous case for area/thickness analysis, effectiveness of N_2 and CO_2 in heavy oil results in a very similar behavior in terms of the matrix and fracture permeabilities. We see that fracture permeabilities higher than 3,000 md are favorable. Fracture permeability is an important reservoir property in this process as it is the primary factor in delivering the injected gas in the further portions of the reservoir from the wellbore, and in delivering the oil, which flows from the matrix into the fractures. Therefore, it is expected to see that higher fracture permeabilities improve the efficiency of the process. In terms of the matrix permeability, while there is a more homogeneous distribution, there is more concentration of higher values in the region where the matrix permeability is less than 40 md. If we consider the black oil and volatile oil, we see a similar but more homogeneous distribution. This indicates that the effectiveness of the process is less sensitive to the system permeability. However, it is still observed that higher fracture permeabilities increase the process efficiency.

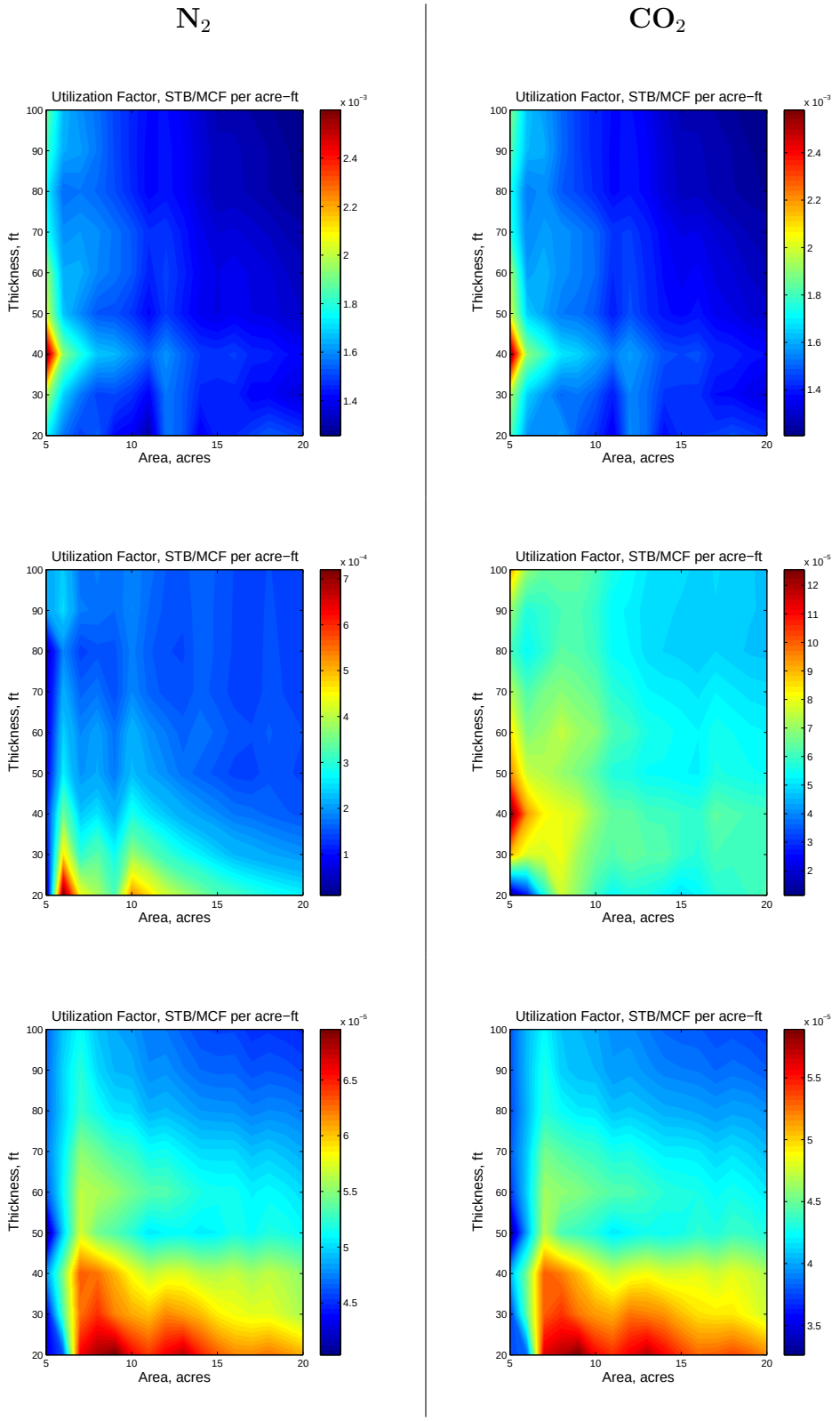

Figure 7.12. Areal distribution plots of utilization factor per acre-ft with changing area and thickness (top: heavy oil, middle: black oil, bottom: volatile oil).

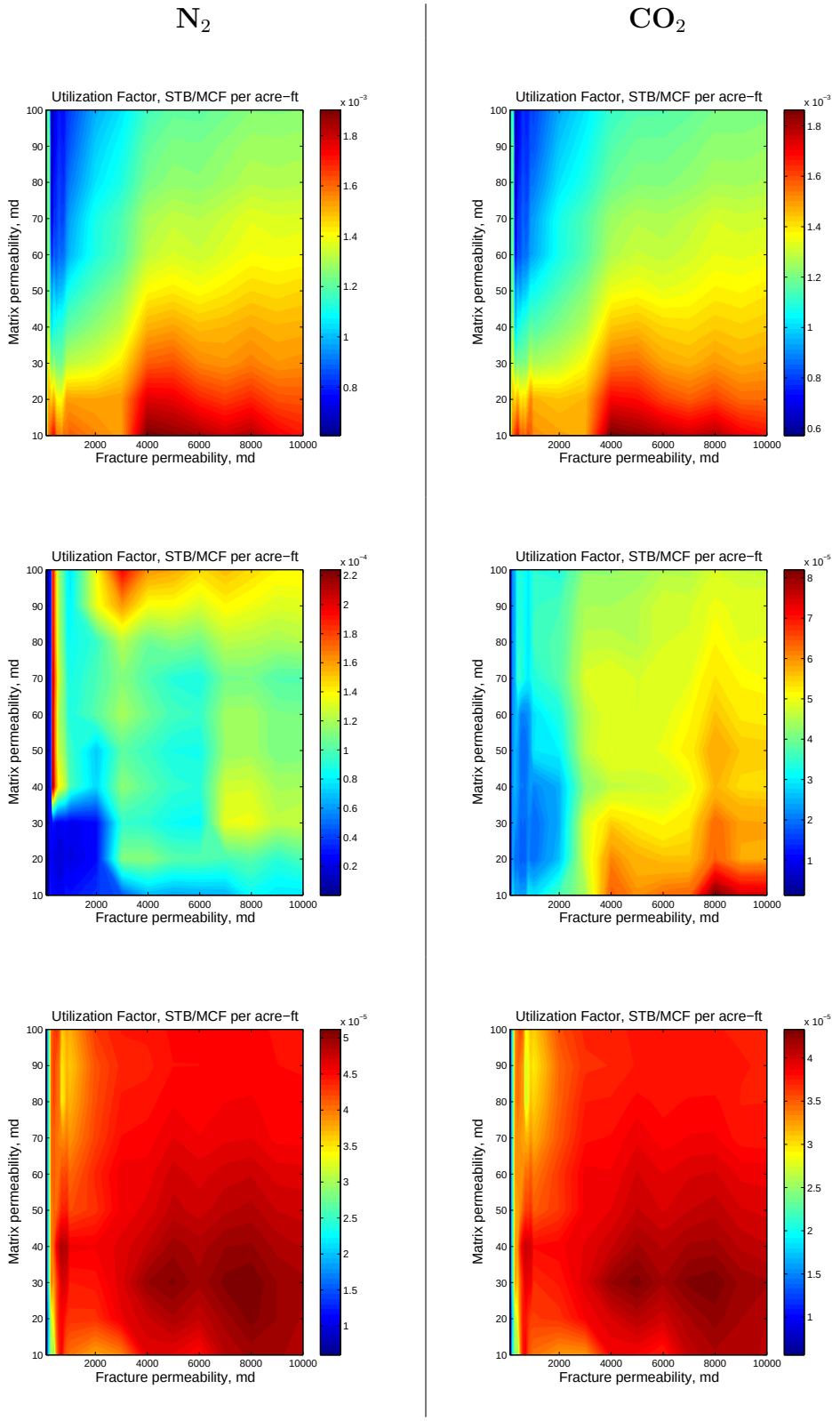

Figure 7.13. Areal distribution plots of utilization factor per acre-ft with changing fracture and matrix permeabilities (top: heavy oil, middle: black oil, bottom: volatile oil).

7.2.3 Pressure/Temperature

Contour plots in Figure 7.14 show the areal distribution of the utilization factor that changes at different initial pressure and temperature conditions. These plots indicate the importance of the liquid/gas mole fraction in the system. The white lines on these contour plots are the quality lines of the phase envelopes shown in Figure 6.5. The numbers indicate the liquid volume percentage in the system. In all cases, we see a strong similarity between N_2 and CO_2. This shows that the choice of the injected gas between CO_2 and N_2 does not change effectiveness of the process at different pressure/temperature conditions. In the case with heavy oil, the majority of the pressure/temperature interval that is under consideration is in the 100% liquid region and almost the whole interval is over 80% liquid quality line. There is a small low-efficiency region that is under the 80% quality line. The efficiency of the process increases with the liquid content. The hottest region is where the temperature is less than 120 F and the pressure is higher than 600 psia. In the case with black oil, there is a wider range of the liquid volume fraction. Within the pressure and temprature ranges investigated, the liquid volume fraction changes between 10% and 90%. Again, in both cases with CO_2 and N_2, we see a gradual increase in the process efficiency through the low temperature - high pressure region where the liquid content approaches 90%. In the case with volatile oil, the distribution is different than the black oil and heavy oil, because of the high gas content in the reservoir. In the interval of interest, the liquid fraction varies between 5% and 50%. Although the liquid fraction is very low, the process efficiency increases as the liquid fraction increases from 5% to 50%. However, the process is also significantly influenced by the high gas fraction in the system. After injecting CO_2 or nitrogen, partial pressures of the reservoir gas and the injected gas come into the picture. When there is a higher gas fraction in the reservoir, the final partial pressure of the reservoir also becomes higher. This forces more gas to go back into the solution and increase the liquid fraction. Therefore, in cases where there is a higher initial gas fraction, more gas goes back into the solution after injecting CO_2/nitrogen and soaking. In the contour plot, we see that these two mechanisms interfere with each other, and the efficiency increases through the constant quality line. In this case, high pressure and temperature regions become the favorable regions for volatile oil.

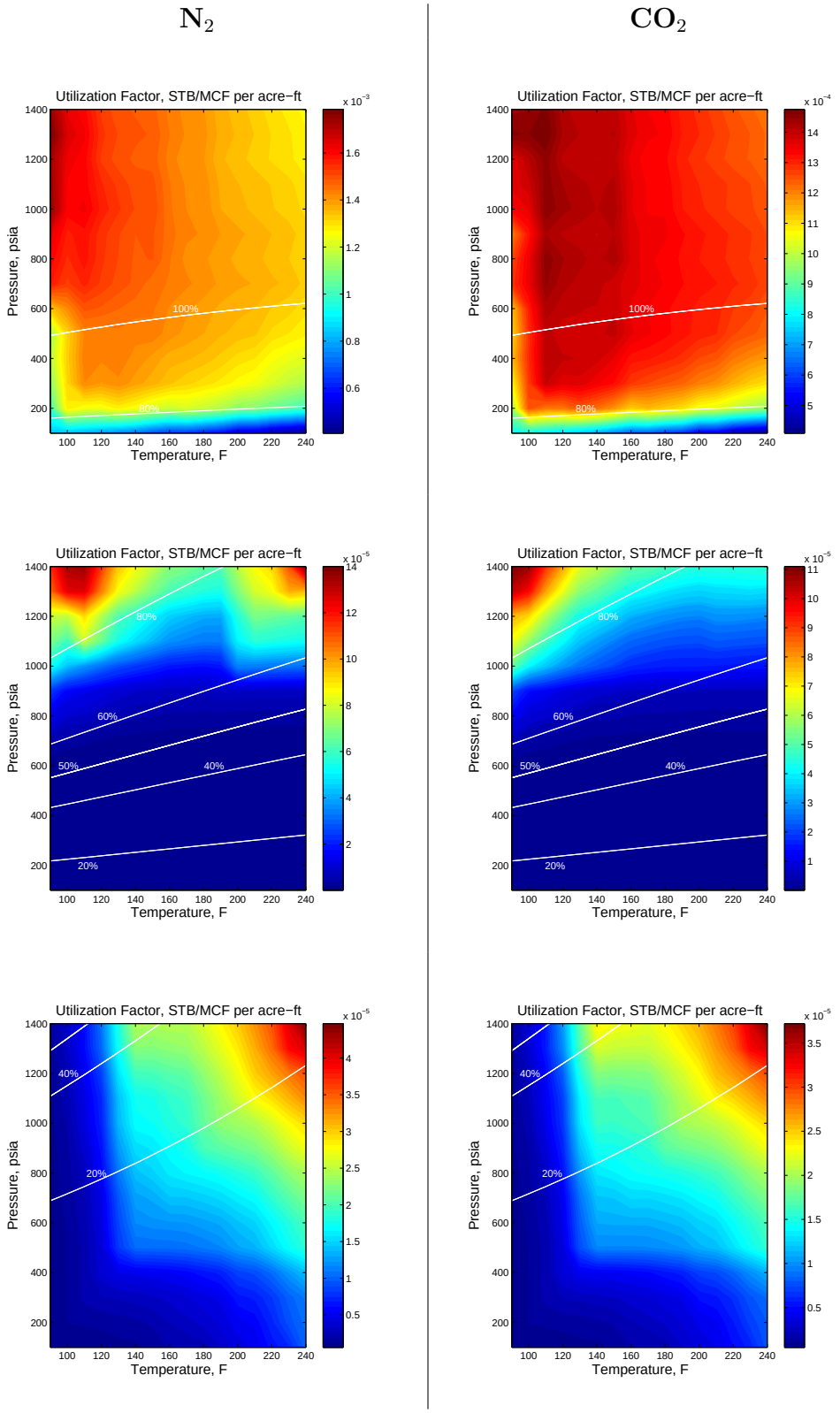

Figure 7.14. Areal distribution plots of utilization factor per acre-ft with changing pressure and temperature (white lines indicate liquid volume % quality lines; top: heavy oil, middle: black oil, bottom: volatile oil).

7.3 Summary and Conclusions

In this chapter, results of a detailed parametric study are presented. The purpose of this study was to develop a better understanding on how operational parameters and reservoir characteristics affect the performance of the cyclic pressure pulsing process. Comparative discussions are presented among cases with CO_2 and N_2 on different reservoir fluids (heavy, black and volatile oils).

The major conclusions of this chapter can be summarized as the following:

1. NPV is mainly a function of incremental oil production as NPVs are affected in a similar fashion at the same operating conditions. Therefore, while the initial peak oil rate is important, the cumulative oil production is the most important criterion from the economics perspective. The peak oil rate increases with the injected gas volume, but the shape of the decline behavior of the production is dependent on other factors.

2. Injection at a higher rate for a shorter period of time is observed to be more effective than injecting for a longer time at a lower rate.

3. Based on the injection rate and amount, optimum soaking time can vary. In the Big Andy Field, for treatments larger than 500 MCF, it was observed that soaking up to 60 days may result in an increase in the NPV for a given injection cycle.

4. With the current oil prices, the cost of injected gas becomes insignificant in the economic considerations. Increased income due to increased oil production overcomes the increased costs with higher volumes of gas. Nitrogen, as a lower-cost gas, was found to be a better choice with higher NPV than CO_2 in the Big Andy Field. Also, because of its low cost, it is not affected negatively from higher number of cycles as is the case with CO_2.

5. The process is found to be more effective in thin reservoirs. Thicknesses ranging between 20-50 ft produced more favorable results.

6. In terms of the area, we see higher efficiency with smaller area (5-8 ft) with heavy oil. For the cases with volatile and black oil, it is seen that the process efficiency is not significantly affected by the area.

7. Higher fracture permeabilities increase the process efficiency.

8. The phase behavior of the reservoir fluid is very important for the performance of the process. Initial pressure/temperature of the reservoir, and therefore, the initial fractions of gas/liquid phases affect the process significantly.

9. The way reservoir characteristics affect the process performance is very similar in cases with CO_2 and N_2, but may differ significantly in different reservoir fluids.

Chapter 8

Optimization Studies

In this part of the study, the goal is to develop optimized design strategies, to maximize the efficiency of the cyclic injection process. The genetic algorithm (GA) is used as the optimization tool (explained in Section 4.2). The approach couples ANN with GA as explained in Section 4.3. In this approach, GA evaluates different design scenarios by using the forward ANN proxy, and searches for the best design scenario that maximizes a specified objective function. First, the optimization tool is tested with simple objective functions, and then more advanced objective functions are used to optimize the cyclic injection process. These studies are presented in this section.

8.1 Testing of the Optimization Tool

Before starting the advanced optimization studies, it is aimed to test the optimization tool, as well as the accuracy of the ANN proxy approximator. This is done by specifying simple objective functions that are easy to optimize even without using an optimization tool (*e.g.*, maximizing the cumulative oil production). An in-house GA code is used, which is based on base-10 system for string representation. The characteristics are shown in Table 8.1. The number of variables is 20, since they represent four primary design parameters for five cycles. These are the variables which are modified to search for the optimum configuration.

As mentioned above, the first test was made with a simple objective function: *maximizing the cumulative oil production.* Although the algorithm provided near-

Table 8.1. GA parameters.

Population size (No. of individuals), N_p	10
Number of variables	20
Number of genes (for each variable)	6
Mutation probability, p_m	0.01
Crossover probability, p_c	0.9
Max. change in fitness for termination, ϵ	0.001
Counter for termination	100
Max. number of generations, n_{max}	1000

optimal solutions, it was observed that the predictions of the ANN approximator were not accurate. The algorithm was trying to search around the variable limits that were input, where the ANN approximator failed to provide accurate answers. This showed that the network was not trained well for cases where the design parameters get values, which are close to limits. Then, fifty new cases were generated and fed into the network for training in addition to the previous cases. It was expected to have the network learn from these cases to provide more accurate outputs in regions close to variable upper/lower limits.

With the new approximator, the GA was run again to provide the solution for maximum oil production. The total cumulative oil production of this design was predicted by the approximator to be 5,362.3 STB, while the maximum value that was included in the training data was 4,674 STB. This shows that the GA was able to go beyond the cases that were shown to the ANN, and suggest a scenario that is better than the ones in the training set. The provided scenario was the one shown in Table 8.2. Maximum gas injection amount, soaking and production periods are suggested as an expected result of maximum oil production objective.

Table 8.2. Recommended scenario for maximum oil production.

Cycle	Inj. rate, MSCF/d	Inj., days	Soak., days	Prod., months
1	100.0	40	40	25
2	100.0	40	40	25
3	100.0	40	40	25
4	100.0	40	40	25
5	100.0	40	40	25

To check the performance of the new approximator, its recommendation was run with the simulator and simulator outputs were checked with the network outputs. Figure 8.1 shows the comparison of actual and network outputs of some critical parameters. X-axis is the cycle number. As can be seen in this figure the new approximator was able to make predictions with reasonable accuracy.

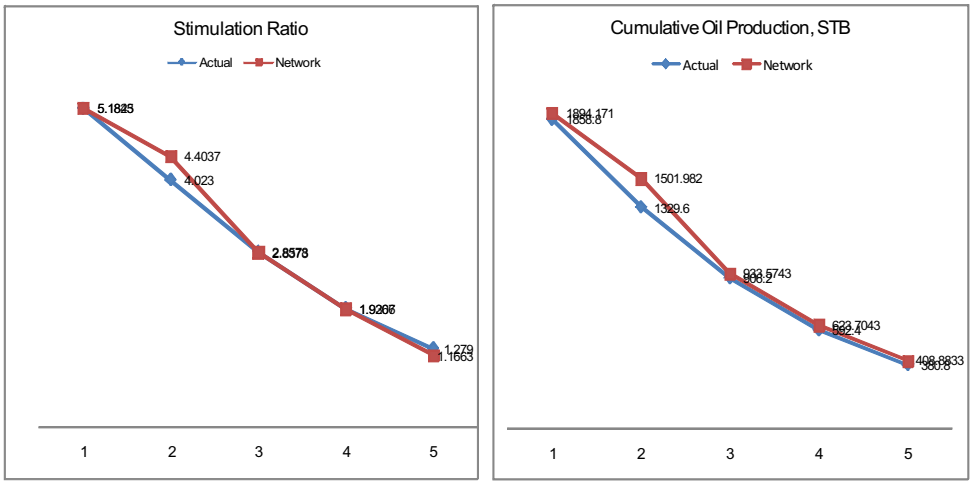

(a) Stimulation ratio

(b) Cumulative oil production

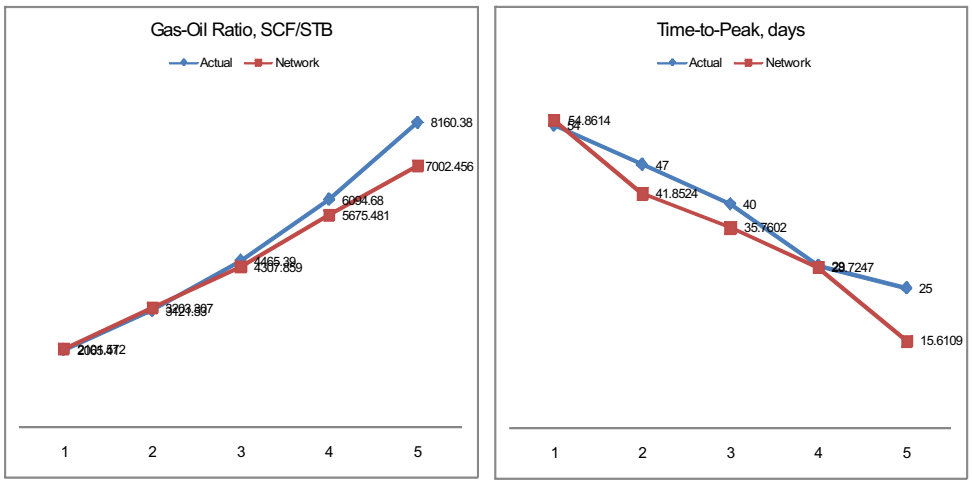

(c) Gas-oil ratio at the end of cycle

(d) Time to reach the peak oil rate

Figure 8.1. Comparison of simulator and network outputs for the scenario recommended by GA to maximize the cumulative oil produced.

Another simple objective function was defined as the ratio of the cumulative oil produced to the cumulative gas injected. Here, we would like to maximize the cumulative oil production, while minimizing the cumulative gas injected. Also known as the utilization factor, this function is an indicator of the overall efficiency of the process rather than oil production only, since it also accounts for the amount of gas that is used to produce the oil. As in the previous case, the GA suggestion provided a ratio of **1.03** STB/SCF, while the maximum value found in the training set is **0.7** STB/SCF. In this case, the provided solution was the one shown in Table 8.3.

Table 8.3. Recommended scenario for maximum oil production and minimum gas injection.

Cycle	Inj. rate, MSCF/d	Inj., days	Soak., days	Prod., months
1	50.0	7	40	25
2	50.0	7	40	25
3	50.0	7	40	25
4	50.0	7	40	25
5	50.0	7	40	25

It is seen from the above table that the following are suggested:

- Minimum gas injection amount
- Maximum soaking period
- Maximum production period

As in the previous case, this recommendation was tested using the simulator, and simulator outputs were checked with the network outputs. Figure 8.2 shows the comparison of actual and network outputs of some critical parameters. As can be seen in this figure the new approximator was able to make predictions with reasonable accuracy.

These studies showed the weakness of the ANN proxy and it was improved by including more cases, which are close to the limits of the ranges. It was observed that the optimization tool was able to provide correct solutions once the approximator is accurate enough to evaluate the objective function. This part of the study

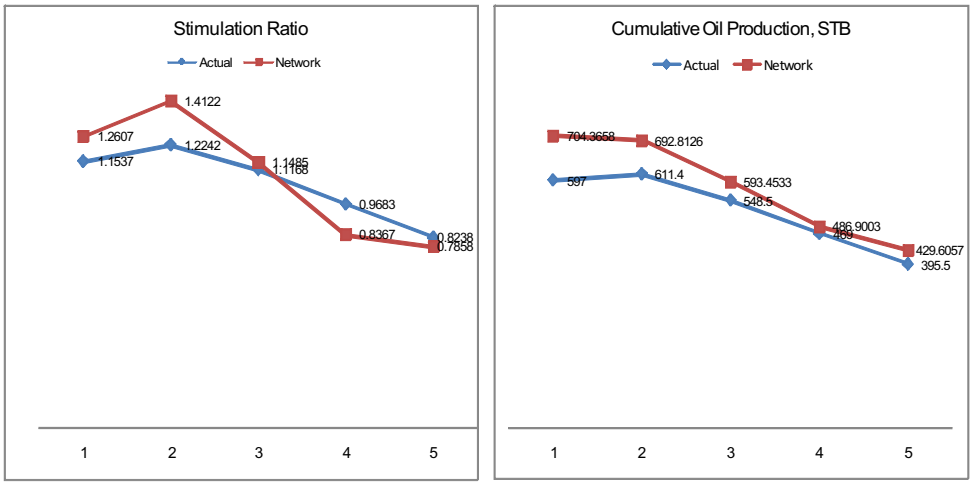

(a) Stimulation ratio

(b) Cumulative oil production

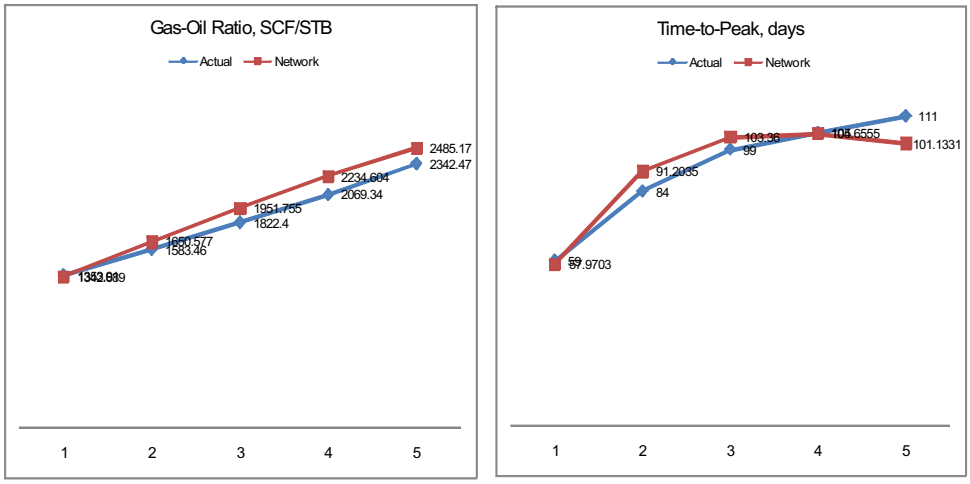

(c) Gas-oil ratio at the end of cycle

(d) Time to reach the peak oil rate

Figure 8.2. Comparison of simulator and network outputs for the scenario recommended by GA to maximize the cumulative oil produced and minimize the amount of gas injected.

was done using the proxy for pure N_2 injection. The following sections include the design optimization of cyclic N_2 and CO_2 processes with more advanced objective functions.

8.2 Optimization in the Big Andy Field

8.2.1 Design Scheme-1

Before beginning an optimization study, it is of crucial importance to determine an objective, which clearly covers our needs. There may be more than one objective, and the objective function that is specified must cover all these objectives. As explained in Chapter 3, maximum efficiency of the cyclic injection process for a given time period can be obtained *vis-à-vis* two important goals:

1. Maximizing the income due to the produced oil
2. Minimizing the operational costs due to the injected gas

In order to design the optimization tool in a way that it would provide us with the design procedures that would make the project achieve these goals, we need to analyze all variables associated with the process. As previously defined, we have process design parameters and performance indicators that are associated with the cyclic injection process. To define our objective function, we need to list all parameters that are involved in the process to see which ones are contributing to the efficiency, and which ones are not. Table 8.4 shows all variables involved in the process and whether they need to be maximized or minimized to achieve the two goals mentioned above.

Considering these, the following objective function was used to optimize N_2 injection:

$$f = \frac{sum(q) + sum(SR) + sum(COP)}{sum(TTP) + sum(GOR) + sum(IP) + sum(SP) + sum(PP) + sum(INJ)} \tag{8.1}$$

Sum indicates the summation of these variables for five cycles. With this objective function, a maximum of **4.36** is obtained, while the training set's maximum was **3.67**. The recommended design is shown in Table 8.5. Comparison of the outputs of this configuration are shown in Figure 8.3.

Table 8.4. Objectives.

Performance indicators	
Parameter	Objective
Flow rates (q1....q9)	*maximize*
Stimulation ratio (SR)	*maximize*
Cumulative oil production (COP)	*maximize*
Incremental oil production (IOP)	*maximize*
Time-to-reach the peak rate (TTP)	*minimize*
Initial and final gas rates (GR1, GR2)	*minimize*
Final gas-oil-ratio (GOR)	*minimize*
Design parameters	
Parameter	Objective
Injection Period (IP)	*minimize*
Soaking period (SP)	*minimize*
Production period (PP)	*minimize*
Amount of injected gas (INJ)	*minimize*

Table 8.5. Recommended scenario for Eqn. 8.1.

Cycle	Inj. rate, MSCF/d	Inj., days	Soak., days	Prod., months
1	50.0	32	7	6
2	100.0	7	7	6
3	100.0	7	7	6
4	50.0	25	7	6
4	50.0	25	7	6

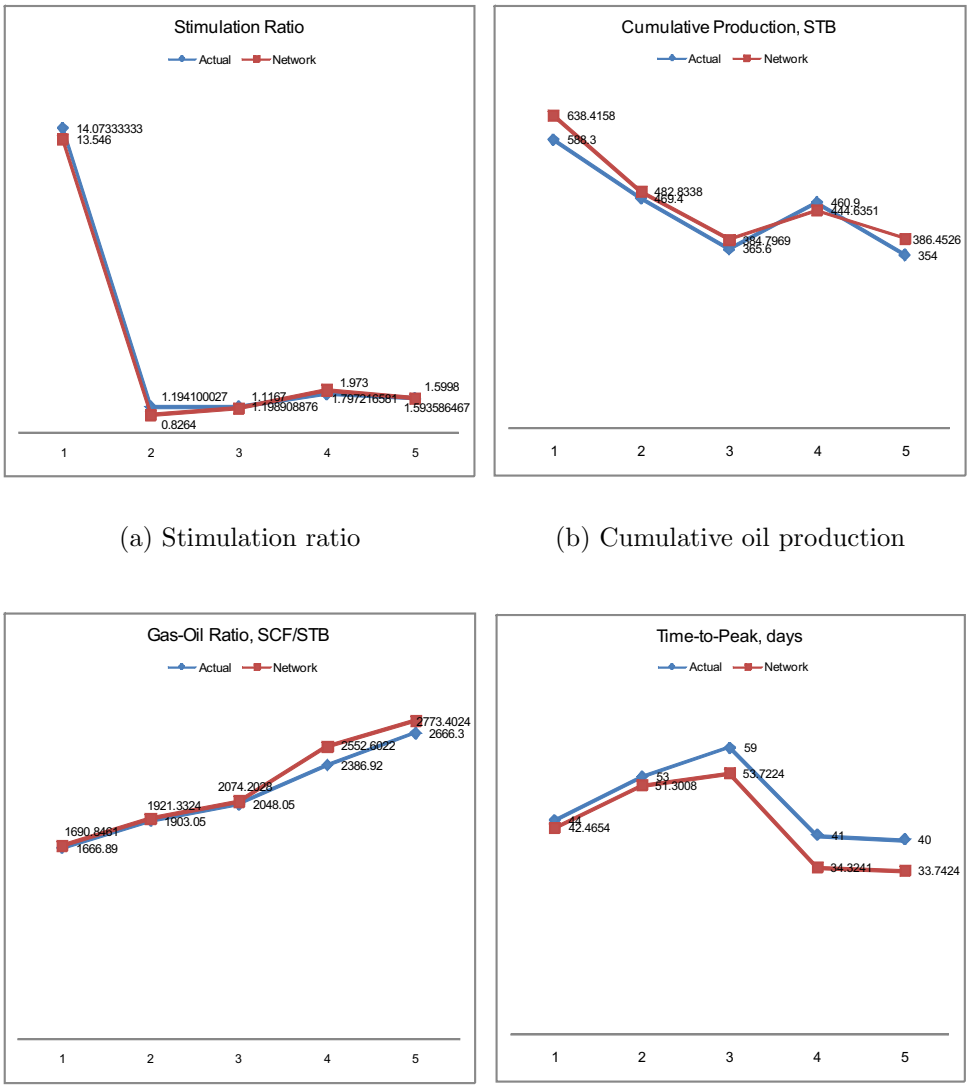

(a) Stimulation ratio

(b) Cumulative oil production

(c) Gas-oil ratio at the end of cycle

(d) Time to reach the peak oil rate

Figure 8.3. Comparison of simulator and network outputs for the scenario recommended by GA for Eqn. 8.1.

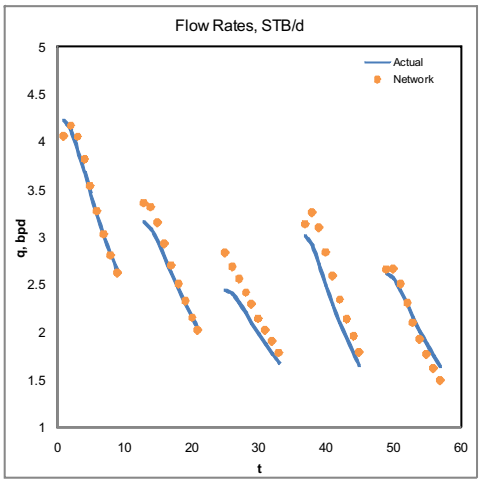

Figure 8.4. Comparison of simulator and network flow rates for the scenario recommended by GA for Eqn. 8.1.

Although this objective function satisfies most of the objectives that were defined, minimization of the production time, and maximization of flow rate summation requirements forced the algorithm for a design scenario having 6 months of production in each cycle. For short-term planning of the project this scenario would be feasible. However, if we look at Figure 8.4, the flow rates at the end of cycles are all larger than 1.5 STB/d. Currently, in the Big Andy Field, the wells are produced until they reach an oil production rate of 0.3 STB/d, which is considered to be economic with current oil prices. Thus, it can be stated that by the recommendation provided by this objective function, each cycle does not produce until actual economic limits to comply with the requirement of shorter production periods with higher rates. Because of that, another objective function can be defined by removing the flow rate and production period specifications:

$$f = \frac{sum(SR) + sum(COP)}{sum(TTP) + sum(GOR) + sum(IP) + sum(SP) + sum(INJ)} \tag{8.2}$$

This objective function is used to determine the optimum design of both N_2 and CO_2 utilization projects. For N_2, the maximum value obtained was **0.83**, while the training set's maximum is **0.58**. For CO_2, the maximum value obtained was **0.82**, while the training set's maximum is **0.44**. Tables 8.6 and 8.7 show the recommended designs.

Table 8.6. Recommended scenario for N_2 injection (objective function: Eqn. 8.2).

Cycle	Inj. rate, MSCF/d	Inj., days	Soak., days	Prod., months
1	50.0	32	7	24
2	100.0	7	7	24
3	50.0	40	7	24
4	50.0	18	7	24
5	50.0	40	7	24

Table 8.7. Recommended scenario for CO_2 injection (objective function: Eqn. 8.2).

Cycle	Inj. rate, MSCF/d	Inj., days	Soak., days	Prod., months
1	72.1	7	7	24
2	100.0	40	7	24
3	100.0	7	7	24
4	50.0	40	7	24
5	50.0	40	7	24

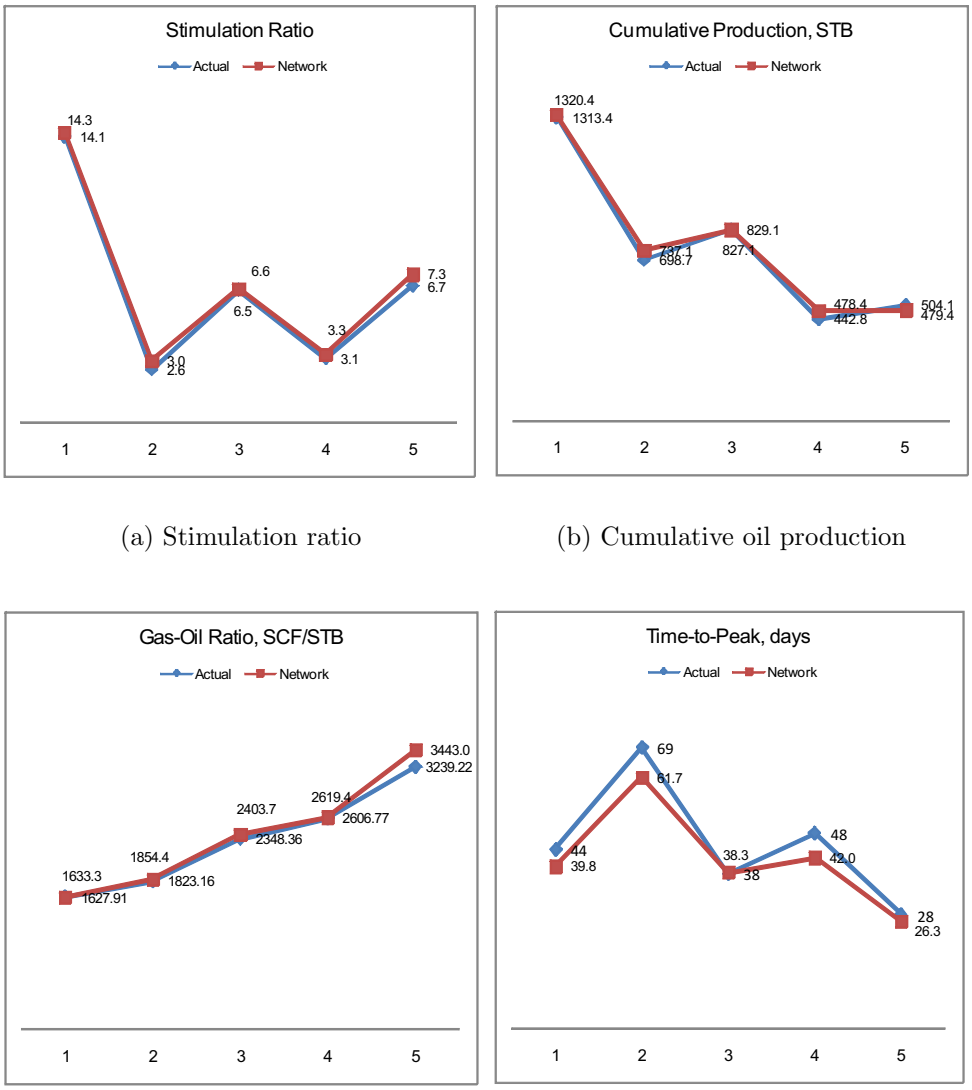

(a) Stimulation ratio

(b) Cumulative oil production

(c) Gas-oil ratio at the end of cycle

(d) Time to reach the peak oil rate

Figure 8.5. Comparison of simulator and network outputs for the scenario recommended by GA for N_2 injection (objective function: Eqn. 8.2).

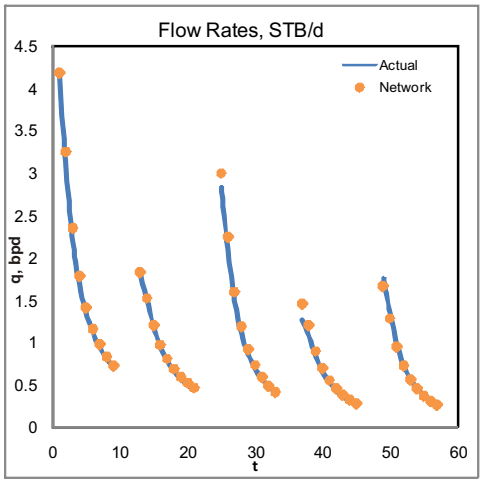

Figure 8.6. Comparison of simulator and network flow rates for the scenario recommended by GA for N_2 injection (objective function: Eqn. 8.2).

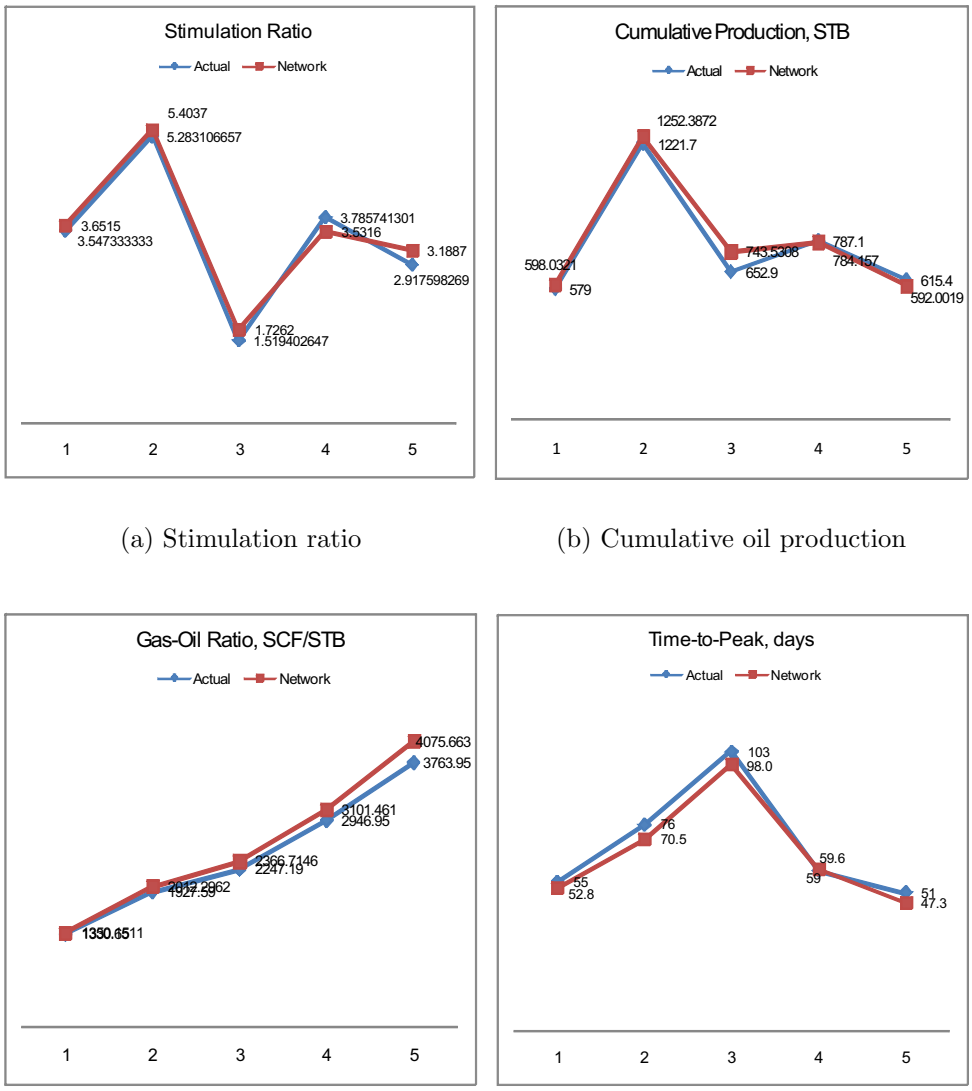

(a) Stimulation ratio

(b) Cumulative oil production

(c) Gas-oil ratio at the end of cycle

(d) Time to reach the peak oil rate

Figure 8.7. Comparison of simulator and network outputs for the scenario recommended by GA for CO_2 injection (objective function: Eqn. 8.2).

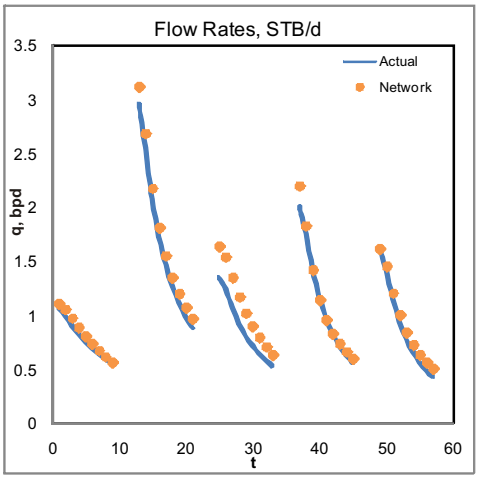

Figure 8.8. Comparison of simulator and network flow rates for the scenario recommended by GA for CO_2 injection (objective function: Eqn. 8.2).

8.2.2 Design Scheme-2

In this part of the optimization studies, the neural network model, which was developed with the Design Scheme-2 is used. In this design scheme the performance indicators used are the NPV and the incremental oil production. NPV is a powerful objective function because it includes all incomes and costs involved and ties them to the time value of the money. Therefore, it is a realistic objective function to evaluate different design scenarios.

Before running the optimization tool, available scenarios in the knowledge base were analyzed to develop an understanding of the parameters that influence the NPV. The best thirty design scenarios were analyzed, which resulted in the highest NPV values among the scenarios. In these cases, it was seen that on average, the injected gas amount is approximately 2,000-2,500 MCF/cycle, with 80-100 MCF/d of injection for approximately 30 days, and soaking for approximately 25 days. The projects' life time tended to be 5-7 years. The histograms plotted for each parameter for the thirty best cases are shown in Figure 8.9.

In order to determine the most optimum design scenario that would maximize the NPV, the genetic algorithm was used to perform a stochastic search over the response surface that is generated by the neural network model. The recommended scenario was close to the average values obtained with available design scenarios, which had higher NPV's as mentioned above. The recommended design scenario is shown in Table 8.8. The network model predicted the NPV of this scenario as **$31,793**, while the forecasted NPV using the numerical model was **$31,595**. This indicates high accuracy in the prediction of the neural network. The recommended scenario's oil production history is shown in Figure 8.10-a, with four cycles of injection. Net cash flow history during the production and injection cycles is shown in Figure 8.10-b. This design scenario resulted in **933.1** STB of incremental oil production.

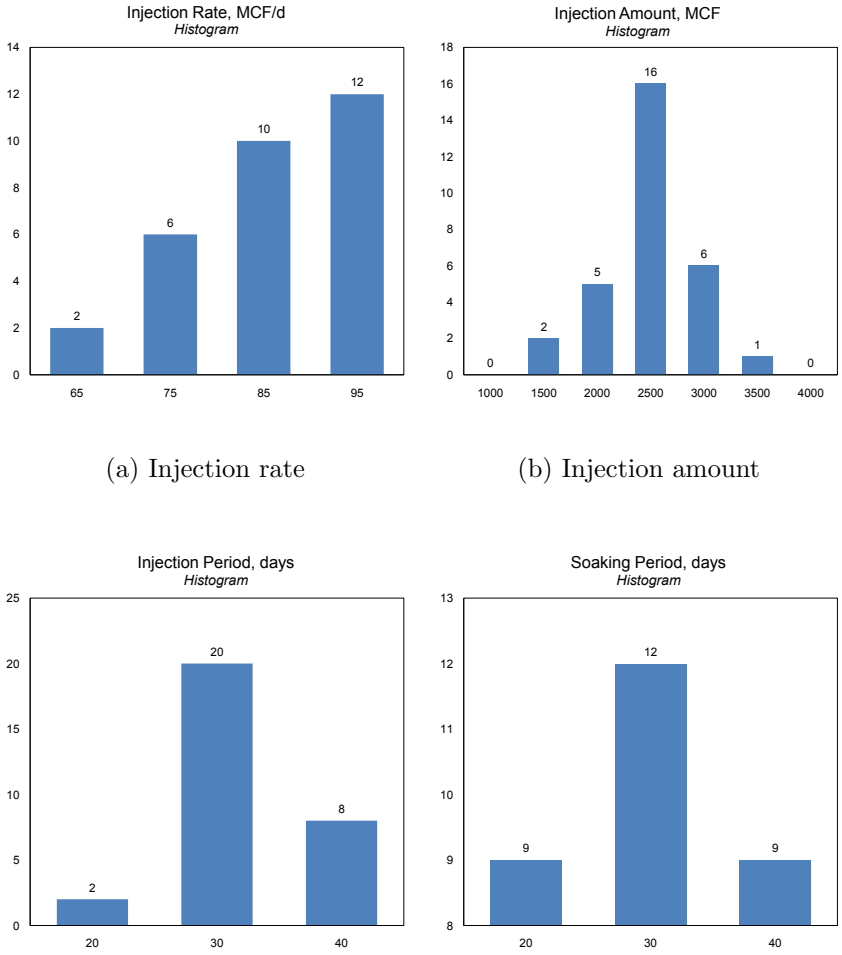

(a) Injection rate

(b) Injection amount

(c) Injection period

(d) Soaking period

Figure 8.9. Histograms for the best 30 design scenarios that resulted in a high NPV.

Table 8.8. Recommended scenario to maximize the NPV.

Project life, years	5
Cycle abandonment rate, STB/d	0.5
Injection rate, MCF/d	72.4
Injection period, days	28
Injection volume, MCF	2,026.4
Soaking period, days	24
Forecasted NPV (neural network prediction)	$31,793
Forecasted NPV (numerical model)	$31,595

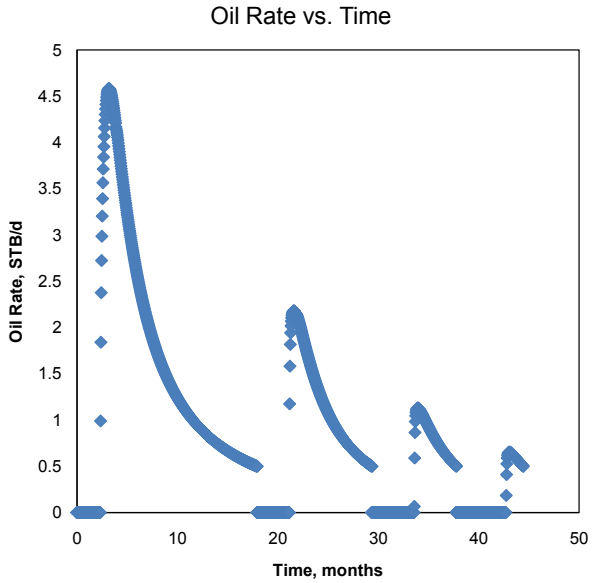

(a) Oil production history

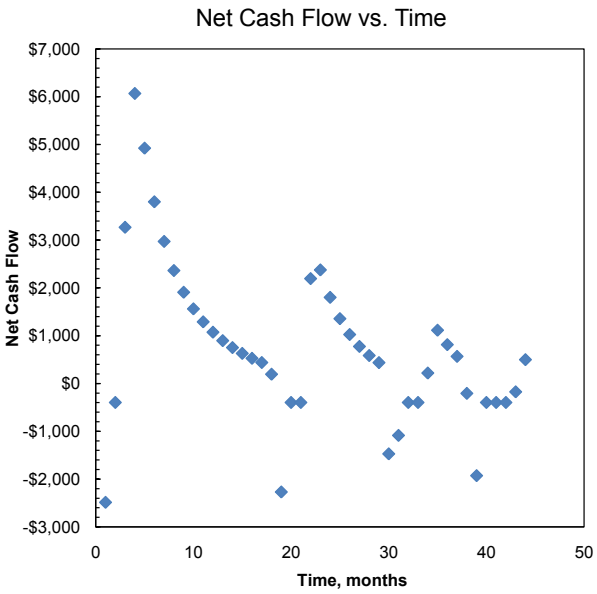

(b) Net cash flow

Figure 8.10. Oil production history and net cash flow output of the recommended design scenario.

8.3 Optimization in Different Reservoirs

In Chapter 6, design and development of universal proxies are presented. These proxies are able to accurately predict the performance of the cyclic pressure pulsing process for any reservoir that has characteristics in the range these proxies were trained (Table 6.1). To optimize the design of the process in reservoirs with different characteristics these proxies can be used for high-performance evaluation of the objective function. In this section, some examples are presented, where these proxies are coupled with the genetic algorithm to provide optimized design scenarios for the reservoir under consideration. To incorporate the time-value of the money in the objective function the cumulative oil production in each cycle is converted to today's (discounted) oil production with the following equation:

$$CP_{t=0} = \sum_{n=1}^{5} \frac{CP_n}{(1+i)^{t_n}} \tag{8.3}$$

where n is the cycle number, CP is the cumulative oil production, i is the interest rate. t_n is the total time from $t = 0$ until the production stops in that cycle. Therefore, it is defined as the summation of the injection, soaking, and production periods for all previous cycles and the cycle under consideration:

$$t_n = \sum_{m=1}^{n} (t_{pp_m} + t_{sp_m} + t_{ip_m}) \tag{8.4}$$

where t_{pp} is the length of the production period, t_{sp} is the length of the soaking period, and t_{ip} is the length of the injection period. The objective is to maximize the cumulative oil production as of today's value for each MCF of gas injected. In this way, the costs associated with the injection are to be minimized. Therefore, the objective function is defined as:

$$f = \frac{CP_{t=0}}{CI} \tag{8.5}$$

where CI is the cumulative volume of the injected gas. The genetic algorithm is used with the parameters shown in Table 8.1. The optimization is done for four different reservoirs. The characteristics of these reservoirs are shown in Table 8.9.

Table 8.9. Reservoir characteristics of example cases used for optimization.

Example No.	1	2	3	4
Reservoir fluid Injected fluid	Volatile Nitrogen	Heavy Nitrogen	Volatile CO_2	Volatile Nitrogen
A, acres	8	7	16	7
h , ft	93	78	99	91
p_i, psia	514	254	251	802
ϕ_m	0.15	0.16	0.15	0.14
ϕ_f	0.03	0.02	0.01	0.02
$k_{m_{x,y}}$, md	86	59	35	59
k_{m_z}, md	2.58	7.08	7.35	12.39
k_f, md	3,623	2,811	3,983	1,011
X_f, ft	14.25	60.8	80.75	71
T, F	137	81	161	235
S_{wi}	0.67	0.47	0.58	0.42

The recommended design scenarios for each reservoir that maximizes the objective function in Eqn. 8.5 are shown in Table 8.10. The comparison of proxy predictions with the simulation outputs for these recommended scenarios is shown in Figure 8.11.

Table 8.10. Recommended scenarios for different reservoirs.

Example Case - 1				
Cycle	Inj. rate, MSCF/d	Inj., days	Soak., days	Prod., months
1	75	13	30	12
2	55	9	10	4
3	67	21	36	5
4	114	18	8	4
5	116	6	41	6
Example Case - 2				
Cycle	Inj. rate, MSCF/d	Inj., days	Soak., days	Prod., months
1	184	46	50	12
2	54	34	50	12
3	158	23	7	8
4	191	31	7	12
5	132	40	50	6
Example Case - 3				
Cycle	Inj. rate, MSCF/d	Inj., days	Soak., days	Prod., months
1	30	37	40	4
2	58	8	10	4
3	71	10	6	6
4	37	37	6	4
5	95	21	6	5
Example Case - 4				
Cycle	Inj. rate, MSCF/d	Inj., days	Soak., days	Prod., months
1	119	8	6	8
2	37	15	40	4
3	48	13	6	6
4	90	11	10	6
5	123	25	8	7

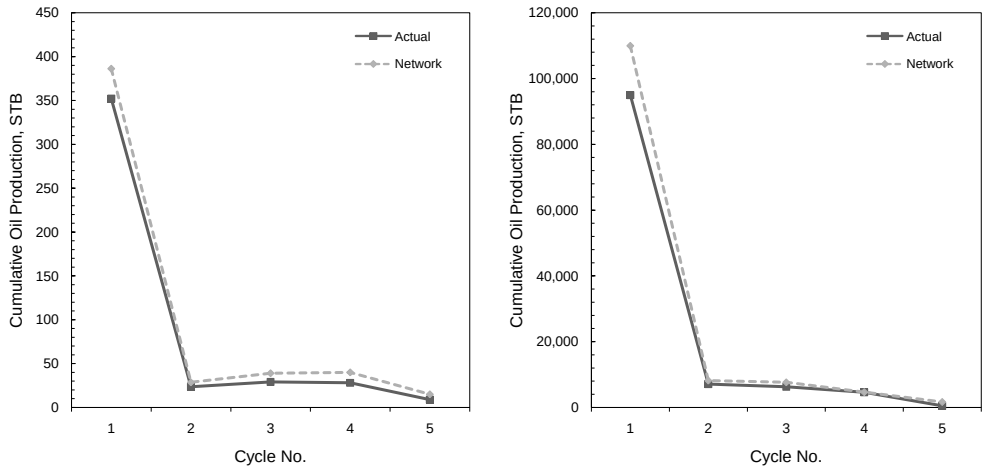

(a) Example Case - 1

(b) Example Case - 2

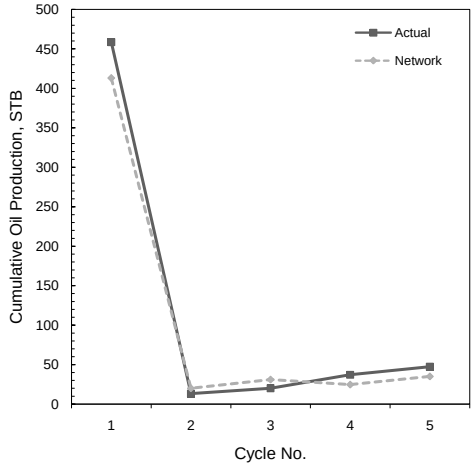

(c) Example Case - 3

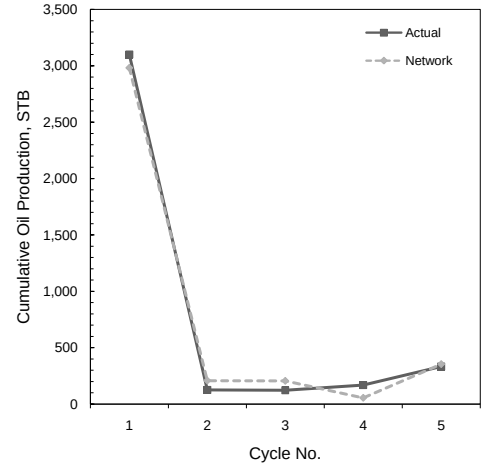

(d) Example Case - 4

Figure 8.11. Comparison of simulator and network outputs for the recommended scenarios by GA for different reservoirs.

8.4 Summary and Conclusions

In this chapter, optimization studies are presented. The hybrid neuro-genetic approach is applied to the cyclic pressure pulsing problem using the ANN-based proxies to evaluate the specified objective function. These studies showed that the optimization tool works well with the ANN approximator, achieving the specified goal (maximizing the specified objective function). It can be stated that GA's can be used to validate the robustness of an ANN approximator, since it searches through regions that may not have been otherwise checked for verification purposes. An important conclusion is that the nature of the problem may change dramatically by including/excluding some process variables. Therefore, it is very important to define the problem very clearly, and select the involved variables and the objective function based on the problem. Excluding some variables may force the algorithm to miss critical attributes of the problem, while including some unnecessary variables may mislead the algorithm to different directions during the search process.

The optimization studies for the Big Andy Field were done for both design schemes used in this study. Using Design Scheme-1, the process design parameters were optimized for five cycles of injection. Different objective functions were defined for a preliminary analysis. It was observed that the recommended scenario changes significantly with different objective functions. Short soaking (7 days) and long production times (24 months) were found to be the most optimum design scenario, when the objective function is re-defined considering the field production rates. While variable cycle injection volumes were recommended for both CO_2 and N_2 injection, the average injection volume in each cycle was 1,600 MCF.

To incorporate all the important process variables that have an influence on the process economics, a neural-network model that predicts the NPV is used with the second design scheme. The optimum treatments that maximize the NPV are found to be around 2,000-2,500 MCF/cycle for a multi-cycle process with a rate of 70-100 MCF/d and soaking for 25-30 days. With the recommended scenario, the project lasted for 4 cycles producing 933.1 STB of incremental oil.

Finally, universal proxies developed in Chapter 6 were used to optimize the process in reservoirs with different characteristics. Four different reservoirs are

used as example case studies. The genetic algorithm provided optimum design scenarios for the objective function defined in Eqn. 8.5. It was observed that the proxy predictions were in agreement with the simulation outputs.

Chapter 9

Concluding Remarks

In this study, cyclic pressure pulsing processes with pure N_2 and pure CO_2 are investigated. The study focuses on naturally fractured reservoirs. Reservoir simulation studies were done to develop a better understanding of the recovery mechanisms involved in this process. For modeling, two design schemes using constant and variable injection volumes were applied. Detailed parametric analyses were done in a wide range of reservoir characteristics to understand the conditions that favor the process. Performance assessment was done by using both NPV and incremental oil production as the performance indicators. A high-performance, neuro-genetic optimization methodology is used to develop optimized design scenarios for the process.

First, the proposed methodology was applied to Big Andy Field in Kentucky. Neural-network based proxy models were constructed that accurately predict the process performance for a given set of design parameters in the same reservoir. Then, universal proxy models were constructed by including variations in reservoir characteristics. Optimization was done using the genetic algorithm as the optimization tool. Developed proxies were used to evaluate the specified objective function. Using proxies for evaluation improved the computational efficiency of the optimization process.

In the following sections, the major conclusions and recommendations for future research are presented.

9.1 Conclusions

The major conclusions of this study are as follows:

1. Cyclic pressure pulsing is an effective IOR method in fractured reservoirs. Volume of the injected gas in each cycle is the most critical parameter in affecting the performance. While soaking has little effect, optimization of soaking would yield higher recovery and NPV. Injection at a higher rate for a shorter period of time is observed to be more effective than injecting for a longer time at a lower rate.

2. The process was found to be more effective in thin reservoirs. Thickness ranging between 20-50 ft produced more favorable results. In terms of the area, higher efficiency was observed with smaller area (5-8 acres) with heavy oil. For the cases with volatile and black oil, it is seen that the process efficiency is not affected by the area significantly. Higher fracture permeabilities increase the process efficiency.

3. The phase behavior of the reservoir fluid is very important for the performance of the process. Initial pressure/temperature of the reservoir, and therefore, the initial fractions of gas/liquid phases affect the process significantly.

4. Artificial neural networks are powerful in constructing proxies to mimic reservoir models. As shown in earlier studies they can be used effectively in screening IOR methods. In this study, they are effectively used in screening and optimizing cyclic pressure pulsing applications.

5. Inverse networks were developed that go beyond the capabilities of a reservoir simulator. These networks provided the design parameters once the desired performance is specified. Development of these networks was more challenging, and a more complicated training algorithm with recurrent connections were used to improve the training.

6. Universal proxies were developed using a more complicated neural network structure to compensate for the additional complexity in the problem for both

design schemes. Same architectures were used for CO_2 and N_2 injection and for heavy, black and volatile oils.

7. Predicted parameters such as the peak oil rate and time-to-peak resulted in larger errors than other parameters because of their instantaneous behavior. Neural networks were more successful in predicting flow rates in a smoothly-declining region where rates do not change sharply from one time-step to another.

8. Analysis of the weights in connection links provided valuable information about the networks. The common observation with both N_2 and CO_2 is that the following are the most critical reservoir properties affecting the process performance:

   - Fracture permeability
   - Ratio of fracture permeability to matrix permeability
   - Area
   - Oil-in-place
   - Ah product
   - Oil saturation

9. During data preparation, the fracture-permeability data are distributed in the data base after considering the sensitivity of the system behavior to permeability. Using the new distribution rather than using a uniform one for the training improved the performance and generalization capabilities of the neural network.

10. The mechanisms involved with N_2 and CO_2 are very similar, with the only difference being the dissolution of CO_2 in the oil at very low pressures. When the costs are involved in the analysis, nitrogen was found to be a better alternative. However, this must be re-evaluated for different prices of oil, N_2 and CO_2.

11. It was shown that the genetic algorithm worked well with neural-network proxies. The nature of the problem may change dramatically by includ-

ing/excluding some process variables, thus yielding different optimum solutions. Therefore, it is very important to define the objective function after considering all dimensions of the problem.

9.2 Recommendations for Future Work

The current study can be further improved with the following potential research:

- Instead of developing different proxies for different types of gases, injected gas composition may be included as a design parameter. Other types of gases such as oxygen and/or natural gas may be included as alternative types of gases.
- The effectiveness of the process in hydraulically fractured wells can be investigated and compared with naturally fractured systems.
- The upper pressure limit may be increased and miscibility conditions at higher pressures may be studied.
- While this study covers a wide range of reservoir characteristics and conditions, the range of parameters studied may be extended even further to cover extreme conditions.
- The proxy models developed may be coupled with other proxy models, which were developed for other IOR applications. This may give the practicing engineer the opportunity to analyze different IOR methods simultaneously for the reservoir under consideration.
- Other evolutionary optimization algorithms may be used and compared with the genetic algorithm.

References

Abboud, A. (2005). *A Study of Cyclic Injection of Nitrogen on Mid-Continent Crude Oil: An Investigation of the Vaporization Process in Low Pressured Shallow Reservoirs*. Master's thesis, The Pennsylvania State University, University Park, Pennsylvania.

Arps, J. (1945). Analysis of Decline Curves. *Trans. AIME*, **160**:228–247.

Asghari, K. and Torabi, F. (2007). Laboratory Experimental Results of Huff-and-Puff CO_2 Flooding in a Fractured Core System. In *SPE Annual Technical Conference and Exhibition Proceedings*. SPE 110577. 11-14 November. Anaheim, California.

Ayala, L. and Ertekin, T. (2005). Analysis of Gas-Cycling Performance in Gas/Condensate Reservoirs Using Neuro-Simulation. In *SPE Annual Technical Conference and Exhibition Proceedings*. SPE 95655. 9-12 October. Dallas, Texas.

Bardon, C., Corlay, P., Longeron, D., and Miller, B. (1994). CO_2 Huff 'n' Puff Revives Shallow Light-Oil-Depleted Reservoirs. *SPERE*, **9**(2):92–100. SPE 22650.

Bardon, C., Karaoguz, D., and Tholance, M. (1986). Well Stimulation by CO_2 in the Heavy Oil Field of Camurlu in Turkey. In *SPE Enhanced Oil Recovery Symposium Proceedings*. SPE 14943. 20-23 April. Tulsa, Oklahoma.

Biswas, D. (1993). *A Study of the Cyclic CO_2 Oil Recovery Process with a Compositional Simulator*. Master's thesis, The University of Texas at Austin, Austin, Texas.

Centilmen, A., Ertekin, T., and Grader, A. S. (1999). Applications of Neural Networks in Multiwell Field Development. In *SPE Annual Technical Conference and Exhibition Proceedings*. SPE 56433. 3-6 October. Houston, Texas.

Claridge, E. (1984). The CO_2 Huff & Puff Process. In *Proceedings of the Enhanced Recovery Week Symposium: EOR Using CO_2*. 6 December. Houston, Texas.

Cook, A. (1957). Alternate Producing and Gas Repressuring for Greater Oil Recovery. *J. Pet. Tech.*, **9**(5):15–18. SPE 778.

Cook, A., Johnson, F., Spencer, G., and Bayazed, A. (1967). The Role of Vaporization in High Percentage Oil Recovery by Pressure Maintenance. *J. Pet. Tech.*, **19**:245–250. SPE 1646.

Crosby, G. and Cochran, R. (1960). Performance of an Alternate Repressuring and Producing Project. *J. Pet. Tech.*, **12**(9):39–41. SPE 1395.

Cullick, A., Johnson, D., and Shi, G. (2006). Improved and More Rapid History Matching With a Nonlinear Proxy and Global Optimization. In *SPE Annual Technical Conference and Exhibition Proceedings*. SPE 101933. 24-27 September. San Antonio, Texas.

Demuth, H., Beale, M., and Hagan, M. (2006). *MATLAB Neural Network Toolbox, Version 5, User's Guide*. Natick, Massachusetts.

Dong, M., Huang, S., and Hutchence, K. (2006). Methane Pressure-Cycling Process with Horizontal Wells for Thin Heavy Oil-Reservoirs. *SPEREE*, **9**(2):154–164. SPE 88500-PA.

Doraisamy, H., Ertekin, T., and Grader, A. (2000). Field Development Studies by Neuro-Simulation: An Effective Coupling of Soft and Hard Computing Protocols. *Computers & Geosciences*, **26**:963–973.

Elman, J. (1990). Finding Structure in Time. *Cog. Sci.*, **14**:179–211.

Emanuel, A., Tang, R., Fong, W., and Langston, M. (1991). Analytic and Numerical Model Studies of Cyclic CO_2 Injection Projects. In *SPE Annual Technical Conference and Exhibition Proceedings*. SPE 22934. 6-9 October. Dallas, Texas.

Fausett, L. (1994). *Fundamentals of Neural Networks: Architectures, Algorithms, and Applications*. Prentice-Hall, Englewood Cliffs, New Jersey.

Felsenthal, M. and Ferrell, H. (1967). Pressure Pulsing - An Improved Method of Waterflooding Fractured Reservoirs. In *SPE Permian Basin Oil Recovery Conference Proceedings*. SPE 1788. 8-9 May. Midland, Texas.

Gökcesu, U. (2005). *Generic Field Development Schemes Using Virtual Intelligence Based Protocols*. Master's thesis, The Pennsylvania State University, University Park, Pennsylvania.

Goldberg, D. and Deb, K. (1991). *A Comparative Analysis of Selection Schemes Used in Genetic Algorithms*, pages 69–93. Morgan Kaufmann Publishers, San Meteo, California. In *Foundations of Genetic Algorithms*, edited by Rawlins, G.

Göndiken, Ş. (1987). Camurlu Field Immiscible CO_2 Huff and Puff Pilot Project. In *Middle East Oil Show Proceedings*. SPE 15749. 7-10 March. Manama, Bahrain.

Güyagüler, B. (2002). *Optimization of Well Placement and Assesment of Uncertainty*. Ph.D. thesis, Stanford University, Stanford, California.

Güyagüler, B., Horne, R., and Rogers, L. (2000). Optimization of Well Placement in a Gulf of Mexico Waterflooding Project. In *SPE Annual Technical Conference and Exhibition Proceedings*. SPE 63221. 1-4 October. Dallas, Texas.

Haskin, H. and Alston, R. (1989). An Evaluation of CO_2 Huff 'n' Puff Tests in Texas. *J. Pet. Tech.*, **41**(2):177–184. SPE 15502.

Haykin, S. (1998). *Neural Networks: A Comprehensive Foundation*. Prentice Hall, second edition.

Hsu, H.-H. and Brugman, R. (1986). CO_2 Huff-Puff Simulation Using a Compositional Reservoir Simulator. In *SPE Annual Technical Conference and Exhibition Proceedings*. SPE 15503. 5-8 October. New Orleans, Lousiana.

Johnson, V. and Rogers, L. (2000). Accuracy of Neural Network Approximators in Simulation-Optimization. *J. Wat. Res. Plan. Mgmt.*, **126**(2):48–56.

Johnson, V. and Rogers, L. (2001). Applying Soft Computing Methods to Improve the Computational Tractability of a Subsurface SimulationOptimization Problem. *J. Pet. Sci. Eng.*, **29**:153–175.

Jordan, M. (1986). Serial Order: A Parallel Distributed Processing Approach. Technical Report 8064, Institute for Cognitive Science, University of Calfornia, San Diego, California.

Khatib, A., Earlougher, R., and Kantar, K. (1981). CO_2 Injection as an Immiscible Application for Enhanced Recovery in Heavy Oil Reservoirs. In *SPE California Regional Meeting Proceedings*. SPE 9928. 25-26 March. Bakersfield, California.

Matlab (2006). *MATLAB Genetic Algorithm and Direct Search Toolbox, Version 2, User's Guide*. The Mathworks, Inc., Natick, Massachusetts.

McCain, J., W. D. (1990). *The Properties of Petroleum Fluids*. PennWell Books, Tulsa, Oklahoma, 2nd edition.

Menzie, D. and Nielsen, R. (1963). A Study of the Vaporization of Crude Oil by Carbon Dioxide Repressurizing. *J. Pet. Tech.*, **15**(11):1247–1252. SPE 568.

Michalewicz, Z. (1994). *Genetic Algorithms + Data Structures = Evolution Programs*. Springer, New York, New York, third edition.

Miller, B. (1990). Design and Results of a Shallow, Light Oilfield-Wide Application of CO_2 Huff 'n' Puff Process. In *SPE/DOE Symposium on Enhanced Oil Recovery Proceedings*. SPE 20268. 22-25 April. Tulsa, Oklahoma.

Miller, B., Bardon, C., and Corlay, P. (1994). CO_2 Huff 'n' Puff Field Case: Five-Year Program Update. In *SPE Permian Basin Oil and Gas Recovery Conference Proceedings*. SPE 27677. 16-18 March. Midland, Texas.

Miller, B. and Gaudin, R. (2000). Nitrogen Huff and Puff Process Breathes New Life into Old Field. World Oil Magazine.

Miller, B. and Hamilton-Smith, T. (1998). Field Case: Cyclic Gas Recovery for Light-Oil Using Carbon Dioxide/Nitrogen/Natural Gas. In *SPE Annual Technical Conference and Exhibition Proceedings*. SPE 49169. 27-30 September. New Orleans, Louisiana.

Mohaghegh, S. (2000). Virtual Intelligence Applications in Petroleum Engineering: Part 1 - Artificial Neural Networks. *J. Pet. Tech.*, **53**(9):64–73. SPE 58046.

Mohaghegh, S., Balan, B., McVey, D., and Ameri, S. (1996). A Hybrid Neuro-Genetic Approach to Hydraulic Fracture Treatment Design and Optimization. In *SPE Annual Technical Conference and Exhibition Proceedings*. SPE 36602. 6-9 October. Denver, Colorado.

Mohaghegh, S., Modavi, A., Hafez, H., Haajizadeh, M., Kenawy, M., and Guruswamy, S. (2006). Development of Surrogate Reservoir Models (SRM) for Fast-Track Analysis of Complex Reservoirs. In *SPE Intelligent Energy Conference and Exhibition Proceedings*. SPE 99667. 11-13 April. Amsterdam, The Netherlands.

Mohammed-Singh, L., Singhal, A., and Sim, S. (2006). Screening Criteria for Carbon Dioxide Huff 'n' Puff Operations. In *SPE/DOE Symposium on Improved Oil Recovery Proceedings*. SPE 100044. 22-26 April. Tulsa, Oklahoma.

Monger, T. and Coma, J. (1988). A Laboratory and Field Evaluation of the CO_2 Huff 'n' Puff Process for Light-Oil Recovery. *SPERE*, **3**:1168–1176. SPE 15501.

Monger, T., Ramos, J., and Thomas, J. (1991). Light Oil Recovery From Cyclic CO_2 Injection: Influence of Low Pressures Impure CO_2, and Reservoir Gas. *SPERE*, **6**(1):25–36. SPE 18084.

Moussine, K., Ibragimov, N., and Khisamov, R. (2007). The Optimization of Gas/Steam Injection Using Numerical Simulation. In *15th SPE Middle East Technical Oil & Gas Show and Conference Proceedings*. SPE 105199. 11-14 March. Kingdom of Bahrain.

Neuroshell (1998). *Neuroshell 2 Tutorial*. Ward Systems, Inc., Frederick, Maryland.

Owens, W. and Archer, D. (1966). Waterflood Pressure Pulsing for Fractured Reservoirs. *J. Pet. Tech.*, **18**:745–752. SPE 1123.

Papp, I., Lakes, B., Palasthy, G., and Tromboczky, S. (1998). Enhanced Recovery for Selected Components of a Highly Volatile Oil. In *SPE/DOE Improved Oil Recovery Symposium Proceedings*. SPE 39689. 19-22 April. Tulsa, Oklahoma.

Parada, C. H. (2008). *An Artificial Neural Network Based Tool-Box for Screening and Designing Improved Oil Recovery Methods*. Ph.D. thesis, The Pennsylvania State University, University Park, Pennsylvania.

Patel, A., Davis, D., Guthrie, C., Tuk, D., Nguyen, T., and Williams, J. (2005). Optimizing Cyclic Steam Oil Production with Genetic Algorithms. In *SPE Western Regional Meeting Proceedings*. SPE 93906. 30 March - 1 April. Irvine, California.

Patton, J., Coats, K., and Spence, K. (1982). Carbon Dioxide Well Stimulation: Part 1-A Parametric Study. *J. Pet. Tech.*, **24**:1798–1804. SPE 9228.

Pratz, M. (1982). *Thermal Recovery*. SPE-AIME. Monograph 7.

Rathmell, J. J., Stalkup, F. I., and Hassinger, R. C. (1971). A Laboratory Investigation of Miscible Displacement by Carbon Dioxide. In *SPE Annual Fall Meeting Proceedings*. SPE 3483. 3-6 October. New Orleans, Louisiana.

Raza, S. (1971). Water and Gas Cyclic Pulsing Method for Improved Oil Recovery. *J. Pet. Tech.*, **23**:1467–1474. SPE 3005.

Rumelhart, D., Hinton, G., and Williams, R. (1986). *Learning Internal Representations by Error Propagation*, chapter 8, pages 675–695. Anderson & Rosenfeld.

Sankur, V. and Emanuel, A. (1983). A Laboratory Study of Heavy Oil Recovery With CO_2 Injection. In *SPE California Regional Meeting Proceedings*. SPE 11692. 23-25 March. Ventura, California.

Sayegh, S. and Maini, B. (1984). Laboratory Evaluation of the CO_2 Huff-n-Puff Process for Heavy Oil Reservoirs. *J. Cdn. Pet. Tech.*, **23**(3):29–36.

Shayegi, S., Jin, Z., Schenewerk, P., and Wolcott, J. (1996). Improved Cyclic Stimulation Using Gas Mixtures. In *SPE Annual Technical Conference and Exhibition Proceedings*. SPE 36687. 6-9 October. Denver, Colorado.

Shelton, J. and Morris, E. (1973). Cyclic Injection of Rich Gas Into Producing Wells To Increase Rates From Viscous-Oil Reservoirs. *J. Pet. Tech.*, **25**(8):890–896.

Silva, P., Clio, M., and Schiozer, D. (2007). Use of Neuro-Simulation Techniques as Proxies to Reservoir Simulator: Application in Production History Matching. *J. Pet. Sci. Eng.*, **57**:273280.

Stone, H. (1973). Estimation of Three-Phase Relative Permeability and Residual Oil Data. *J. Cdn. Pet. Tech*, **12**(4):53.

Stright, D., Jr., Aziz, K., Settari, A., and Starratt, F. (1977). Carbon Dioxide Injection Into Bottom-Water, Undersaturated Viscous Oil Reservoirs. *J. Pet. Tech.*, **29**:1248–1258. SPE 6116.

Thomas, G. and Monger-McClure, T. (1991). Feasibility of Cyclic CO_2 Injection for Light-Oil Recovery. *SPERE*, **6**(2):179–184. SPE 20208.

Towler, B. and Wagle, Y. (1992). Modelling the CO_2 Huff 'n' Puff Process in Solution-Gas-Drive Reservoirs Using a Black-Oil Simulator. *J. Pet. Sci. Eng.*, **8**:167–179.

Warren, J. E. and Root, P. J. (1963). The Behaviour of Naturally Fractured Reservoirs. *SPEJ*, **3**(3):245–255. 426-PA.

Wehner, S. and Prieditis, J. (1996). CO_2 Huf-n-Puff: Initial Results from a Waterflooded SSC Reservoir. In *Permian Basin Oil & Gas Recovery Conference Proceedings*. SPE 35223. 27-29 March. Midland, Texas.

Wolcott, J., Schenewerk, P., Berzins, T., and Karim, F. (1995). A Parametric Investigation of the Cyclic CO_2 Injection Process. *J. Pet. Sci. Eng.*, **14**:35–44.

Yan, S. and Minsker, B. (2006). Optimal Groundwater Remediation Design Using an Adaptive Neural Network Genetic Algorithm. *Water Resour. Res.*, **42**:1–14.

Yeten, B., Durlofsky, L., and Aziz, K. (2003). Optimization of Nonconventional Well Type, Location, and Trajectory. *SPEJ*, **8**(3):200–210. SPE 86880.

Yu, T., Wilkinson, W., and Castellini, A. (2008). Constructing Reservoir Flow Simulator Proxies Using Genetic Programming for History Matching and Production Forecast Uncertainty Analysis. *Journal of Artificial Evolution and Applications*, **2008**:13 pages. Article ID 263108.

Zangl, G., Giovannoli, M., and Stundner, M. (2006). Application of Artificial Intelligence in Gas Storage Management. In *SPE Europec/EAGE Annual Conference and Exhibition Proceedings*. SPE 100133. 12-15 June. Vienna, Austria.

Appendix

Graphical-User-Interface Application for Proxy Models

Constructed proxy models were incorporated in a graphical-user-interface (GUI) application. The application was developed using Visual Basic 6.0. With this user-friendly interface, it is possible to evaluate a large number of scenarios and search for the optimized design scenario easily. In this appendix, features of this GUI application are presented. The interface includes two main components: screening and optimization.

Screening

In the screening part (Figure A.1), the forward proxy models provide estimated production profiles for a given design scenario for five cycles of injection. There are two main sections to input data:

1. Reservoir Description: Reservoir rock properties, initial conditions, well spacing, and reservoir fluid type are to be inputted in this section. Information about phase diagrams and compositions of reservoir fluids are stored in another window, and it pops up when the '?' button is clicked.

2. Process Design Description: Design parameters for five cycles of injection are inputted in this section. To use the same values for all cycles, 'Copy to All' button can be used to copy the design parameters for Cycle-1 to other cycles. The injected gas (nitrogen or CO_2) is also selected in this section.

After all the data is entered, 'Fire the Proxy' is to be clicked to call the appropriate proxy model for the given injected gas and reservoir fluid type. In the results section, estimated cumulative productions, peak oil rates, and production times are printed. In addition to expected performance of each cycle, the expected base production in this reservoir and the incremental oil that can be produced with the given design scenario are provided. In the bottom, oil production rate vs. time plot is displayed.

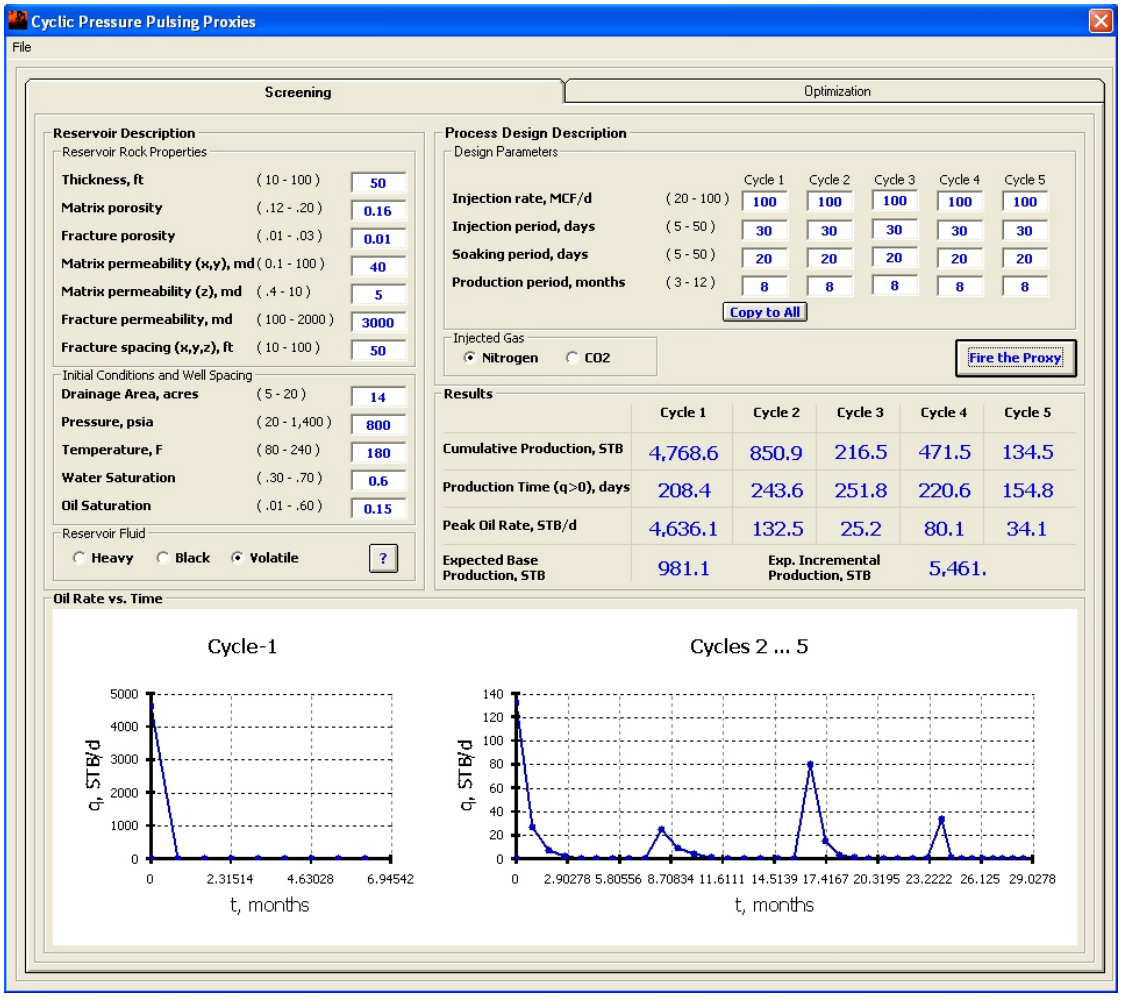

Figure A.1. Screening.

Optimization

Optimization part (Figure A.2) includes a genetic algorithm that searches for the optimized design scenario for the reservoir under consideration. The objective function is:

$$f = \frac{IOP_{t=0}}{CI} \tag{A.1}$$

where $IOP_{t=0}$ is the current incremental oil production, and CI is the cumulative volume of the injected gas. GA parameters such as the population size, number of generations, crossover and mutation probabilities can be changed. After the generations are completed, the recommended design scenario is printed together with the expected base and incremental oil productions from this reservoir. A summary of each GA generation is given at the bottom, with the best fitness values found. The 'Apply Design' button can be used to use the recommended design as input to the proxy model. After clicking the button, the design is applied and the screening tab is displayed with the expected oil production performance (Figure A.3).

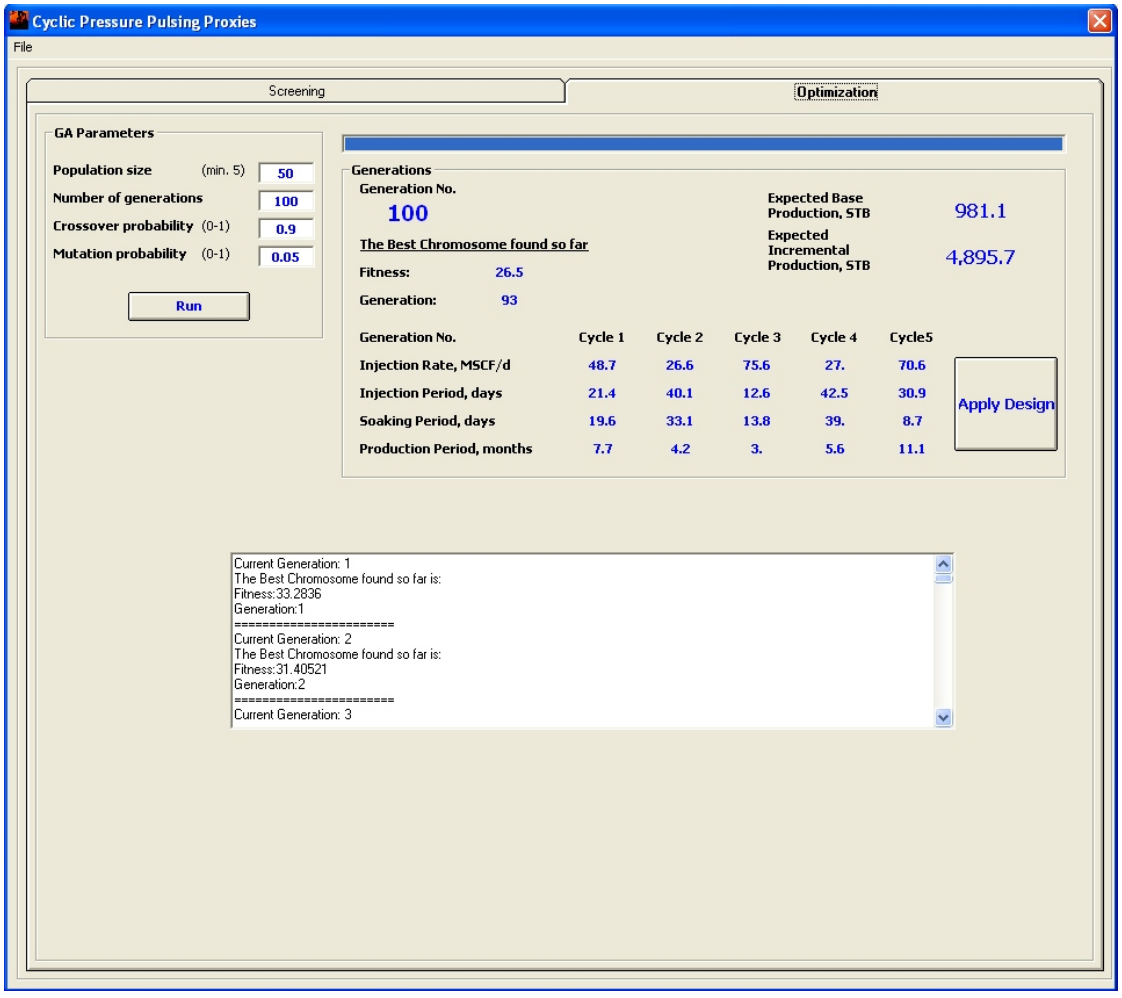

Figure A.2. Optimization.

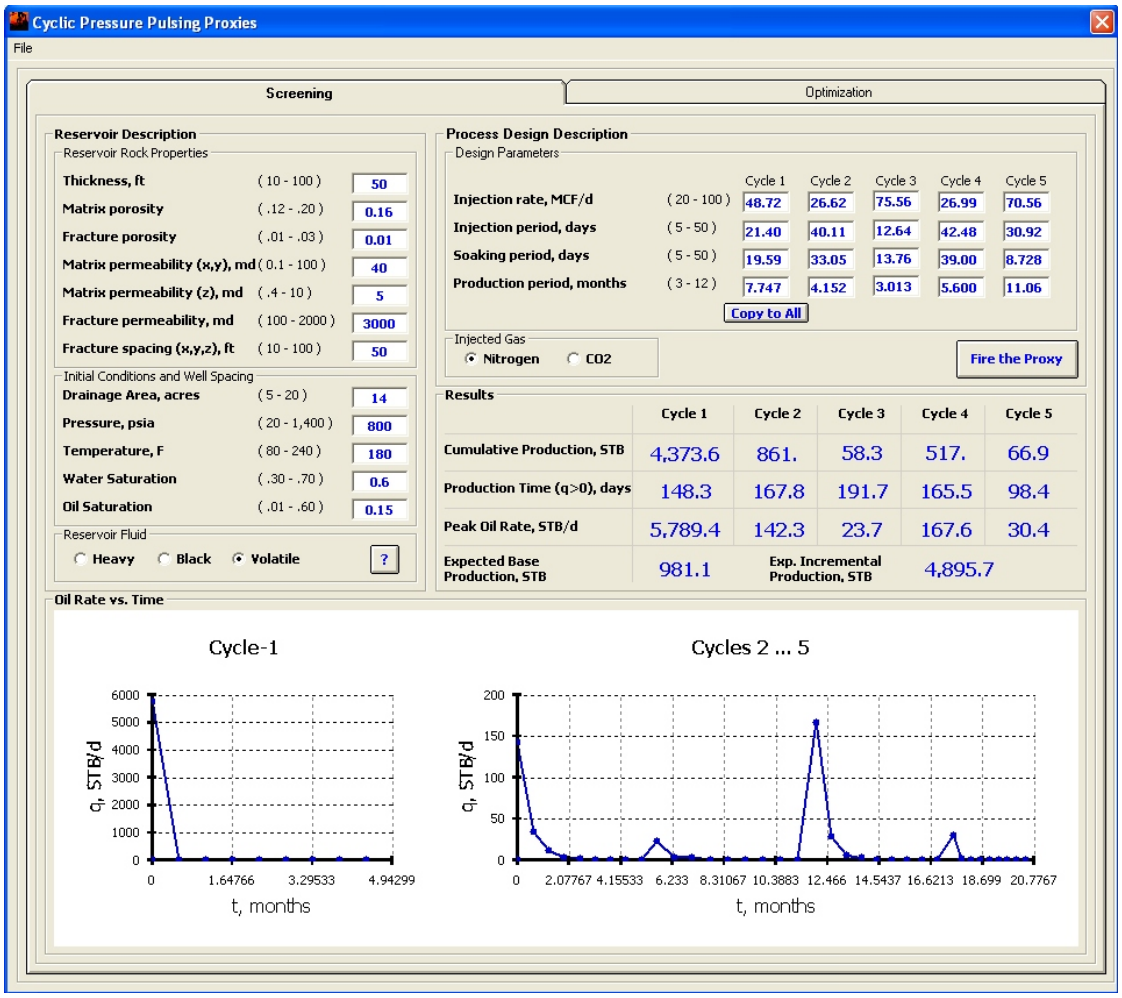

Figure A.3. Applying the optimized design.

Vita

F. Emre Artun

Fazıl Emre Artun was born in Ankara, Turkey, on June 19, 1982. He graduated from TED Ankara Koleji (TED Ankara College Foundation Private High School) in 1999. He received a baccalaureate degree in Petroleum and Natural Gas Engineering from Orta Doğu Teknik Üniversitesi (Middle East Technical University), Ankara, Turkey, in June, 2003. After graduation, he came to the United States for graduate studies. He received a master's degree in Petroleum and Natural Gas Engineering from West Virginia University, Morgantown, West Virginia, and he joined The Pennsylvania State University for his doctoral studies in August, 2005. Since then, he has been a Ph.D. candidate in the Petroleum and Natural Gas Engineering Program, and he has been pursuing a Graduate Minor in Computational Science.

Mr. Artun received the Best Student Paper Award at the 2005 AAPG Eastern Section Meeting. He was a 2^{nd} place winner at the 2008 Penn State Annual Graduate Exhibition's Engineering Research Division and he was awarded with the 2007/2008 PNGE Graduate Merit Award. His research work has been published in technical journals, and in the proceedings of national and international conferences. He is a member of the Society of Petroleum Engineers.

Mr. Artun successfully defended his Ph.D. dissertation on June 3, 2008, and he has accepted a position with Chevron Energy Technology Company as a reservoir simulation engineer in Houston, Texas.